

**Natural and Enhanced Attenuation
of Soil and Groundwater at the
Monument Valley, Arizona,
DOE Legacy Waste Site**

2008 Pilot Study Status Report

August 2009



U.S. DEPARTMENT OF
ENERGY

Legacy
Management

This page intentionally left blank

**Natural and Enhanced Attenuation of Soil and Groundwater
at the Monument Valley, Arizona, DOE Legacy Waste Site**

2008 Pilot Study Status Report

August 2009

This page intentionally left blank

Contents

Abbreviations	vii
Executive Summary	ix
1.0 Introduction	1-1
2.0 Soil Moisture	2-1
2.1 Irrigation Schedule	2-1
2.2 Neutron Hydroprobe Monitoring	2-1
2.3 Percolation Flux Monitoring	2-4
3.0 Soil Chemistry Monitoring	3-1
3.1 Source Area Nitrogen and Sulfur	3-1
3.2 Land Farm Nitrogen and Sulfur Sampling Design	3-5
3.2.1 Background	3-5
3.2.2 Sampling Protocol for 2009	3-6
3.3 Root Distribution in the Source Area Plantings	3-7
3.3.1 Need for Direct Estimation of Root Depth	3-7
3.3.2 Sampling and Analysis Protocol	3-7
3.4 Manganese Toxicity Investigation	3-9
3.4.1 Background	3-9
3.4.2 Manganese Chemistry	3-9
3.4.3 Presence and Formation Iron-Manganese Concretions	3-9
3.4.4 Manganese Abundance at the Site	3-11
3.4.5 Origin of Reduced Soluble Manganese at the Site	3-11
3.4.6 Conclusions and Recommendations	3-12
4.0 Summary of Interrelationships of NH ₄ , NO ₃ , SO ₄ , and Moisture Content	4-1
5.0 Vegetation Monitoring: Plume Grazing Enclosures	5-1
6.0 Monitoring Vegetation Status and Evapotranspiration Using Ground-Calibrated Remote Sensing Methods	6-1
6.1 Background and Rationale for Remote Sensing Methods	6-1
6.2 Remote Sensing Products	6-1
6.3 Mapping Vegetation with Quickbird Imagery	6-3
6.4 Approximating LAI and Standing Biomass from Quickbird Images	6-7
6.5 MODIS EVI for Tracking Vegetation Changes Over Time	6-7
6.6 MODIS EVI* for Estimating ET and LAI	6-9
6.7 MODIS Estimates of ET and LAI Over the Site, 2000-2008	6-10
7.0 Ethanol-Enhanced Denitrification of the Alluvial Aquifer	7-1
7.1 Background	7-1
7.2 Summary of Work Plan	7-2
8.0 Data Archive	8-1
9.0 References	9-1

Figures

Figure 2–1.	(Top) Soil moisture levels in 2007 and 2008 in non-irrigated Control plots and in four areas within the Original Field in the source area at the Monument Valley site. (Bottom) Soil moisture levels in Control plots and in the Extended Field, the Evaporation Pond, and the Land Farm, 2007 and 2008. Bars are standard errors of means; results are averaged across all soil depths at each port.....	2–2
Figure 2–2.	Soil moisture levels at different depths in the soil profile in Control plots and irrigated plots in the source area at the Monument Valley site. Results are averaged across ports at each site.	2–3
Figure 2–3.	Schematic of a passive wick WFM (from Gee et al. 2009).	2–5
Figure 2–4.	Hourly volumetric water content at four depths down to 300 cm monitored with WCRs at WFM Stations.	2–6
Figure 3–1.	Nitrate and ammonium concentrations in the original source area field (1999 planting) from 2000 to 2008. Results are the analysis of 100 auger holes sampled at 3–5 soil depths at each sample interval. Error bars are standard errors of means. Data were analyzed by one-way analysis of variance with sample interval as the independent variable; both nitrate and ammonium have decreased ($P < 0.001$).....	3–1
Figure 3–2.	Regression of $\delta^{15}\text{N}$ on the natural log of nitrate and ammonium concentration in samples from the subpile soil taken in 2004. Samples were taken at different depths and locations in and out of irrigated areas to assure a wide range of concentration values. The results show significant ($P < 0.001$) increase in $\delta^{15}\text{N}$ values with decreasing concentrations, indicating that microbial processes are reducing the concentrations through production of nitrous oxide or nitrogen gas.	3–2
Figure 3–3.	(Top) Mean and standard errors of nitrate, ammonium and sulfate concentrations in the original field in the subpile soil area in 2008. (Bottom) Reduction in nitrate and ammonium from 2000–2008 as a function of soil depth.	3–3
Figure 3–4.	Distribution of ammonium (A), nitrate (B), and sulfate (C) in the original field of the source area in 2008 as a function of sampling location. The field was divided into four sections in the east-west direction: e = east; em = east middle; wm = west middle; and w = west. Each section was divided into five subzones in the north-south direction with 1 = northernmost subzone and 5 = southernmost subzone.....	3–4
Figure 3–5.	Distribution of nitrate and ammonium in the extended field (EF) and evaporation ponds (EP) in 2007 and 2008. Bars are means and standard errors. There were no significant differences ($P < 0.05$) in 2007 and 2008 means.....	3–5
Figure 3–6.	Augering for collection of soil samples. Half the samples were taken underneath canopies and half in the space between canopies (shown).	3–8
Figure 3–7.	Top of the auger hole shown in Figure 3–6. Note the roots in the soil even though this sample was taken between shrub canopies.	3–8
Figure 5–1.	Comparison of Shrub Density Estimates (Combined Method), 2007 to 2008 ...	5–3

Figure 6-1.	Top: MODIS pixel footprints overlain on a high-resolution 2007 Quickbird image for the Monument Valley site. Bottom: a shape file of the Monument Valley site prepared on a Quickbird image and overlain on a MODIS image for July, 2007. The red dot shows the location of the irrigated field in the source area for each image; note the close correspondence in location between the two images.	6-2
Figure 6-2.	Top: Outline of the North Enclosure at the Monument Valley site on a classified Quickbird image (left) compared to the original sharpened panchromatic image. Bottom: illustration of the point-intercept method of visually estimating f_c by shrubs on a Quickbird image. Yellow points are grid intersections that were scored as ATCA or SAVE shrubs.	6-5
Figure 6-3.	Relationship between shrub canopy area measured on the ground with areas measured on a Quickbird image for the Monument Valley site.	6-6
Figure 6-4.	Comparison of shrub density at the Monument Valley site in 1997 and 2007. The 1997 image is an aerial photograph while the 2007 image is a Quickbird scene. The Quickbird image shows the development of the volunteer stand of ATCA (A) and the irrigated field (B) in the fenced area over time.	6-7
Figure 6-5.	Relationship between standing biomass and ground cover of ATCA shrubs at the Monument Valley site.	6-8
Figure 6-6.	Top: ET estimated by MODIS at the Monument Valley site (open circles). Closed circles with error bars show ET measured by sap flux sensors in 2006 and 2007. Closed circles without error bars show ET projected from sap flux measurements and a best-fit model of ET based on temperature data during the sap flux measurements. Bottom: LAI estimated by MODIS (open circles) compared to ground measurements in 2006 and 2007.	6-11
Figure 6-7.	MODIS pixel footprints superimposed on a Quickbird image showing the irrigated field and volunteer ATCA stand inside the fence at the Monument Valley site.	6-12
Figure 6-8.	Two MODIS pixels representing the SAVE stand outside the fence at the Monument Valley site.	6-13
Figure 6-9.	MODIS pixels (red dots) selected to represent the sparse ATCA stand over the plume at the Monument Valley site.	6-14
Figure 6-10.	ET estimated by MODIS for selected areas at the Monument Valley site.	6-15
Figure 6-11.	LAI estimated by MODIS for selected areas at the Monument Valley site.	6-16
Figure 7-1.	Location of proposed new wells PW1 and PW2	7-2
Figure 7-2.	Location of proposed new wells P3 and P4	7-3

Tables

Table 3-1.	Manganese and Iron Soil Chemical Data	3-10
Table 5-1.	Vegetation Cover Inside and Outside Grazing Enclosure Plots	5-2
Table 5-2.	Shrub Density Inside and Outside Grazing Enclosure Plots.....	5-2
Table 6-1.	Estimates of fractional ground cover of shrubs by different methods at the Monument Valley site, July 2007	6-6

Appendixes

Appendix A: Publications and Presentations

Appendix B: List of Pilot Study Maintenance Activities in 2008

Appendix C: Conceptual Model of Groundwater Solute Attenuation at the Former Uranium Mill Tailings Site, Monument Valley, Arizona

Appendix D: Journal of Hydrology Manuscript

Appendix E: Ecohydrology Journal Manuscript

Appendix F: Work Plan for Pilot Study of Ethanol-Enhanced Groundwater Denitrification

Appendix G: Data Archive Outline

Abbreviations

ATCA	<i>Atriplex canescens</i>
Ca	calcium
cm	centimeter
cm ³	cubic centimeter
CNS	carbon nitrogen sulfur
CV	coefficient of variation
DOE	U.S. Department of Energy
EA	enhanced attenuation
EF	extended field
EP	evaporation ponds
ERL	University of Arizona Environmental Research Laboratory
ET	evapotranspiration
EVI	enhanced vegetation index
EVI*	EVI converted to scaled values
Fe	iron
ft	foot
ha	hectares
kg	kilogram
LAI	leaf area index
m	meter
mg/kg	milligram per kilogram
mg/L	milligram per liter
mm/yr	millimeter per year
Mn	manganese
MODIS	Moderate Resolution Imaging Spectrometer
MV	Monument Valley
NIR	near-infrared
p	probability
ppm	parts per million
r ²	coefficient of determination
SAVE	<i>Sarcobatis vermiculatus</i>
T _a	daily temperature

$\mu\text{g/g}$ micrograms per gram
VI vegetation index
WCR water content reflectometer
WFM water fluxmeter

Executive Summary

The U.S. Department of Energy (DOE) Office of Legacy Management (LM), the Navajo Uranium Mill Tailings Remedial Action program, the University of Arizona, and Diné College are exploring alternative remedies for groundwater contamination at Monument Valley, Arizona, that include natural and enhanced attenuation (EA) processes. DOE removed radioactive tailings from Monument Valley, a former uranium mill site, in 1994. Nitrate and ammonium, waste products of the milling process, remain in a shallow groundwater plume spreading from a mill site soil source. A conventional cleanup strategy might involve drilling wells and pumping groundwater to a treatment facility on the surface. Pilot studies jointly funded by LM and the University of Arizona are answering two questions: (1) what is the capacity of natural processes to remove nitrate and slow plume dispersion, and (2) can we efficiently enhance natural attenuation if necessary? Below are 2008 highlights of pilot study results that are helping to answer these questions.

Source Containment and Removal

Phreatophytes were planted in the nitrate plume source area (soils remaining after tailings were removed) to limit percolation and leaching of nitrate by controlling the soil-water balance. About 1.7 hectares (ha) of the source area was planted in 1999 and the remaining 1.6 ha was planted in 2006, primarily with the native desert shrub, four-wing saltbush (*Atriplex canescens*).

Source Area Nitrogen and Sulfur

Soil cores were collected in the Source Area soil from the 1999 planting (original field) and the 2006 planting (extended fields) in March 2007 and May 2008 and analyzed for nitrate-N, ammonium-N, and sulfate-S. Both nitrate and ammonium have decreased significantly since 2000. The decrease in nitrate may have slowed, as expected for a substrate-dependent, exponential decay process. On the other hand, ammonium levels are still decreasing. Nitrification (of ammonium) is a likely reason for the slow decrease in nitrate.

Enrichment of ^{15}N ($\delta^{15}\text{N}$) provides additional evidence that loss of nitrogen is due to denitrification in the case of nitrate, and of nitrification followed by denitrification in the case of ammonium. Denitrification favors ^{14}N over ^{15}N , so residual nitrate in the soil becomes enriched in ^{15}N as nitrate becomes depleted.

Overall, the results show that planting and irrigating of native shrubs has produced a marked reduction in both nitrate and ammonium in the source area over an 8-year period. Total nitrogen has been reduced from 350 milligrams per kilogram (mg/kg) in 2000 to less than 200 mg/kg in 2008. Microbial processes rather than plant uptake are responsible for most of the nitrogen reduction. However, the plants help control of the site water balance, preventing additional leaching of nitrogen compounds into the aquifer.

Manganese Chemistry

Source Area soils have elevated levels of calcium (Ca) and iron (Fe) in places that display a discolored surface in aerial photographs. On the ground, several color phases including black, red, green, and pink have been observed. Some Source Area soils also have a shallow layer of

dark brown mottled material, which has been associated with areas of stunted plant growth. Manganese (Mn) concretions (Fe and Mn precipitates) were identified in samples from the mottled soil areas. Oxides of Mn at different oxidation states, deposited in the soil during extraction of uranium, may be the source. These different oxidation states could be responsible for the "rainbow" colors around drip emitters in the stained areas, and especially in the former evaporation pond.

Uranium processing included the use of sulfuric acid solutions passed through leached bed to mobilize uranium ions. With the low-pH, reduced, and anaerobic soil, naturally occurring Mn was likely also leached and translocated within the vadose zone. The most likely forms of Mn at the site are sulfate-containing species. At this arid site, it is also likely that soluble (reduced) forms of Mn were formed during the period of operations. But after operation ceased, dry conditions set in precluding the re-oxidation of Mn to much more stable and common forms of Mn such as pyrolusite. Now that the site is irrigated, oxidation (at least in the unsaturated zone) of Mn is likely occurring, leading to more stable forms over time. This process may be responsible for the formation of nucleation sites that form the dark brown concretions rich in Mn and the rainbow rings around drip nozzles that have been observed on irrigation soils at this site.

Because the levels of Mn are within values for normal soils, and well below any levels of concern for human health risks, further testing or remediation is not recommended. Current irrigation practices and natural attenuation processes will likely continue to convert the soluble forms of Mn into insoluble oxides normally present in soils.

Groundwater Attenuation

Interrelationships of NH₄, NO₃, SO₄, and Moisture Content

Contamination of the alluvial aquifer by nitrate, ammonium, and sulfate are the major concerns at Monument Valley site. In 2008, transport and fate processes that influence ammonium, nitrate, and sulfate concentrations were evaluated, and a manuscript comparing nitrate attenuation characterization methods developed for Monument Valley was submitted to the *Journal of Hydrology*.

Results from the collection of spatial and temporal concentration data from a transect of monitoring wells located along the plume centerline indicate that nitrate, ammonium, and sulfate concentrations are decreasing due to natural attenuation processes. Adsorption appears to partly control the transport and fate of ammonium in the plume. Sulfate concentrations are most likely controlled by equilibrium formation/dissolution of the solid mineral phase gypsum. Naturally formed gypsic lenses are already found in soils at the site. Calcium ions in the soil react with sulfate in the Source Area and contamination plume to produce gypsum deposits, which are relatively immobile.

Nitrification may be occurring in the upgradient part of the plume as well as in the Source Area (see above). Nitrate biotransformation occurs through reduction to atmospheric nitrogen gas (i.e., denitrification) in both the irrigated subpile soils and the downgradient region of the plume.

The occurrence and rate of denitrification was evaluated through microcosm experiments, nitrogen isotopic fractionation analysis, and solute transport modeling. First-order rate coefficients calculated with each method were comparable. The composite natural attenuation rate coefficient was slightly larger but similar to the denitrification rate coefficient, which suggests that microbially-induced decay primarily controls nitrate attenuation at the site. Sulfate reductive biotransformation was not evident from the available data.

An estimated 30–70 percent of nitrate in the plume has been lost through natural denitrification since the mill was closed in 1968. Estimates of sulfate losses through gypsum formation are not yet available, but eventually an equilibrium level is expected to be established at the solubility of calcium sulfate in the hotspots of the plume, and lower where the plume has been diluted.

Ethanol-Enhanced Denitrification of the Alluvial Aquifer

EA can be defined as initiating and/or augmenting natural and sustainable attenuation processes. The goal is to increase the magnitude of attenuation by natural processes beyond that which occurs without intervention. Enhancing in situ biological denitrification through injection of amendments has been deemed a promising method for remediation of nitrate-contaminated groundwater.

The Monument Valley site is considered to be an excellent candidate for in situ EA denitrification. The region of high nitrate contamination in the plume is confined in a relatively small volume of the aquifer. Treatment of this high-concentration portion of the plume could allow natural attenuation of the remainder of the plume. Questions that remain to be addressed are the degree of enhancement that can be achieved and the optimal means of implementation. These questions will be addressed with a pilot-scale demonstration in 2009 supplemented with mathematical modeling analyses. This report includes a detailed work plan for a field-scale injection of ethanol as a denitrification enhancement substrate.

Changes in Vegetation

Preliminary studies demonstrated that grazing protection overlying the plume may have positive effects on biomass productivity, ground cover, and rates of phreatophyte transpiration and nitrogen uptake. In 2005, two large plots were fenced to evaluate grazing protection on a landscape scale. Vegetation canopy cover and shrub density were sampled in 2007 and 2008 in the two grazing exclosure plots and compared with adjacent control plots not protected from grazing. Results suggest that to date, no clear trends in the response of vegetative cover and shrub density to reduced grazing are apparent. However, grazing exclosures do appear to have increased overall leaf area index (LAI) and evapotranspiration (ET) (see below).

Remote Sensing Monitoring Methods

Phreatophytic shrub populations at Monument Valley play a role in controlling movement of the groundwater nitrate plume and also in limiting soil percolation in the source area of the plume. The Monument Valley site will require long-term monitoring of vegetation cover and ET if natural and enhanced attenuation methods are selected for the final remedy. Vegetation abundance over the source area helps determine the extent of recharge of water from the source area and from surrounding uplands into the plume, because water used by vegetation decreases

the amount that can migrate into the aquifer. Vegetation abundance over the plume helps determine the rate of plume migration away from the site, because water used by vegetation decreases the amount available to expand the volume of the plume over time.

In 2008, an unobtrusive approach for evaluating changes in phreatophytic shrub populations based on remote sensing technologies developed from research at Monument Valley. These methods may result in reduced long-term surveillance and maintenance costs at Monument Valley and also may be applicable at other LM sites. The body of this report discusses the need for vegetation monitoring and how ground data can be combined with high-resolution and low-resolution imagery to monitor ET, LAI, and fractional cover. The method developed for Monument Valley was published in the journal *Ecohydrology* in 2008.

1.0 Introduction

The U.S. Department of Energy (DOE) is conducting pilot studies of enhanced attenuation remedies for contaminated groundwater at a former uranium mill tailings sites near Monument Valley, Arizona. Nitrate, ammonium, and sulfate levels are elevated in an alluvial aquifer spreading away from a source area where tailings were removed.

The pilot studies at Monument Valley were mandated by a DOE Environmental Assessment. The EA gives direction for an evaluation of alternative remedies before a final strategy is selected (DOE 2004a). Preliminary studies suggested that natural and enhanced phytoremediation may be viable options for reducing nitrate and sulfate levels in the alluvial aquifer and at the plume source (DOE 2002, DOE 2004b). Phytoremediation is also in harmony with revegetation and land management goals for the site.

In May 2005, DOE and the Navajo Nation jointly approved a second (and final) phase of pilot studies as proposed in a work plan published by DOE in 2004 (DOE 2004c). The purpose of the final phase is to evaluate the capacity of natural processes, and methods to enhance natural processes, that degrade and slow the migration of contaminants both in the alluvial aquifer and at its source. The pilot studies are focusing on phytoremediation and bioremediation processes. Phytoremediation relies on the roots of plants to remove, degrade, and slow the migration of contaminants. Bioremediation relies on microbial processes to reduce concentrations of nitrate, ammonium, and sulfate in the source area and plume.

In 2006, DOE published first-year (2005) results of the pilot study, a synopsis of the enhanced natural attenuation approach, and a decision framework for using the results of the pilot studies to choose a final remedy for nitrate, ammonia, and sulfate at Monument Valley (DOE 2006). Summaries of the 2006 and 2007 results of the Monument Valley pilot studies were subsequently published (DOE 2007, DOE 2008). Summaries of the 2008 results of Monument Valley's pilot studies are presented in Sections 2.0 through 8.0 of this report. The reader can find additional background information on the rationale and designs of the Monument Valley pilot studies in the DOE reports cited above. Appendix A is a complete list of journal and proceedings publications, presentations, and DOE reports produced since the inception of the project.

The pilot studies are based on large plantings and irrigation systems that require regular maintenance. Maintenance activities in 2008, outlined in Appendix B, included repairs of the drip irrigation system and raising transplant replacements for dead four-wing saltbush and black greasewood as needed.

This page intentionally left blank

2.0 Soil Moisture

Monument Valley pilot study plots are irrigated to support growth of planted phreatophytic shrubs and to enhance denitrification. The plots are purposely under-irrigated to prevent leaching of nitrate into the aquifer. The original source area (subpile) plot has been irrigated each year since it was installed in 2000, with the exception of 2003. The irrigated area was increased in 2006 with the expansion of the subpile plot, planting of the evaporation pond, and planting of plume phytoremediation plots (Passive Phytoremediation Plots).

2.1 Irrigation Schedule

In 2007 and 2008 the irrigation schedules were altered to provide more water to the fields in an attempt to enhance plant growth and denitrification, while still preventing leaching of contaminants into the aquifer. In 2007, plots were irrigated for 2 hours per day (0.95 millimeters per day [mm/day] on an area basis) from April 25 to May 21 (total of 24 mm), then for 6 hours per day (2.85 mm/day) from May 22 to November 1 (total of 472 mm). The total annual application was 496 mm, about three times higher than in previous years.

In 2008, irrigation rates were reduced because neutron hydroprobe readings and water content reflectometers (WCRs) suggested that some parts of the fields were over-irrigated and may be producing drainage. Plots were irrigated for 4 hours per day (1.9 mm/day) from March 28 to May 25 (total of 110 mm) and for 3 hours per day (1.4 mm/day) from May 26 to October 1 (total of 175 mm). The total application in 2008 was 285 mm. The Passive Phytoremediation Plots received 6 hours per day of irrigation both years to encourage deep root growth, but soil moisture was not measured. Irrigation schedules of some of the plots in the Land Farm were altered in both years due to lower-than-expected yield from the high-nitrate well.

2.2 Neutron Hydroprobe Monitoring

Soil moisture levels were measured monthly during the irrigation season at approximately 0.31-meter (m) intervals in a series of 60-neutron hydroprobe ports distributed in four plots in the Original Field (the subpile plots established in 2000); in three plots in the Extended Field (established in 2006); in the Evaporation Pond plot (established in 2006); and in the Land Farm (established in 2006). Additional control ports were located in non-irrigated portions of the subpile soil, representing denuded areas and areas with vegetation.

Results were analyzed for April, July, and September readings for 2007 and 2008. Mean readings over all depths for each plot are shown by month and year in Figure 2-1. A three-way analysis of variance was conducted in which year, month, and site (Controls, Original Field, Extended Fields, Evaporation Pond, and Land Farm) were independent variables and soil moisture (cubic centimeters [cm³] H₂O per cm³ soil) averaged over all depths was the dependent variable. Year was marginally significant ($P = 0.051$), while month ($P = 0.001$) and site ($P < 0.001$) were highly significant. The interaction term (year \times site) was also highly significant ($P < 0.001$), showing that the sites responded differently to the altered irrigation schedules. Control ports were not significantly different between years ($P = 0.652$), whereas the Original Field was slightly wetter in 2008 than 2007 ($P = 0.003$) and the Extended Field was slightly dried in 2008 than 2007 ($P < 0.001$). The Extended Field was slightly wetter in July than in April

or September in both years ($P < 0.001$) but seasonal differences were otherwise non-significant ($P > 0.05$).

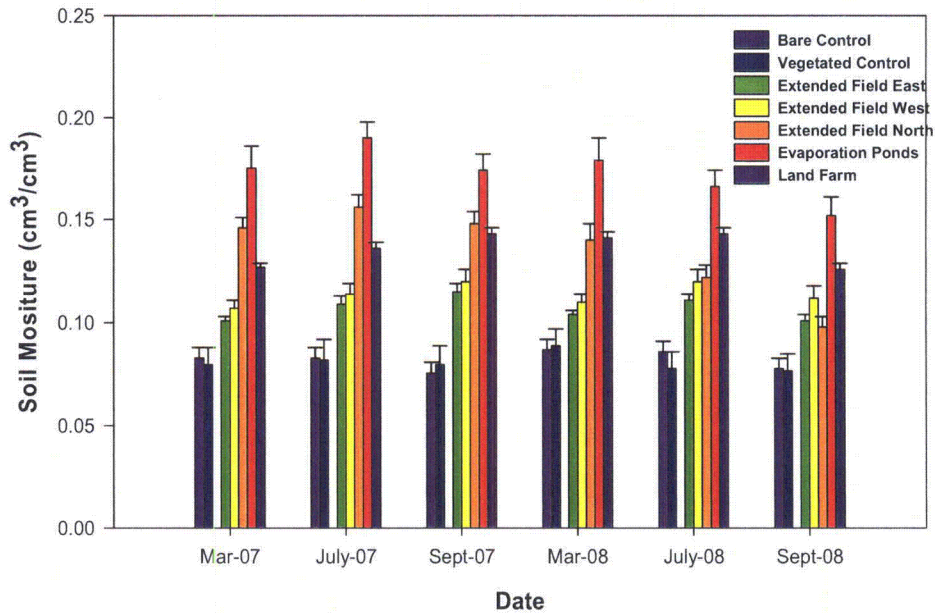
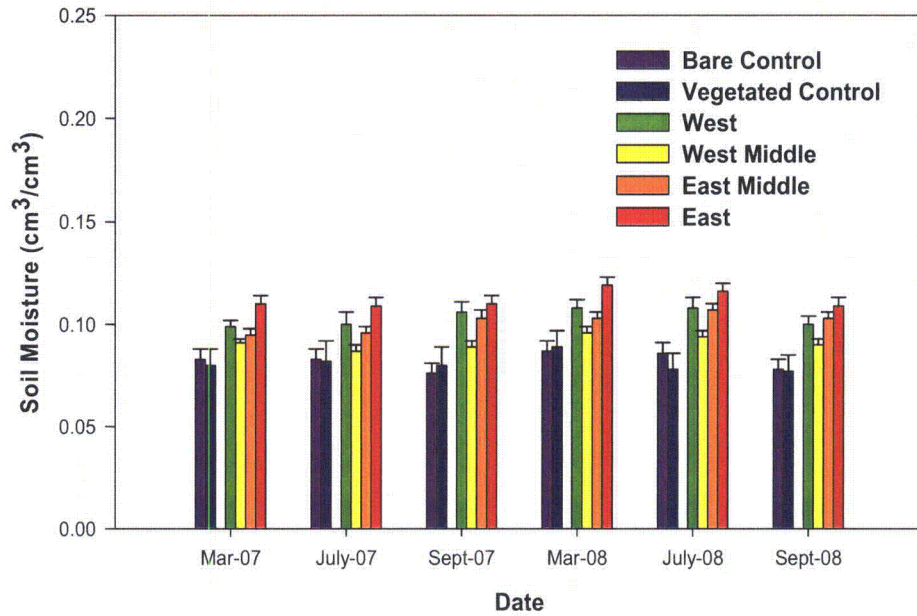


Figure 2-1. (Top) Soil moisture levels in 2007 and 2008 in non-irrigated Control plots and in four areas within the Original Field in the source area at the Monument Valley site. (Bottom) Soil moisture levels in Control plots and in the Extended Field, the Evaporation Pond, and the Land Farm, 2007 and 2008. Bars are standard errors of means; results are averaged across all soil depths at each port.

Bare and vegetated control plots had similar moisture levels (about $0.08 \text{ cm}^3/\text{cm}^3$), significantly lower than in all irrigated plots (Figure 2-1). Moisture levels in the Original Field were about $0.10 - 0.12 \text{ cm}^3/\text{cm}^3$ (Figure 2-1, top), which are below the assumed field capacity (about $0.15 \text{ cm}^3/\text{cm}^3$). However, field capacity needs to be determined by measurement in these fields. Moisture levels were slightly higher in the Extended Field and Land Farm than in the Original Field, but were much higher in the Evaporation Pond, above $0.15 \text{ cm}^3/\text{cm}^3$ (Figure 2-1, bottom).

Variations in soil moisture by depth is shown in Figure 2-2. Control plots had low soil moisture near the surface but moisture content increased with depth, and was higher than in the Original Field, Extended Field, and Evaporation Pond at the 4.3-m depth (the 4.6-m depth is not plotted in Figure 3-2 because many of the ports did not extend to this depth). The Evaporation Pond had groundwater at a shallow depth, a condition that existed before irrigation began. These results suggest that some recharge of the aquifer takes place in the non-irrigated portion of the site due to infiltration of precipitation. Some recharge is also likely to take place in parts of the irrigated fields, especially the Evaporation Pond. Overall, however, an irrigation rate of 285 millimeters per year (mm/yr) as used in 2008 should stimulate plant growth and denitrification while minimizing leaching of contaminants to the aquifer.

Soil Moisture by Depth Combined 2007 - 2008 Data

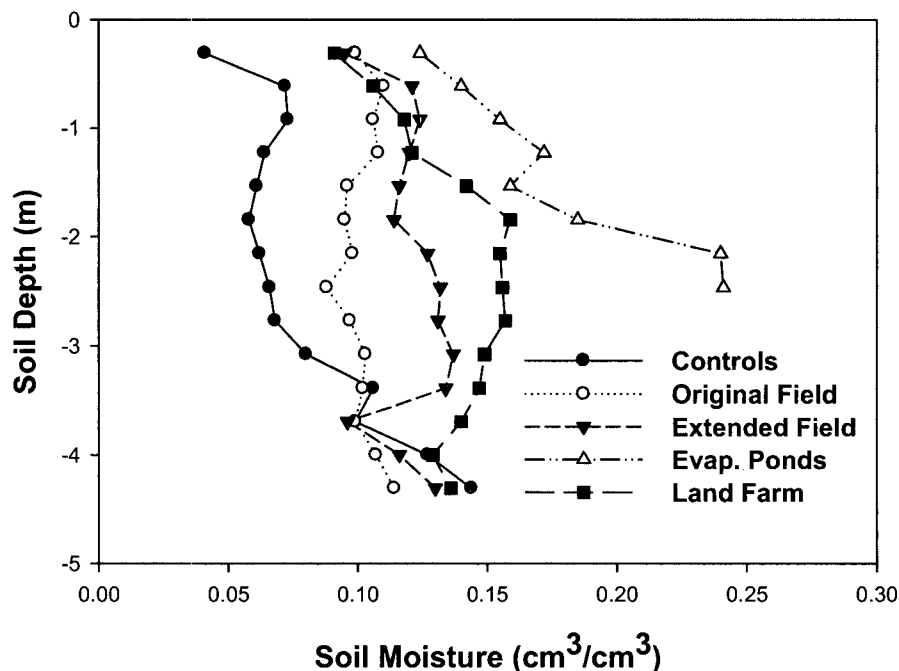


Figure 2-2. Soil moisture levels at different depths in the soil profile in Control plots and irrigated plots in the source area at the Monument Valley site. Results are averaged across ports at each site.

2.3 Percolation Flux Monitoring

WCRs and Water Fluxmeters (WFMs) were installed in 2006 at four locations within the subpile plantings for real-time monitoring of soil moisture profiles and percolation flux. The four WFMs were installed to monitor percolation of water below the root zone that could potentially leach contaminants. Instrument clusters were installed in the south-central area of the 1999 planting (WFM1) and in the northeast (WFM2), northwest (WFM3), and southeast (WFM4) areas of the 2006 planting. Instrument clusters consisted of one WFM placed about 370 cm deep in the soil profile with four WCRs placed above the WFM at 30–60, 90–120, 180–210, and 270–300-cm depths.

WCRs are designed to measure volumetric water content of soils and other porous media. The water content information is derived from the probe sensitivity to the dielectric constant of the medium surrounding the probe rods (Campbell Scientific, 2006). Because of apparent discrepancies in our in-house calibrations of WCRs, calibration coefficients derived in the Campbell Scientific soils laboratory were used to reduce 2008–2009 periodicity data:

$$\text{Water Content (\%vol)} = (-0.0663 - 0.0063 * \text{period} + 0.0007 * \text{period}^2) * 100$$

The WCR output is period, measured in microseconds. The result of the calibration equation is percent volumetric water content.

The WFMs were installed near the bottom of the root zone and are capable of directly monitoring saturated and unsaturated water fluxes ranging from 0.02 mm/yr to more than 1,000 mm/yr (Gee et al. 2002). Two WFMs were installed in March 2006; the other two were installed in July 2006.

The WFMs are passive wick lysimeters that monitor percolation flux from a soil-filled funnel (Gee et al., 2009). The soil captures flow from a predetermined area where it drains into the funnel neck occupied by a conductive material capable of applying a capillary pressure to the overlying soil. Water flux is measured directly by placing a water monitoring device (e.g., miniature tipping bucket or recording autosiphon) below the lower end of the wick (Figure 2–3).

The funnel neck is 2.5 cm in diameter and is filled with a fiberglass wick material that creates a hanging water column. The top 15 cm of the wick material was separated into single strands, which were used to line the interior of the funnel. To prevent soil from filtering through the funnel and the wick, a thin layer of diatomaceous earth was placed in the bottom of the funnel above the wick. Diatomaceous earth material is highly conductive and does not restrict flow within the WFM. The wick extended vertically below the soil-filled funnel.

The WFMs incorporate a method to control convergence or divergence of flow. The control tube consists of a plastic pipe, about the same diameter as the top end of the funnel and extends from the funnel top up to a height of 60 cm. The inside diameter of the control tube is 20 cm with corresponding surface area of 314 cm². The saturated hydraulic conductivity of the wick is extremely high and under normal flow conditions offers little resistance to the overall flow in the WFM.

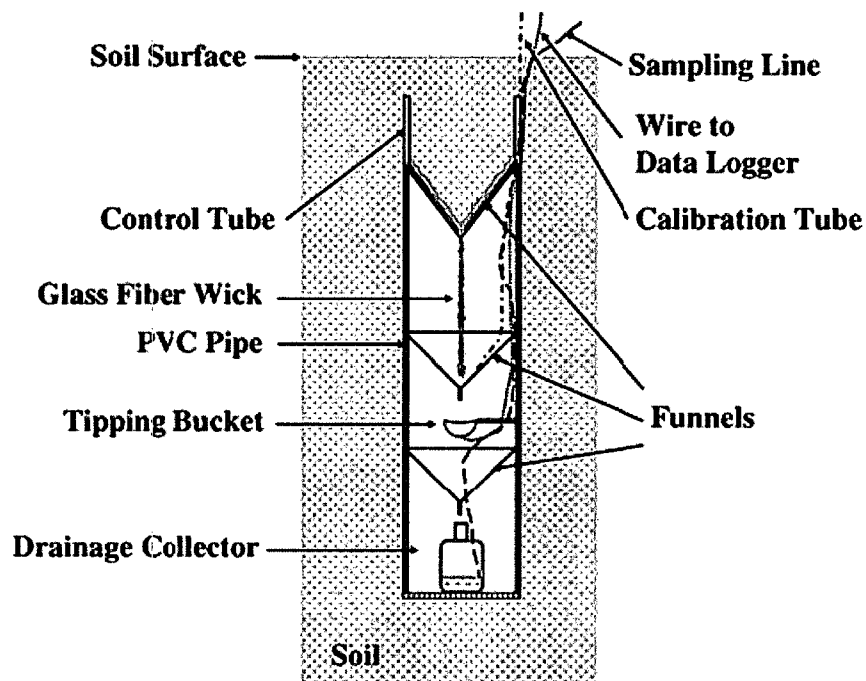


Figure 2-3. Schematic of a passive wick WFM (from Gee et al. 2009).

The four WFMs have recorded zero percolation since they were installed in March and July 2006. These results support the conclusion that infiltration from the combination of ambient precipitation and irrigation has been stored in the fine sand profile and is not percolating and leaching nitrate. In October 2008 and again in March 2009, water was injected in the WFM calibration tubes. All instruments recorded tips showing that all were functioning correctly and capable of recording percolation events should they occur.

Results from WCRs placed above WFMs show that soil volumetric water content is somewhat variable both spatially and temporally (Figure 2-4). Many patterns were expected. Seasonal fluctuations in water content are a response to meteorological conditions and the irrigation schedule. Seasonal fluctuations in water content deeper in the profiles lag fluctuations closer to the surface. Rapid wetting and drying is evident closer to the surface whereas changes in water content are more gradual producing smoother curves for WCRs located deeper in the profiles.

Water content was consistently higher at WFM1, a location with more mature plants in the 1999 planting. The deepest WCR at the WFM1 location has recorded yearly increases in water content since 2006, suggesting that deep percolation and leaching of nitrate is more likely there. WFM2 and WFM3, located in areas of the 2006 planting where shrubs have grown largest, have recorded yearly declines in water content at all depths, which is likely a response to increasing leaf area and evapotranspiration (ET). The lowest values occurred at the 270–300-cm depth in WMF3.

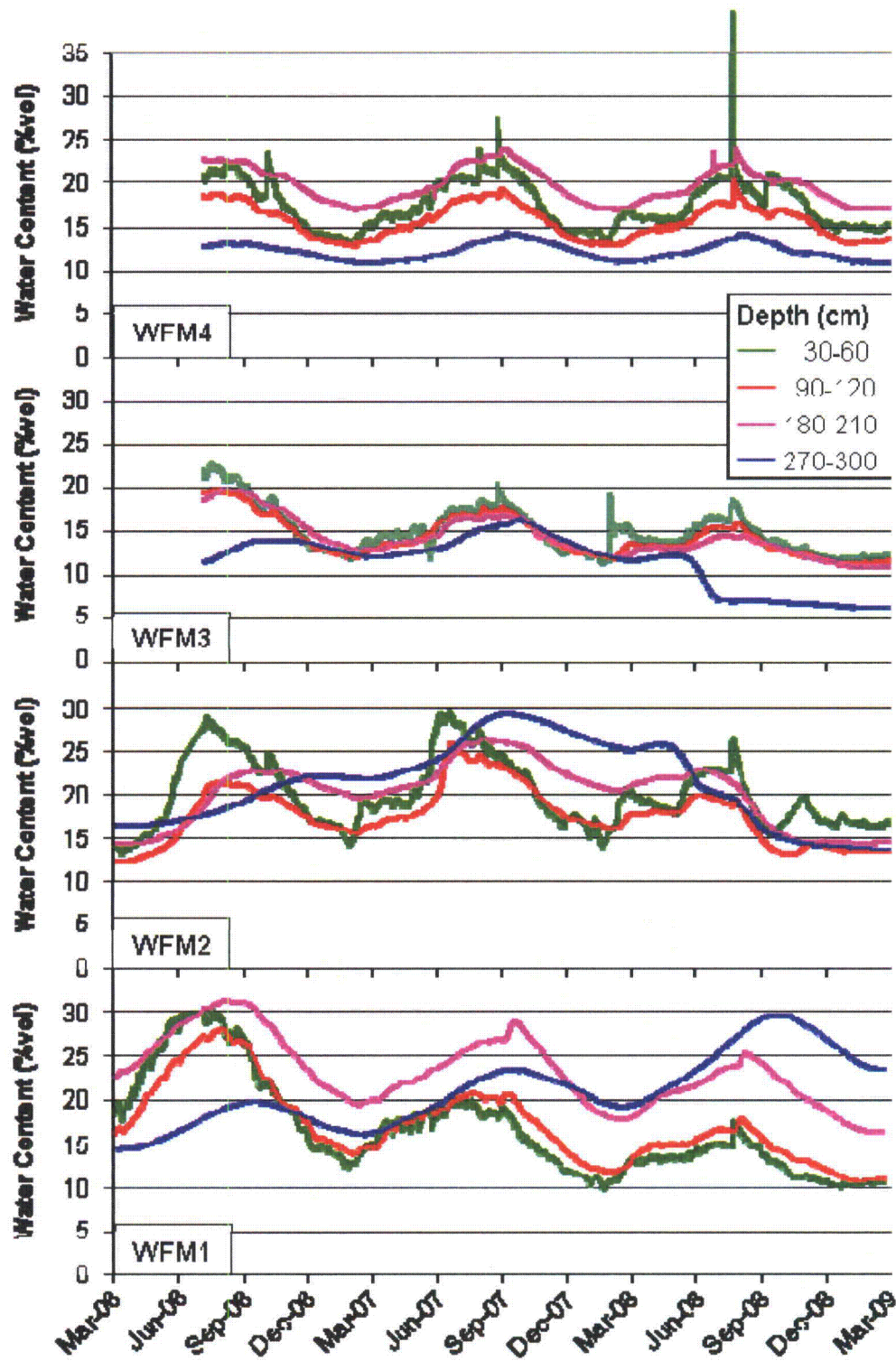


Figure 2-4. Hourly volumetric water content at four depths down to 300 cm monitored with WCRs at WFM Stations.

3.0 Soil Chemistry Monitoring

3.1 Source Area Nitrogen and Sulfur

Soil cores were collected in the Source Area soil from the 1999 planting (original field) and the 2006 planting (extended fields) in March, 2007 and May, 2008 and analyzed for nitrate-N, ammonium-N, and sulfate-S. Figure 3–1 shows mean soil nitrate and ammonium results from the original field for the period 2000–2008. Both nitrate and ammonium have decreased significantly ($P < 0.001$) since 2000. The decrease in nitrate appears to have slowed, as expected for a substrate-dependent, exponential decay process. On the other hand, ammonium levels are still decreasing. Nitrification (of ammonium) is a likely reason for the slow decrease in nitrate. Overall, total nitrogen has been reduced from 350 milligrams per kilogram (mg/kg) to 200 mg/kg.

**Nitrate and Ammonium in
Original Subpile Field**

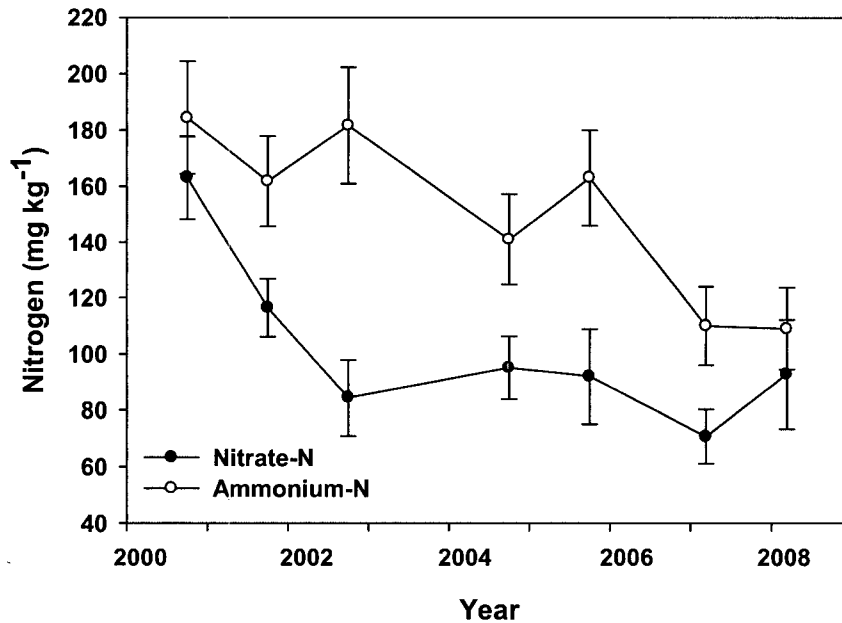


Figure 3–1. Nitrate and ammonium concentrations in the original source area field (1999 planting) from 2000 to 2008. Results are the analysis of 100 auger holes sampled at 3–5 soil depths at each sample interval. Error bars are standard errors of means. Data were analyzed by one-way analysis of variance with sample interval as the independent variable; both nitrate and ammonium have decreased ($P < 0.001$).

Soil samples taken throughout the original field in 2004 show that ^{15}N enrichment ($\delta^{15}\text{N}$) is linearly related to the log of nitrate and ammonium concentrations, and that slopes of enrichment curves are the same (Figure 3–2). This is evidence that loss of nitrogen is due to denitrification in the case of nitrate, and of nitrification followed by denitrification in the case of ammonium. Denitrification favors ^{14}N over ^{15}N , so residual nitrate in the soil becomes enriched in ^{15}N as nitrate becomes depleted.

$\delta^{15}\text{N}$ in Nitrate and Ammonium Samples from the Subpile Soil at Monument Valley

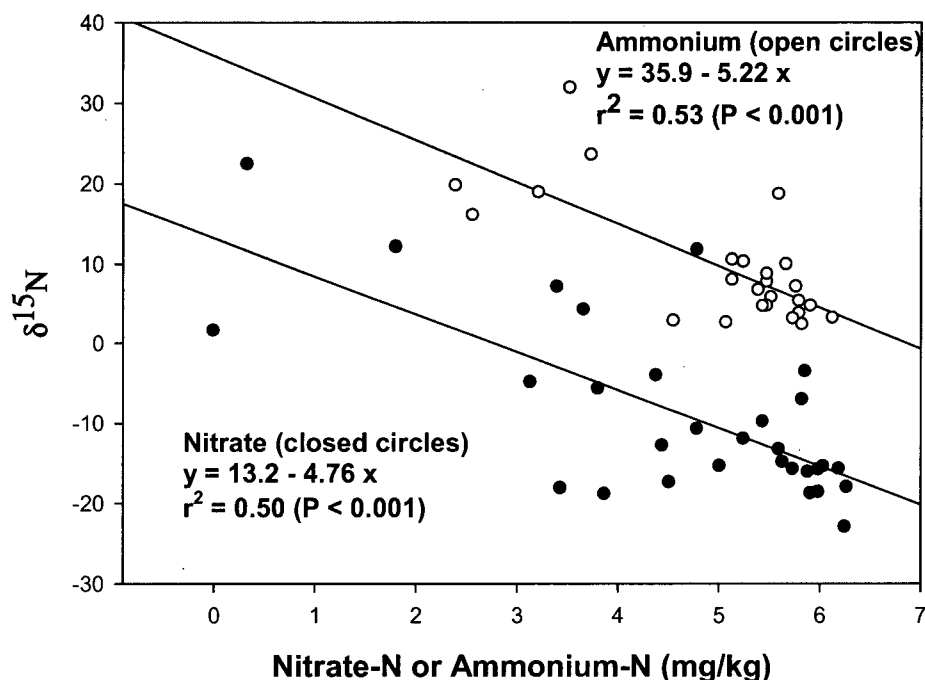
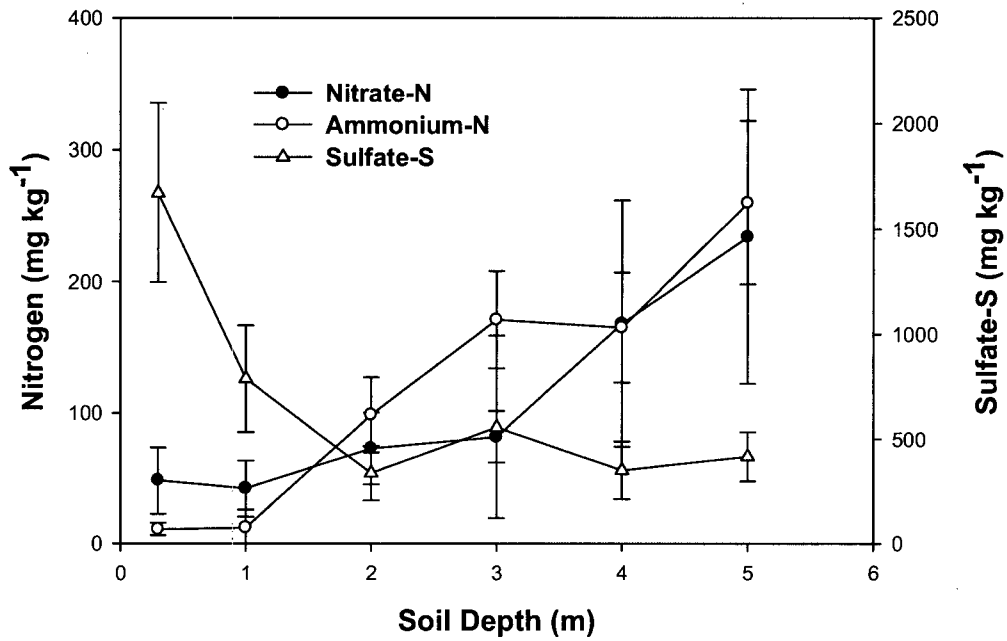


Figure 3–2. Regression of $\delta^{15}\text{N}$ on the natural log of nitrate and ammonium concentration in samples from the subpile soil taken in 2004. Samples were taken at different depths and locations in and out of irrigated areas to assure a wide range of concentration values. The results show significant ($P < 0.001$) increase in $\delta^{15}\text{N}$ values with decreasing concentrations, indicating that microbial processes are reducing the concentrations through production of nitrous oxide or nitrogen gas.

Figure 3–3 (top) shows the distribution of nitrate, ammonium and sulfate by depth in 2008, and Figure 3–3 (bottom) shows the distribution of nitrogen losses by depth from 2000 to 2008. Nitrate and ammonium both increase in concentration with soil depth, whereas sulfate is most concentrated at shallow depths. Most nitrate losses have come from the middle of the soil profile (peak at 3–m depth) whereas most ammonium losses have come from shallow soil depths (peak at 1 m). Nitrification of ammonium to nitrate is an oxidative process that is more likely to occur in shallow (aerated) soil, whereas denitrification is an anaerobic process more likely to occur in deeper, less aerated soil.

Figure 3–4 shows the distribution of nitrate, ammonium and sulfate in the original field by sampling location. The field is divided into four zones running east to west, and each zone is divided into 5 subzones running north to south. Data were averaged across soil depths. Ammonium (Figure 3–4A) and nitrate (Figure 3–4B) concentrations differed significantly by zone ($P < 0.001$), whereas sulfate did not differ significantly by zone or subzone ($P = 0.15$). Nitrate hotspots are now mainly in the eastern edge of the original field, whereas ammonium hotspots are still present throughout the original field.

Nitrate, Ammonium and Sulfate by Soil Depth, 2008



Loss of Nitrate and Ammonium by Soil Depth, 2000 - 2008

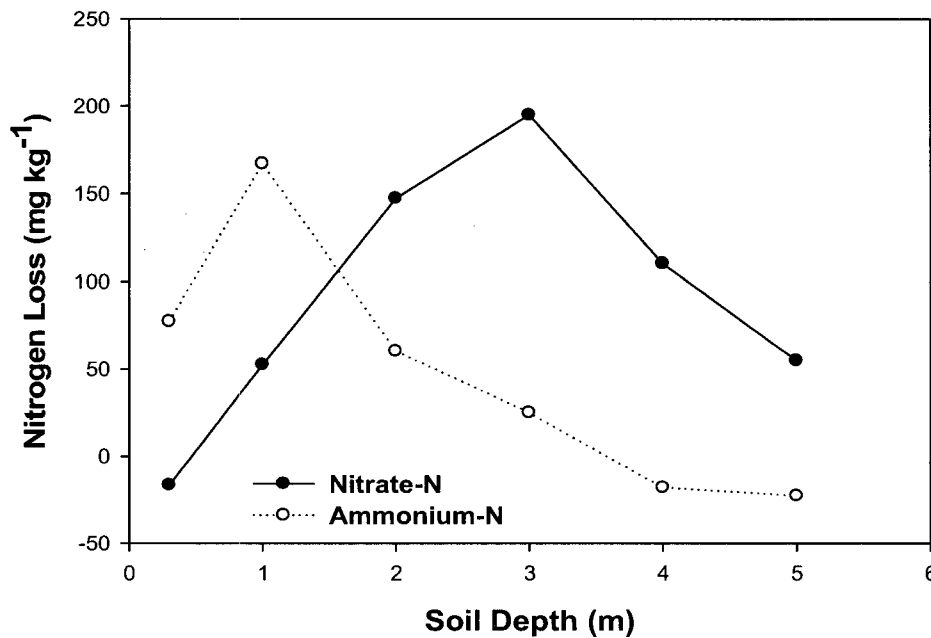


Figure 3-3. (Top) Mean and standard errors of nitrate, ammonium and sulfate concentrations in the original field in the subpile soil area in 2008. (Bottom) Reduction in nitrate and ammonium from 2000–2008 as a function of soil depth.

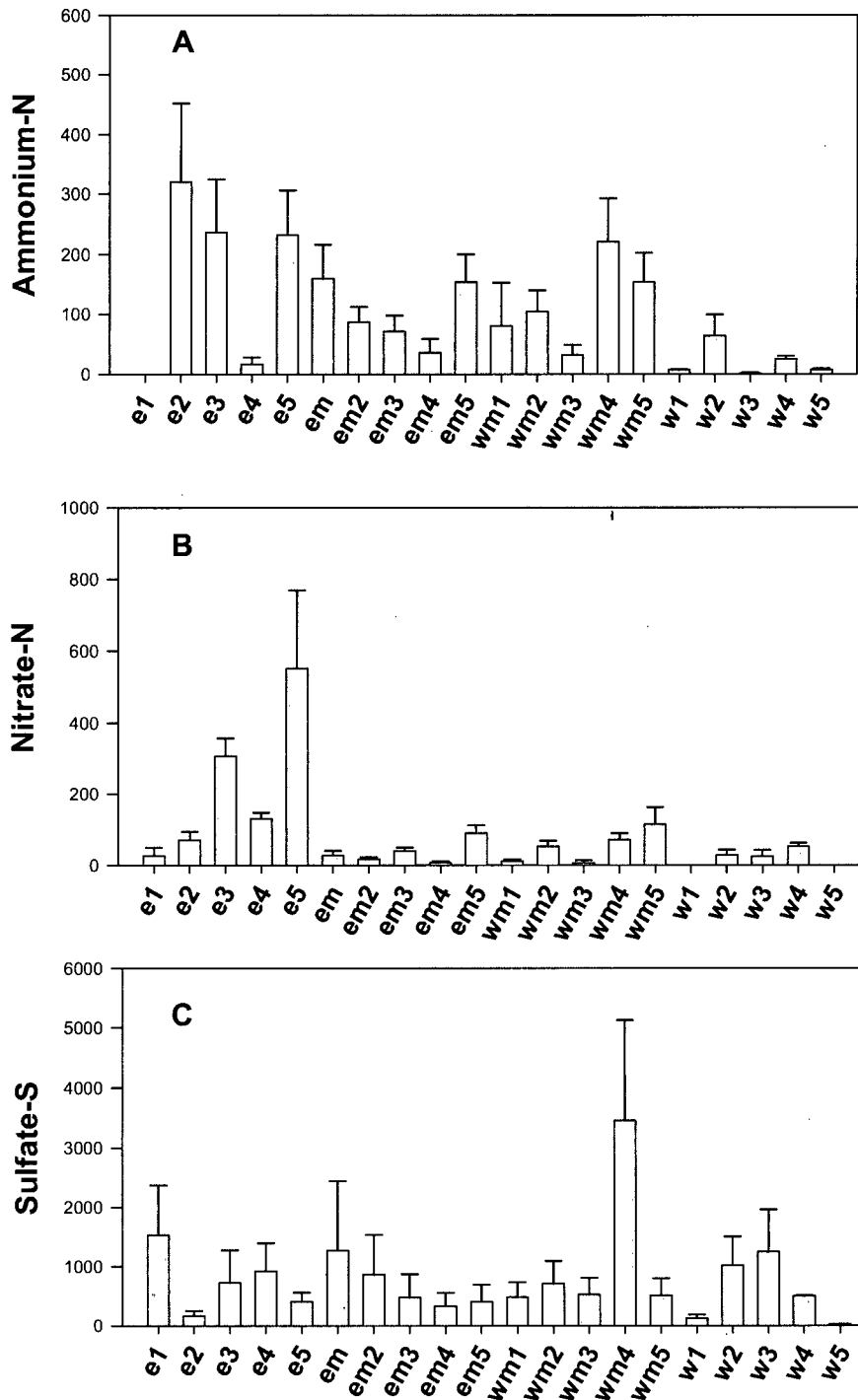


Figure 3-4. Distribution of ammonium (A), nitrate (B), and sulfate (C) in the original field of the source area in 2008 as a function of sampling location. The field was divided into four sections in the east-west direction: e = east; em = east middle; wm = west middle; and w = west. Each section was divided into five subzones in the north-south direction with 1 = northernmost subzone and 5 = southernmost subzone.

Nitrate and ammonium concentrations in the extended field and former evaporation ponds are shown in Figure 3–5. Nitrate and ammonium decreased between 2007 and 2008, but results were not significant ($P > 0.05$). The former evaporation ponds now have low levels of both nitrate and ammonium. The extend field areas still have elevated levels of both nitrate and ammonium.

Nitrate and Ammonium in 2006 Plantings, 2007 - 2008

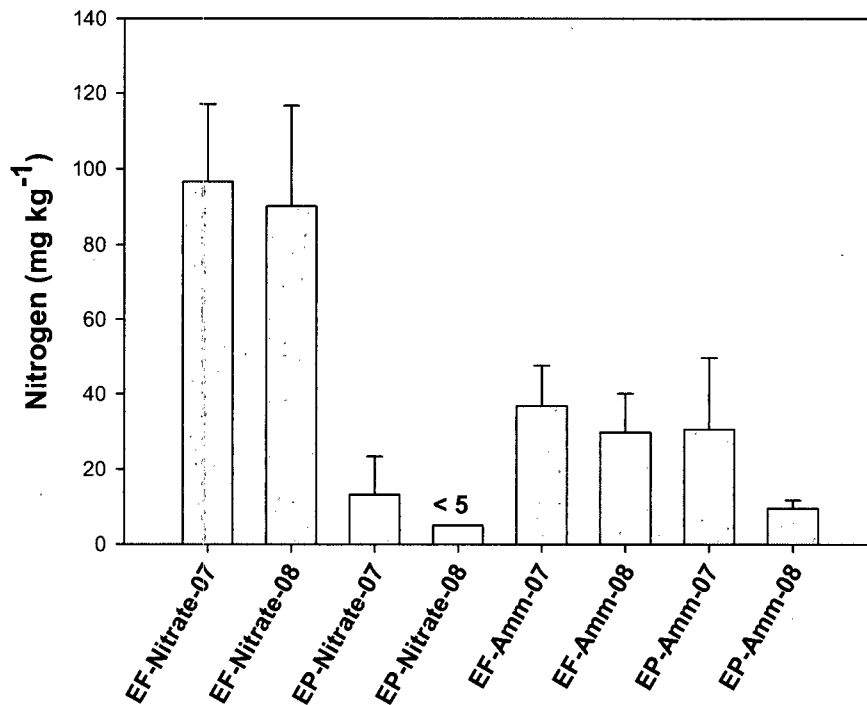


Figure 3–5. Distribution of nitrate and ammonium in the extended field (EF) and evaporation ponds (EP) in 2007 and 2008. Bars are means and standard errors. There were no significant differences ($P < 0.05$) in 2007 and 2008 means.

The results show that planting and irrigating of native shrubs has produced a marked reduction in both nitrate and ammonium in the source area over an eight year period. Microbial processes rather than plant uptake are responsible for nearly all of the nitrogen reduction. However, the plants contribute to the control of the site water balance, preventing leaching of nitrogen compounds into the aquifer (see Section 2.0).

3.2 Land Farm Nitrogen and Sulfur Sampling Design

3.2.1 Background

Land farming was selected as possible *active* remedy for the nitrate and sulfate plumes. Land farming will be considered only if the more passive alternatives are found to be inadequate. The farm would serve several functions: (1) extract nitrates in irrigation water pumped from the plume; (2) convert nitrates into useful plant biomass; (3) reduce sulfate levels in the alluvial aquifer, (4) minimize water infiltration and leaching of contaminants back into the aquifer; and

(5) enhance restoration of the disturbed ecosystem. Land farming consists of pumping the contaminated alluvial aquifer to irrigate and fertilize a farming operation on areas disturbed during the surface remediation. The land farm would produce a crop such as native plant seed for mine land reclamation. Pumping would continue until nitrate concentrations in the alluvial aquifer drop below the 44 milligrams per liter (mg/L) maximum concentration limit for nitrate.

The treatment structure for the land farm pilot study consisted of two main factors: (1) nitrate concentration in irrigation water supply and (2) crop species. There were four nitrate levels; no nitrate, 250 mg/L nitrate (a level not likely toxic to crop plants or to livestock feeding on the crop) 500 mg/L nitrate (a level not likely toxic to crops but possibly toxic to livestock) and 750 mg/L nitrate (a level possibly toxic to crops and livestock). The two crops are *Atriplex canescens* (ATCA) and *Sarcobatus vermiculatus* (SAVE).

The treatment structure has been altered several times due mainly to the low yield of water from well 649, the source of high nitrate water. Initially, plants in the control (or no nitrate) plots received 2 gallons of clean water per day. Plants in the 250-parts-per-million (ppm) nitrate plots were irrigated for 60 minutes with water from well 649 and 180 minutes with water from the DeChelley aquifer (non-contaminated water) to total 2 gallons per day. Plants in the 500-mg/L nitrate plots were irrigated for 180 minutes with contaminated water and 60 minutes with clean water. Plants in the 750-ppm plots received 2 gallons of contaminated water per day from well 649.

In 2007, we attempted to increase the irrigation volumes to 4 gallons per day to enhance plant growth. However, we found that well 649 was drawing down after 2 hours of operation making it impossible to supply enough high nitrate water to meet the treatment structure. Hence, the 250-ppm and 500-ppm treatments were switched to water from the DeChelley aquifer, and the four high-nitrate plots were the only ones receiving water from Well 649. Even with this modified design, the high nitrate plots received less water than the other plots due to the low yield of the well, and the 750-ppm plots had significantly lower soil moisture levels than the control plots. Nevertheless, ATCA plants on the 750-ppm treatment produced three times as much biomass as ATCA plants on the other treatments. Hence, the experiment showed that contrary to initial expectations, high nitrate levels did not inhibit plant growth. In fact, it stimulated growth by providing nitrogen, indicating that direct irrigation of ATCA with water from the plume hotspot would be feasible. SAVE plants were difficult to establish due to very slow initial growth and damage by rabbits. No treatment effects were evident in 2007.

3.2.2 Sampling Protocol for 2009

Both ATCA and SAVE plants are now well established in the plots and have grown sufficiently that the experiment can be terminated and analyzed. Soil and plant tissue samples are needed to answer the two other questions regarding irrigating with high nitrate water:

- Will nitrate and sulfate accumulate in the soil profile?
- Will tissue levels of nitrate and sulfate be acceptable for livestock?

We recommend sampling according to the original experimental design. Even though the treatment structure was altered, the two intermediate treatment levels did receive some nitrate supplementation during the initial year of irrigation, so treatment effects might remain.

Since the individual plots are the experimental units for analysis, we recommend taking multiple plant tissue samples within each plot, then pooling them by plot for analyses. Branches from five randomly selected ATCA and SAVE plants in each plot will be clipped and bagged. Plant samples will be dried in a solar drier at the Environmental Research Laboratory in Tucson. Samples will then be separated into stems and leaves by hand-sorting. One composite leaf sample and one composite stem sample will be prepared for ATCA and SAVE plants from the materials harvested for each plot. These will be analyzed by Carbon-Nitrogen-Sulfur (CNS) analyzer for carbon, total nitrogen, and total sulfur. Nitrate will be determined in aqueous extracts from leaves and stems by colorimetry (Hach Cadmium Reduction Method). One soil core will be taken from each plot and sampled at 1-foot [ft], 3-ft, 5-ft, 7-ft, 9-ft and 12-ft depths. Samples will be dried in a solar drier then submitted for analysis of total nitrogen, total sulfur and nitrate, using aqueous extracts analyzed as for plant tissues. Sampling will be conducted in October 2009.

Levels of nitrogen, sulfur, and nitrate will be compared in soils and tissues by two-way analysis of variance with nitrate treatment and plant type as categorical variables. Tissue nitrate and sulfur levels will be compared to recommended limits for ingestion by livestock. Based on the results, the overall feasibility of land farming for remediation of nitrates in the plume hotspot will be evaluated.

3.3 Root Distribution in the Source Area Plantings

3.3.1 Need for Direct Estimation of Root Depth

ATCA and SAVE are both deep-rooted phreatophytes. We previously found that ATCA and SAVE plants over the plume were extracting water from deep in the vadose zone and from the top of the aquifer at soil depths of 9–13 m. However, ATCA is a facultative phreatophyte, capable of forming an extensive shallow root system to capture shallow soil water from rainfall events (and from irrigation) as well as deep roots to tap groundwater, when available. The irrigated plantings in the source area are deficit irrigated (irrigated with less water than they could use based on potential ET), and bedrock is encountered at 3–5 m. An alluvial aquifer occurs at a depth of about 4 m on the far eastern end of the plots. It is important to determine the rooting depths of ATCA and SAVE in the source area to determine how roots are distributed relative to the wetting pattern induced by irrigation. Rooting depth determines how deeply plants can be safely irrigated without causing leaching of water past the root zone. Rooting depth might also influence the distribution of denitrification within the soil profile, as the carbon deposited by root growth could stimulate microbial denitrification. Previous field and laboratory assays showed that denitrification is carbon limited in source area soils.

3.3.2 Sampling and Analysis Protocol

In April 2009, soil cores were collected to determine root biomass in the original field and in the extended fields. One core was collected from the West, three from West Middle, four from East Middle and four from East plots in the original field. One core was collected from Extended Field West, four were collected from Extended Field South, and three were collected from the Extended Field North. Of the 20 samples collected, half were directly underneath plant canopies and half were in bare soil between canopies. Soil samples were collected at 0.3-m, 1-m, 2-m, 3-m, 4-m and 5-m soil depths where possible. Depth to bedrock was determined at each auger site.

Figures 3–6 and 3–7 show the auguring procedure. Figure 3–7 shows that extensive roots were present in canopies at the 1-ft soil depth, but these became less obvious with increasing soil depth. The soil samples were returned fresh in sealed plastic bags to the Environmental Research Laboratory. Presence of roots in samples will be scored by direct examination of soils under a dissecting microscope and by a flotation method (Al-Khafaf et al. 1977), in which roots soil samples are placed in a saturated NaCl solution, which allows roots and other organic materials to float to the top. They can then be collected, sorted, and weighed to determine root biomass per kilogram of soil.

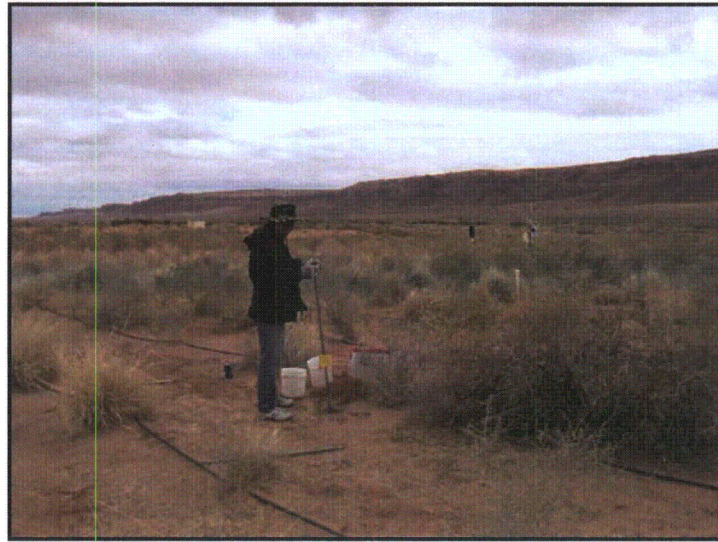


Figure 3–6. Auguring for collection of soil samples. Half the samples were taken underneath canopies and half in the space between canopies (shown).

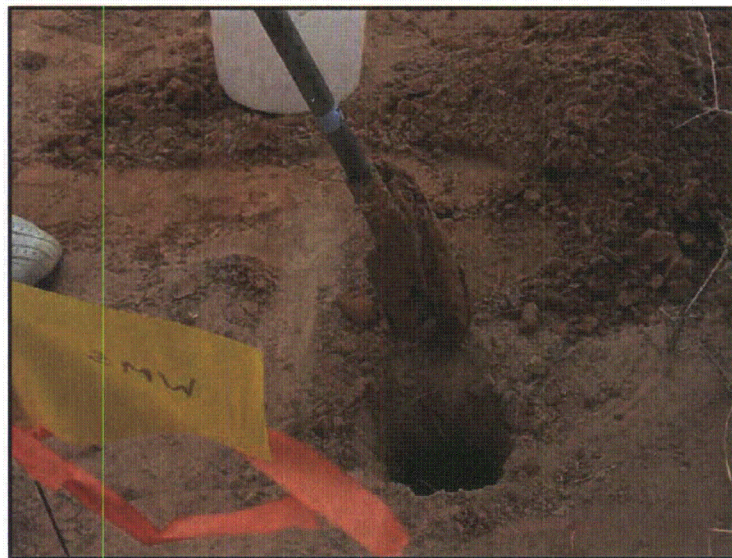


Figure 3–7. Top of the auger hole shown in Figure 3–6. Note the roots in the soil even though this sample was taken between shrub canopies.

3.4 Manganese Toxicity Investigation

3.4.1 Background

The subpile soil has elevated levels of calcium (Ca) and iron (Fe) in places and exhibits stained areas (which appear white on aerial photographs but have several other color phases including black, red, green, and pink when examined on the ground). Parts of the field also have a shallow layer of black mottled material below the soil surface, which is associated with areas of stunted plant growth. The Soil, Water and Plant Analysis Laboratory at the University of Arizona identified Manganese (Mn) nodules (Fe and Mn precipitates) in samples from the mottled soil areas. They hypothesized that oxides of Mn at different oxidation states were deposited in the soil during extraction of yellowcake at the site. These different oxidation states could be responsible for the "rainbow" appearance of colors around drip emitters in the stained areas, and especially in the former evaporation pond. Dr. Janick F. Artiola conducted further analyses to determine if Mn might present a health risk at the site.

3.4.2 Manganese Chemistry

Mn is a relatively abundant element in soils (600 mg/kg), ranging from 20–3,000 mg/kg. The chemistry of Mn in soils is very complex because it can have three possible oxidation states (II, III, IV) within the pH-redox range of most soil systems (Lindsay 1979). Many Mn complexes are colored. The most reduced forms (Mn II), like Alabandite (natural MnS (Mn II), found in Arizona, are dark brown with green streaks. Because reduced forms of Mn tend to be more soluble in water they can form secondary minerals such as: oxides, hydroxides and carbonates in the soil, examples include; carbonates like rhodochrosite (pink) and ankerite (dark gray), pyrochroite ($\text{Mn}(\text{OH})_2$) (dark gray), and Mn sulfates, such as MnSO_4 which is reddish-pink in color. As Mn oxidizes, it can also react with sulfates with green colors, for example $\text{Mn}_2(\text{SO}_4)_3$. Eventually Mn oxidizes and forms the most stable forms (least soluble) of Mn(IV) like pyrolusite (beta- MnO_2), and manganite (MnOOH)(III) (gray or brown with reddish or black streak). Other stable forms are psilomalane, $\text{BaMnMn}_8\text{O}_{16}(\text{OH})_4$ formed by weathering of carbonates and silicates, found in A; others are Mn-rich veins of limestones, which are opaque black, forming crusts and stalactites and filling cavities.

3.4.3 Presence and Formation Iron-Manganese Concretions

The formation or dissolution of Mn nodules is typically associated and has been mostly studied in marine environments. But soils with significant redox fluctuations can also have and actively form Mn nodules and concretions. Mn concretions, initially erroneously classified as nodules (approximately 1–3 mm in diameter), have been shown to be present in Monument Valley soils.

Water soluble (likely reduced) forms of Mn have been observed at the site as rainbow-like rings around drip irrigation emitters. Since this site is under irrigation and revegetation, these recent events may be significantly altering the redox reactions of Mn (usually facilitated via wet/dry cycles). Although not proven, the presence of colored bands near dry nozzles may indicate the presence of some soluble and redox-active Mn species that could either co-precipitate or dissolve in response to soil-water redox changes. One possible scenario may be the recent induced change from less oxidized and more mobile forms of Mn to more oxidized Mn species and less soluble Mn species due to increased biological activity (irrigation, plant rhizoidal-microbial activity).

Fifteen surface soils samples were analyzed for total and water-soluble Mn and total Fe to establish the presence of these concretion forming factors. Additionally, several dark concretions were gathered, homogenized, acid-digested, and analyzed for total Mn and Fe. See Table 3-1.

Table 3-1. Manganese and Iron Soil Chemical Data

Color	Concretions	Site Sample ID	Total Mn (µg/g)	H2O-Sol-Mn (µg/g)	Total Fe (µg/g)
Dark red	HBC	MV EM 4-9	133.97	0.094	4,294
Dark red	LBC	MV EM 2-1	21.62	0.634	3,974
Medium red	LBC	MV EM 4-6	9.32	0.006	4,620
Dark red	LBC	MV E 4-1	89.50	0.120	4,418
Medium red	LBC	MV W 3-6	47.82	0.714	3,508
Dark red	MBC	MV E 4-15	283.50	0.334	4,722
Medium red	MBC	MV EFW 2-1	114.21	0.230	2,837
Medium red	MBC	MV EFW 3-1	170.00	0.036	3,486
Light red	MBC	MV WM 2-1	293.04	0.026	3,414
Dark red	NC	MV E 1-3	111.40	0.022	3,937
Dark red	NC	MV E 5-1	220.01	0.012	4,467
Medium red	NC	MV EM 3-12	5.59	0.038	4,587
Dark red	NC	MV E 1-2	7.70	0.028	3,988
Light red	NC	MV E 2-6	121.92	0.036	3,851
Medium red	VLBC	MV W 1-3	583.57	0.016	3,206
		Average	148	0.16	3,950
		%CV	104	147	14
Concretions Analysis					
			Total Mn	Total Fe	
HBC = heavy black concretions			(µg/g)	(µg/g)	
LBC = light black concretions			2,808	3,076	
MBC = medium black concretions					
NC = no visible concretions					
VLBC = very light black concretions					

µg/g = micrograms per gram
 MV = Monument Valley
 CV = coefficient of variation

We observe from the analysis of the pure concretions that the amounts of Mn and Fe are very similar, suggesting that these dark concretions are in fact soil particles or aggregates enriched with Mn. The total iron content in these concretions shows an approximate 20 percent reduction (by mass) in Fe suggesting, as one would expect, that these concretions are likely more dense than soil aggregates due to the precipitation of Mn oxides. The data shows that on average these concretions are nearly 20 times richer in Mn than the surrounding soil. Also, the total and soluble Mn (%CV = 104 and 147, respectively) soil concentrations are much more variable than the total Fe concentrations (%CV= 14). This suggests that Mn is or has in the past been mobilized and localized within this soil system. The uneven numbers of concretions in these 15 soil samples was clearly observed, ranging from “no visible concretions”, to “heavy, black concretions” (see Table 3-1), suggesting that these Mn-rich sites are highly spatially variable in these soils.

The observed variability in soluble Mn also supports the digenesis process of these Mn-rich concretions. Although the measured soil soluble Mn concentrations are very small (< 1mg/kg), their high variability (among the 15 soil samples) suggest that some soluble forms of Mn still remain in these soils. This, together with anecdotal evidence that the rainbow rings are diminishing with each irrigation event, suggests that the onset of regular irrigation events mobilized significant amounts of soluble forms of Mn. However, with time (wet-dry cycles), soluble Mn is rapidly coalescing (precipitating) into stable Mn oxides, forming Mn-rich concretions. The mobilization of Mn at this site likely occurred during the leaching of uranium-rich minerals with acid, as described in the last section.

3.4.4 Manganese Abundance at the Site

The results shown in the table above suggest that the range and average concentration of Mn in soils at the site is well within normal soil values. Total Mn averages 148 mg/kg with a maximum of 583.6 mg/kg. These levels are below the soil average of 600 mg/kg (range of 20–3,000 mg/kg) reported in Section 3.4.2, “Manganese Chemistry”. Although not modeled, soluble Mn concentrations, likely above those expected in soil-water extracts with stable Mn species in well-aerated, alkaline soils, might occur on site. Six of the 15 soil samples showed soluble Mn values above 0.05 mg/kg, suggesting the presence of some reduced, soluble forms of Mn oxides and carbonates like pyrochroite and rhodochrosite or even residual Mn sulfates that are not stable in soil systems. With more wet-dry cycles it is expected that these forms of Mn will be converted to oxidized, very stable and insoluble forms of Mn such as pyrolusite.

3.4.5 Origin of Reduced Soluble Manganese at the Site

Manganese reduction and leaching in soils with low pH (high acidity) and saturated conditions is well documented in the literature of wetland and hydric soils (Schwermann and Fanning 1976, Zhang and Karathanasis 1997). Fuller and Warrick (1985) document the effects of strong acid leachates (such as 2N sulfuric acid) through soils. Among the many elements leached by strong sulfuric acid solutions, Mn stands out, generating huge pulses (thousands of ppm) within the first pore volumes of column fluent. During these laboratory studies, changes in the color of the acidic fluents were observed, ranging from faded pink and green to brown. This sequential “rainbow effect” indicated the progressive leaching of several Mn species found in soils.

Uranium processing included the use of sulfuric acid solutions passed through leached bed to mobilize uranium ions. It stands to reason under these extreme conditions (low pH, reduced and anaerobic soil) that naturally occurring Mn also leached and was translocated within the vadose zone of the site. The most likely forms of Mn at the site were/are sulfate-containing species since this is the most prevalent anion at the site. Since this site/location is very dry, it is also likely that soluble (reduced) forms of Mn were formed during the period of operations. But upon decommissioning the site, dry conditions set in, precluding the re-oxidation of Mn to much more stable and common forms (at least surface soils) of Mn such as pyrolusite. However, since the site is now being irrigated as part of the revegetation strategy, oxidation (at least in the unsaturated zone) of Mn is likely occurring, leading to more stable forms over time. This process may be responsible for the formation of nucleation sites that form dark brown concretions rich in Mn and the rainbow rings around drip nozzles that have been observed on irrigation soils at this site.

3.4.6 Conclusions and Recommendations

The levels of Mn are within values for normal soils, and well below any levels of concern for human health risks. Therefore, we do not recommend further testing or remediation at the site. The irrigation practices and natural attenuation processes will continue to convert the soluble forms of Mn into insoluble oxides normally present in soils.

4.0 Summary of Interrelationships of NH_4 , NO_3 , SO_4 , and Moisture Content

Contamination of groundwater by nitrate, ammonium, and sulfate are the major concerns for remediation of the Monument Valley site, and there is great interest in the impact of natural attenuation on risk and management of groundwater contaminant plumes. Transport and fate processes that influence ammonium, nitrate, and sulfate concentrations were evaluated, and a full report is attached as Appendix C. A manuscript comparing nitrate attenuation characterization methods developed for Monument Valley was submitted to the *Journal of Hydrology* (Appendix D).

Spatial and temporal concentration data collected from a transect of monitoring wells located along the plume centerline were analyzed to evaluate the overall rates of natural attenuation. The results indicate that nitrate, ammonium, and sulfate concentrations are decreasing due to natural attenuation processes. Adsorption appears to partly control the transport and fate of ammonium in the plume. Sulfate concentrations are most likely controlled by equilibrium formation/dissolution of the solid mineral phase gypsum. Naturally formed gypsum lenses are already found in soils at the site. Excess Ca ions in the soil react with sulfate in the source area and contamination plume to produce gypsum deposits, which are relatively immobile.

As documented in Section 3.1, ammonium has decreased in the irrigated subpile soils in the source area through microbial processes (nitrification followed by denitrification). Ammonium biotransformation to nitrate (i.e., nitrification) may also be occurring in the upgradient part of the plume. Nitrate biotransformation occurs through reduction to atmospheric nitrogen gas (i.e., denitrification) in both the irrigated subpile soils and the downgradient region of the plume.

The occurrence and rate of denitrification was evaluated through microcosm experiments, nitrogen isotopic fractionation analysis, and solute transport modeling. First-order rate coefficients calculated with each method were comparable. The composite natural attenuation rate coefficient was slightly larger but similar to the denitrification rate coefficient, which suggests that microbially induced decay primarily controls nitrate attenuation at the site. Sulfate reductive biotransformation was not evident from the available data.

Overall, approximately half of the nitrate and ammonium originally present in the source area has been remediated since 1999 through planting and irrigating of native shrubs, and an estimated 30–70 percent of nitrate in the plume has been lost through natural denitrification since the mill was closed in 1968. Estimates of sulfate losses through gypsum formation are not yet available, but eventually an equilibrium level is expected to be established at the solubility of calcium sulfate (Ca 2,000 mg/L) in the hotspots of the plume, and lower where the plume has been diluted.

This page intentionally left blank

5.0 Vegetation Monitoring: Plume Grazing Enclosures

In 2005, two grazing enclosure plots (north and south) were constructed at the site. Previous studies of these and earlier enclosures demonstrated that grazing protection may have positive effects on biomass productivity, ground cover, and rates of phreatophyte transpiration and nitrogen uptake (McKeon et al. 2006; Glenn et al. 2008). Vegetation canopy cover and shrub density were sampled in the two enclosure plots and adjacent control plots not protected from grazing in 2007 and 2008. The purpose of the study is to better understand how grazing protection may change plant community composition and phreatophyte shrub abundance over several years.

A relevé sampling protocol was performed (Bonham 1989) within each enclosure plot and within each control area to generally characterize the vegetation cover. The most common species in all areas were four-wing saltbush (*Atriplex canescens*) and Russian thistle (*Salsola tragus*). A greater number of species were found inside both enclosure plots than in their respective outside control areas. Greasewood (*Sarcobatus vermiculatus*), shadscale (*Atriplex confertifolia*), suaeda (*Suaeda torreyana*), and broom snakeweed (*Gutierrezia sarothrae*) were found both inside and outside the south plot but not the north. Resinbush (*Vancoveria stylosa*), purple sage (*Poliomintha incana*), and threadstem sandmat (*Chamaesyce revoluta*) were found both inside and outside the north plot, but not the south. Differences in depth to groundwater probably contribute to observed differences in species composition between the north and south.

Line transects were used to quantify differences in plant canopy cover. Twenty 5-m transects were randomly placed within each native grazing enclosure and equal-sized control area. The cover types directly under points at 1-decimeter intervals on each transect tape were recorded. T-tests were used to compare means and identify statistically significant differences. Results of the 2008 transect samples are summarized in Table 5-1.

Phreatophyte shrub cover and total vegetative cover are significantly higher in the south grazing enclosure than its control area ($p < .0005$). The north enclosure showed no statistically significant trends for phreatophyte shrub cover, but in 2008, vegetative cover was actually higher in the control than in the enclosure ($p < .005$), mainly the result of higher cover of resinbush and Russian thistle. In 2007, the north enclosure experienced grazing pressure when the fence was damaged, allowing prolonged entry of livestock. Therefore, the South Plot may represent the effect of grazing enclosures after three growing seasons better than the North Plot, which is more equivalent to one growing season.

Vegetative cover has not changed significantly between 2007 and 2008 except that higher cover of some forb species (e.g. herb sophia [*Descurainia sophia*] and Russian thistle) was observed in 2008. This is most likely because sampling occurred in early September in 2008 but later in the year (early November) in 2007, when many such annuals had already died back. Also, the cover of resinbush, Russian thistle, and four-wing saltbush increased outside the north enclosure increased relative to inside in 2008. Comparison to future trends in this area may help explain this trend.

Table 5–1. Vegetation Cover Inside and Outside Grazing Exclosure Plots

Cover Type	Native South Inside	Native South Outside	Native North Inside	Native North Outside
<i>Atriplex canescens</i>	14.5	0.7	11.9	13.8
<i>Sarcobatus vermiculatus</i>	8.8	5.3	-	-
Total phreatophyte shrubs	23.3	6.0	11.9	13.8
<i>Ephedra viridis</i>	-	-	0.2	-
<i>Gutierrezia sarothrae</i>	-	0.7	-	-
<i>Poliomintha incana</i>	-	-	3.1	0.4
<i>Vancleavea stylosa</i>	-	-	1.3	8.0
<i>Yucca angustifolia</i>	-	-	-	0.6
Total non-phreatophyte shrubs	0.0	0.7	4.6	9.0
<i>Ambrosia acanthicarpa</i>	-	0.9	1.5	1.4
<i>Chamaesyce revoluta</i>	-	-	1.0	0.1
<i>Chenopodium</i> sp.	-	-	0.9	0.2
<i>Descurainia sophia</i>	-	-	0.1	-
<i>Salsola tragus</i>	15.7	10.5	4.1	7.4
<i>Suaeda torreyana</i>	1.6	0.2	0.0	-
Total forbs	17.3	11.6	7.6	9.1
<i>Sporobolus cryptandrus</i>	-	-	0.4	-
Total grasses	0.0	0.0	0.4	0.0
Plant litter	11.7	9.2	15.0	13.7
Bare ground	47.7	72.5	60.5	55.0
Total vegetative cover	40.6	18.3	24.5	31.3

To estimate shrub density, the distance from each sampling point to the nearest phreatophyte shrub of a given species was recorded (point-to-plant distance) as well as the distance between that shrub and its nearest conspecific neighbor (plant-to-plant distance). Density was calculated for each species using (1) closest individual method, (2) nearest neighbor method, and (3) a combined method, summarized in the 2007 report (DOE 2007). The combined method is considered to be more accurate than the other methods. Results of the density calculations are presented in Table 5–2. Size and age classes of shrubs were not measured in 2008.

Table 5–2. Shrub Density Inside and Outside Grazing Exclosure Plots

Area	Closest Individual	Nearest Neighbor	Combined Method
Native South Inside	329.08	285.33	476.43
Native South Outside	252.22	378.60	292.32
Native North Inside	1,106.85	1,394.76	804.79
Native North Outside	523.45	959.16	490.15

The average density of shrubs was higher inside the grazing exclosures than outside (641 inside vs. 391 outside, combined method). The density of shrubs in the north plots was higher than the density in the south (647 in the north vs. 384 in the south, combined method).

Shrub density changed substantially between 2007 and 2008 (Figure 5–1). In 2007, density was higher outside the exclosures, but in 2008, density was higher inside. Shrub density dropped drastically outside the north enclosure in 2008. In 2007, approximately 85 percent of the shrubs in the control area outside the north enclosure were characterized as “small” (young shrubs); approximately 77 percent of the shrubs inside the north enclosure were small. It is probable that grazing pressure was responsible for the substantial drop in shrub density outside.

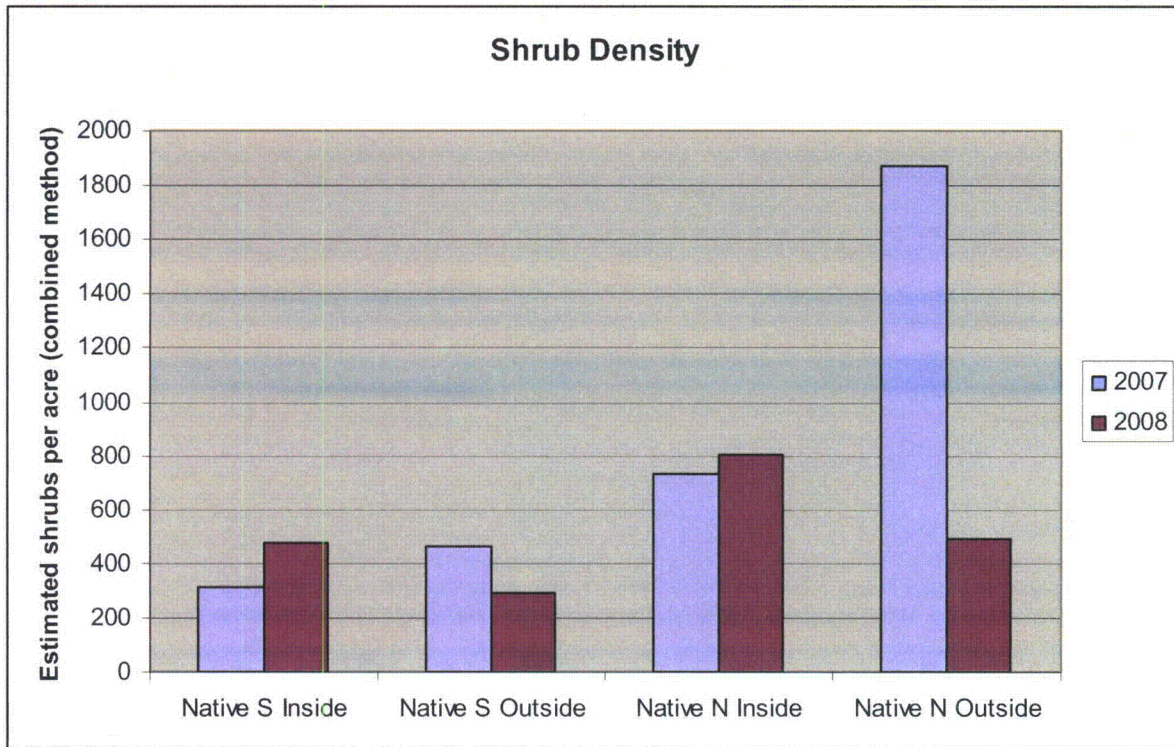


Figure 5–1. Comparison of Shrub Density Estimates (Combined Method), 2007 to 2008

This page intentionally left blank

6.0 Monitoring Vegetation Status and Evapotranspiration Using Ground-Calibrated Remote Sensing Methods

Phreatophytic shrub populations at Monument Valley will play a continuing role in controlling movement of the groundwater nitrate plume and also in limiting soil percolation in the source area of the plume. This section presents an unobtrusive method for evaluating changes in phreatophytic shrub populations based on remote sensing technologies. The approach developed for Monument Valley was published in the journal *Ecohydrology* (Appendix E). These methods may result in reduced long-term surveillance and maintenance costs at Monument Valley and also may be applicable at other Legacy Management sites. The following sections discuss the need for vegetation monitoring and how ground data can be combined with high-resolution and low-resolution imagery to monitor ET, leaf area index (LAI), and fractional cover.

6.1 Background and Rationale for Remote Sensing Methods

The Monument Valley site will require long-term monitoring of vegetation cover and ET, especially if lengthy *in situ* (rather than pump and treat) technologies are selected as mitigation strategies. Vegetation abundance over the source area helps determine the extent of recharge of water from the source area and from surrounding uplands into the plume, because water used by vegetation decreases the amount that can migrate into the aquifer. Vegetation abundance over the plume helps determine the rate of plume migration away from the site, because water used by vegetation decreases the amount available to expand the volume of the plume over time.

The dominant vegetation over both the source area and plume is a mixed ATCA, *Atriplex confertifolia*, and SAVE phreatophyte shrub community. Direct measurements of transpiration by ATCA and SAVE over the plume in 2006 and 2007 indicated that individual shrubs have relatively high rates of water use on a leaf-area and canopy-area basis. Estimated ET rates from dense stands of plants approached the rate of potential ET for this location. On an area basis, dense stands had annual ET rates several times higher than the annual precipitation, indicating that they were extracting water from the plume and source area and could contribute greatly to controlling the site water balance.

Currently, relatively heavy grazing is practiced at the site, and shrub cover is only about 9–10 percent over most of the plume. Annual ET over the plume is approximately equal to annual precipitation. However, exclosure studies have shown that the ground cover could conceivably be increased to 25 percent through controlled grazing. A small change in annual ET over the plume through enhanced vegetation abundance could tip the water balance from recharge to discharge. Conversely, increased grazing pressure or loss of vegetation through climate change could tip the balance towards recharge, leading to further migration of the plume away from the source area. We estimated that an increase of just 30 mm/yr in annual ET over the plume could tip the water balance of the aquifer from recharge to discharge.

6.2 Remote Sensing Products

The protocol developed for Monument Valley uses annual, high resolution (0.5 m) Quickbird imagery (DigitalGlobe, Inc., Longmont, CO) and 16-day composite low-resolution (250 m) imagery from the Moderate Resolution Imaging Spectrometer (MODIS) sensors on NASA's Terra satellite (Figure 6–1, top). Both sources of images are supplied as geometrically and

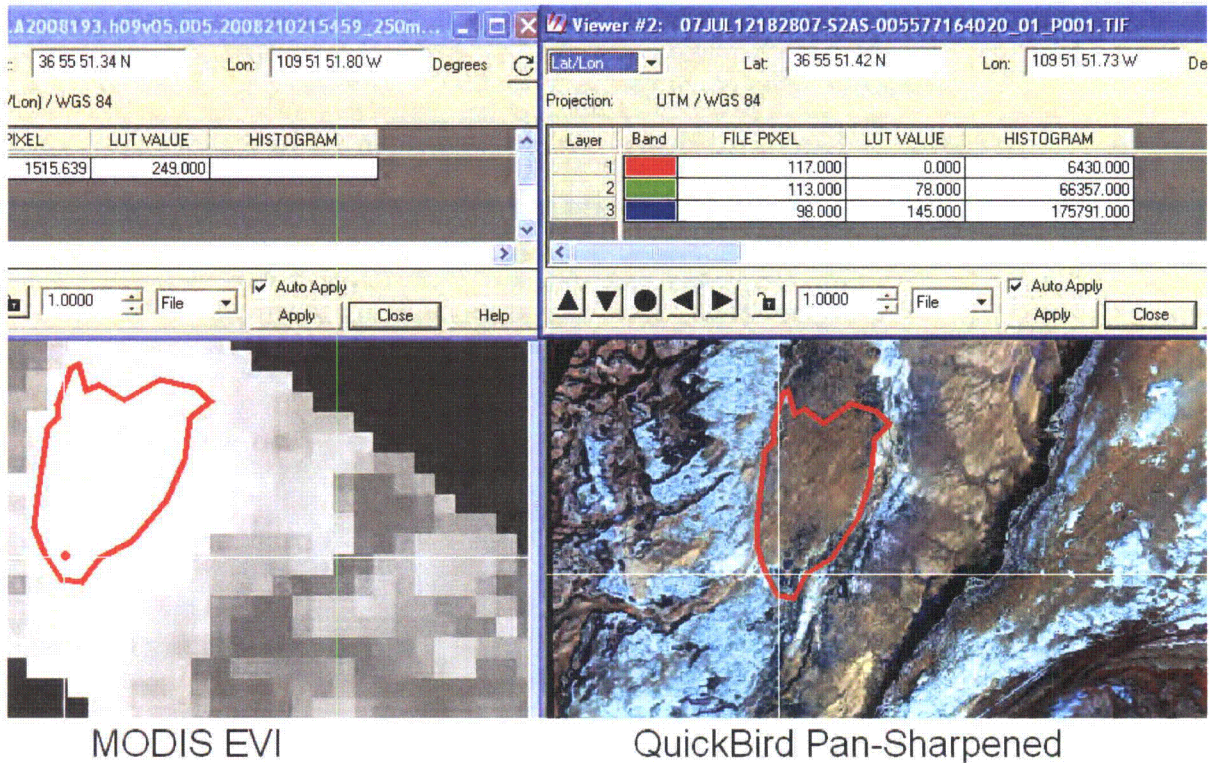
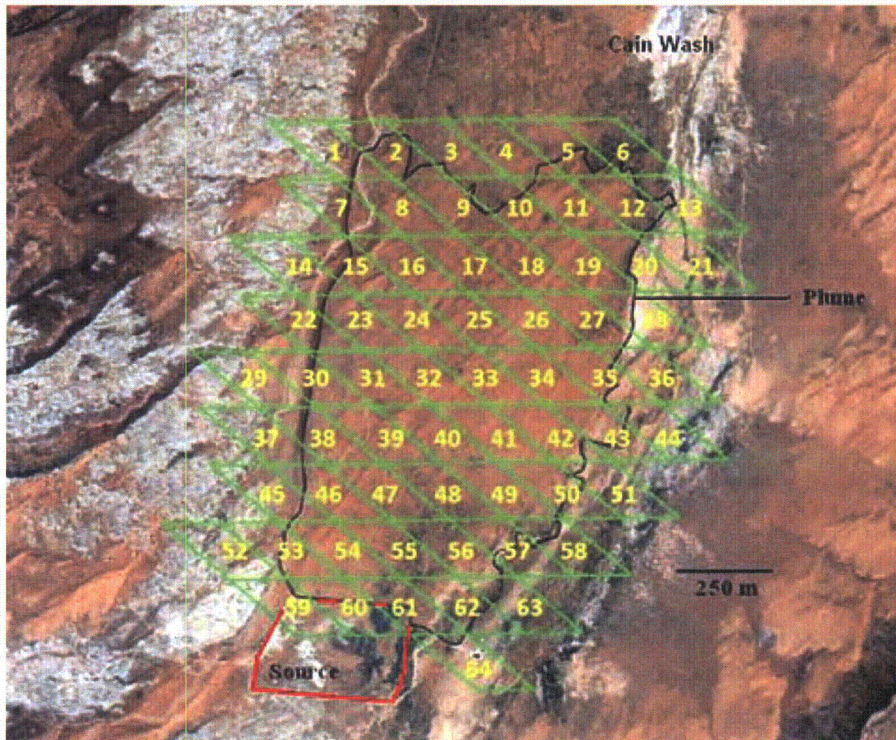


Figure 6–1. Top: MODIS pixel footprints overlain on a high-resolution 2007 Quickbird image for the Monument Valley site. Bottom: a shape file of the Monument Valley site prepared on a Quickbird image and overlain on a MODIS image for July, 2007. The red dot shows the location of the irrigated field in the source area for each image; note the close correspondence in location between the two images.

atmospherically corrected products, ready for use without further processing by the end-user. Quickbird is a commercial product and a series of replacement satellites is planned. Similarly, a series of inter-calibrated Terra-type NASA satellites is planned to provide continuity for Earth Observation Sciences for decades to come.

Quickbird pan-sharpened images combine 0.5-m resolution panchromatic black-and-white images with 2.4-m resolution multi-spectral (color) images, and they have sufficient resolution to map the distribution of individual shrubs over the site to determine fractional vegetation cover (f_c) and changes in vegetation patterns over time. One 16.5 km \times 16.5 km scene, sufficient to cover the entire Monument Valley site, costs approximately \$1,200. The images are custom-acquired within a window of approximately 60 days from time of order to date of acquisition.

MODIS imagery is collected on a near-daily basis, and is processed into 16-day composite values by the EROS Data Center in South Dakota. Vegetation changes can be monitored using the two vegetation indexes (VIs) supplied by EROS: the Enhanced Vegetation Index (EVI) and the Normalized Difference Vegetation Index (NDVI) (Huete et al. 2002). Quickbird also offers multi-spectral images at 2.4 m resolution from which NDVI can be calculated. These VIs ratio the reflection of light in the Red to reflection in the Near Infrared (NIR) received by the satellite sensors. Green vegetation absorbs nearly all of the Red radiation and reflects nearly all of the NIR radiation, producing VIs distinctly different from soil or water. Hence, VIs can be used to map vegetation patterns and quantify the density of foliage over an area of interest. They can be calibrated with ground data to quantify physiological processes that depend on light absorption by the canopy. These include ET and Gross Primary Productivity. They can also be calibrated to quantify biophysical variables such as fractional vegetation cover (f_c), LAI, and standing biomass. These are the primary variables that determine the vigor of the site vegetation community.

MODIS imagery is free, and can be acquired online from the Oak Ridge National Laboratory DAAC site (<http://daac.ornl.gov/>). This site uses Google Earth to aid the user in defining an area of interest, and then displays the footprint of the MODIS pixels to be ordered on a recent, high-resolution Quickbird image of the scene. Hence, areas covered by MODIS pixels can be precisely collocated on high-resolution Quickbird images as well as on the ground in field surveys. This greatly facilitates calibrating satellite data to ground measurements. The geometric accuracy of MODIS and Quickbird images is high, allowing areas of interest to be located first on the Quickbird image, then overlain as shape files on the MODIS image to extract NDVI or EVI values for change detection over time (Figure 6–1, bottom). Images are available at 16-day intervals from 2000 to the present. The archives are continuously updated with a lag of about 30 days between date of acquisition and date of posting.

6.3 Mapping Vegetation with Quickbird Imagery

Fractional cover can be easily determined on Quickbird images because the dark-colored shrubs stand out clearly against light-colored sand at the Monument Valley site. Two methods can be used to quantify vegetation cover. The first method uses an unsupervised, image classification program in ERDAS Imagine software (Leica Geosystems, Inc., Atlanta, Georgia). Each pixel in the area of interest is partitioned into one of four color-coded classes using a statistical nearest-neighbor approach. One class clearly corresponds to shrubs, as seen by comparing the classified

image with the original image (Figure 6–2, top). The program displays the number of pixels in each class, from which fractional cover of shrubs can be calculated.

The second method uses a point-intercept analysis of the original image in Adobe Photoshop or other photo interpretation software. A grid is overlaid on the area of interest on the image, and each grid intersection is scored as vegetated or unvegetated (Figure 6–2, bottom). This method is more time consuming and more subjective than the automatic classification method, but avoids misclassification of dark objects such as vehicles and sheds as shrubs, a problem with automatic classification programs.

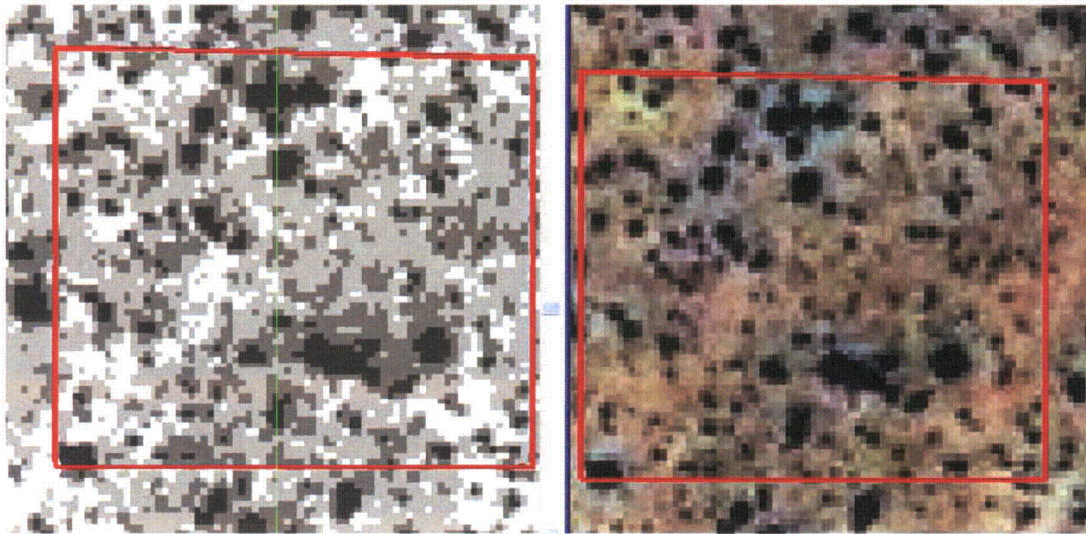
Both methods are sensitive to shadows cast by shrubs. Shadow length is dependent on time of day and day of the year. Quickbird is in a sun-synchronous orbit and acquires images at approximately 10:30 a.m., resulting in small shadows that cannot be distinguished from shrub canopies on the panchromatic images. Quickbird images are acquired at view angles that can be as great as 20 percent off-nadir. Images are corrected so that distances measured on the ground are accurate, but three dimensional objects can still be slightly distorted. We measured ATCA and SAVE shrub canopy areas on the ground and regressed them against measurements on a July 12, 2007 Quickbird image (Figure 6–3). Ground measurements were only 83 percent of Quickbird measurements, presumably due to shadows counted in the shrub category. Shadow effects diminish as stand density increases, because shadows are cast within the canopy rather than on bare soil. An iterative correction formula that takes this into account is:

$$f_c = f_{cQB} \times (0.83 + 0.17 \times f_{cQB}) \quad (1)$$

where f_{cQB} is the apparent cover measured on the Quickbird image. As stand density approaches 1.0, the correction factor approaches 0.

Comparison of Quickbird estimates of f_c with ground estimates made in the South and North Exclosure plots in 2007 by line transects are in Table 6–1. Estimates show a reasonable level of agreement. The visual, point-intercept methods corresponded more closely to ground measurements than the computer classification method. The Quickbird methods are able to distinguish ATCA and SAVE shrubs from other (less dense) vegetation classes. However, images should be acquired before the summer monsoon season to avoid interference from annual forbs that can be prolific in wet years. Furthermore, we do not know if the correction factor for shadows can be applied to all Quickbird images.

The high resolution of the Quickbird images also allows them to be used to map the distribution of shrubs over the site. Figure 6–4 shows how shrub density increased dramatically in the fenced source area from 1997 to 2007. Classified images from different dates can be analyzed by automated change-detection programs in ERDAS or ArcInfo programs to map changes in shrub densities over time. These programs display differences in pixel values as they change over time. However, Quickbird images have a positional error of about 12 m between different dates. To use change detection programs, the images must first be geo-referenced by matching common features on each image using ERDAS or ArcInfo software. This has not yet been done for the Monument Valley site.



South Exclsoure - Classified vrs. Pan-Sharpended Image

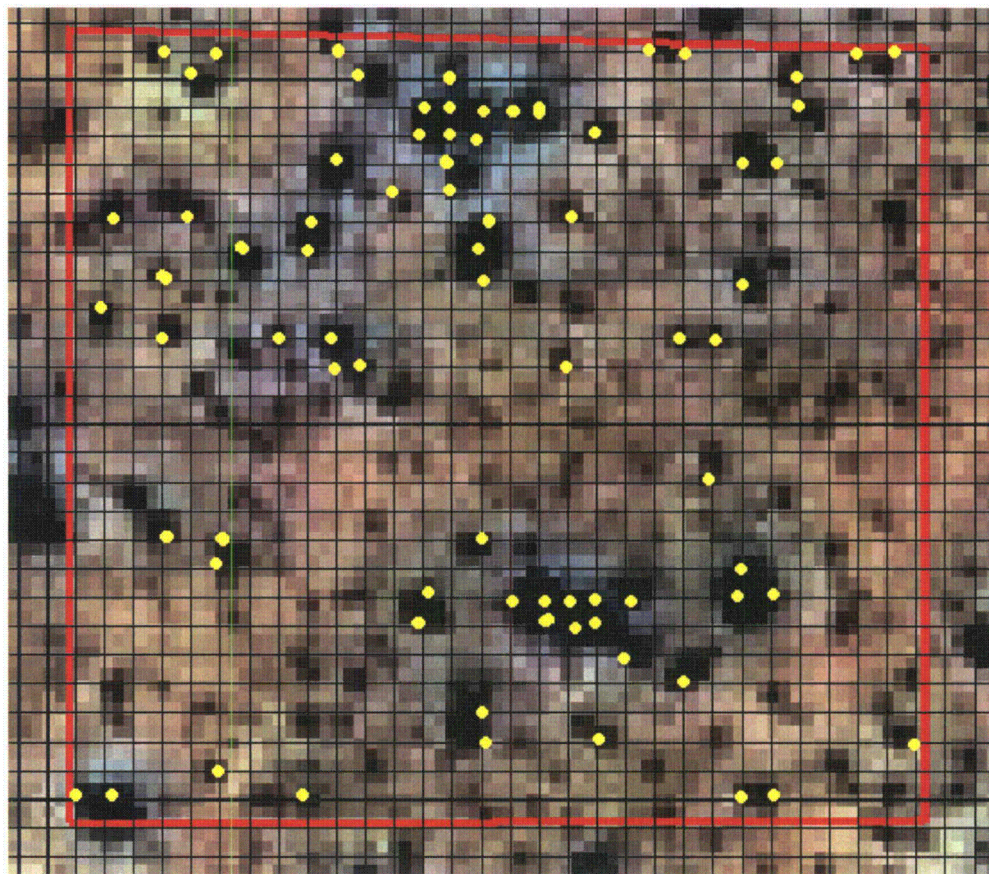


Figure 6–2. Top: Outline of the North Exclosure at the Monument Valley site on a classified Quickbird image (left) compared to the original sharpened panchromatic image. Bottom: illustration of the point-intercept method of visually estimating f_c by shrubs on a Quickbird image. Yellow points are grid intersections that were scored as ATCA or SAVE shrubs.

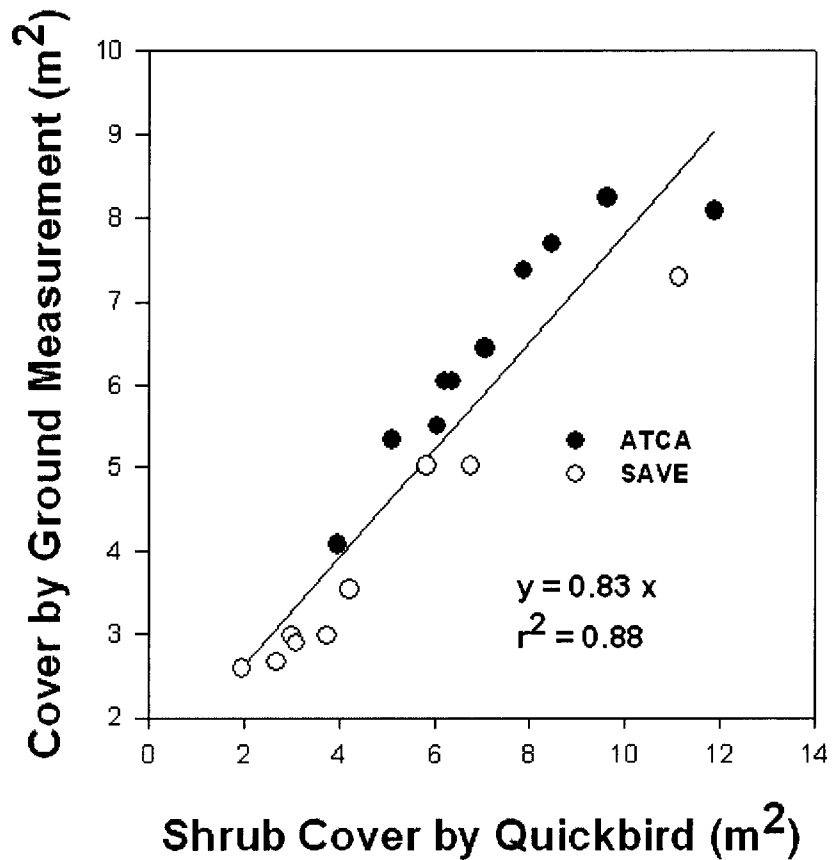


Figure 6–3. Relationship between shrub canopy area measured on the ground with areas measured on a Quickbird image for the Monument Valley site.

Table 6–1. Estimates of fractional ground cover of shrubs by different methods at the Monument Valley site, July 2007

Method	South Exclosure	North Exclosure
Ground Survey	0.273	0.106
Quickbird Classified	0.331	0.078
Quickbird Point Intercept	0.241	0.103

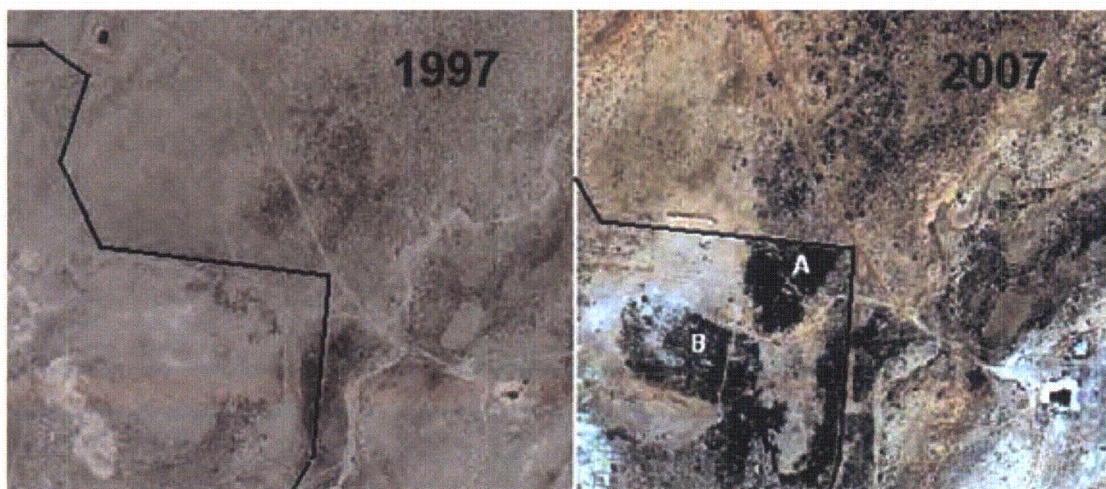


Figure 6-4. Comparison of shrub density at the Monument Valley site in 1997 and 2007. The 1997 image is an aerial photograph while the 2007 image is a Quickbird scene. The Quickbird image shows the development of the volunteer stand of ATCA (A) and the irrigated field (B) in the fenced area over time.

6.4 Approximating LAI and Standing Biomass from Quickbird Images

Ground measurements can be combined with Quickbird estimates of f_c to determine LAI and standing biomass. We measured LAI by leaf-harvesting on 64 ATCA and 64 SAVE plants in 2006 and 2007 (Glenn et al. 2008b). In 2007, the weighted mean LAI value of ATCA and SAVE plants over the site was 3.84, and f_c was 0.0964. Hence, this value can be used to determine an approximate value for mid-summer LAI over the site in 2007:

$$\text{Site LAI} = 3.84 \times 0.0964 = 0.37 \quad (2)$$

To estimate standing biomass, we regressed f_c of individual shrubs against biomass for ATCA plants determined by destructive harvesting. We found a linear relationship between f_c and shrub biomass over the range of shrub sizes found on the plume (Figure 6-5). Standing biomass over the site for 2007 can be approximated by:

$$\text{Standing Biomass (kg/m}^2\text{)} = 1.39 \times 0.0964 = 0.134 \quad (3)$$

These estimates should only be used as approximations, because both LAI and biomass are sensitive to time of year and the condition of the range. For example, LAI in the irrigated ATCA field in 2007 was only 2.05, because these plants are deficit-irrigated and are not tapped into groundwater. Furthermore, the ground measurements were only conducted in a few areas and seriously under-sampled the whole site. As outlined below, Quickbird analyses should be combined with MODIS EVI measurements to provide a dynamic picture of site conditions.

6.5 MODIS EVI for Tracking Vegetation Changes Over Time

Vegetation indices are one of the oldest tools in remote sensing (reviewed in Glenn et al. 2008a). As ratios of two adjacent bands in the electromagnetic spectrum, they are relatively insensitive to changes in atmospheric properties at different acquisition dates, and they can be inter-calibrated

Ground Cover vs. Dry Biomass

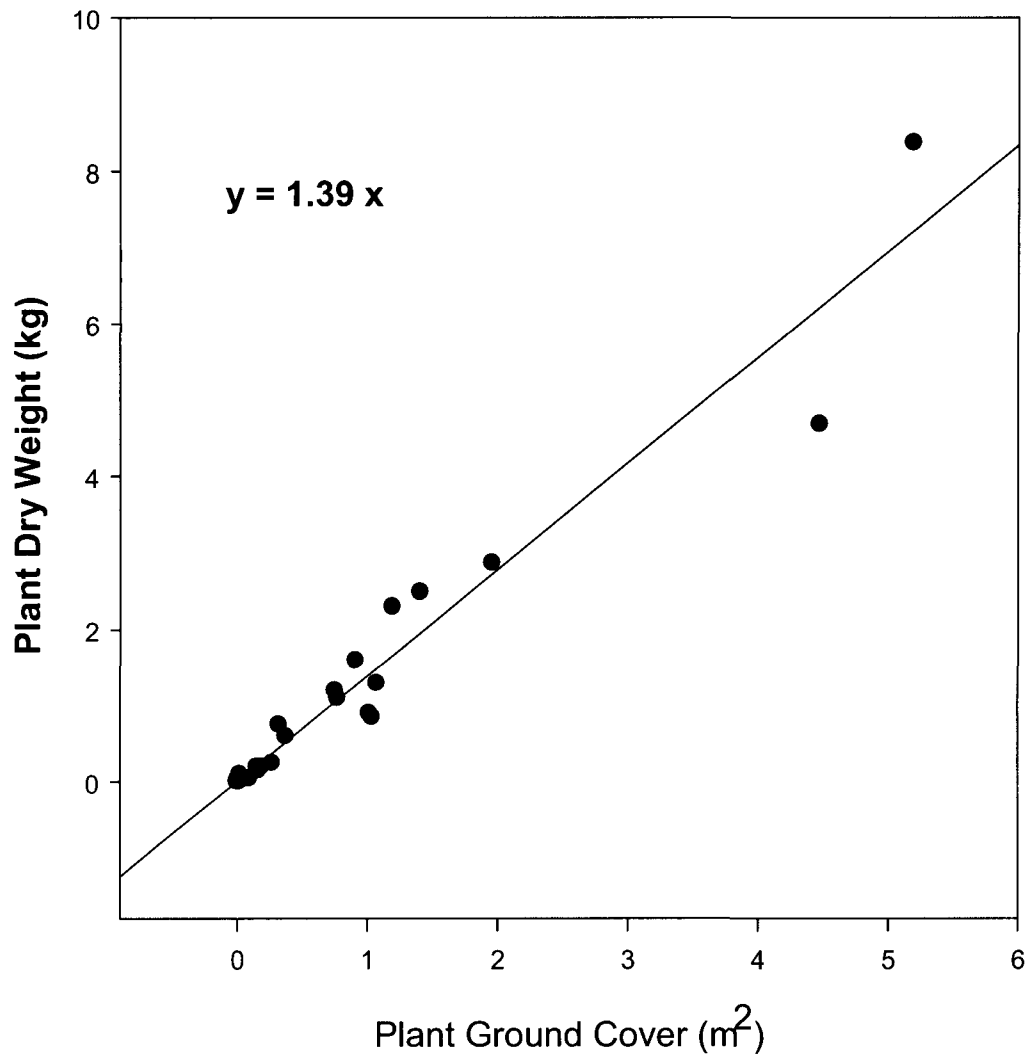


Figure 6-5. Relationship between standing biomass and ground cover of ATCA shrubs at the Monument Valley site.

among different sensor systems to allow comparisons among different satellite products over time. We selected the MODIS sensor system to monitor vegetation at the Monument Valley site because it provides near-daily coverage at a useful resolution (250 m), and because the VI products are quality-controlled and have been inter-calibrated with ground measurements and with other satellite sensor systems. We selected EVI because in a previous study in which we correlated MODIS EVI and NDVI with moisture flux tower ET data at 11 sites in the western U.S. (Glenn et al. 2008a), ET was better correlated with EVI ($r = 0.83$) than NDVI (0.72) across

sites. Unlike the NDVI, EVI uses reflection the Blue band as well as reflection in the Red and NIR bands:

$$EVI = 2.5 \times (\rho_{NIR} - \rho_{Red}) / (1 + \rho_{NIR} + (6 \times \rho_{Red} - 7.5 \times \rho_{Blue})) \quad (4)$$

where the coefficient “1” accounts for canopy background scattering and the blue and red coefficients, 6 and 7.5, minimize residual aerosol variations (Huete et al. 2002). The EVI is more functional on NIR reflectance than on Red absorption, and therefore it does not “saturate” as rapidly as NDVI in dense vegetation, and it has been shown to be highly correlated with photosynthesis and plant transpiration in a number of studies (Glenn et al. 2008a).

We converted EVI to scaled values (EVI*) for comparison with other data sets. Scaling sets of EVI for bare soil at zero and for a fully vegetated surface at 1.0, using EVI values of 0.091 for EVI_{min} and 0.542 for EVI_{max} determined on large data sets (Nagler et al. 2005):

$$EVI^* = 1 - (EVI_{max} - EVI) / (EVI_{max} - EVI_{min}) \quad (5)$$

6.6 MODIS EVI* for Estimating ET and LAI

VIs are often used to estimate individual biophysical properties of vegetation, such as f_c and LAI. However, their greatest strength is that VIs represent the composite properties of green vegetation that determine light absorption by chlorophyll; these include f_c , LAI, leaf angles within the canopy, chlorophyll content, and light scattering by leaves (Glenn et al. 2008a). They are less useful in estimating individual biophysical properties than in estimating physiological properties that depend on overall light absorption, such as ET and gross primary production. Fortunately, these are the parameters of interest in monitoring changes in sites such as Monument Valley over time.

We used EVI* and maximum daily temperature (T_a) values to calculate ET:

$$ET \text{ (mm/m}^2\text{/day)} = 11.5 \times (1 - \exp^{-1.63EVI^*}) \times 0.883 / (1 + \exp^{-(T_a - 27.9)/2.57}) \quad (6)$$

The algorithm was determined by regressing ET measured at nine flux tower stations against EVI* and T_a over a 4-year period; the coefficient of determination (r^2) was 0.76 (Nagler et al. 2005).

The expression containing EVI* is based on the formula for light extinction through a canopy. The temperature term is in the form of a sigmoidal curve, where there is a minimum temperature due to the physiological status of the plants; a middle, exponential portion of the curve which fits the vapor pressure deficit:temperature response in the Penman-Moneith equation; and an upper limit, where physiological limitations to ET also apply. Hence, air temperature is a scalar from 0 to 1.0 that accounts for both atmospheric water demand and the physiological limitations on E, at the low and high end of the temperature scale (Nagler et al. 2005).

Equation (6) is identical to the one derived in Nagler et al. (2005) based on moisture flux tower data at nine phreatophyte sites in western riparian corridors, except that the original algorithm had a constant term representing minimum (bare soil) ET, which was 1.07 mm/day in the

original study of riparian vegetation (Nagler et al. 2005). It was required because none of the tower-based values of ET reached zero even in winter or when EVI* approached 0, due to bare soil evaporation. However, in this study the sap flow sensors measured plant transpiration only, and bare soil evaporation is very low due to lack of surface moisture and scant rainfall, so we did not include the constant term in Equation (6).

To estimate LAI, we used the ERDAS unsupervised classification method to determine f_c for each of 60 MODIS pixels, by projecting the pixel footprint onto a July 2007 Quickbird image of the Monument Valley site. We then converted f_c values to LAI using Equation (2). We regressed summer 2007 LAI values calculated for each pixel against mean June–August 2007 EVI* values:

$$\text{LAI} = 3.21 \text{ EVI}^* \quad (7)$$

The regression had $r^2 = 0.77$ and Standard Error of the Mean = 0.22.

MODIS estimates of ET and LAI from 2000–2007 are in Figure 6–6 (top and bottom, respectively). 2006 and 2007 ground estimates of ET and LAI are also plotted. Ground estimates of ET closely matched MODIS estimates. The 2007 LAI estimates were similar by both methods, but 2006 MODIS LAI was lower than the ground estimate. The ground estimates were made on plants in and around the North and South Enclosures, whereas the MODIS estimate includes the entire site, hence exact agreement in LAI was not expected.

6.7 MODIS Estimates of ET and LAI Over the Site, 2000–2008

MODIS pixels locations are highly stable over time, allowing single pixels or clusters of pixels to be used for change detection studies without the need to co-register the images to each other. Selected MODIS pixels were used to track changes in ET and LAI at the Monument Valley site over time. One pixel encompassed most of the planted fields in the source area (plus adjacent unvegetated areas) while an adjacent pixel encompassed the volunteer, non-irrigated dense ATCA stand inside the fence (Figure 6–7). Two adjacent pixels represented the moderately dense SAVE stand outside the fence and over the hotspot of the plume (Figure 6–8), while 29 pixels represented the sparse ATCA stand over the rest of the plume area (Figure 6–9).

ET (Figure 6–10) and LAI (Figure 6–11) for all four areas were similar and relatively low from 2000–2003. The site had only recently been fenced, and the irrigated fields were initiated in 2000. Furthermore, heavy grazing was practiced over the site during those years. From 2004–2008, ET and LAI increased inside the fenced area, due to the development of dense plant stands as indicated in Figure 6–4. The dense stands represented 57.9 percent and 38.5 percent of the areas covered by the irrigated field and volunteer ATCA pixels, respectively. Projected peak summer ET rates in the dense stands in 2008 were 4.88 mm/day and 7.01 mm/day, respectively. These estimates are consistent with differences in LAI measured on the ground (2.05 and 3.68, respectively); the field plantings are constrained by the deficit irrigation strategy, whereas the volunteer plants are presumed to be rooted into the shallow portion of the plume and have unlimited access to water.

From 2004 to 2008, ET and LAI generally increased over the unfenced parts of the plume as well. We attribute this to relaxed grazing pressure. The dip in ET in LAI in 2006 might have been due to low precipitation (89 mm) compared to 172 mm in 2005 and 117 mm in 2007.

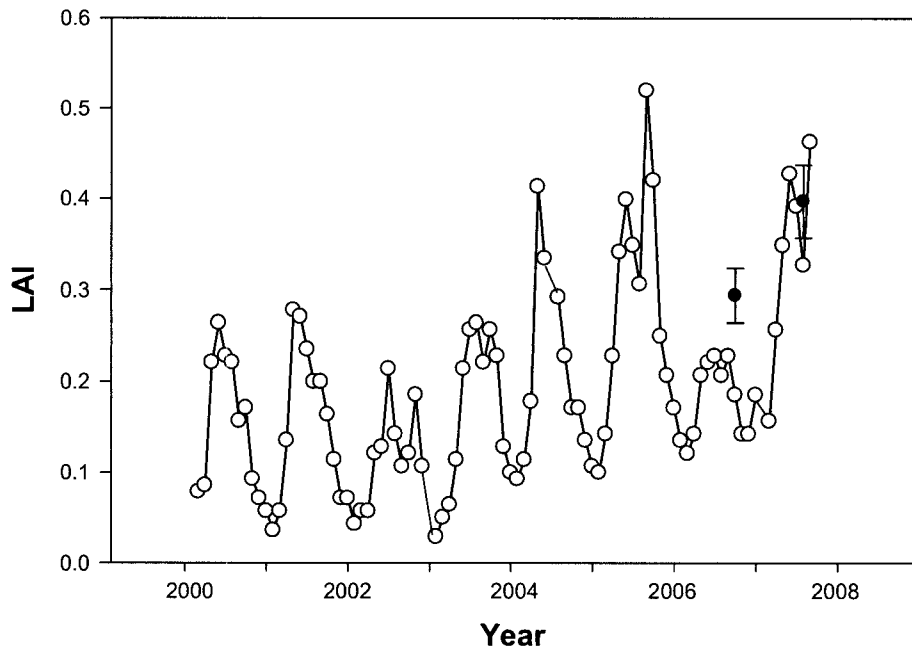
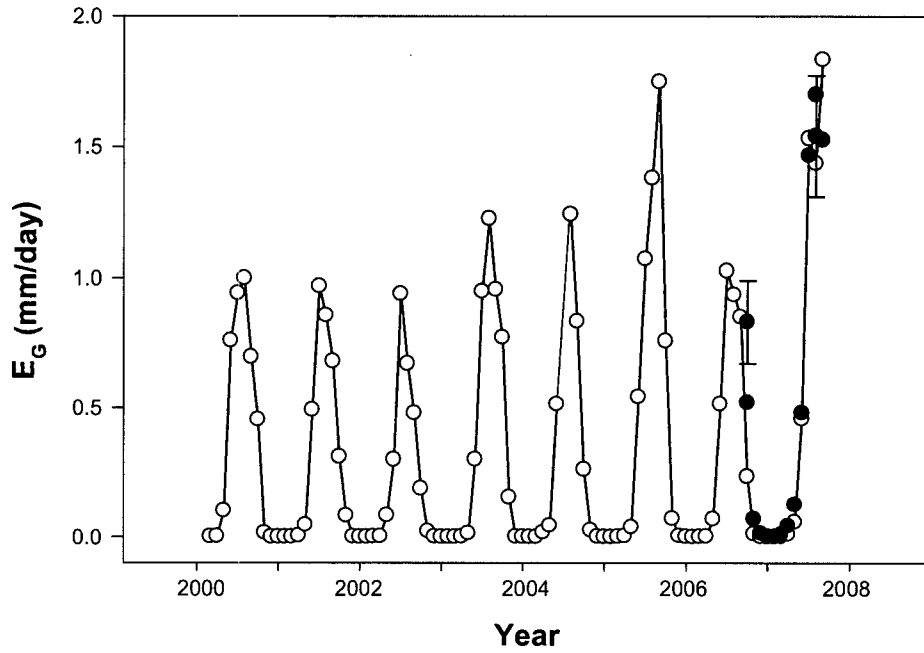


Figure 6-6. Top: ET estimated by MODIS at the Monument Valley site (open circles). Closed circles with error bars show ET measured by sap flux sensors in 2006 and 2007. Closed circles without error bars show ET projected from sap flux measurements and a best-fit model of ET based on temperature data during the sap flux measurements. Bottom: LAI estimated by MODIS (open circles) compared to ground measurements in 2006 and 2007.



Figure 6–7. MODIS pixel footprints superimposed on a Quickbird image showing the irrigated field and volunteer ATCA stand inside the fence at the Monument Valley site.



Figure 6–8. Two MODIS pixels representing the SAVE stand outside the fence at the Monument Valley site.

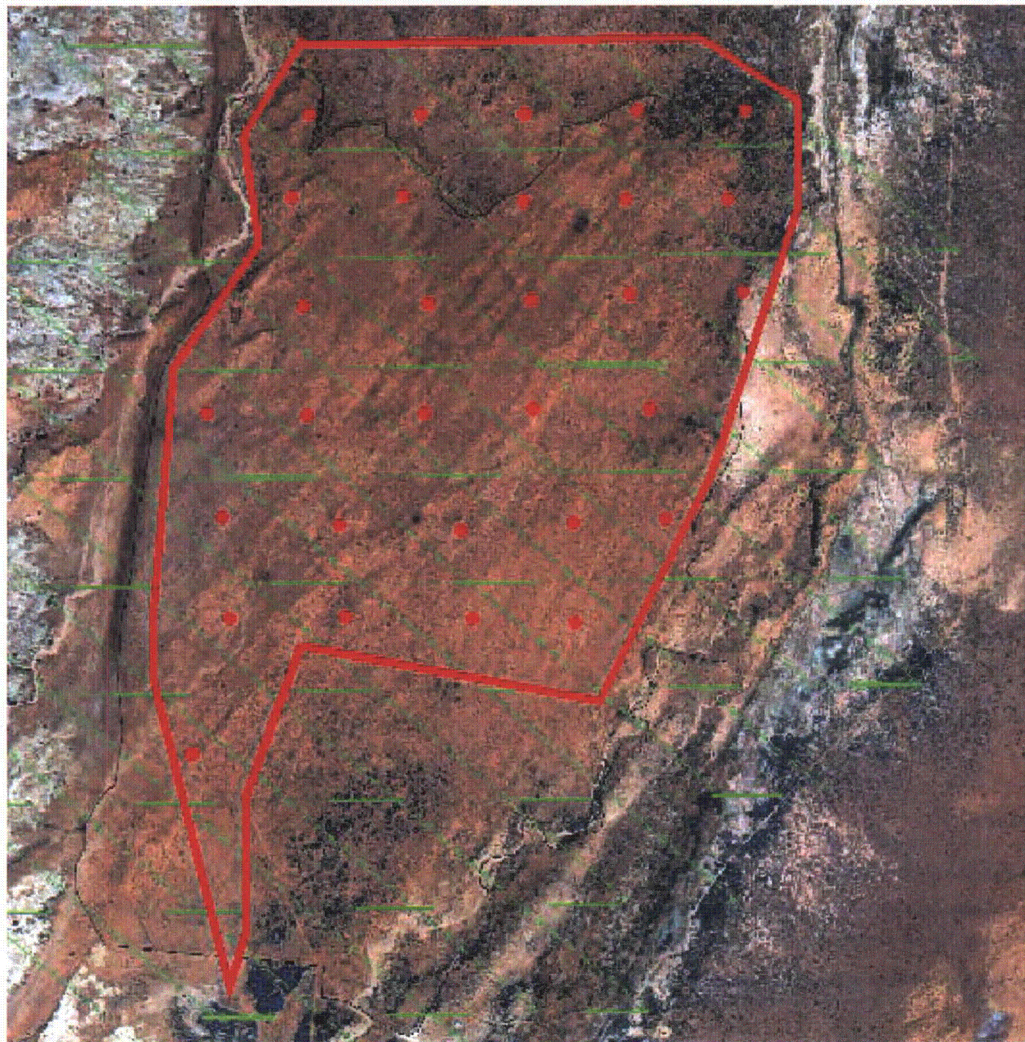


Figure 6–9. MODIS pixels (red dots) selected to represent the sparse ATCA stand over the plume at the Monument Valley site.

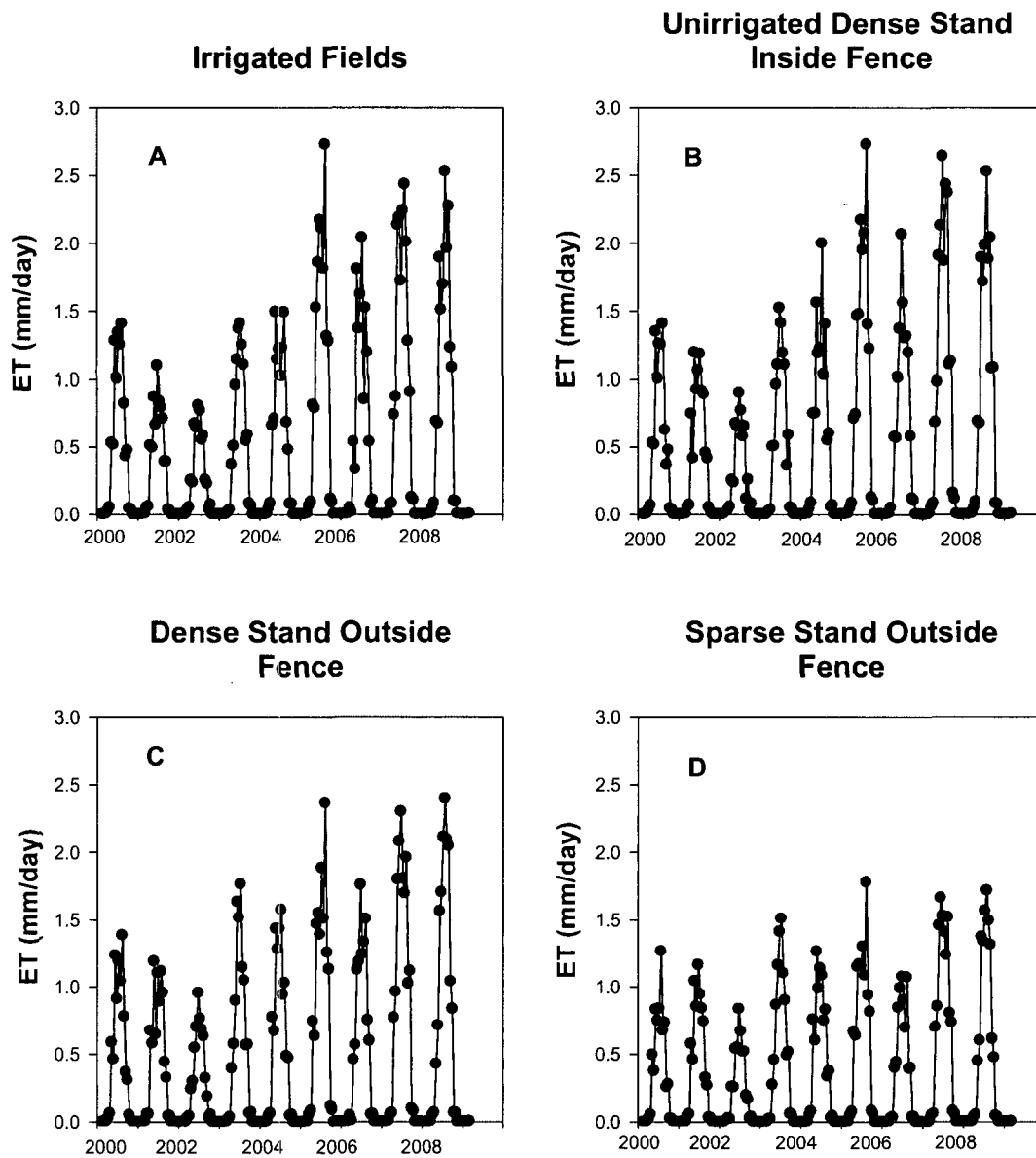


Figure 6–10. ET estimated by MODIS for selected areas at the Monument Valley site.

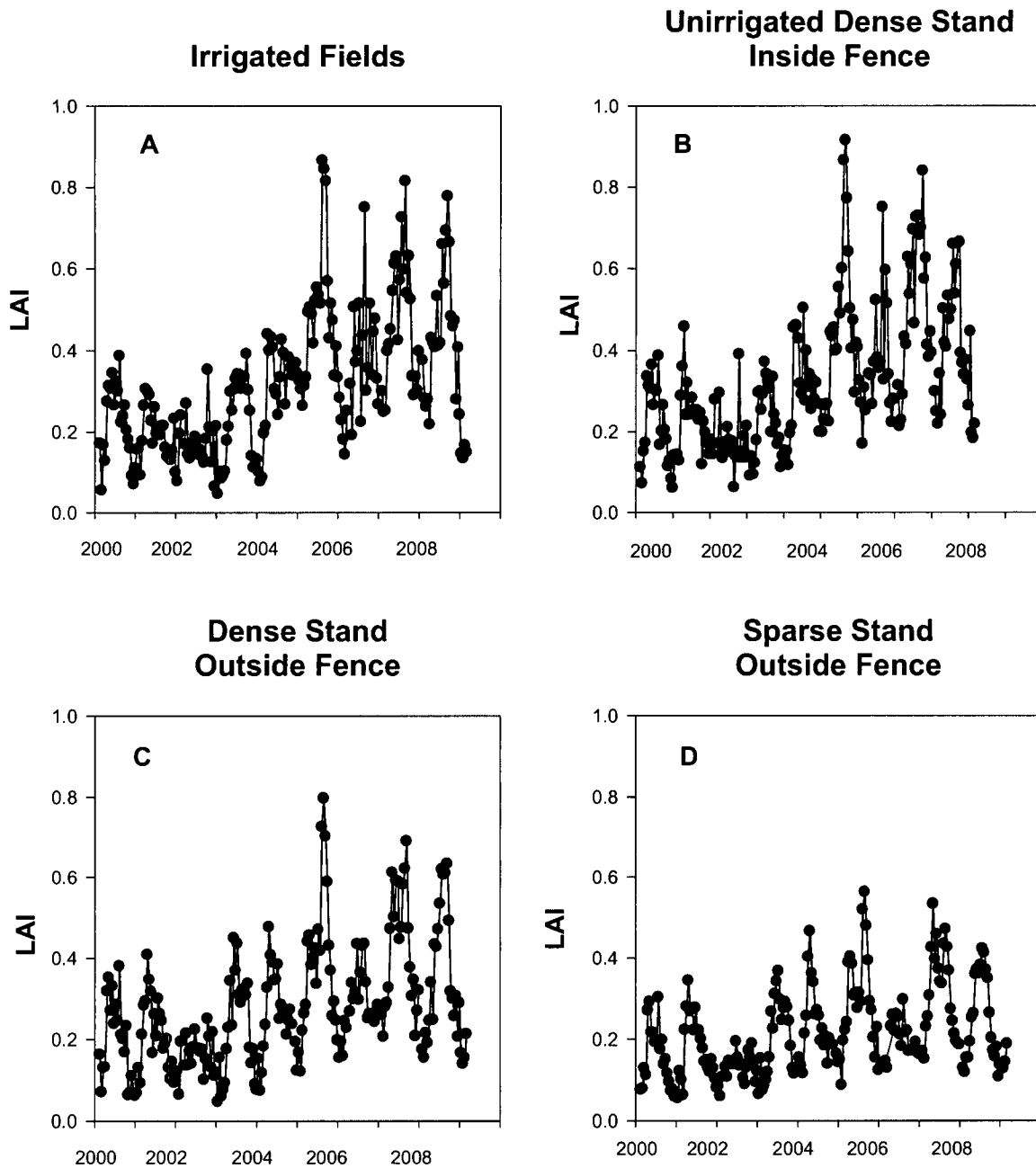


Figure 6–11. LAI estimated by MODIS for selected areas at the Monument Valley site.

MODIS ET estimates include the contribution by annual plants, which can be substantial in wet years. Figures 6–10 and 6–11 illustrate how MODIS can be used to detect changes in vegetation over the site unobtrusively. Apparent changes detected by MODIS surveillance can then be followed up by detailed analyses of Quickbird images, followed by ground surveys if necessary. If a hydrological model of the source and plume is developed, the ET estimates could be used to project changes in plume volume and movement over time.

7.0 Ethanol-Enhanced Denitrification of the Alluvial Aquifer

7.1 Background

Enhanced attenuation (EA) can be defined as initiating and/or augmenting natural and sustainable attenuation processes. The goal is to increase the magnitude of attenuation by natural processes beyond that which occurs without intervention. Enhancing in situ biological denitrification through injection of amendments has been deemed a promising method for remediation of nitrate contaminated groundwater. A small number of field tests of this method have been reported. These studies have shown that substantial reductions of nitrate concentrations were achieved upon injection of the chosen amendment. The New Mexico South Valley case study described in the ITRC report (2000) is very similar to the Monument Valley site in terms of volume and area of the plume, nitrate concentrations, and mobility of the plume.

The Monument Valley site is an excellent candidate for in situ EA remediation of nitrate in the plume. We have already demonstrated that denitrification can be stimulated in the vadose zone of the source area through irrigation of native shrubs. Nitrate levels in the source area have decreased from 171 mg/L in 2001 to 71 mg/L in 2006. The region of high nitrate contamination in the plume is confined in a relatively small volume of the aquifer. Treatment of this high-concentration portion of the plume could allow natural attenuation of the remainder of the plume, thereby reducing the long-term exposure risk to valley residents, wildlife, and livestock.

The degree to which a reagent-injection based method will be successful for a particular site depends greatly on the ability to deliver the reagent to the target zone. Hydrogeologic properties of the subsurface control this aspect, with physical material heterogeneity (i.e., hydraulic conductivity) the primary characteristic of concern. Based on previous site characterization, the alluvial aquifer consists primarily of fine to medium grained sand deposits that vary in thickness from 0 to 120 ft. Thin, non-laterally extensive, finer-grained layers are found in the thickest sections of the aquifer. The hydraulic conductivity for portions of the aquifer has been reported to range between 1 and 30 ft/d. A hydraulic gradient of approximately 0.01 has been reported, with average pore water velocities estimated to be approximately 1 ft/day. These properties are relatively ideal for subsurface injection of reagents. The region of elevated nitrate concentrations is contained within an area of the aquifer that has a radius of approximately 800 ft. Therefore, substrate could be injected into this part of the plume within 2 to 3 years, assuming 1 ft/day of pore water velocity.

Considering the information presented above, it appears that enhanced denitrification via reagent injection is a feasible method for the Monument Valley site. Questions that remain to be addressed are the degree of enhancement that can be achieved and the optimal means of implementation. These questions will be addressed with a pilot-scale demonstration test supplemented with mathematical modeling analyses. With this information, the time required to remediate the target zone to a selected cleanup objective can be estimated. Laboratory microcosm evaluations of denitrification have determined that ethanol amendments may increase reaction rate coefficients by approximately a factor of 100, which would decrease remediation times substantially. The remediation enhancement with ethanol injection must be tested at the pilot-scale to evaluate the feasibility of this technology.

7.2 Summary of Work Plan

The detailed work plan (Appendix F) describes the proposed investigation of a field-scale injection of ethanol as a denitrification enhancement substrate at the Monument Valley site. This pilot-scale investigation will focus on a small area of the alluvial aquifer. The results of this pilot study will support the feasibility analysis of full-scale ethanol application at the Monument Valley site for enhanced attenuation of nitrate concentrations and the remediation of groundwater contamination.

A total of 4 new wells will be installed (see Figures 7-1 and 7-2 for new well locations). The estimated local groundwater gradient is shown on the attached figures along with the proposed locations for the new wells. We will inject ethanol and tracers into wells 655 and 765 and monitor concentrations in downgradient monitoring wells, including the four new wells. These new wells will be designed to be similar to the injection wells at each site (i.e., well total depth and screened interval should be consistent with injection well for each site).

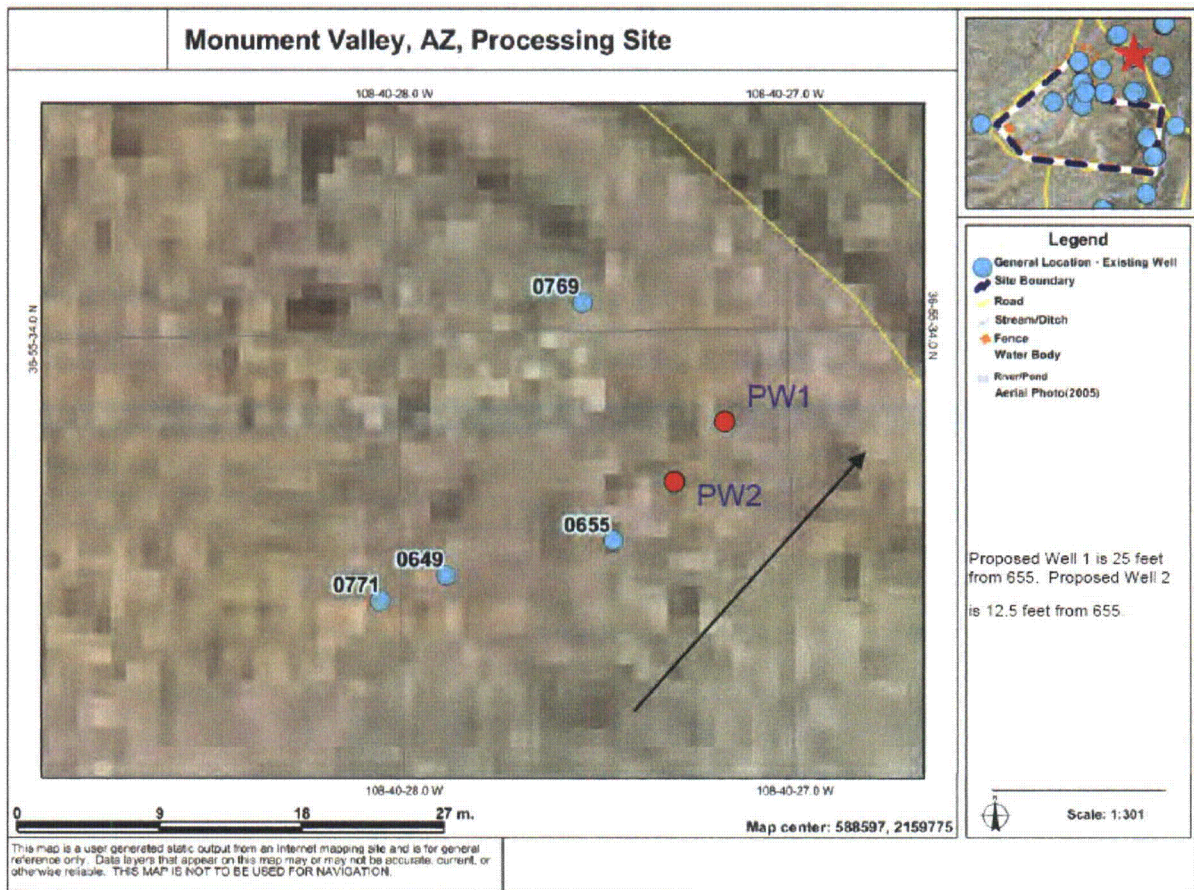


Figure 7-1. Location of proposed new wells PW1 and PW2

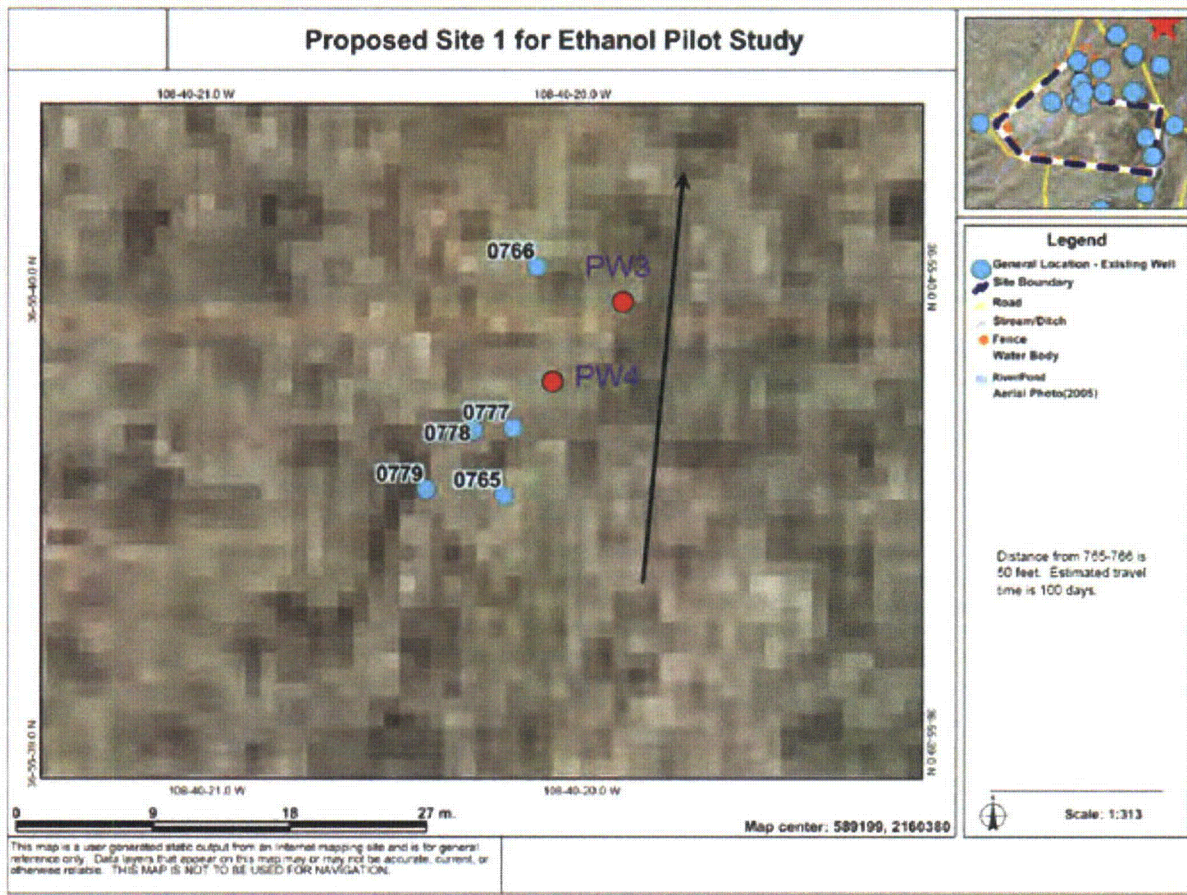


Figure 7-2. Location of proposed new wells P3 and P4

This page intentionally left blank

8.0 Data Archive

The University of Arizona's Environmental Research Laboratory (ERL) has worked with the Grand Junction office of the DOE since 1999 at the Monument Valley, Arizona site. Several different contractors have worked on the project during that period, and other personnel and contractors worked at the Monument Valley site prior to 1999. Long term evaluation of remediation efforts at this site will require maintaining consistent data sets over a period of decades. Hence, it is important to document the methods used in data collection and to archive the data sets so they will be available for re-analysis in the future.

As a first step in this process, we have collected all the original data sets generated by ERL as well as others provided to us by DOE. These are listed in outline format in Appendix G. The nine main topic areas include:

- Source Area Atriplex Plantings (moisture profiles by neutron probe; plant growth and development; plant uptake of CNS);
- Salt Balance Study (conducted to determine if nitrates were leaching from the soil due to irrigation or were undergoing denitrification);
- Subpile Soil Denitrification Studies;
- Field Application of Ethanol Solutions;
- Land Farm Studies;
- Stunted Growth Studies;
- Natural Attenuation in the Plume Studies;
- Enhanced Natural Attenuation in the Plume Studies; and
- Evapotranspiration and Water Balance Studies.

All of the primary data files are Excel spreadsheets. However, a great many additional files (not listed below) were generated in Systat and Sigmaplot and GIS programs in analyzing and interpreting the data sets. These files will also be made available as needed to interpret the Excel files. The following additional steps should be taken to create a permanent data archive:

- [1] Consolidate individual files into larger Excel files with descriptive titles covering broad topic areas (e.g., consolidate each year's probe data into a single file with multiple sheets representing each year).
- [2] Annotate each file with text information on dates of data collection, purpose of data collection, and a complete description of methodology, such that the work could be repeated in the future to detect trends.
- [3] Work with S.M. Stoller to develop final hard-copy, electronic, and Web-based data depository for this and other project data.

This page intentionally left blank

9.0 References

- Al-Khafaf, S., P. Wierenga and B. Williams, 1977. A flotation method for determining root mass in soil, *American Society of Agronomy* 69: 1025–1026.
- Bonham, C.D., 1989. *Measurements for Terrestrial Vegetation* (New York: John Wiley and Sons).
- Coplen, T., A. Herczeg, and C. Barnes, 2000. “Isotope Engineering Using Stable Isotopes of the Water Molecule to Solve Practical Problems,” in P.G. Cook and A.L. Herczeg (eds.), *Environmental Tracers in Subsurface Hydrology* (Norwell, MA: Kluwer Academic Publishers), 79–10.
- Cottam, Grant, and J.T. Curtis, 1956. “The Use of Distance Measures in Phytosociological Sampling,” *Ecology*, 37: 451–460.
- DOE (U.S. Department of Energy), 2002. *Phytoremediation of Nitrogen Contamination in Subpile Soils and in the Alluvial Aquifer at the Monument Valley, Arizona, Uranium Mill Tailings Site*, GJO-2002-312-TAR, U.S. Department of Energy, Grand Junction, Colorado.
- DOE (U.S. Department of Energy), 2004a. *Environmental Assessment of Ground Water Compliance at the Monument Valley, Arizona, Uranium Mill Tailings Site*, Draft, DOE/EA-1313, U.S. Department of Energy, Office of Legacy Management, Grand Junction, Colorado.
- DOE (U.S. Department of Energy), 2004b. *Phytoremediation of the Nitrogen-Contaminated Subpile Soil at the Former Uranium Mill Tailings Site in Monument Valley, Arizona: 2004 Status Report*, DOE-LM/GJ768-2004 (ESL-RPT-2004-07), Environmental Sciences Laboratory, U.S. Department of Energy, Grand Junction, Colorado.
- DOE (U.S. Department of Energy), 2004c. *Monument Valley Ground Water Remediation: Pilot Study Work Plan*, DOE-LM/GJ757-2004, Office of Legacy Management, U.S. Department of Energy, Grand Junction, Colorado.
- DOE (U.S. Department of Energy), 2006. *Soil and Ground Water Phytoremediation Pilot Studies at Monument Valley, Arizona: 2005 Status Report*, DOE-LM/1254-2006, Office of Legacy Management, U.S. Department of Energy, Grand Junction, Colorado.
- DOE (U.S. Department of Energy), 2007. *Natural and Enhanced Attenuation of Soil and Ground Water at Monument Valley, Arizona, and Shiprock, New Mexico: 2006 Status Report*, DOE-LM/1428, Office of Legacy Management, U.S. Department of Energy, Grand Junction, Colorado.
- Ellsworth, P. and D. Williams, 2007. “Hydrogen isotope fractionation during water uptake by woody xerophytes,” *Plant and Soil*, 291: 93–107.
- Fuller, W.H, and A.W. Warrick, 1985. *Soils in Waste Treatment and Utilization: Volume II*, CRC Press.

Glenn, E., A. Huete, P. Nagler, and S. Nelson, 2008a. Relationship between remotely sensed vegetation indices, canopy attributes and plant physiological processes: What vegetation indices can and cannot tell us about the landscape. *Sensors* 8, 2136–2160.

Glenn, E., K. Morino, K. Didan, F. Jordan, K. Carroll, P. Nagler, K. Hultine, L. Shearer, and W.J. Waugh, 2008b. Scaling sap flux measurements of grazed and ungrazed shrub communities with fine and coarse-resolution remote sensing, *Ecohydrology* 1(4):316–329.

Huete, A., K. Didan, T. Miura, E. Rodriguez, X. Gao, and L. Ferreira., 2002. Overview of the radiometric and biophysical performance of the MODIS vegetation indices, *Remote Sensing of Environment* 83, 195–213.

Jordan, F., W.J. Waugh, E.P. Glenn L. Sam, T Thompson, and T.L. Thompson, 2008. “Natural bioremediation of a nitrate-contaminated soil-and-aquifer system in a desert environment,” *Journal of Arid Environments*, 72(5): 748–763.

Lin, G., S. Phillips, and J. Ehleringer, 1996. “Monsoonal precipitation responses of shrubs in a cold desert community on the Colorado Plateau,” *Oecologia*, 106: 8–17.

Lindsay, W.L., 1979. *Chemical Equilibria in Soils*. Wiley-Interscience.

McKeon, C., E.P. Glenn, W.J. Waugh, C. Eastoe, F. Jordan and S.G. Nelson, 2006. “Growth and Water and Nitrate Uptake Patterns of Grazed and Ungrazed Desert Shrubs Growing Over a Nitrate Contamination Plume,” *Journal of Arid Environments* 64(1):1–21.

Nagler, P., R. Scott, C. Westenburg, J. Cleverly, E. Glenn, and A. Huete, 2005. Evapotranspiration on western U.S. rivers estimated using the Enhanced Vegetation Index from MODIS and data from eddy covariance and Bowen ratio flux towers, *Remote Sensing of Environment* 97, 337–351.

Schwertmann, U. and D. S. Fanning, 1976. “Iron-manganese Concretions in Hydrosequences of Soils in Loess in Bavaria,” *Soil Science Society of America Journal*. 40:731–738.

Waugh, W.J., 2002. *Distance (Plotless) Methods for Estimating Shrub Density on the Monticello ACAP Lysimeter*, U.S. Department of Energy Grand Junction Office, Grand Junction, Colorado.

Zhang, M., and A. D. Karathanasis, 1997. Characterization of iron-manganese concretions in Kentucky Alfisols with perched water tables, *Clays and Clay Minerals*; June 1997; 45(3): 428–439.

Appendix A
Publications and Presentations

This page intentionally left blank

Journal Publications

Carroll, K.C., F.L. Jordan, E.P. Glenn, W.J. Waugh, and M.L. Brusseau, SUBMITTED. Comparison of nitrate attenuation characterization methods at the uranium mill tailing site in Monument Valley, Arizona. *Journal of Hydrology*.

Glenn, E.P., K. Morino, K. Didan, F. Jordan, K. Carroll, P. Nagler, K. Hultine, L. Sheader, and W.J. Waugh, 2008. "Scaling sap flux measurements of grazed and ungrazed shrub communities with fine and coarse-resolution remote sensing." *Ecohydrology* 1(4):316-329.

Jordan, F., W.J. Waugh, E.P. Glenn, L. Sam, T Thompson, and T.L. Thompson, 2008. Natural bioremediation of a nitrate-contaminated soil-and-aquifer system in a desert environment. *Journal of Arid Environments* 72(5):748-763.

McKeon, C., E.P. Glenn, W.J. Waugh, C. Eastoe, F. Jordan and S.G. Nelson, 2006. Growth and water and nitrate uptake patterns of grazed and ungrazed desert shrubs growing over a nitrate contamination plume. *Journal of Arid Environments* 64(1):1-21.

McKeon, C., F.L. Jordan, E.P. Glenn, W.J. Waugh, and S.G. Nelson, 2005. Rapid nitrate and ammonium loss from a contaminated desert soil. *Journal of Arid Environments* 61(1):119-136.

Glenn, E.P., W.J. Waugh, D. Moore, C. McKeon, and S. Nelson, 2001. Evaluation of revegetation methods at an abandoned uranium mill site on the Colorado Plateau, Arizona. *Journal of Environmental Quality* 30:1154-1162.

Lash, D., E.P. Glenn, W.J. Waugh, and D. Baumgartner. 1999. Effects of grazing exclusion and reseeding on a former uranium mill site in the Great Basin Desert, Arizona. *Arid Soil Research and Rehabilitation* 13:253-264.

Glenn, E.P., D. Moore, S. Sanderson, J. Brown, D. Lash, M. Nelson, and W.J. Waugh, 1998. Comparison of growth and morphology of *Atriplex canescens* varieties *occidentalis* and *angustifolia*. *Southwestern Naturalist* 43:176-182.

Symposia and Workshop Abstracts

Carroll, K.C., F.L. Jordan, E.P. Glenn, W.J. Waugh, and M.L. Brusseau, 2008. *Comparison of Nitrate Attenuation Characterization Methods for Groundwater Remediation* (poster). American Geophysical Union Annual Meeting, December 15-19, 2008, San Francisco, California.

Jordan, F., C. McKeon, E.P. Glenn, W.J. Waugh, and S.G. Nelson, 2005. *Rapid Nitrate Loss from the Vadose Zone of a Contaminated Desert Soil*. Soil Water Conservation Society Annual Meeting, July 30–August 4, 2005, Rochester, New York.

Jordan, F., E.P. Glenn, J.C. Glier, C.A. McKeon, and W.J. Waugh, 2006. *Restricting Grazing to Enhance Phytoremediation of a Shallow Aquifer*. Soil Water Conservation Society Annual Meeting, July 22-26, 2006, Keystone, Colorado.

Jordan, F., W.J. Waugh, E.P. Glenn, 2008. *A Plant-Based Approach to Remediating a Nitrate-Contaminated Soil/aquifer System in a Desert Environment*. 2008 Joint Meeting of The Geological Society of America and Soil Science Society of America, October 5-9, 2008. Houston, Texas.

Maxwell, B., M. Carroll, W.J. Waugh, F. Jordan, and E.P. Glenn, 2007. *Remediation of Soil and Ground Water Using Native Desert Phreatophytes*. National Water Conference, USDA-Cooperative State Research, Education, and Extension Service, January 28 - February 1, 2007, Savannah, Georgia.

McKeon, C., E.P. Glenn, D. Moore, and W.J. Waugh, 2001. *Phytoremediation of Nitrate-Contaminated Groundwater by Desert Phreatophytes*. Proceedings of 2001 International Containment and Remediation Technology Conference and Exhibition, June 10-13, 2001, Orlando, Florida.

Waugh, W.J., 2006. *Phytoremediation: Growing Answers for Soil and Ground Water Contamination on the Navajo Nation*. 3rd Annual Navajo Nation Drinking Water Conference, June 12-14, 2006, Window Rock, Arizona (invited paper).

Waugh, W.J., F. Jordan, E.P. Glenn, and R. Bush, 2006. *Enhanced Attenuation of Soil and Ground Water Using Native Desert Phreatophytes*. 2006 Ground Water Summit, National Ground Water Association, April 22-27, San Antonio, Texas (invited paper).

Waugh, W.J., E.P. Glenn, and F. Jordan, 2007a. *Ground Water Restoration at Abandoned Uranium Mills on the Navajo Nation Using Native, Desert Phreatophytes*. Ecological Society of America / Society for Ecological Restoration Joint Meeting, August 5-10, 2007, San Jose, California.

Waugh, W.J., E.P. Glenn, and F. Jordan, 2007b. *Phytoremediation: Growing Answers for Soil and Ground Water Contamination at Monument Valley, Arizona*. Navajo Nation Division of Natural Resources Conference, June 11-14, 2007, Flagstaff, Arizona (invited seminar).

Department of Energy Publications

DOE (U.S. Department of Energy), 1998. *Native Plant Farming and Phytoremediation Pilot Study*. MAC-GWMON 1.8, U.S. Department of Energy, Grand Junction, Colorado.

DOE (U.S. Department of Energy), 2004a. *Monument Valley Ground Water Remediation Pilot Study Work Plan: Monitored Natural Attenuation, Enhanced Attenuation, and Land Farming Pilot Studies*. DOE-LM/GJ757-2004, Office of Legacy Management, U.S. Department of Energy, Grand Junction, Colorado.

DOE (U.S. Department of Energy), 2004b. *Phytoremediation of the Nitrogen-Contaminated Subpile Soil at the Former Uranium Mill Tailings Site in Monument Valley, Arizona: 2004 Status Report*. DOE-LM/GJ768-2004 (ESL-RPT-2004-07), Environmental Sciences Laboratory, U.S. Department of Energy, Grand Junction, Colorado.

DOE (U.S. Department of Energy), 2006. *Soil and Ground Water Phytoremediation Pilot Studies at Monument Valley, Arizona: 2005 Status Report*. DOE-LM/1254-2006, U.S. Department of Energy Office of Legacy Management, Grand Junction, Colorado.

DOE (U.S. Department of Energy), 2007. *Natural and Enhanced Attenuation of Soil and Ground Water at Monument Valley, Arizona, and Shiprock, New Mexico: 2006 Status Report*. DOE-LM/1428, U.S. Department of Energy Office of Legacy Management, Grand Junction, Colorado.

DOE (U.S. Department of Energy), 2008. *Natural and Enhanced Attenuation of Soil and Ground Water at Monument Valley, Arizona, and Shiprock, New Mexico: 2007 Status Report*, LMS/MON/S04243. U.S. Department of Energy Office of Legacy Management, Grand Junction, Colorado.

Waugh, W.J., and E.P. Glenn, 2002. *Phytoremediation of Nitrogen Contamination in Subpile Soils and in the Alluvial Aquifer at the Monument Valley, Arizona, Uranium Mill Tailings Site*. GJO-2002-312-TAR, UMTRA Ground Water Research Project, U.S. Department of Energy Grand Junction Office, Grand Junction, Colorado.

Glenn, E.P. and W.J. Waugh, 2001. *Disposal Cell Cover Moisture Content and Hydraulic Conductivity, Long-Term Surveillance and Maintenance Program Shiprock, New Mexico Site*. GJO-2001-204-TAR, U.S. Department of Energy Grand Junction Office, Grand Junction, Colorado.

Glenn, E.P., W.J. Waugh, and D. Moore, 2000. *Pilot Test Work Plan for Forage Crop Production by Phytoremediation of Nitrate in Ground Water at the Monument Valley UMTRA Site*. U.S. DOE, Grand Junction, Colorado.

Glenn, E.P., W.J. Waugh, C. McKeon, and D. Moore, 1999. *Monument Valley, Arizona, Phytoremediation Pilot Studies*. GJO-99-133-TAR, U.S. Department of Energy, Grand Junction, Colorado.

Waugh, W.J., and E.P. Glenn, 1998. *Monument Valley Ground Water Remediation Work Plan: Native Plant Farming and Phytoremediation Pilot Study*. MAC-GWMON 1.8, UMTRA Ground Water Project, U.S. Department of Energy, Grand Junction, Colorado.

Appendix B
List of Pilot Study Maintenance Activities in 2008

This page intentionally left blank

2008 Site Maintenance Activities

Perform routine maintenance to start irrigation – March 2008:

- Environmental Research Laboratory shop crew repaired freeze damage to PVC lines, serviced batteries, and started irrigation.
- The Stanleys:
 - Repaired damage to irrigation tubing caused by animals; a common problem throughout fields.
 - Replaced emitters as needed.
 - Conducted extensive trimming of overgrown plants to provide:
 - access to irrigation lines for maintenance,
 - access to hydroprobe ports for soil moisture readings, and
 - access throughout field for soil sampling, plant measurements.

Raise transplants in greenhouse:

- Prepared several hundred each *Atriplex canescens* and *Sarcobatus vermiculatus* using seed collected at the site.
- Irrigated, fertilized, and removed weeds as necessary.
- Over the course of the summer, transported transplants to site during routine trips in amounts that the Stanleys could transplant.

Complete irrigation system design modifications (2007, 2008):

- Solar batteries to Well 649 discharged in original Land Farm irrigation schedule because of long run time and cloudy weather.
- Placed all Land Farm plots on 0 parts per million (ppm) N water, Well 618, except for the four plots with 750 ppm N, which remained on Well 649. Irrigation time for the 750 ppm N plots reduced from 4 hours/day to 2 hours/day.
- Additional problem: damage to Well 649 pump and controller caused by low water supply.
- Replaced time clock due to damage caused by power surges, probably from electrical storms. Installed relays to prevent further damage.

Winterize irrigation system:

- Closed valve from Well 618.
- Opened drain valves.
- Installed additional access valves to facilitate draining lines. Vacuumed lines to remove excess water.

Appendix C
**Conceptual Model of Groundwater Solute Attenuation at
the Former Uranium Mill Tailings Site,
Monument Valley, Arizona**

This page intentionally left blank

**CONCEPTUAL MODEL OF GROUNDWATER SOLUTE ATTENUATION AT THE
FORMER URANIUM MILL TAILING SITE, MONUMENT VALLEY, ARIZONA**

Prepared for:

U.S. DEPARTMENT OF ENERGY
Grand Junction Office
Grand Junction, Colorado

Prepared by:

K.C. Carroll, F.L. Jordan, M.L. Brusseau, and E.P. Glenn
**THE SOIL, WATER, AND ENVIRONMENTAL
SCIENCE DEPARTMENT**
University of Arizona
Tucson, Arizona

February 25, 2009

This page intentionally left blank

EXECUTIVE SUMMARY

Contamination of groundwater by nitrate and sulfate continues to be a pervasive issue, and there is great interest in the impact of natural attenuation on risk and management of groundwater contaminant plumes. Transport and fate processes that influence ammonium, nitrate, and sulfate concentrations at a field site near Monument Valley, Arizona, were evaluated. Spatial and temporal concentration data collected from a transect of monitoring wells located along the plume centerline were analyzed to evaluate the overall rates of natural attenuation. The results indicate that nitrate, ammonium, and sulfate concentrations are decreasing due to attenuation processes. Adsorption appears to partly control the transport and fate of ammonium. Sulfate concentrations are most likely controlled by equilibrium formation/dissolution of the solid mineral phase gypsum. Ammonium biotransformation to nitrate (i.e. nitrification) may be occurring in the upgradient, or source, regions, whereas nitrate biotransformation occurs through reduction to atmospheric nitrogen gas (i.e. denitrification) in the downgradient region. The occurrence and rate of denitrification was evaluated through microcosm experiments, nitrogen isotopic fractionation analysis, and solute transport modeling. First-order rate coefficients calculated with each method were comparable. The composite natural attenuation rate coefficient was slightly larger but similar to the denitrification rate coefficient, which suggests that microbially induced decay primarily controls nitrate attenuation at the site. Sulfate reductive biotransformation was not evident from the available data.

1.0 INTRODUCTION

Nitrate is a contaminant that can be persistent in aerobic groundwater systems (e.g., Knowles, 1982; Korom, 1992; Lee et al., 2006). However, reductive biotransformation, or denitrification, can naturally attenuate nitrate in low oxygen or anaerobic subsurface environments (e.g., Knowles, 1982; Korom, 1992; DeSimone and Howes, 1998; Pauwels et al., 1998; McGuire et al., 2002; Smith et al., 2004; McCray et al., 2005). Significant interest has developed in using monitored natural attenuation (MNA) for remediation of nitrate-contaminated groundwater (e.g., ITRC, 2000; Sidle et al., 2000; Smets and Pritchard, 2003; Beller et al., 2004; Groffman et al., 2006; Lee et al., 2006; Oa et al., 2006; Repert et al., 2006; Heatwole and McCray, 2007; Singleton et al., 2007; Jordan et al., 2008; McMahan et al., 2008). Thorough site characterization is essential to evaluate site-specific feasibility and viability of MNA (e.g., Wiedemeier, 1999; Ford et al., 2007). The goals of MNA characterization should include the evaluation of the occurrence, mechanisms, and rates of various processes that may be acting to decrease contaminant concentrations.

Several approaches have been employed to characterize nitrate attenuation in subsurface environments. Spatial and temporal trends in concentrations of nitrate, other nitrogen species, and nitrogen gas in groundwater have been used to assess denitrification (e.g., Bohlke and Denver, 1995; Smith et al., 1996; Blicher-Mathiesen et al., 1998; DeSimone and Howes, 1998; Pauwels et al., 1998; Bohlke et al., 2002; McGuire et al., 2002; Repert et al., 2006). Denitrification has also been evaluated through the use of microbiological methods including microcosm incubations and/or isolation and growth of bacterial strains (e.g., Whitelaw and Rees, 1980; Howard, 1985; Smith and Duff, 1988;

Desimone and Howes, 1996; Aelion et al., 1997; D'Angelo and Reddy, 1999; Oa et al., 2006). Nitrogen stable-isotope fractionation has been used to characterize denitrification (e.g., Mariotti et al., 1988; Bottcher et al., 1990; Smith et al., 1991; Feast et al., 1998; McMahon et al., 1999; Mengis et al., 1999; Sidle et al., 2000; Bohlke et al., 2002; Fukada et al., 2003; Schurmann et al., 2003; Beller et al., 2004; Smith et al., 2004; Chen et al., 2006; Singleton et al., 2007; McMahon et al., 2008). Several solute transport modeling investigations have been presented that included denitrification (e.g., Starr and Parlange, 1975; Schwan et al., 1984; Widdowson et al., 1988; Kinzelbach et al., 1991; Postma et al., 1991; Engesgaard and Kipp, 1992; Lensing et al., 1994; Clement et al., 1997; Conan et al., 2003; Lee et al., 2006; Heatwole and McCray, 2007; Wriedt et al., 2007). Recent reviews have assessed the multitude of methods currently used to characterize denitrification (Smets and Pritchard, 2003; Groffman et al., 2006), and have suggested that denitrification characterization may be improved through comparison of multiple lines of evidence.

2.0 SITE BACKGROUND AND INVESTIGATION METHODS

2.1 Site Description

The Monument Valley site is a former uranium mill tailing site located in northern Arizona (DOE, 1999). Uranium was mined at the site from 1943 to 1968, and seepage through mill tailing stockpiles into the shallow alluvial aquifer has resulted in a groundwater contamination plume. Surface reclamation activities conducted from 1992 through 1994 under the UMTRCA Program consisted of removing the radioactive tailing material from the site (DOE, 1999; McKeon et al., 2005). Nitrate (expressed hereafter as

nitrate-nitrogen or $\text{NO}_3\text{-N}$), sulfate, and ammonium concentrations in groundwater have since begun to decrease, which suggests that MNA may be a viable remediation strategy for the site. Additionally, a phytoremediation pilot study was conducted to remove excess $\text{NO}_3\text{-N}$ from the soil in the former tailing area. Results of the study suggest that denitrification is responsible for $\text{NO}_3\text{-N}$ transformation at the site (McKeon et al., 2006; Jordan et al., 2008). However, groundwater at the Monument Valley site continues to exceed the 10 mg L^{-1} regulatory standard.

Prior site characterization efforts have described the site geology, hydrogeology, and contamination distribution (DOE, 1999). The ammonium, sulfate, and $\text{NO}_3\text{-N}$ contamination occurs in the shallow, unconsolidated alluvial aquifer down-gradient and north of the former tailing area. There is negligible groundwater pumping in the area, and groundwater levels have remained relatively constant over the monitoring period, with an average hydraulic gradient of 0.01 across the entire site (Figure 1). Hydraulic testing suggests that the alluvial aquifer has hydraulic conductivity values that range from 0.5 to 1.0 m day^{-1} from testing done at Well 655, and values ranging from 3.5 to 10.8 m day^{-1} from testing done at Well 765 (DOE, 1999).

Ammonium solutions were used in the uranium processing, sulfate was a reaction product of the leaching process, and leakage of sulfate, $\text{NO}_3\text{-N}$, and ammonium from the unlined tailing material is believed to have generated the groundwater contamination. The tailing material removal (1992 to 1994) coincided with a decrease in the dissolved oxygen concentrations in the alluvial aquifer. Sulfate is generally considered nonreactive, or stable, in groundwater systems. Adsorption to aquifer material is negligible in alkaline groundwater. However, it can precipitate from solution to form the

mineral phase gypsum, which can subsequently re-dissolve when sulfate concentrations decrease. Decreases in redox and dissolved oxygen were the likely cause of NO₃-N decay to atmospheric nitrogen through denitrification, which requires low dissolved oxygen conditions (e.g., Hubner, 1986; Korom, 1992). Although all radioactive tailing materials were removed by 1994, the alluvial aquifer still contains ammonium that may be continually decaying to NO₃-N via nitrification, which would constitute a source for NO₃-N. Previous investigations suggest that NO₃-N undergoes minimal adsorption to the alluvial aquifer material (Sam, 2006). Thus, the primary processes mediating NO₃-N attenuation likely include diffusion, dispersion, and denitrification.

2.2 Groundwater Sampling and Analysis

Groundwater samples were obtained from monitoring wells screened in the alluvial aquifer along a transect extending approximately two km from the source area (or former tailing area). For the present investigation, a series of wells (referred to as transect A-A') located along the major axis of the NO₃-N plume, coincident with the mean hydraulic gradient, were evaluated including numbered Wells 606, 771, 655, 765, 653, 648, and 650 at distances of 91, 308, 311, 533, 828, 828, and 1943 meters from the source area, respectively. Samples were collected and analyzed for NO₃-N and ammonium. Prior to sample collection, wells were purged with a micro-purge pumping unit for approximately three well-bore volumes. Two liters of water were collected from each well and placed in sterile Nalgene bottles. All samples were stored on ice in a cooler or at 4°C until analyzed. Sample analysis for ammonium was conducted using EPA method 350.3 (0.01 mg L⁻¹ detection limit), and NO₃-N analysis was conducted

using EPA method 353.2 (0.004 mg L⁻¹ detection limit). Additionally, prior groundwater sampling and chemical analysis for site-wide monitoring of pH, oxidation-reduction potential, sulfate, NO₃-N, ammonium, and dissolved oxygen between 1985 and 2007 were considered herein.

2.3 Microcosm Experiments

Microcosm assays were conducted using sediment samples collected from the NO₃-N contaminated alluvial aquifer 10-11 m below land surface to obtain direct evidence of denitrification, and to calculate denitrification rate coefficients. Experimental methods followed those employed by Jordan et al. (2008), who conducted similar microcosm experiments with sediments from the site with and without ethanol amendment. The microcosm experiments presented herein were conducted to replicate prior results and extend the analysis to evaluate denitrification kinetics with no amendment, ethanol amendment, and methanol amendment using both concentration decay and isotopic fractionation analysis. Results of the experiments were analyzed by various methods including observation of NO₃-N loss, evaluation of nitrous oxide (N₂O) production, and determination of nitrogen stable isotope fractionation. Quantifying denitrification with stable isotope fractionation requires a significant depletion of NO₃-N to effect a detectable change in ¹⁵N, which may be accomplished by adding a substrate to enhance denitrification (Blackmer and Bremner, 1977).

Replicate slurries were made using 10 g of sediment and 1 mg NO₃-N supplemented with or without 7.5 mg carbon substrate (e.g., ethanol or methanol). N₂O production and NO₃-N depletion were assayed in 250 ml glass microcosms containing

10% acetylene in the headspace to prevent the conversion of N₂O to N₂. Samples were collected from the microcosms at 0, 4, 12, 20, and 43 days after initiation for N₂O and residual NO₃-N analysis. Each treatment initially contained ten replicate flasks and two flasks were sacrificed for NO₃-N and ¹⁵N measurements at each time. The microcosms were maintained at 23(±2)°C. N₂O concentrations were quantified using a Shimadzu GC-14A gas chromatograph with a ⁶³Ni electron capture detector, a 2 ml sampling loop, and two stainless steel packed columns: Porapak Q and Haysep Q both 80/100 mesh (Supelco, Bellefonte, PA). NO₃-N loss was also monitored through time.

Additional microcosm experiments were conducted to test the nitrification potential activity of soil samples collected from the phytoremediation plots near the historic tailing material. Six replicate soil samples (5 g) for each site were placed in glass bottles (125 ml), washed with sodium phosphate buffer (1mM; pH 7.2) to remove soluble NO₃-N, and resuspended in 50 ml of the same buffer containing NH₄Cl (1.5 mM). The slurries were shaken continuously in the dark at 25° C for 3-5 days. The pH was adjusted daily to 7 over the course of the experiment. Half of the samples were treated with 1% (vol/vol) acetylene to inactivate autotrophic ammonia oxidation activity. Aliquots of slurry (2 ml) were taken at 0, 24, and 48 hours. The samples were centrifuged and analyzed for nitrite plus NO₃-N using the colorimetric Szechrome reagent (Jordan et al., 2008).

2.4 Nitrate-N Isotopic Analysis

Stable isotopes of nitrogen (¹⁴N and ¹⁵N) were analyzed in the following manner. Fifty ml from each sacrificed microcosm were added to a 500 ml flask containing 0.4 g

MgO, which was placed on a hotplate for 4 hours at 45° C to remove ammonium (Mulvaney and Khan, 1999). A subsample was analyzed to ensure complete liberation of ammonium prior to evaporating the samples at room temperature in acid washed, oven-dried crucibles. The nitrogen content of the solid crystalline residue was measured on a continuous-flow gas-ratio mass spectrometer (Finnigan Delta PlusXL) at the Geosciences Department, University of Arizona, and the samples were combusted using an elemental analyzer (Costech) coupled to the mass spectrometer. Standardization was based on acetanilide for elemental concentration, and IAEA-N-1 and IAEA-N-2 were used for ¹⁵N with a 95% confidence interval precision of ±0.19 ‰ (or per mil). These analyses differentiated between the two isotopes of nitrogen and quantified total NO₃-N per liter of water.

3.0 DATA ANALYSIS

When evaluating transformation processes and quantifying rate coefficients, it is important to distinguish between composite and process-specific rate coefficients. Composite attenuation rate coefficients incorporate all processes contributing to attenuation of the target contaminant, and are calculated by analyzing changes in aqueous concentration data as a function of space or time. Process-specific rate coefficients represent a specific attenuation mechanism. For example, biotransformation rate coefficients represent microbial-mediated transformation processes. Of particular interest for this investigation, denitrification is a multi-step process through which NO₃-N is reduced to atmospheric nitrogen (e.g., Knowles, 1982; Korom, 1992; Kendall and McDonnell, 1998), and it is commonly the most significant attenuation process for NO₃-

N in groundwater. For this study, natural attenuation and biological denitrification were both assumed to follow first-order decay. This simplified approach has been deemed reasonable for quantifying denitrification in previous studies (e.g., Pauwels et al., 1998; Smith et al., 2004; McCray et al., 2005).

3.1 Spatial Data Analysis

The field-scale composite rate coefficient describes the changes in concentration with distance (measured at a point in time) away from a source area along the major axis of the plume. Least squares regression was used to determine the exponential equation that best described the data:

$$C(x) = C_0 e^{-(k/v)x} \quad (1)$$

where $C(x)$ is the concentration at distance x , v is the velocity of the solute transported in groundwater, and k is the composite-rate coefficient for MNA.

3.2 Stable Isotope Analysis

Denitrification was assessed by determining compound-specific stable isotope fractionation. Biological denitrification leads to an enrichment of the heavy isotope, ^{15}N , within the remaining $\text{NO}_3\text{-N}$ because denitrification favors the light isotope, ^{14}N (Mariotti et al., 1988). The nitrogen isotopic composition is typically reported as $\delta^{15}\text{N} \text{‰}$ (Kendall and Aravena, 1999):

$$\delta^{15}\text{N}(\text{‰}) = \left(\frac{R_{\text{sample}}}{R_{\text{standard}}} - 1 \right) \times 1000 \quad (2)$$

where R_{sample} is the isotopic ratio ($^{15}\text{N}/^{14}\text{N}$) measured in a sample and R_{standard} is the ratio of the atmospheric standard. Denitrification attributed enrichment of ^{15}N in each sample

was quantified by a simplified form of the Rayleigh equation (Kendall and McDonnell, 1998; Kendall and Aravena, 1999; Fukada et al., 2003):

$$\delta_R = \delta_{R_0} + \varepsilon \ln\left(\frac{C_t}{C_0}\right) \quad (3)$$

where δ_R is the $\delta^{15}\text{N}$ value of the $\text{NO}_3\text{-N}$ at time (t), δ_{R_0} is the initial $\delta^{15}\text{N}$ value of the $\text{NO}_3\text{-N}$, ε is the enrichment factor, C_t is the $\text{NO}_3\text{-N}$ concentration at time (t) and C_0 is the initial $\text{NO}_3\text{-N}$ concentration. The enrichment factor can be used to estimate the extent of biological denitrification occurring in a groundwater system compared to other processes that might reduce $\text{NO}_3\text{-N}$ levels (Smith et al., 2004). First-order rate coefficients for denitrification were calculated from the nitrogen stable-isotope enrichment data upon calculation of the enrichment factor. The rate coefficients (k) were calculated as (Morrill et al., 2005):

$$\alpha = \frac{1000 + \delta_R}{1000 + \delta_{R_0}} \quad (4)$$

$$\varepsilon = 1000(\alpha - 1) \quad (5)$$

$$\left(\frac{\delta_R}{1000} + 1\right) = \left(\frac{\delta_{R_0}}{1000} + 1\right) \exp(k[(1 - \alpha)t]) \quad (6)$$

where α is the fractionation factor, and k is the rate coefficient for denitrification. The $\delta^{15}\text{N}$ results of the samples collected during the microcosm experiments were used to obtain the enrichment factors (ε) and fractionation factors (α) that were used to calculate denitrification rate coefficients. Equation 6 was used to quantify denitrification in the laboratory microcosm experiments.

Isotopic evidence for denitrification may also be observed in the field if sufficient transformation has occurred to result in a measurable fractionation of ^{15}N . Over time,

NO₃-N from the source area has been transported down-gradient in the aquifer. If denitrification has occurred in the plume, NO₃-N at the leading edge of the plume should be more enriched in ¹⁵N than NO₃-N closer to the source area. The rate of denitrification in the plume can therefore be calculated by measuring ¹⁵N enrichment in samples taken from the plume at increasing distances from the source area. Subsamples of groundwater collected at several monitoring wells along the A-A' transect were analyzed for nitrogen stable isotopes ¹⁵N and ¹⁴N using the methods discussed above for the microcosm samples but with larger sample volumes (200 ml), and the δ¹⁵N results were used to obtain the field-scale denitrification rate coefficient (k) (Equation 6) assuming the initial value for δ¹⁵N (-7) was the most enriched value measured from the groundwater samples.

3.4 Geochemical Modeling Analysis

PHREEQC Version 2.2 (Parkhurst and Appelo, 1999), an equilibrium speciation and mineral-water mass-transfer code developed by the United States Geological Survey, was used for the calculation of aqueous complex speciation and mineral saturation indices based on the aqueous composition of the groundwater obtained from chemical analysis of samples collected at Well 653. Chemical reactions and thermodynamic constants required for the calculations were taken from a standard database that is distributed with the software. The model was used to evaluate the composition of the groundwater, and was used to predict solid minerals that may form (precipitate) from the groundwater solution or are approximately at equilibrium with the groundwater.

3.5 Numerical Modeling Analysis

Numerical modeling was used to quantify solute transport and attenuation processes including denitrification for the NO₃-N plume at the Monument Valley site. A one-dimensional groundwater flow model was developed and calibrated to provide the pore-water velocity for the solute-transport model. The numerical model MODFLOW (Harbaugh and McDonald, 1996) was used for the groundwater flow simulations. The model discretization consisted of 64 cells that were each 30.5 m long, which extended from the source area to beyond Well 650 along the A-A' transect. Constant-head boundary conditions were imposed on the first (1472 m above sea level) and last cell (1455 m above sea level). The results of the groundwater flow modeling were used within the identical model domain for simulating transport of NO₃-N along the A-A' transect.

The commonly used numerical solute transport model MT3DMS (Zheng and Wang, 1999) was employed to solve the advection-dispersion equation:

$$\frac{\partial(\theta C)}{\partial t} = \frac{\partial}{\partial x_i} \left(\theta D_{ij} \frac{\partial C}{\partial x_j} \right) - \frac{\partial}{\partial x_i} (\theta v_i C) - k \theta C \quad (8)$$

where θ is the porosity, C is the groundwater solute concentration, t is time, x is distance, D is the hydrodynamic dispersion coefficient tensor, v is the pore-water velocity, and k is the first-order rate coefficient for denitrification. The dispersion tensor accounts for diffusion/dispersion in three dimensions through the evaluation of the longitudinal, horizontal transverse, and vertical transverse dispersivities and associated velocities. The NO₃-N concentration distribution observed from the monitoring-well data in 1993 was used for the initial condition. Initial simulations indicated that the model required a source boundary condition at the up-gradient boundary to facilitate calibration to the

NO₃-N concentration data. A source decay rate (0.02 yr⁻¹) was calculated from the local-composite attenuation rate coefficient at Well 606, which is adjacent to the source zone.

The results of miscible-displacement experiments conducted with porous media collected from the alluvial aquifer near Well 606 were used to evaluate adsorption and dispersion properties (Sam, 2006). NO₃-N exhibited minor retardation ($R = 1.2$) due to adsorption, which was accounted for in the transport modeling assuming a linear isotherm ($K_d = 0.028 \text{ L Kg}^{-1}$). The column-scale dispersivity (0.05 cm) was up-scaled to the field scale (14.5 cm) using a standard linear scaling approach (Gelhar et al., 1992). Horizontal and vertical transverse dispersivities were assumed to be 10% of the longitudinal dispersivity. The porosity was assumed to be 0.25, and the molecular diffusion coefficient ($8.64 \times 10^{-5} \text{ m}^2 \text{ day}^{-1}$) was calculated from a correlation relating the diffusion coefficient to the molecular weight (Schwarzenbach et al., 1993). Model simulations were calibrated to the measured NO₃-N concentration distribution along the A-A' transect for the years 1998, 2003, and 2007 by varying the denitrification first-order rate coefficient.

4.0 RESULTS AND DISCUSSION

4.1 Laboratory Microcosm Experiments and Analyses

The results of the microcosm experiments are presented in Figure 2 as the biotransformation of NO₃-N and production of N₂O over time. The results show that N₂O production, which is the decay product of denitrification in the presence of acetylene, coincides with the decay of NO₃-N. The denitrification of NO₃-N without amendment was relatively slow compared to the decay observed with both ethanol and

methanol amendments, which showed nearly complete denitrification of NO₃-N over the assay periods. The magnitude and rate of denitrification enhancement was greater for ethanol amended compared to the methanol amended and nonamended microcosms. The denitrification rate coefficients calculated from microcosm concentration results were 0.7 yr⁻¹ without substrate amendment, 14.5 yr⁻¹ with methanol amendment, and 17.6 yr⁻¹ with ethanol amendment (Table 1).

The NO₃-N isotopic fractionation data obtained from the laboratory microcosm experiments are presented in Figure 3. The nonamended microcosms did not undergo denitrification to the extent required to observe fractionation, and denitrification in the ethanol amended microcosms occurred prior to measurement of fractionation. Thus isotopic analyses were conducted only for the methanol-amended samples. The rate coefficients for the methanol-amended microcosms were very similar for both the concentration decay and isotopic fractionation analyses (Table 1). The results of a linear regression analysis are also shown that was used to calculate the fractionation factor ($\alpha = 1 + \text{slope}$) attributed to denitrification in the methanol-amended microcosm (Figure 3).

4.2 Temporal and Spatial Analysis of Field Data

The pH and redox values and concentrations of sulfate, ammonium, dissolved oxygen, and NO₃-N in groundwater samples collected from monitoring wells along the A-A' transect (Figure 1) were plotted versus time since 1985 to evaluate natural attenuation behavior. The pH values remained relatively constant (Figure 4a), whereas the oxidation-reduction potential significantly decreased during the surface reclamation period of 1992-1996 (Figure 4b). Both sulfate (Figure 4c) and ammonium concentrations

(Figure 4d) followed a decreasing trend throughout time for each of the monitoring wells along A-A'. The dissolved oxygen concentrations (data not shown) in the aquifer decreased from 1992 to 1994 to between 0.1 and 1 mg L⁻¹, which is in the range required to initiate denitrification (e.g., Robertson and Kuenen, 1984; Hubner, 1986). Decreases in groundwater NO₃-N concentrations were observed near the source area (Figure 4e), whereas increasing NO₃-N concentrations were observed at distances down-gradient from the source area (e.g., Wells 653 and 650). Regression analyses are also shown for selected wells on the ammonium and NO₃-N plots, and indicate that exponential decay (Equation 1) provides a reasonable description of the data. The local-scale composite rate coefficient calculated with the data from Well 606 (0.02 yr⁻¹) represents the rate of NO₃-N attenuation adjacent to the source zone (Table 1). The low magnitude suggests that concentration attenuation at that location is limited. Additionally, the local-scale composite rate coefficients for ammonium and NO₃-N at Well 606 are similar, which suggests that nitrification is acting as the current source of NO₃-N. The increasing concentration trends at the edge of the plume suggest that the plume is moving or expanding.

The spatial behavior of the groundwater contamination plume was evaluated by plotting NO₃-N concentrations versus distance along the A-A' transect from the source area. The pH values increase with distance downgradient away from the source area (Figure 5a), whereas the oxidation-reduction potential significantly decreased after 1994 to a relatively stable range throughout the transect (Figure 5b). Figures 5c, 5d, and 5e contain the sulfate, ammonium, and NO₃-N spatial data for selected years, respectively. The concentrations of both ammonium and NO₃-N decrease with distance from the

source area for each of the years evaluated. The sulfate decreases with distance, overall. However, the concentrations vary about a mean of approximately 1000 mg/L over the majority of investigation area with the decrease only occurring at the furthest downgradient monitoring well. The stability of the sulfate suggests that mineral/groundwater equilibrium may be controlling the concentrations for the majority of the groundwater plume. The geochemical modeling of groundwater speciation was used to predict the minerals that are at equilibrium or might be able to precipitate from the groundwater solution, and the results are listed in Table 2. The results suggest that gypsum is at equilibrium with the groundwater at Well 653, and the precipitation/redissolution of gypsum could control the groundwater concentration distribution. However, there are insufficient available data to determine if sulfate is undergoing reduction or which other attenuation processes may be impacting sulfate.

The dissolved oxygen content (data not shown) has decreased over time, especially for the region greater than approximately 610 m from the source area. The 1992 data suggest an increase in dissolved oxygen concentration or a concentration spike at approximately 300 m down-gradient of the source area. However, since that time oxygen concentrations have shown a decreasing trend with distance from the source area. The $\text{NO}_3\text{-N}$ plume extends further from the source than the ammonium plume, which would be expected if nitrification and/or adsorption of ammonium were occurring. Exponential regression analysis for selected years indicates that exponential decay provides a reasonable description of the data. The field-scale composite rate coefficient calculated for $\text{NO}_3\text{-N}$ from the regression equation was 0.7 yr^{-1} for the 1993 data and 0.6

yr⁻¹ for the 2007 data, which suggests a relative consistency in attenuation rates over time at the site (Table 1).

The NO₃-N isotopic fractionation data obtained from the groundwater analysis are presented in Figure 6. Field-scale denitrification was quantified through δ¹⁵N enrichment analysis of groundwater samples collected along the A-A' transect monitoring wells. The NO₃-N becomes progressively more enriched in ¹⁵N relative to ¹⁴N with travel time/distance from the source area (Figure 6a), which suggests that denitrification is preferentially transforming ¹⁴N as opposed to ¹⁵N. The enrichment of ¹⁵N increases with decreasing NO₃-N concentration, suggesting that ¹⁵N fractionation occurs as a result of denitrification and therefore that enrichment can be used to evaluate the magnitude and rate of denitrification. The results of a linear regression analysis are presented that were used to calculate the fractionation factor attributed to denitrification in the alluvial aquifer along transect A-A' (Figure 6b), which was used for the calculation of the denitrification rate coefficient (0.3 yr⁻¹, Table 1).

4.3 Numerical Modeling Analysis

The results of the MODFLOW model calibration are presented in Figure 7a along with the observed groundwater elevations from 2002 and 2007. Calibration of the model was accomplished by comparing simulated and measured groundwater elevation data for 2007. The simulated groundwater elevations compare favorably with the observed data along A-A' (Figure 7a) with a root mean square error (RMSE) of 0.4 m (0.01% average error).

Two zones of different hydraulic conductivities were used in the simulations, which resulted in the change in groundwater elevation gradient observed in Figure 7a. The values calibrated for the two zones were 4.9 m day^{-1} for the region extending from the source zone to 610 m down-gradient, and 7.6 m day^{-1} for the zone from 610 m to 1951 m. The previously mentioned hydraulic testing data suggests that hydraulic conductivity increases in the direction of groundwater flow from Well 655 to Well 765, and model calibrated values are within the previously measured range from 0.5 m day^{-1} at Well 655 to 10.8 m day^{-1} at Well 765.

The simulated spatial distribution of $\text{NO}_3\text{-N}$ concentrations obtained from calibration of the solute-transport model to the measured data is presented in Figure 7b. The calibrated simulation compares well with the observed concentration data with a RMSE of 3.9 mg L^{-1} (0.7% average error) for 2007. The optimal calibration was achieved by using two zones with different rates of denitrification. The first zone, with a rate coefficient of 0.07 yr^{-1} , was applied from the source area to approximately 610 m down-gradient, and a rate coefficient of 0.44 yr^{-1} was used for the zone from 610 m to 1951 m down-gradient of the source. The zone locations were selected based on observation of a change in ammonium concentrations and redox conditions along the A-A' transect, and correspond to the hydraulic conductivity zones. The apparent spatial variability in denitrification activity may be a result of spatial variability in the nitrification process (greater near the source zone) and in dissolved oxygen concentrations (which are lower down-gradient).

4.4 Comparison of Rate Coefficient Data

Potential source-zone processes were evaluated through comparison of the local-scale and field-scale composite rate coefficients. The NO₃-N and ammonium local-scale composite rate coefficients are similar at Well 606. This suggests that nitrification may be a source of NO₃-N at the site. The results of microcosm experiments conducted to evaluate potential nitrification activity indicated a positive potential for nitrification in the area near the source zone (data not shown). These results support the possibility that nitrification is a continuing source of NO₃-N. The local-scale composite NO₃-N decay coefficient was significantly lower than the field-scale composite value (Table 1). This suggests that the source-zone decay rate, as assumed to be represented by the local-scale rate coefficient, is more rate limiting than the solute transport attenuation rate, as provided by the composite-scale rate coefficient. Thus, source-zone decay appears to be the rate-limiting step for NO₃-N attenuation at this site.

An integrated characterization approach using various methods was used in this investigation to determine first-order rate coefficients for natural attenuation and denitrification. An interesting result is that the rate coefficients were comparable for the different methods used (Table 1). The spatially-weighted average of the model-calibrated denitrification rate coefficients (0.3 yr⁻¹) is identical to the denitrification rate coefficient calculated from the field isotopic data. These two field-scale values are slightly lower than, but similar to, the laboratory-scale rate coefficient (0.7 yr⁻¹). This observation is contrary to typical observations wherein denitrification rate coefficients determined at the laboratory scale are significantly higher than field-scale rate coefficients. The field-scale denitrification rate coefficients are slightly smaller than but similar to the field-scale

composite rate coefficient (which accounts for all natural attenuation processes). This suggests that microbially induced decay primarily controls nitrate attenuation at the site. The rate coefficients reported herein fall within the wide range (0.02 to 6 yr⁻¹) of values reported in prior studies (e.g., McMahon et al., 2008).

4.5 Conceptualization of Sulfur and Nitrogen Interactions

Characterizing the behavior and fate of nitrate, sulfate, and ammonium at the Monument Valley site is required for the development of a site-wide conceptual model and for the development of a groundwater remediation strategy for the site. The interactions of these chemical species with the microbial community as well as their retention properties in the aquifer are of particular interest. Interactions with the microbial community involve microbially mediated transformation reactions. Additional reactions of interest involve adsorption or formation/dissolution of solid mineral phases.

Various researchers have investigated the interactions of nitrate and sulfate with solid aquifer materials, which include adsorption and mineral forming reactions. The major factors defining anion sorption are the concentration of the ion, the presence of specific or non-specific binding sites, the pH of the system, and the presence of competing electrolytes. The primary mechanism of both sulfate and nitrate sorption is non-specific electrostatic interaction, but both anions are capable of forming more specific complexes with solid aquifer materials. Specific sorption is the result of ligand exchange, and occurs primarily in soils with high concentrations of aluminum and iron hydroxides and oxyhydroxides (Fuller et al, 1985), and may result in the formation of stable and relatively static covalent structures (Bohn, 1985). Both sorption mechanisms

are highly pH dependent, with the majority of sorption occurring at lower pH values (e.g., pH<6 for sulfate). Competitive reactions also play a role in nitrate and sulfate sorption processes. Xu et al. (2005) demonstrated that low molecular weight organic acids, released by plant roots may compete for anionic sorption sites in the rhizosphere, reducing the number of available sites for electrostatic binding of nitrate, and presumably sulfate. At Monument Valley, pH values (Figure 4a) are more alkaline than those typically expected to demonstrate significant anionic sorption. Thus, it is unlikely that sulfate or nitrate undergo significant adsorption at the site, which is supported by the previous NO₃-N sorption experiment discussion (Section 3.5). NO₃-N does not typically form soil minerals. However, sulfate does form gypsum in soils, which is a calcium-sulfate mineral.

Ammonium is a cation that, unlike anions NO₃-N and sulfate, has significant sorption behavior in alkaline soils, and the sorption is primarily controlled by the quantity and accessibility of negatively charged mineral surfaces (Buss et al, 2004). Such surfaces are typically seen in alkaline soils, such as those found at Monument Valley. At the neutral and higher pH values typical of the subpile area and downgradient plume, metal hydroxides and oxy-hydroxides are the mineral surfaces expected to be most important in ammonium interactions with the solid phase, (Sverjensky and Sahai, 1996; DeSimone et al, 1997), and Parks (1965) states that Mn oxides are more likely to contribute to ammonium sorption than Fe hydroxides. The cation exchange capacity of a soil is also an important parameter to consider, as well as the order of preferential cation exchange [Al³⁺ > Ca²⁺ > Mg²⁺ > NH⁴⁺ > H⁺ > Na⁺ (Domenico and Schwartz, 1998)].

Loss of ammonium through nitrification affects its fate and transport, as well. Nitrification is the biotransformation of ammonium to $\text{NO}_3\text{-N}$. Oxygen availability is often the limiting factor for aerobic nitrification processes. This can confine the zone of active nitrification to the edges of an ammonium plume. Aerobic nitrification typically occurs at pH values between 6 and 8.5 (USEPA 1993).

It has been hypothesized that sequential or concurrent nitrification and denitrification may play a role in the persistence of nitrate at the Monument Valley site. Concurrent nitrification and denitrification have been reported most commonly in wastewater treatment systems, but also in soil, as well. *Diaphorobacter* sp. isolated from a wastewater treatment plant is reported to be capable of both nitrification and denitrification in aerobic conditions (Khardenavis et al 2007). Abbasi and Adams (2000) used intact cores from the upper 7.5cm of a soil profile and showed concurrent nitrification/denitrification in a sandy clay loam of approximately pH 5.

$\text{NO}_3\text{-N}$ and sulfate can both be reduced in anaerobic groundwater systems. Though the canonical presentation of terminal electron acceptors states that $\text{NO}_3\text{-N}$ is preferentially reduced before sulfate, there are limited reports of $\text{NO}_3\text{-N}$ and sulfate being co-reduced. McGuire et al (2002) found that when introduced into a sandy aquifer together, $\text{NO}_3\text{-N}$ and sulfate were co-reduced *in situ*. This co-reduction was found to occur only *in situ*, which suggests that the reactions utilize aquifer mineral phases as well as dissolved species. Co-reduction has also been reported at a landfill in Denmark (Jakobsen and Postma, 1999). However, as noted above, at the Monument Valley Site there is insufficient data to fully evaluate the potential for sulfate reduction or natural attenuation.

5.0 SUMMARY

The results of various methods used for the characterization of groundwater contamination attenuation at the Monument Valley UMTRA site have been presented herein. Surface remediation of tailing materials at the site occurred prior to 1994. However, ammonium, sulfate, $\text{NO}_3\text{-N}$ remain in the groundwater system, and $\text{NO}_3\text{-N}$ concentrations measured at monitoring wells continue to exceed the regulatory limit. The results reported herein indicate that $\text{NO}_3\text{-N}$, ammonium, and sulfate concentrations are decreasing due to attenuation processes. Adsorption appears to partly control the transport and fate of ammonium. Sulfate concentrations are most likely controlled by equilibrium formation/dissolution of the solid mineral phase gypsum. Sulfate reductive biotransformation was not evident from the available data. ammonium biotransformation to $\text{NO}_3\text{-N}$ (i.e. nitrification) may be occurring in the upgradient, or source, regions, whereas $\text{NO}_3\text{-N}$ -biotransformation occurs through reduction to atmospheric nitrogen gas (i.e. denitrification) in the downgradient region. The rate of denitrification was characterized through a variety of methods including microcosm concentration decay, microcosm isotopic fractionation, field-scale isotopic fractionation, and solute-transport modeling. The field-scale composite rate coefficient as calculated from groundwater concentration data was similar to the field-scale denitrification rate coefficient, which suggests that denitrification is the predominant process contributing to the overall $\text{NO}_3\text{-N}$ attenuation. The results suggest that $\text{NO}_3\text{-N}$ in the Monument Valley alluvial aquifer is undergoing natural attenuation.

6.0 REFERENCES

- Abbasi, M.K., Adams, W.A., 2000. Estimation of simultaneous nitrification and denitrification in grassland soil associated with urea-N using N-15 and nitrification inhibitor. *Biology and Fertility of Soils*, 31(1), 38-44.
- Aelion, C.M., Shaw, J.N., Wahl, M., 1997. Impact of suburbanization on ground water quality and denitrification in coastal aquifer sediments. *Journal of Experimental Marine Biology and Ecology* 213, 31-51.
- Beller, H.R., Madrid, V., Hudson, G.B., McNab, W.W., Carlsen, T., 2004. Biogeochemistry and natural attenuation of nitrate in groundwater at an explosives test facility. *Applied Geochemistry* 19, 1483-1494.
- Blackmer, A.M., Bremner, J.M., 1977. Denitrification of Nitrate in Soils under Different Atmospheres. *Soil Biology & Biochemistry* 9, 141-142.
- Blicher-Mathiesen, G., McCarty, G.W., Nielsen, L.P., 1998. Denitrification and degassing in groundwater estimated from dissolved dinitrogen and argon. *Journal of Hydrology* 208, 16-24.
- Bohlke, J.K., Denver, J.M., 1995. Combined Use of Groundwater Dating, Chemical, and Isotopic Analyses to Resolve the History and Fate of Nitrate Contamination in 2 Agricultural Watersheds, Atlantic Coastal-Plain, Maryland. *Water Resources Research* 31, 2319-2339.
- Bohlke, J.K., Wanty, R., Tuttle, M., Delin, G., Landon, M., 2002. Denitrification in the recharge area and discharge area of a transient agricultural nitrate plume in a glacial outwash sand aquifer, Minnesota. *Water Resources Research* 38, Doi 10.1029/2001wr000663.
- Bohn, H.L., McNeal, B.L., O'Connor, G.A., 1985. *Soil Chemistry*. 2nd ed. New York: John Wiley & Sons. 341 p.
- Bottcher, J., Strebel, O., Voerkelius, S., Schmidt, H.L., 1990. Using Isotope Fractionation of Nitrate Nitrogen and Nitrate Oxygen for Evaluation of Microbial Denitrification in a Sandy Aquifer. *Journal of Hydrology* 114, 413-424.
- Buss, S.R., Herbert, A.W., Morgan, P., Thornton, S.F., Smith, J.W.N., 2004. A review of ammonium attenuation in soil and groundwater. *Quarterly Journal of Engineering Geology and Hydrogeology*, 37, 347-359.
- Chen, J.Y., Tang, C.Y., Yu, J.J., 2006. Use of O-18, H-2 and N-15 to identify nitrate contamination of groundwater in a wastewater irrigated field near the city of Shijiazhuang, China. *Journal of Hydrology* 326, 367-378.

Clement, T.P., Peyton, B.M., Skeen, R.S., Jennings, D.A., Petersen, J.N., 1997. Microbial growth and transport in porous media under denitrification conditions: Experiments and simulations. *Journal of Contaminant Hydrology* 24, 269-285.

Conan, C., Bouraoui, F., Turpin, N., de Marsily, G., Bidoglio, G., 2003. Modeling flow and nitrate fate at catchment scale in Brittany (France). *Journal of Environmental Quality* 32, 2026-2032.

D'Angelo, E.M., Reddy, K.R., 1999. Regulators of heterotrophic microbial potentials in wetland soils. *Soil Biology & Biochemistry* 31, 815-830.

Desimone, L.A., Howes, B.L., 1996. Denitrification and nitrogen transport in a coastal aquifer receiving wastewater discharge. *Environmental Science & Technology* 30, 1152-1162.

DeSimone, L.A., Howes, B.L., 1998. Nitrogen transport and transformations in a shallow aquifer receiving wastewater discharge: A mass balance approach. *Water Resources Research* 34, 271-285.

DeSimone, L.A., Howes, B.L., Barlow, P.M., 1997. Mass-balance analysis of reactive transport and cation exchange in a plume of wastewater-contaminated groundwater. *Journal of Hydrology*, 203(1-4), 228-249.

DOE, 1999. Final Site Observational Work Plan for the UMTRA Project Site at the Monument Valley, Arizona. U.S. Department of Energy, Office of Legacy Management, Document:U0018101.

Domenico, P.A., Schwartz, F.W., 1998. *Physical and Chemical Hydrogeology* 2nd ed. New York: John Wiley & Sons. 533 p.

Engesgaard, P., Kipp, K.L., 1992. A Geochemical Transport Model for Redox-Controlled Movement of Mineral Fronts in Groundwater-Flow Systems - a Case of Nitrate Removal by Oxidation of Pyrite. *Water Resources Research* 28, 2829-2843.

Feast, N.A., Hiscock, K.M., Dennis, P.F., Andrews, J.N., 1998. Nitrogen isotope hydrochemistry and denitrification within the Chalk aquifer system of north Norfolk, UK. *Journal of Hydrology* 211, 233-252.

Ford, R.G., Wilkin, R.T., Puls, R.W., 2007. Monitored Natural Attenuation of Inorganic Contaminants in Ground Water Volume 1 - Technical Basis for Assessment. In: Agency, U.S.E.P. (Ed.). National Risk Management Research Laboratory Office of Research and Development. U.S. Environmental Protection Agency, Cincinnati, Ohio.

Fukada, T., Hiscock, K.M., Dennis, P.F., Grischek, T., 2003. A dual isotope approach to identify denitrification in groundwater at a river-bank infiltration site. *Water Research* 37, 3070-3078.

- Fuller, R. D., David, M. B., Driscoll, C. T., 1985. Sulfate adsorption relationships in forested spodosols of the northeastern USA. *Soil Science Society of America Journal*, 49(4), 1034-1040.
- Gelhar, L.W., Welty, C., Rehfeldt, K.R., 1992. A critical review of data on field-scale dispersion in aquifers. *Water Resources Research* 28, 1955-1974.
- Groffman, P.M., Altabet, M.A., Bohlke, J.K., Butterbach-Bahl, K., David, M.B., Firestone, M.K., Giblin, A.E., Kana, T.M., Nielsen, L.P., Voytek, M.A., 2006. Methods for measuring denitrification: Diverse approaches to a difficult problem. *Ecological Applications* 16, 2091-2122.
- Harbaugh, A.W., McDonald, M.G., 1996. User's documentation for MODFLOW-96, an update to the U.S. Geological Survey modular finite-difference ground-water flow model. USGS Open-File Report 96-485.
- Heatwole, K.K., McCray, J.E., 2007. Modeling potential vadose-zone transport of nitrogen from onsite wastewater systems at the development scale. *Journal of Contaminant Hydrology* 91, 184-201.
- Howard, K.W.F., 1985. Denitrification in a Major Limestone Aquifer. *Journal of Hydrology* 76, 265-280.
- Hubner, H., 1986. Isotope effects of nitrogen in the soil and biosphere. In: Fritz, P., Fontes, J.C. (Eds.). *Handbook of Environmental Isotope Geochemistry*, Vol 2b, The Terrestrial Environment. Elsevier, pp. 361-425.
- ITRC, 2000. *Emerging Technologies for Enhanced In Situ Bionitrification (EISBD) of Nitrate-Contaminated Ground Water*.
- Jakobsen, R., Postma, D., 1999. Redox zoning, rates of sulfate reduction and interactions with Fe-reduction and methanogenesis in a shallow sandy aquifer, Romo, Denmark. *Geochimica et Cosmochimica Acta*, 63(1), 137-151.
- Jordan, F., Waugh, W.J., Glenn, E.P., Sam, L., Thompson, T., Thompson, T.L., 2008. Natural bioremediation of a nitrate-contaminated soil-and-aquifer system in a desert environment. *Journal of Arid Environments* 72, 748-763.
- Kendall, C., Aravena, R., 1999. Nitrate isotopes in groundwater systems. In: Cook, P., Herczeg, A. (Eds.). *Environmental Tracers in Subsurface Hydrology*. Kluwer Academic Publishers, Norwell, MA pp. 261-297.
- Kendall, C., McDonnell, J.J. (Eds.), 1998. *Isotope Tracers in Catchment Hydrology*. Elsevier, New York.
- Kinzelbach, W., Schafer, W., Herzer, J., 1991. Numerical Modeling of Natural and Enhanced Denitrification Processes in Aquifers. *Water Resources Research* 27, 1123-1135.

- Khardenavis, A.A., Kapley, A., Purohit, H.J., 2007. Simultaneous nitrification and denitrification by diverse diaphorobacter sp. *Applied Microbiology and Biotechnology*, 77(2), 403-409.
- Knowles, R., 1982. Denitrification. *Microbiological Reviews* 46, 43-70.
- Korom, S.F., 1992. Natural Denitrification in the Saturated Zone - a Review. *Water Resources Research* 28, 1657-1668.
- Lee, M.S., Lee, K.K., Hyun, Y.J., Clement, T.P., Hamilton, D., 2006. Nitrogen transformation and transport modeling in groundwater aquifers. *Ecological Modelling* 192, 143-159.
- Lensing, H.J., Vogt, M., Herrling, B., 1994. Modeling of Biologically Mediated Redox Processes in the Subsurface. *Journal of Hydrology* 159, 125-143.
- Mariotti, A., Landreau, A., Simon, B., 1988. N-15 Isotope Biogeochemistry and Natural Denitrification Process in Groundwater - Application to the Chalk Aquifer of Northern France. *Geochimica Et Cosmochimica Acta* 52, 1869-1878.
- McCray, J.E., Kirkland, S.L., Siegrist, R.L., Thyne, G.D., 2005. Model parameters for simulating fate and transport of on-site wastewater nutrients. *Ground Water* 43, 628-639.
- McGuire, J.T., Long, D.T., Klug, M.J., Haack, S.K., Hyndman, D.W., 2002. Evaluating behavior of oxygen, nitrate, and sulfate during recharge and quantifying reduction rates in a contaminated aquifer. *Environmental Science & Technology* 36, 2693-2700.
- McKeon, C., Glenn, E.P., Waugh, W.J., Eastoe, C., Jordan, F., Nelson, S.G., 2006. Growth and water and nitrate uptake patterns of grazed and ungrazed desert shrubs growing over a nitrate contamination plume. *Journal of Arid Environments* 64, 1-21.
- McKeon, C.A., Jordan, F.L., Glenn, E.P., Waugh, W.J., Nelson, S.G., 2005. Rapid nitrate loss from a contaminated desert soil. *Journal of Arid Environments* 61, 119-136.
- McMahon, P.B., Bohlke, J.K., Bruce, B.W., 1999. Denitrification in marine shales in northeastern Colorado. *Water Resources Research* 35, 1629-1642.
- McMahon, P.B., Bohlke, J.K., Kauffman, L.J., Kipp, K.L., Landon, M.K., Crandall, C.A., Burow, K.R., Brown, C.J., 2008. Source and transport controls on the movement of nitrate to public supply wells in selected principal aquifers of the United States. *Water Resources Research* 44, Doi 10.1029/2007wr006252.
- Mengis, M., Schiff, S.L., Harris, M., English, M.C., Aravena, R., Elgood, R.J., MacLean, A., 1999. Multiple geochemical and isotopic approaches for assessing ground water NO₃- elimination in a riparian zone. *Ground Water* 37, 448-457.
- Morrill, P.L., Lacrampe-Couloume, G., Slater, G.F., Sleep, B.E., Edwards, E.A., McMaster, M.L., Major, D.W., Lollar, B.S., 2005. Quantifying chlorinated ethene

degradation during reductive dechlorination at Kelly AFB using stable carbon isotopes. *Journal of Contaminant Hydrology* 76, 279-293.

Mulvaney, R.L., Khan, S.A., 1999. Use of diffusion to determine inorganic nitrogen in a complex organic matrix. *Soil Science Society of America Journal* 63, 240-246.

Oa, S.W., Kim, G., Kim, Y., 2006. Determination of electron donors by comparing reaction rates for in situ bioremediation of nitrate-contaminated groundwater. *Journal of Environmental Science and Health Part a-Toxic/Hazardous Substances & Environmental Engineering* 41, 2359-2372.

Parkhurst DL, Appelo CAJ. 1999. User's guide to PHREEQC (Version 2) - A computer program for speciation, batch-reaction, one-dimensional transport, and inverse geochemical calculations. *Water-Resources Investigations Report 99-4259*. U.S. Geological Survey, Denver, CO.

Parks, G.A., 1965. Isoelectric points of solid oxides solid hydroxides and aqueous hydroxo complex systems. *Chemical Reviews*, 65(2), 177-198.

Pauwels, H., Kloppmann, W., Foucher, J.C., Martelat, A., Fritsche, V., 1998. Field tracer test for denitrification in a pyrite-bearing schist aquifer. *Applied Geochemistry* 13, 767-778.

Postma, D., Boesen, C., Kristiansen, H., Larsen, F., 1991. Nitrate Reduction in an Unconfined Sandy Aquifer - Water Chemistry, Reduction Processes, and Geochemical Modeling. *Water Resources Research* 27, 2027-2045.

Repert, D.A., Barber, L.B., Hess, K.M., Keefe, S.H., Kent, D.B., Leblanc, D.R., Smith, R.L., 2006. Long-term natural attenuation of carbon and nitrogen within a groundwater plume after removal of the treated wastewater source. *Environmental Science & Technology* 40, 1154-1162.

Robertson, L.A., Kuenen, J.G., 1984. Aerobic Denitrification - a Controversy Revived. *Archives of Microbiology* 139, 351-354.

Sam, L.B., 2006. Simulated Natural attenuation and Enhanced Bioremediation of Nitrate-Contaminated Aquifer Materials in Monument Valley, Arizona. Department of Soil, Water, and Environmental Science. University of Arizona, Tucson, p. 52.

Schurmann, A., Schroth, M.H., Saurer, M., Bernasconi, S.M., Zeyer, J., 2003. Nitrate-consuming processes in a petroleum-contaminated aquifer quantified using push-pull tests combined with N-15 isotope and acetylene-inhibition methods. *Journal of Contaminant Hydrology* 66, 59-77.

Schwan, M., Kramer, D., Gericke, C., 1984. Simulation of the Nitrate Degradation in Groundwater. *Acta Hydrochimica Et Hydrobiologica* 12, 163-171.

- Schwarzenbach, R.P., Gschwend, P.M., Imboden, D.M., 1993. Environmental organic chemistry. J. Wiley, New York.
- Sidle, W.C., Roose, D.L., Yzerman, V.T., 2000. Isotope evaluation of nitrate attenuation in restored and native riparian zones in the Kankakee watershed, Indiana. *Wetlands* 20, 333-345.
- Singleton, M.J., Esser, B.K., Moran, J.E., Hudson, G.B., McNab, W.W., Harter, T., 2007. Saturated zone denitrification: Potential for natural attenuation of nitrate contamination in shallow groundwater under dairy operations. *Environmental Science & Technology* 41, 759-765.
- Smets, B.F., Pritchard, P.H., 2003. Elucidating the microbial component of natural attenuation. *Current Opinion in Biotechnology* 14, 283-288.
- Smith, R.L., Bohlke, J.K., Garabedian, S.P., Revesz, K.M., Yoshinari, T., 2004. Assessing denitrification in groundwater using natural gradient tracer tests with N-15: In situ measurement of a sequential multistep reaction. *Water Resources Research* 40, Doi 10.1029/2003wr002919.
- Smith, R.L., Duff, J.H., 1988. Denitrification in a Sand and Gravel Aquifer. *Applied and Environmental Microbiology* 54, 1071-1078.
- Smith, R.L., Garabedian, S.P., Brooks, M.H., 1996. Comparison of denitrification activity measurements in groundwater using cores and natural-gradient tracer tests. *Environmental Science & Technology* 30, 3448-3456.
- Smith, R.L., Howes, B.L., Duff, J.H., 1991. Denitrification in Nitrate-Contaminated Groundwater - Occurrence in Steep Vertical Geochemical Gradients. *Geochimica Et Cosmochimica Acta* 55, 1815-1825.
- Starr, J.L., Parlange, J.Y., 1975. Nonlinear Denitrification Kinetics with Continuous-Flow in Soil Columns. *Soil Science Society of America Journal* 39, 875-880.
- Sverjensky, D.A., Sahai, N., 1996. Theoretical prediction of single-site surface-protonation equilibrium constants for oxides and silicates in water. *Geochimica et Cosmochimica Acta*, 60(20), 3773-3797.
- USEPA, 1993. Manual. Nitrogen control. Report EPA/625/-93/010. US Environmental Protection Agency, Washington DC.
- Whitelaw, K., Rees, J.F., 1980. Nitrate-Reducing and Ammonium-Oxidizing Bacteria in the Vadose Zone of the Chalk Aquifer of England. *Geomicrobiology Journal* 2, 179-187.
- Widdowson, M.A., Molz, F.J., Benefield, L.D., 1988. A Numerical Transport Model for Oxygen-Based and Nitrate-Based Respiration Linked to Substrate and Nutrient Availability in Porous-Media. *Water Resources Research* 24, 1553-1565.

Wiedemeier, T.H., 1999. Natural attenuation of fuels and chlorinated solvents in the subsurface. John Wiley, New York.

Wriedt, G., Spindler, J., Neef, T., Meissner, R., Rode, M., 2007. Groundwater dynamics and channel activity as major controls of in-stream nitrate concentrations in a lowland catchment system? *Journal of Hydrology* 343, 154-168.

Xu, R.K., Yang, M.L., Wang, Q.S., Ji, G.L., 2005. Effect of low molecular weight organic anions on the adsorption of NO₃⁻ by variable charge soils. *Soil Science and Plant Nutrition*, 51(5), 663-666.

Zheng, C., Wang, P.P., 1999. MT3DMS: A modular three-dimensional multispecies model for simulation of advection, dispersion and chemical reactions of contaminants in groundwater systems; Documentation and Users Guide, Contract Report SERDP-99-1. U.S. Army Engineer Research and Development Center, Vicksburg, MS.

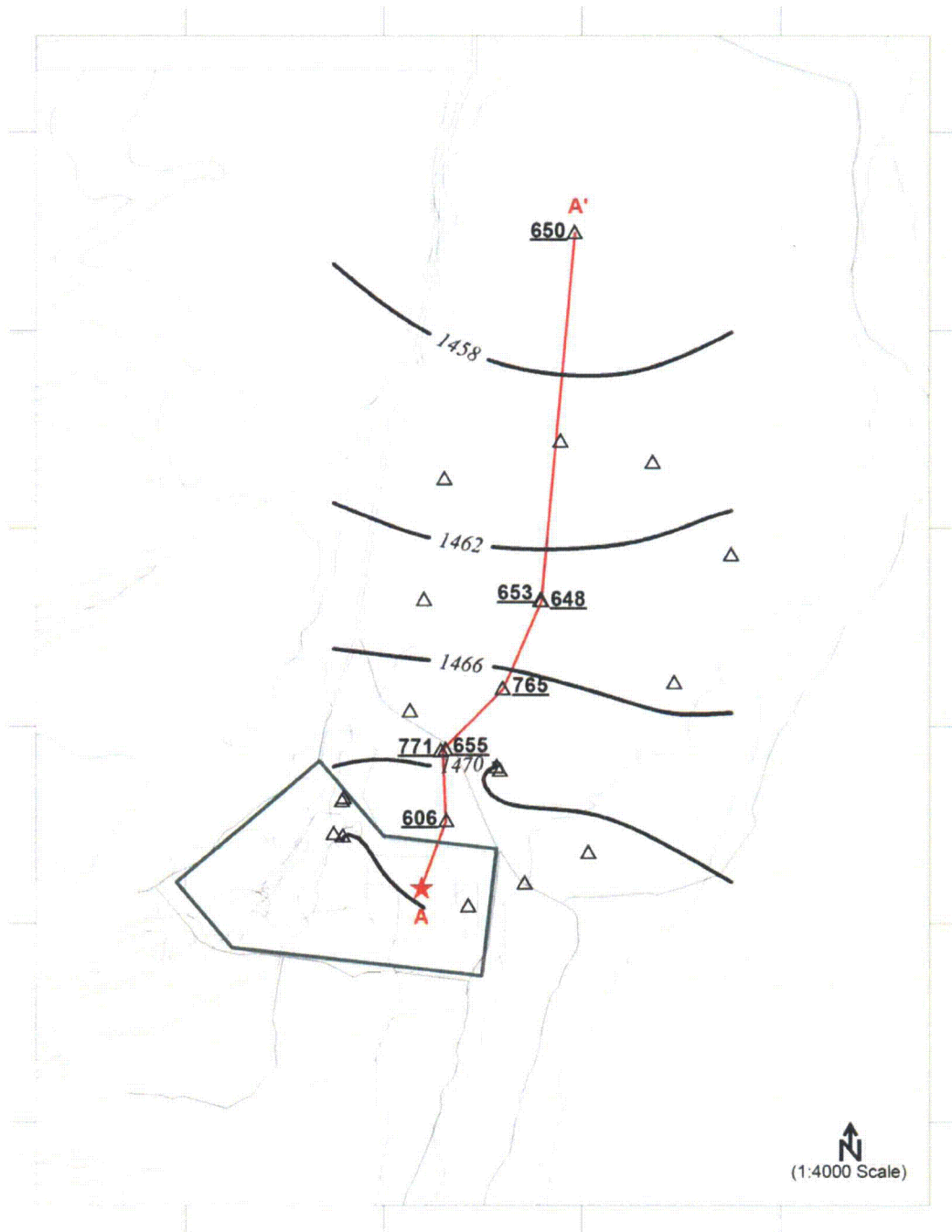


Figure 1: Site map indicating source zone location (star), groundwater elevation contours (meters above sea level), monitoring wells locations (triangles), and transect A-A' (line with underlined wells labeled).

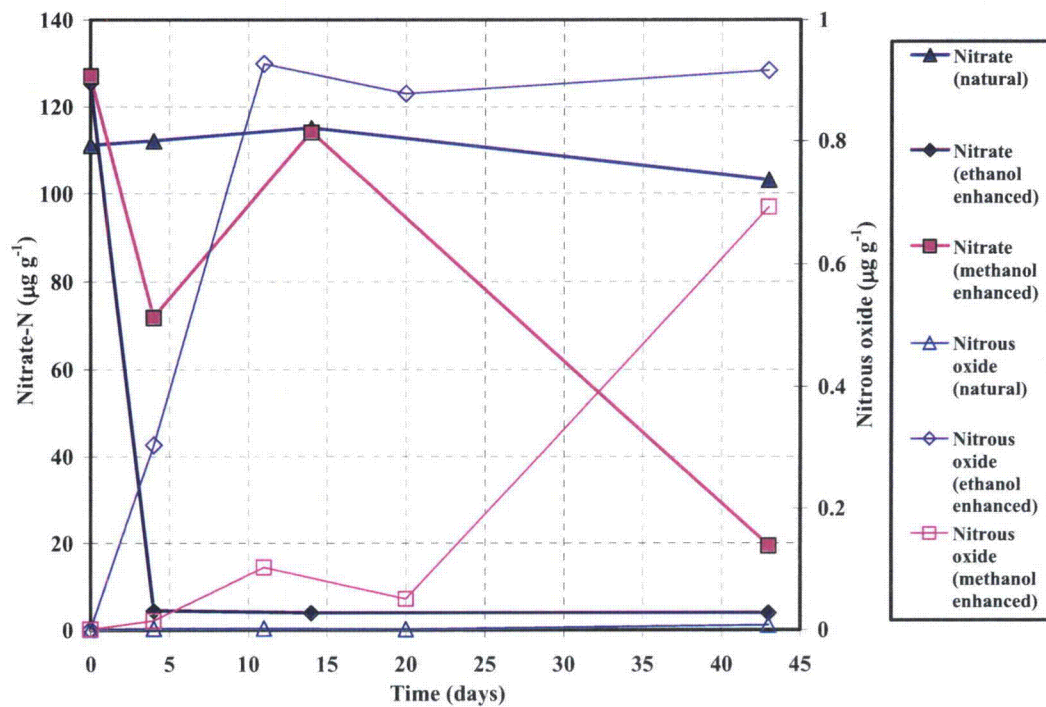


Figure 2. Nitrate depletion and nitrous oxide production in soil slurry laboratory microcosms as a function of time. Results designated as natural refer to denitrification without substrate addition, and results designated as methanol or ethanol enhanced refer to carbon substrate amended denitrification.

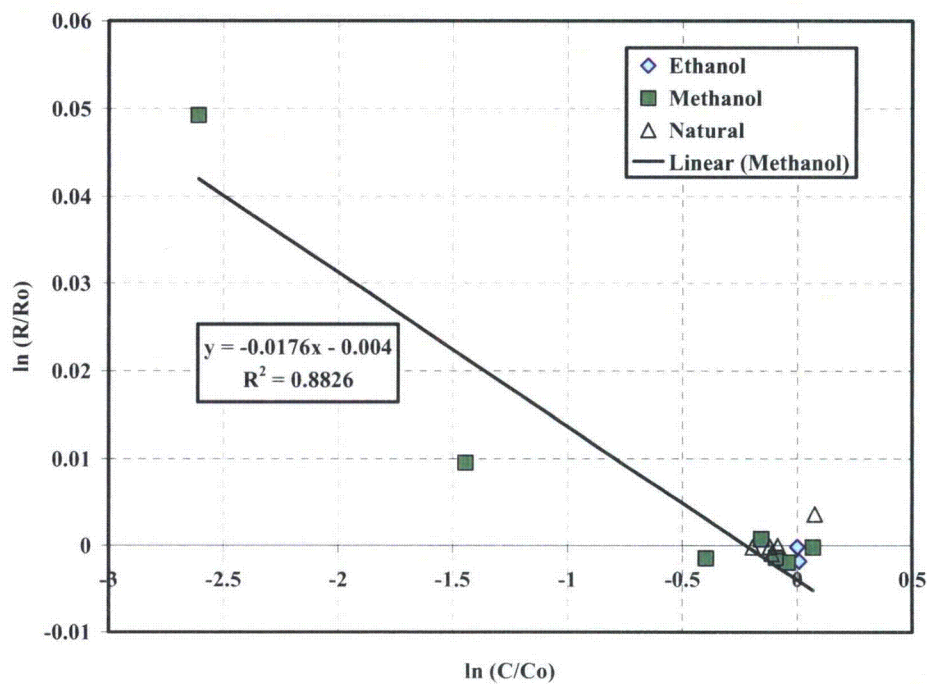
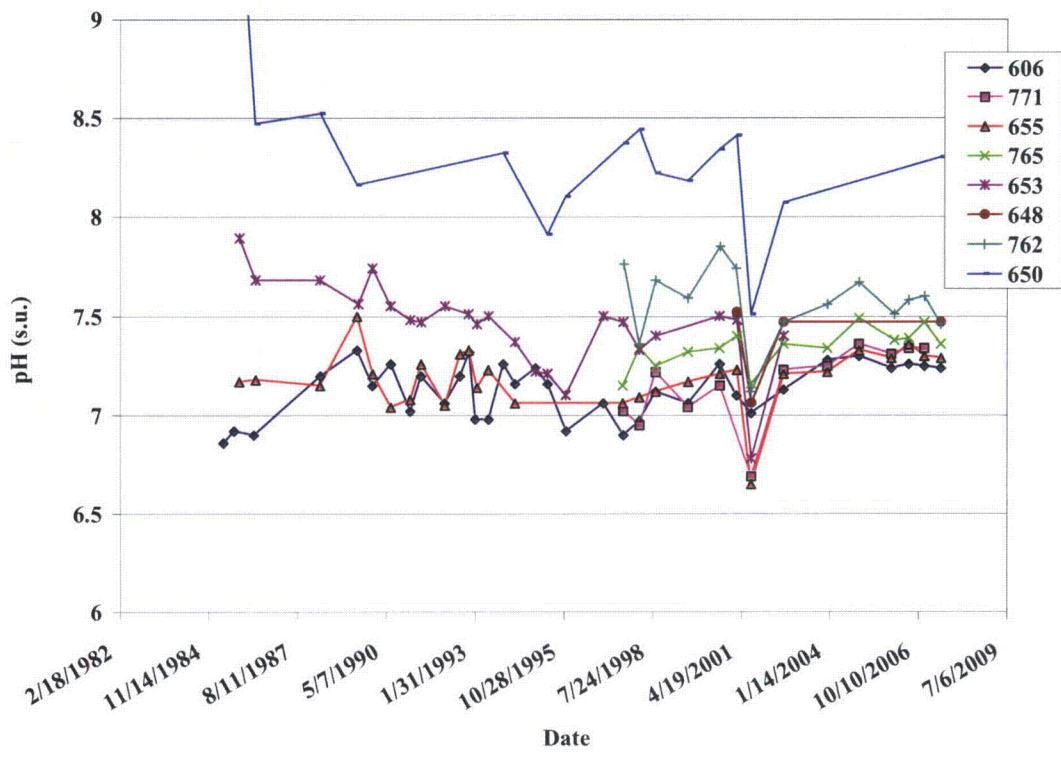
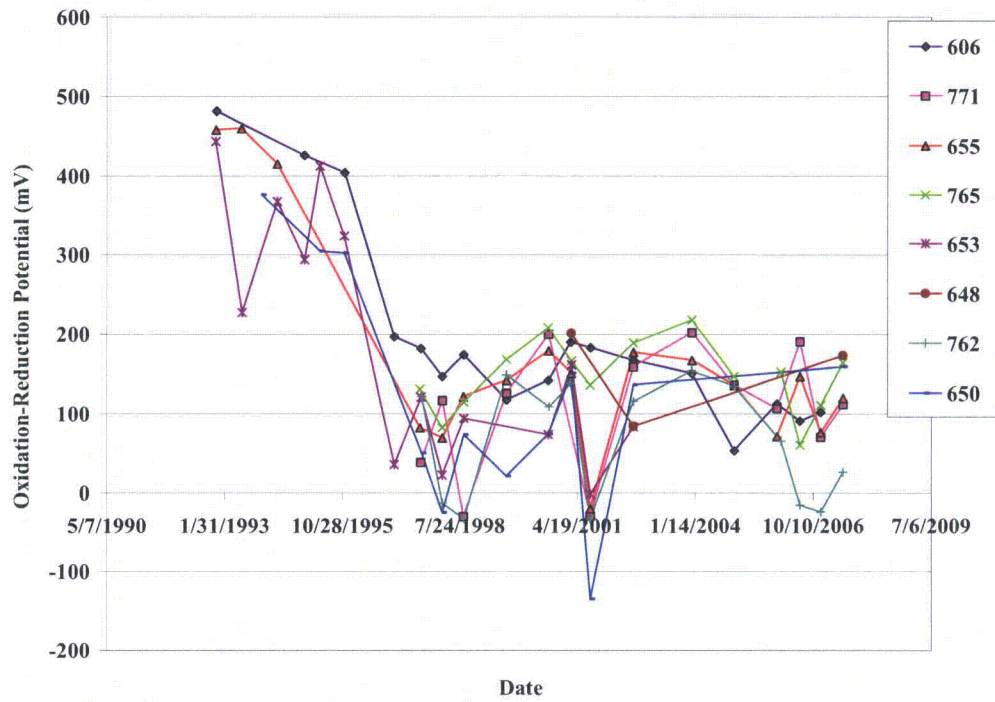


Figure 3. Nitrogen stable isotope fractionation (isotopic ratios relative to initial values versus concentrations relative to initial values) observed during laboratory microcosm experiments with and without amendment. The symbols refer to isotopic composition data, and the lines present the results of regression analysis.

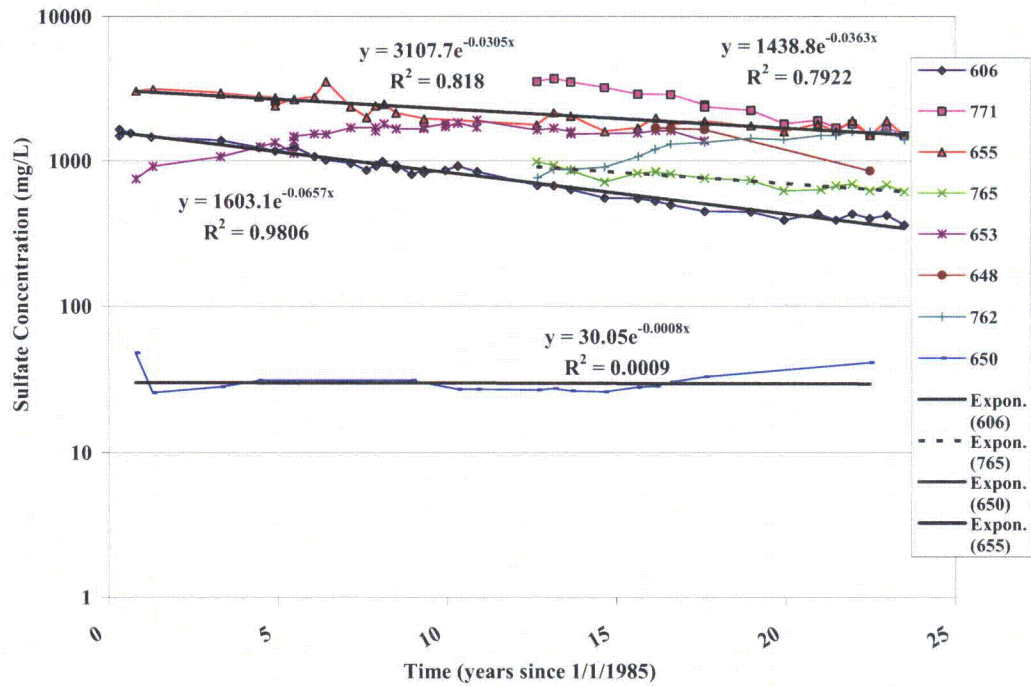
A.



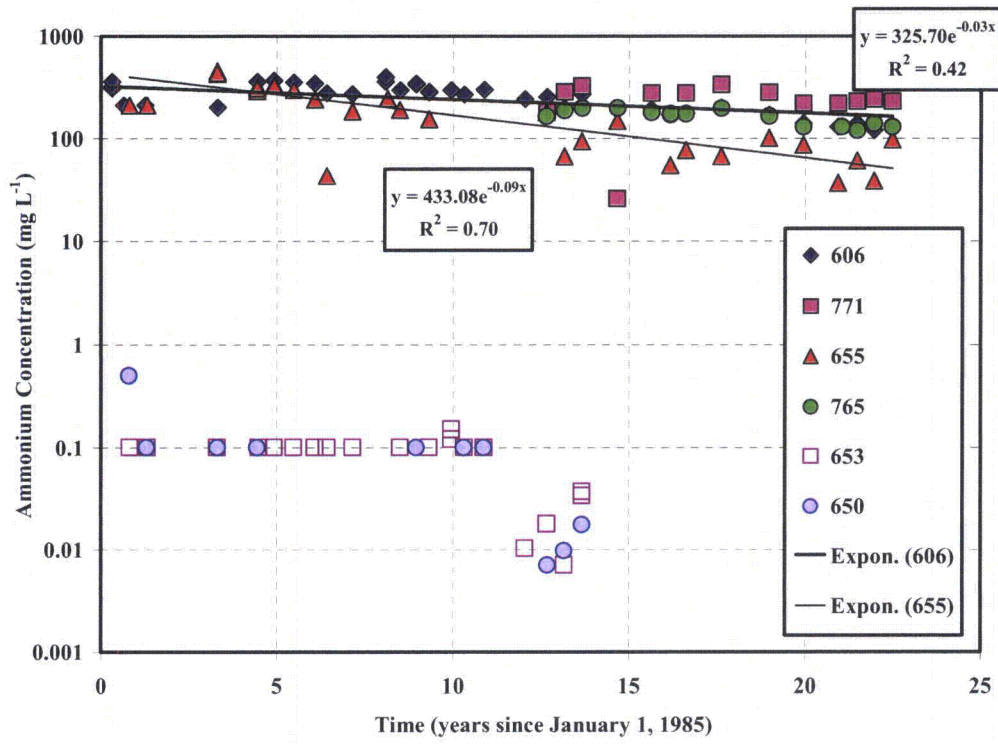
B.



C.



D.



E.

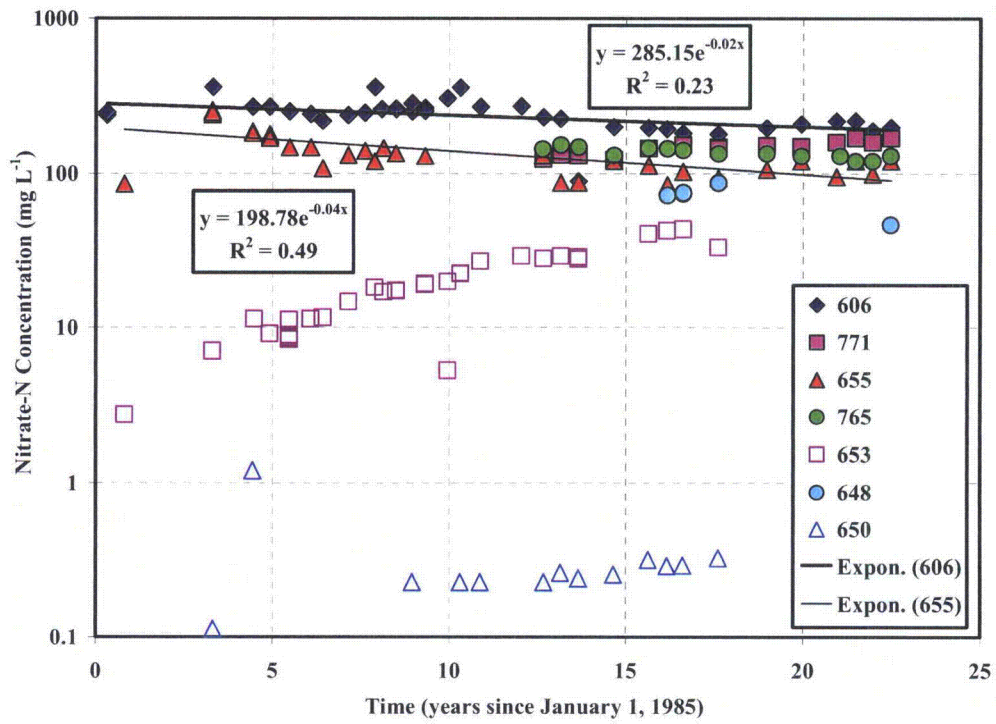
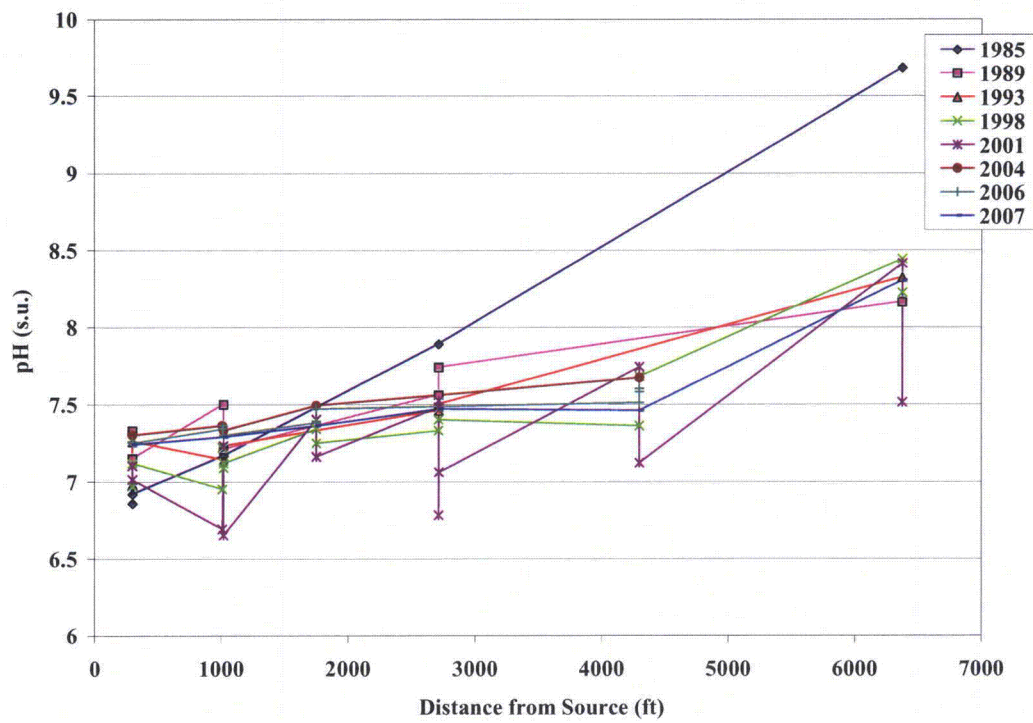
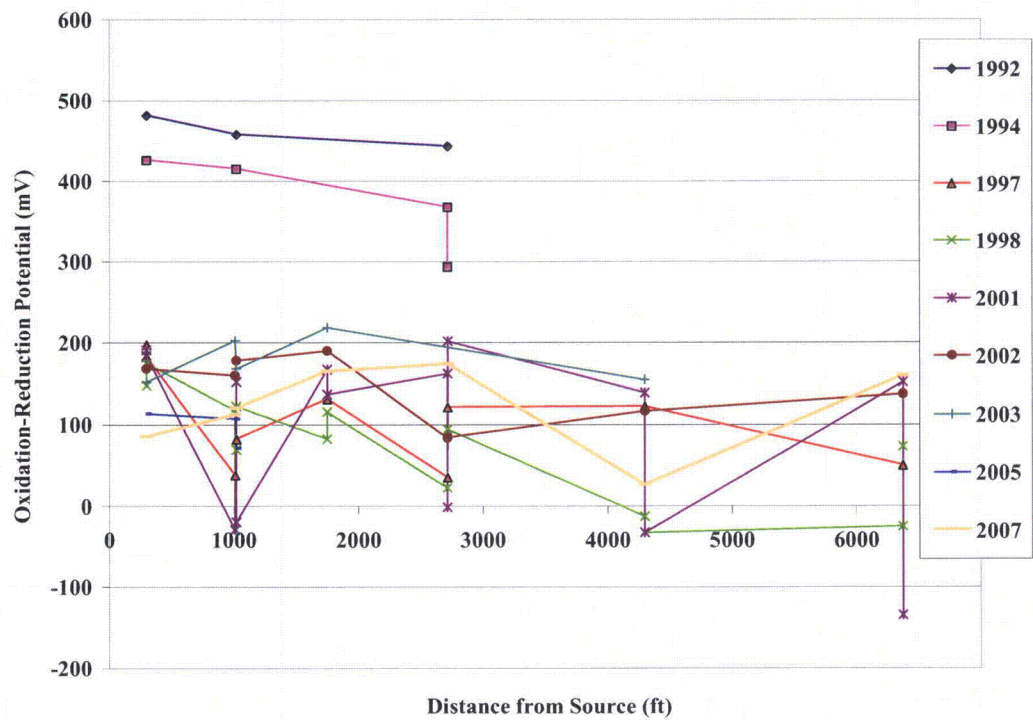


Figure 4. Groundwater pH (a), oxidation-reduction potential (b), sulfate (c), ammonium (d) and nitrate (e) concentrations obtained from sampling of monitoring wells along transect A-A' as a function of time. The symbols indicate data for numbered wells, and the lines are the results of exponential regression for selected wells.

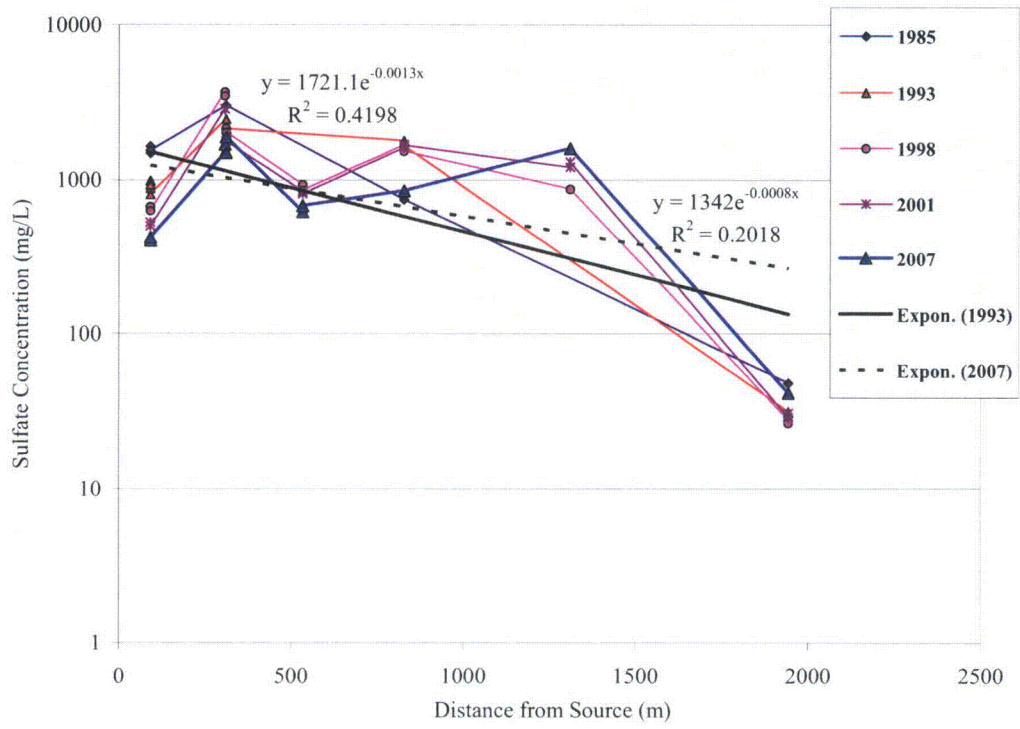
A.



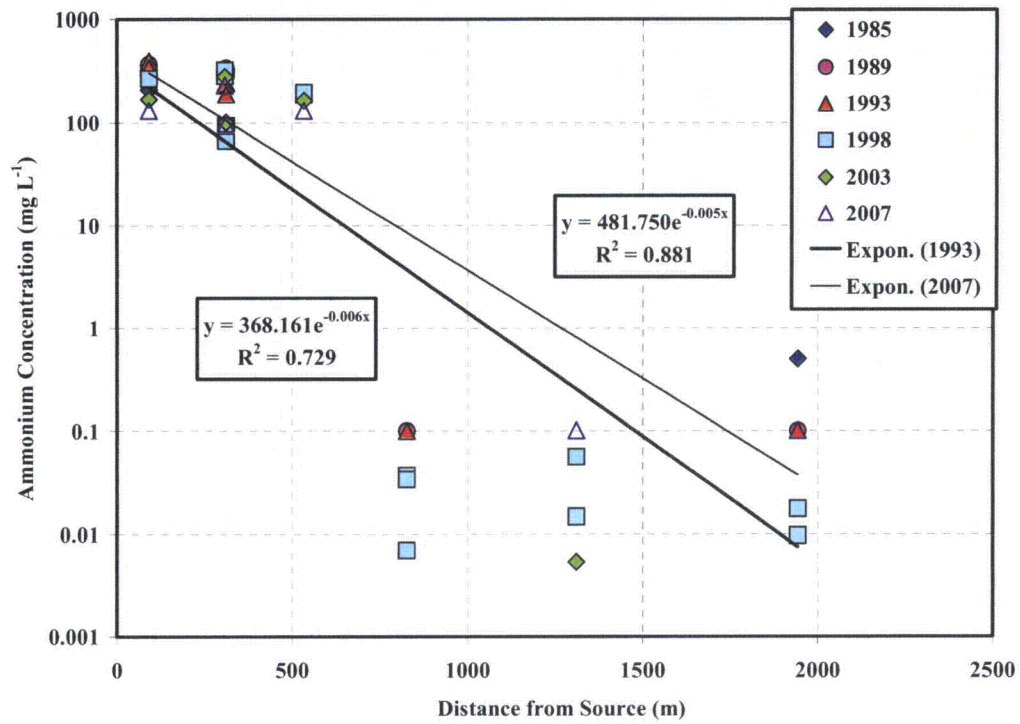
B.



C.



D.



E.

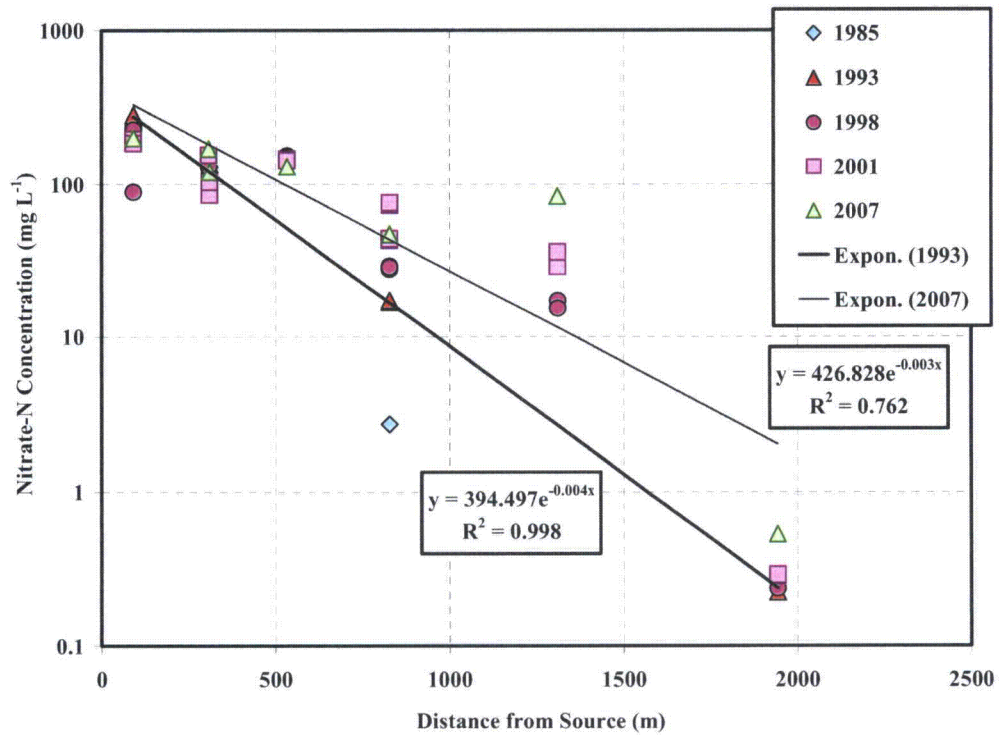
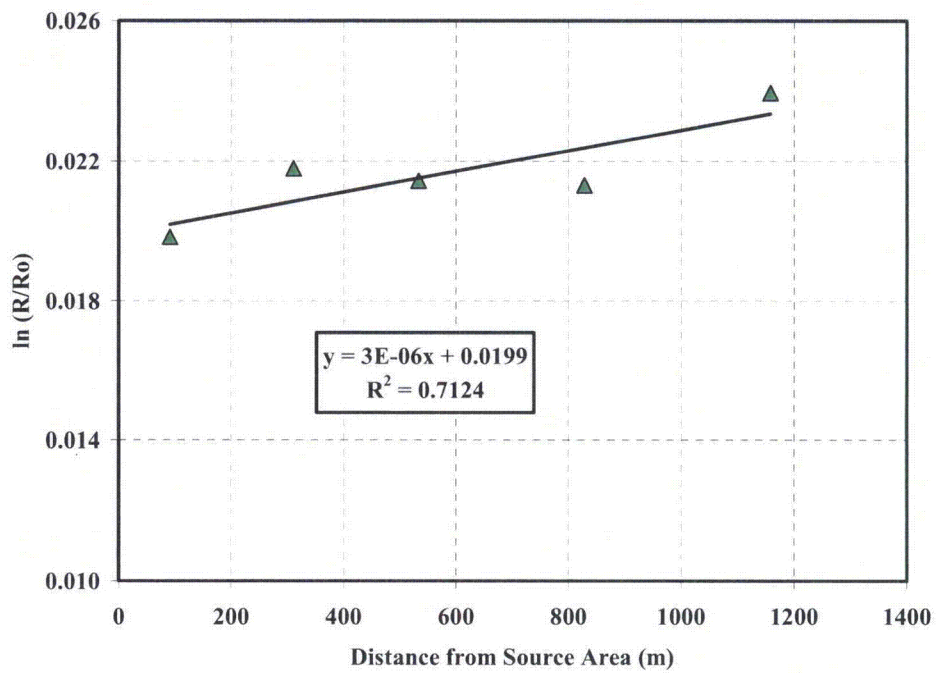


Figure 5. Groundwater pH (a), oxidation-reduction potential (b), sulfate (c), ammonium (d) and nitrate (e) concentrations obtained from sampling monitoring wells at various times as a function of distance along transect A-A'. The symbols indicate data for samples collected at the same time, and the lines are the results of exponential regression for selected years.

A.



B.

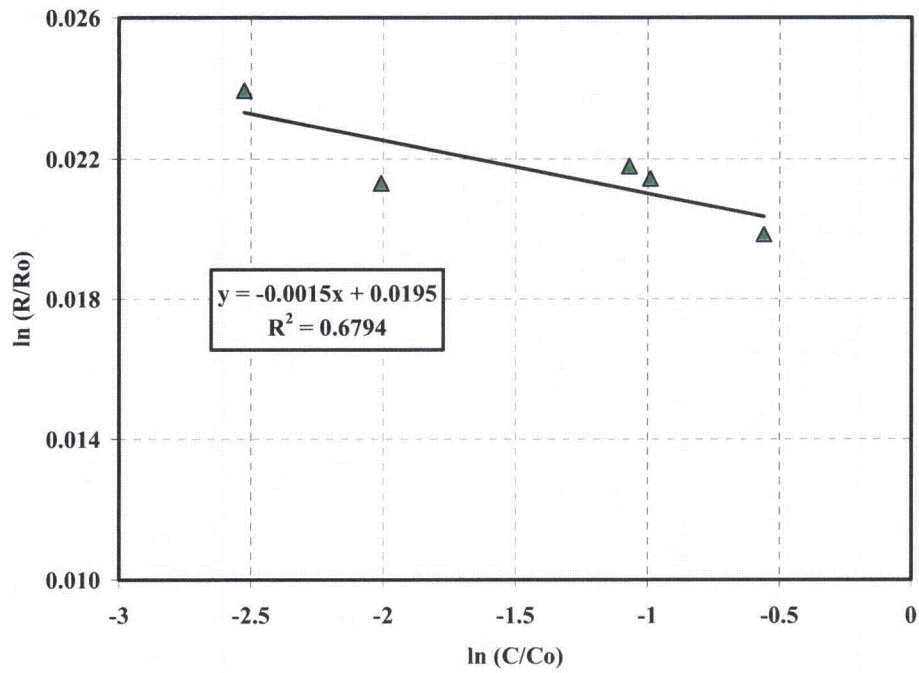
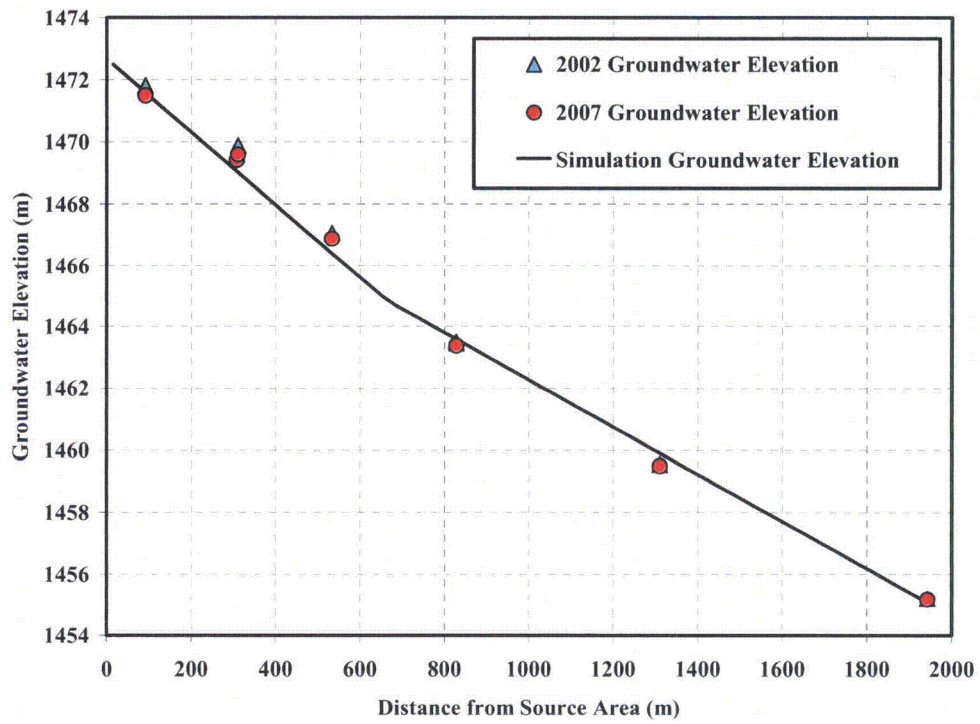


Figure 6. Nitrogen stable isotope fractionation (isotopic ratios relative to initial values) observed upon analysis of groundwater samples (without substrate amendment) collected from monitoring wells as a function of distance along transect A-A' (a) and as a function of relative concentration (b). The symbols refer to isotopic composition data, and the lines present the results of regression analysis.

A.



B.

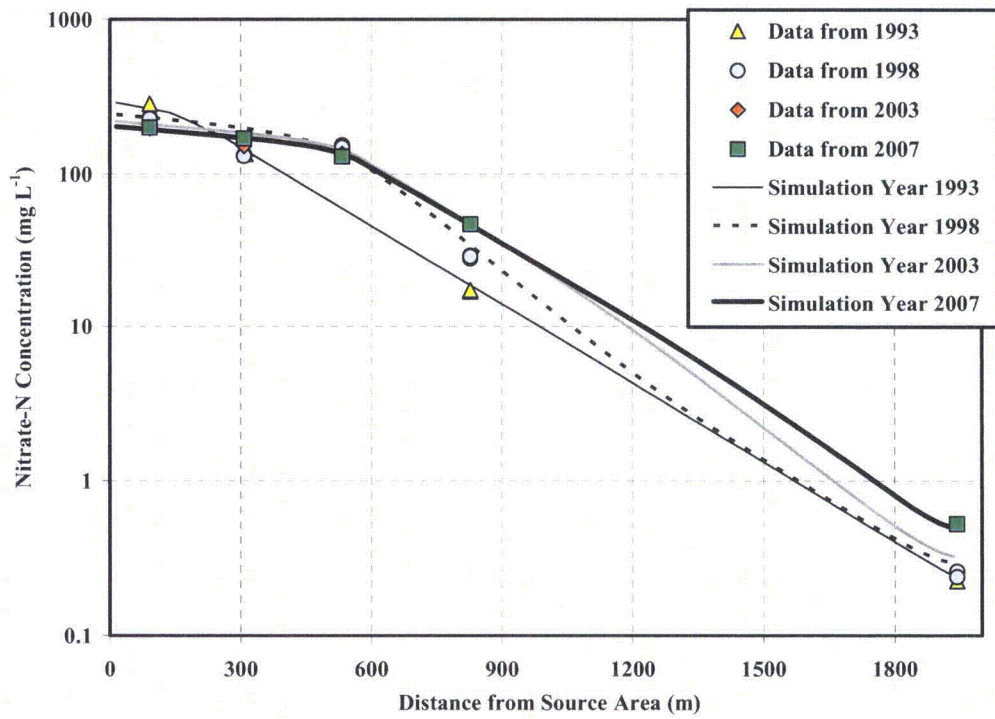


Figure 7. Comparison of observed (data points) and simulated (lines) groundwater elevation (a) with distance along transect A-A' upon calibration of the MODFLOW model, and comparison of observed (data points) and simulated (lines) groundwater nitrate concentrations (b) with distance along transect A-A' upon calibration of the MT3DMS transport model.

Table 1. Geochemical equilibrium modeling results indicating minerals that may precipitate (supersaturated) or are at equilibrium with the groundwater composition at Well 653.

Phase	Composition	Saturation Index	Description
SnSO4	SnSO4	18.31	Supersaturated
Magnetite	Fe3O4	11.99	Supersaturated
Hematite	Fe2O3	9.05	Supersaturated
Clausthalite	PbSe	8.16	Supersaturated
SnO2	SnO2	6.93	Supersaturated
U4O9	U4O9	6.22	Supersaturated
Ba3(AsO4)2	Ba3(AsO4)2	5.04	Supersaturated
Fe(OH)2.7Cl.3	Fe(OH)2.7Cl.3	4.19	Supersaturated
Hercynite	FeAl2O4	3.98	Supersaturated
U3O8	U3O8	3.5	Supersaturated
Goethite	FeOOH	3.35	Supersaturated
Cr2O3	Cr2O3	3.08	Supersaturated
Lepidocrocite	FeOOH	2.8	Supersaturated
Diaspore	AlOOH	2.76	Supersaturated
Magnesioferrite	Fe2MgO4	2.46	Supersaturated
Maghemite	Fe2O3	1.96	Supersaturated
H2Sn(OH)6	H2Sn(OH)6	1.48	Supersaturated
Gibbsite	Al(OH)3	1.38	Supersaturated
Cr(OH)3(am)	Cr(OH)3	1.25	Supersaturated
FeCr2O4	FeCr2O4	1.22	Supersaturated
Uraninite	UO2	1.01	Supersaturated
Boehmite	AlOOH	0.97	At Equilibrium
Tyuyamunite	Ca(UO2)2(VO4)2	0.95	At Equilibrium
Barite	BaSO4	0.83	At Equilibrium
Al4(OH)10SO4	Al4(OH)10SO4	0.76	At Equilibrium
Ferrihydrite	Fe(OH)3	0.58	At Equilibrium
Semetal(hex)	Se	0.53	At Equilibrium
CdSe	CdSe	0.43	At Equilibrium
SbO2	SbO2	0.38	At Equilibrium
Sn(OH)4	Sn(OH)4	0.24	At Equilibrium
Semetal(am)	Se	-0.09	At Equilibrium
Carnotite	KUO2VO4	-0.2	At Equilibrium
Gypsum	CaSO4:2H2O	-0.36	At Equilibrium
Alunite	KAl3(SO4)2(OH)6	-0.37	At Equilibrium
Anhydrite	CaSO4	-0.66	At Equilibrium
Al2O3	Al2O3	-0.68	At Equilibrium
Celestite	SrSO4	-0.68	At Equilibrium
UO2(OH)2(beta)	UO2(OH)2	-0.69	At Equilibrium

Table 2. Compilation of natural, ethanol-, and methanol-enhanced first-order rate coefficients obtained from laboratory- and field-scale data.

Natural and enhanced denitrification-rate coefficients from laboratory microcosm data.			
<i>First-order rate description</i>	<i>Estimation Method</i>	<i>k (yr-1)</i>	<i>Half Life (yr)</i>
Natural (unamended)	Concentration Decay	0.7	1
Enhanced (methanol)	Concentration Decay	14.5	< 1
Enhanced (ethanol)	Concentration Decay	17.6	< 1
Natural and enhanced denitrification-rate coefficients obtained from ¹⁵N isotopic enrichment data.			
<i>Substrate Description</i>	<i>α</i>	<i>k (yr-1)</i>	<i>Half Life (yr)</i>
Enhanced (methanol) microcosm	0.9824	14.5	< 1
Natural A-A' field data	0.9985	0.3	2
Natural denitrification-rate coefficients obtained from solute transport model calibration.			
<i>Transect Zone of Application</i>	<i>Estimation Method</i>	<i>k (yr-1)</i>	<i>Half Life (yr)</i>
Near source (0-594 m)	Concentration Calibration	0.07	9
Away from source (594-1950 m)	Concentration Calibration	0.4	2
Sulfate Natural attenuation first-order rate coefficients obtained from field concentration data.			
<i>First-order rate description</i>	<i>Estimation Method</i>	<i>k (yr-1)</i>	<i>Half Life (yr)</i>
Data from Well 606	Local-Scale Composite	0.07	11
Data from Well 655	Local-Scale Composite	0.03	23
Data from 1993	Field-Scale Composite	0.07	9
Data from 2007	Field-Scale Composite	0.07	9
Ammonium Natural attenuation first-order rate coefficients obtained from field concentration data.			
<i>First-order rate description</i>	<i>Estimation Method</i>	<i>k (yr-1)</i>	<i>Half Life (yr)</i>
Data from Well 606	Local-Scale Composite	0.03	23
Data from Well 655	Local-Scale Composite	0.09	8
Data from 1993	Field-Scale Composite	1.1	1
Data from 2007	Field-Scale Composite	0.9	1
Nitrate natural attenuation first-order rate coefficients obtained from field concentration data.			
<i>First-order rate description</i>	<i>Estimation Method</i>	<i>k (yr-1)</i>	<i>Half Life (yr)</i>
Data from Well 606	Local-Scale Composite	0.02	40
Data from Well 655	Local-Scale Composite	0.04	17
Data from 1993	Field-Scale Composite	0.7	1
Data from 2007	Field-Scale Composite	0.6	1

Appendix D
Journal of Hydrology Manuscript

This page intentionally left blank

**COMPARISON OF NITRATE ATTENUATION CHARACTERIZATION
METHODS AT THE URANIUM MILL TAILING SITE IN MONUMENT
VALLEY, ARIZONA**

Kenneth C. Carroll^{1,2}, Fiona L. Jordan³, Edward P. Glenn¹, W. Jody Waugh⁴, and Mark
L. Brusseau^{1,2*}

¹Department of Soil, Water and Environmental Science, University of Arizona,
429 Shantz Building #38, P.O. Box 210038, Tucson, AZ, USA

²Department of Hydrology and Water Resources, University of Arizona,
Harshbarger Building #11, Tucson, AZ, USA

³Golder Associates Inc., 5200 Pasadena Ave. N.E., Suite C, Albuquerque, NM, USA

⁴Environmental Sciences Laboratory, S.M. Stoller Corporation, Grand Junction, CO,
USA

Submitted for publication in:

Journal of Hydrology

January 13, 2009

*Corresponding author (Brusseau@ag.arizona.edu)

1 **ABSTRACT**

2 Contamination of groundwater by nitrate continues to be a pervasive issue, and there is
3 great interest in the use of natural and enhanced attenuation to manage subsurface nitrate
4 contamination. Several methods for characterizing the occurrence and rate of nitrate
5 attenuation were tested at a field site near Monument Valley, Arizona. Spatial and
6 temporal nitrate concentration data collected from a transect of monitoring wells located
7 along the plume centerline were analyzed to evaluate the overall rates of natural
8 attenuation. The occurrence and rate of denitrification was evaluated through microcosm
9 experiments, nitrogen isotopic fractionation analysis, and solute transport modeling.
10 First-order rate coefficients calculated with each method were comparable. The
11 composite natural attenuation rate coefficient was slightly larger but similar to the
12 denitrification rate coefficient, which suggests that microbially induced decay primarily
13 controls nitrate attenuation at the site. This research highlights the benefits associated
14 with a multiple-method approach for the characterization of natural attenuation.

15

16 **Keywords**--nitrate, natural attenuation, stable isotope, rate coefficient, denitrification

17 **1.0 INTRODUCTION**

18 Nitrate is a contaminant that can be persistent in aerobic groundwater systems
19 (e.g., Knowles, 1982; Korom, 1992; Lee et al., 2006). However, reductive
20 biotransformation, or denitrification, can naturally attenuate nitrate in low oxygen or
21 anaerobic subsurface environments (e.g., Knowles, 1982; Korom, 1992; DeSimone and
22 Howes, 1998; Pauwels et al., 1998; McGuire et al., 2002; Smith et al., 2004; McCray et
23 al., 2005). Significant interest has developed in using monitored natural attenuation
24 (MNA) for remediation of nitrate-contaminated groundwater (e.g., ITRC, 2000; Sidle et
25 al., 2000; Smets and Pritchard, 2003; Beller et al., 2004; Groffman et al., 2006; Lee et al.,
26 2006; Oa et al., 2006; Repert et al., 2006; Heatwole and McCray, 2007; Singleton et al.,
27 2007; Jordan et al., 2008; McMahan et al., 2008). Thorough site characterization is
28 essential to evaluate site-specific feasibility and viability of MNA (e.g., Wiedemeier,
29 1999; Ford et al., 2007). The goals of MNA characterization should include the
30 evaluation of the occurrence, mechanisms, and rates of various processes that may be
31 acting to decrease contaminant concentrations.

32 Several approaches have been employed to characterize nitrate attenuation in
33 subsurface environments. Spatial and temporal trends in concentrations of nitrate, other
34 nitrogen species, and nitrogen gas in groundwater have been used to assess denitrification
35 (e.g., Bohlke and Denver, 1995; Smith et al., 1996; Blicher-Mathiesen et al., 1998;
36 DeSimone and Howes, 1998; Pauwels et al., 1998; Bohlke et al., 2002; McGuire et al.,
37 2002; Repert et al., 2006). Denitrification has also been evaluated through the use of
38 microbiological methods including microcosm incubations and/or isolation and growth of
39 bacterial strains (e.g., Whitelaw and Rees, 1980; Howard, 1985; Smith and Duff, 1988;

40 Desimone and Howes, 1996; Aelion et al., 1997; D'Angelo and Reddy, 1999; Oa et al.,
41 2006). Nitrogen stable-isotope fractionation has been used to characterize denitrification
42 (e.g., Mariotti et al., 1988; Bottcher et al., 1990; Smith et al., 1991; Feast et al., 1998;
43 McMahon et al., 1999; Mengis et al., 1999; Sidle et al., 2000; Bohlke et al., 2002; Fukada
44 et al., 2003; Schurmann et al., 2003; Beller et al., 2004; Smith et al., 2004; Chen et al.,
45 2006; Singleton et al., 2007; McMahon et al., 2008). Several solute transport modeling
46 investigations have been presented that included denitrification (e.g., Starr and Parlange,
47 1975; Schwan et al., 1984; Widdowson et al., 1988; Kinzelbach et al., 1991; Postma et
48 al., 1991; Engesgaard and Kipp, 1992; Lensing et al., 1994; Clement et al., 1997; Conan
49 et al., 2003; Lee et al., 2006; Heatwole and McCray, 2007; Wriedt et al., 2007). Recent
50 reviews have assessed the multitude of methods currently used to characterize
51 denitrification (Smets and Pritchard, 2003; Groffman et al., 2006), and have suggested
52 that denitrification characterization may be improved through comparison of multiple
53 lines of evidence.

54 The purpose of the research described herein was to evaluate the efficacy of a
55 multi-method approach for characterizing the occurrence and rate of nitrate attenuation in
56 groundwater. The methods employed included microcosm experiments, stable-isotope
57 fractionation, concentration-trend evaluation, and solute-transport modeling. A former
58 uranium mill site in northern Arizona was used as a model site for the study.

59

60

61

62

63 **2.0 MATERIALS AND METHODS**

64 *2.1 Site Description*

65 The Monument Valley site is a former uranium mill tailing site located in
66 northern Arizona (DOE, 1999). Uranium was mined at the site from 1943 to 1968, and
67 seepage through mill tailing stockpiles into the shallow alluvial aquifer has resulted in a
68 groundwater contamination plume. Surface reclamation activities conducted from 1992
69 through 1994 under the UMTRCA Program consisted of removing the radioactive tailing
70 material from the site (DOE, 1999; McKeon et al., 2005). Nitrate (expressed hereafter as
71 nitrate-nitrogen or $\text{NO}_3\text{-N}$) and ammonium (NH_4) concentrations in groundwater have
72 since begun to decrease, which suggests that MNA may be a viable remediation strategy
73 for the site. Additionally, a phytoremediation pilot study was conducted to remove
74 excess $\text{NO}_3\text{-N}$ from the soil in the former tailing area. Results of the study suggest that
75 denitrification is responsible for $\text{NO}_3\text{-N}$ transformation at the site (McKeon et al., 2006;
76 Jordan et al., 2008). However, groundwater at the Monument Valley site continues to
77 exceed the 10 mg L^{-1} regulatory standard.

78 Prior site characterization efforts have described the site geology, hydrogeology,
79 and contamination distribution (DOE, 1999). The NH_4 and $\text{NO}_3\text{-N}$ contamination occurs
80 in the shallow, unconsolidated alluvial aquifer down-gradient and north of the former
81 tailing area. There is negligible groundwater pumping in the area, and groundwater
82 levels have remained relatively constant over the monitoring period, with an average
83 hydraulic gradient of 0.01 across the entire site (Figure 1). Hydraulic testing suggests
84 that the alluvial aquifer has hydraulic conductivity values that range from 0.5 to 1.0 m

85 day⁻¹ from testing done at Well 655, and values ranging from 3.5 to 10.8 m day⁻¹ from
86 testing done at Well 765 (DOE, 1999).

87 NH₄ solutions were used in the uranium processing, and leakage of NO₃-N and
88 NH₄ from the unlined tailing material is believed to have generated the groundwater
89 contamination. The tailing material removal (1992 to 1994) coincided with a decrease in
90 the dissolved oxygen concentrations in the alluvial aquifer. Decreases in redox and
91 dissolved oxygen were the likely cause of NO₃-N decay to atmospheric nitrogen through
92 denitrification, which requires low dissolved oxygen conditions (e.g., Hubner, 1986;
93 Korom, 1992). Although all radioactive tailing materials were removed by 1994, the
94 alluvial aquifer still contains NH₄ that may be continually decaying to NO₃-N via
95 nitrification, which would constitute a source for NO₃-N. Previous investigations suggest
96 that NO₃-N undergoes minimal adsorption to the alluvial aquifer material (Sam, 2006).
97 Thus, the primary processes mediating NO₃-N attenuation likely include diffusion,
98 dispersion, and denitrification.

99

100 *2.2 Groundwater Sampling and Analysis*

101 Groundwater samples were obtained from monitoring wells screened in the
102 alluvial aquifer extending approximately two km from the source area (or former tailing
103 area). For the present investigation, a series of wells (referred to as transect A-A')
104 located along the major axis of the NO₃-N plume, coincident with the mean hydraulic
105 gradient, were evaluated including numbered Wells 606, 771, 655, 765, 653, 648, and
106 650 at distances of 91, 308, 311, 533, 828, 828, and 1943 meters from the source area,
107 respectively. Samples were collected and analyzed for NO₃-N and NH₄. Prior to sample

108 collection, wells were purged with a micro-purge pumping unit for approximately three
109 well-bore volumes. Two liters of water were collected from each well and placed in
110 sterile Nalgene bottles. All samples were stored on ice in a cooler or at 4°C until
111 analyzed. Sample analysis for NH₄ was conducted using EPA method 350.3 (0.01 mg L⁻¹
112 detection limit), and NO₃-N analysis was conducted using EPA method 353.2 (0.004 mg
113 L⁻¹ detection limit). Additionally, prior groundwater sampling and chemical analysis for
114 site-wide monitoring of NO₃-N and NH₄ and field monitoring of dissolved oxygen
115 between 1985 and 2007 were considered herein.

116

117 *2.3 Microcosm Experiments*

118 Microcosm assays were conducted using sediment samples collected from the
119 NO₃-N contaminated alluvial aquifer 10-11 m below land surface to obtain direct
120 evidence of denitrification, and to calculate denitrification rate coefficients.
121 Experimental methods followed those employed by Jordan et al. (2008), who conducted
122 similar microcosm experiments with sediments from the site with and without ethanol
123 amendment. The microcosm experiments presented herein were conducted to replicate
124 prior results and extend the analysis to evaluate denitrification kinetics with no
125 amendment, ethanol amendment, and methanol amendment using both concentration
126 decay and isotopic fractionation analysis. Results of the experiments were analyzed by
127 various methods including observation of NO₃-N loss, evaluation of nitrous oxide (N₂O)
128 production, and determination of nitrogen stable isotope fractionation. Quantifying
129 denitrification with stable isotope fractionation requires a significant depletion of NO₃-N

130 to effect a detectable change in ^{15}N , which may be accomplished by adding a substrate to
131 enhance denitrification (Blackmer and Bremner, 1977).

132 Replicate slurries were made using 10 g of sediment and 1 mg $\text{NO}_3\text{-N}$
133 supplemented with or without 7.5 mg carbon substrate (e.g., ethanol or methanol). N_2O
134 production and $\text{NO}_3\text{-N}$ depletion were assayed in 250 ml glass microcosms containing
135 10% acetylene in the headspace to prevent the conversion of N_2O to N_2 . Samples were
136 collected from the microcosms at 0, 4, 12, 20, and 43 days after initiation for N_2O and
137 residual $\text{NO}_3\text{-N}$ analysis. Each treatment initially contained ten replicate flasks and two
138 flasks were sacrificed for $\text{NO}_3\text{-N}$ and ^{15}N measurements at each time. The microcosms
139 were maintained at $23(\pm 2)^\circ\text{C}$. N_2O concentrations were quantified using a Shimadzu
140 GC-14A gas chromatograph with a ^{63}Ni electron capture detector, a 2 ml sampling loop,
141 and two stainless steel packed columns: Porapak Q and Haysep Q both 80/100 mesh
142 (Supelco, Bellefonte, PA). $\text{NO}_3\text{-N}$ loss was also monitored through time.

143 Additional microcosm experiments were conducted to test the nitrification
144 potential activity of soil samples collected from the phytoremediation plots near the
145 historic tailing material. Six replicate soil samples (5 g) for each site were placed in glass
146 bottles (125 ml), washed with sodium phosphate buffer (1mM; pH 7.2) to remove soluble
147 $\text{NO}_3\text{-N}$, and resuspended in 50 ml of the same buffer containing NH_4Cl (1.5 mM). The
148 slurries were shaken continuously in the dark at 25°C for 3-5 days. The pH was adjusted
149 daily to 7 over the course of the experiment. Half of the samples were treated with 1%
150 (vol/vol) acetylene to inactivate autotrophic ammonia oxidation activity. Aliquots of
151 slurry (2 ml) were taken at 0, 24, and 48 hours. The samples were centrifuged and

152 analyzed for nitrite plus NO₃-N using the colorimetric Szechrome reagent (Jordan et al.,
153 2008).

154

155 *2.4 Nitrate-N Isotopic Analysis*

156 Stable isotopes of nitrogen (¹⁴N and ¹⁵N) were analyzed in the following manner.
157 Fifty ml from each sacrificed microcosm were added to a 500 ml flask containing 0.4 g
158 MgO, which was placed on a hotplate for 4 hours at 45° C to remove NH₄ (Mulvaney and
159 Khan, 1999). A subsample was analyzed to ensure complete liberation of NH₄ prior to
160 evaporating the samples at room temperature in acid washed, oven-dried crucibles. The
161 nitrogen content of the solid crystalline residue was measured on a continuous-flow gas-
162 ratio mass spectrometer (Finnigan Delta PlusXL) at the Geosciences Department,
163 University of Arizona, and the samples were combusted using an elemental analyzer
164 (Costech) coupled to the mass spectrometer. Standardization was based on acetanilide for
165 elemental concentration, and IAEA-N-1 and IAEA-N-2 were used for ¹⁵N with a 95%
166 confidence interval precision of ±0.19 ‰ (or per mil). These analyses differentiated
167 between the two isotopes of nitrogen and quantified total NO₃-N per liter of water.

168

169 **3.0 DATA ANALYSIS**

170 When evaluating transformation processes and quantifying rate coefficients, it is
171 important to distinguish between composite and process-specific rate coefficients.
172 Composite attenuation rate coefficients incorporate all processes contributing to
173 attenuation of the target contaminant, and are calculated by analyzing changes in aqueous
174 concentration data as a function of space or time. Process-specific rate coefficients

175 represent a specific attenuation mechanism. For example, biotransformation rate
176 coefficients represent microbial-mediated transformation processes. Of particular interest
177 for this investigation, denitrification is a multi-step process through which NO₃-N is
178 reduced to atmospheric nitrogen (e.g., Knowles, 1982; Korom, 1992; Kendall and
179 McDonnell, 1998), and it is commonly the most significant attenuation process for NO₃-
180 N in groundwater. For this study, natural attenuation and biological denitrification were
181 both assumed to follow first-order decay. This simplified approach has been deemed
182 reasonable for quantifying denitrification in previous studies (e.g., Pauwels et al., 1998;
183 Smith et al., 2004; McCray et al., 2005).

184

185 *3.1 Spatial Data Analysis*

186 The field-scale composite rate coefficient describes the changes in concentration
187 with distance (measured at a point in time) away from a source area along the major axis
188 of the plume. Least squares regression was used to determine the exponential equation
189 that best described the data:

$$190 \quad C(x) = C_0 e^{-(k/v)x} \quad (1)$$

191 where C(x) is the concentration at distance x, v is the velocity of the solute transported in
192 groundwater, and k is the composite-rate coefficient for MNA.

193

194 *3.2 Stable Isotope Analysis*

195 Denitrification was assessed by determining compound-specific stable isotope
196 fractionation. Biological denitrification leads to an enrichment of the heavy isotope, ¹⁵N,
197 within the remaining NO₃-N because denitrification favors the light isotope, ¹⁴N (Mariotti

198 et al., 1988). The nitrogen isotopic composition is typically reported as $\delta^{15}\text{N}$ ‰ (Kendall
 199 and Aravena, 1999):

$$200 \quad \delta^{15}\text{N}(\text{‰}) = \left(\frac{R_{\text{sample}}}{R_{\text{standard}}} - 1 \right) \times 1000 \quad (2)$$

201 where R_{sample} is the isotopic ratio ($^{15}\text{N}/^{14}\text{N}$) measured in a sample and R_{standard} is the ratio
 202 of the atmospheric standard. Denitrification attributed enrichment of ^{15}N in each sample
 203 was quantified by a simplified form of the Rayleigh equation (Kendall and McDonnell,
 204 1998; Kendall and Aravena, 1999; Fukada et al., 2003):

$$205 \quad \delta_R = \delta_{R_o} + \varepsilon \ln \left(\frac{C_t}{C_o} \right) \quad (3)$$

206 where δ_R is the $\delta^{15}\text{N}$ value of the $\text{NO}_3\text{-N}$ at time (t), δ_{R_o} is the initial $\delta^{15}\text{N}$ value of the
 207 $\text{NO}_3\text{-N}$, ε is the enrichment factor, C_t is the $\text{NO}_3\text{-N}$ concentration at time (t) and C_o is the
 208 initial $\text{NO}_3\text{-N}$ concentration. The enrichment factor can be used to estimate the extent of
 209 biological denitrification occurring in a groundwater system compared to other processes
 210 that might reduce $\text{NO}_3\text{-N}$ levels (Smith et al., 2004). First-order rate coefficients for
 211 denitrification were calculated from the nitrogen stable-isotope enrichment data upon
 212 calculation of the enrichment factor. The rate coefficients (k) were calculated as (Morrill
 213 et al., 2005):

$$214 \quad \alpha = \frac{1000 + \delta_R}{1000 + \delta_{R_o}} \quad (4)$$

$$215 \quad \varepsilon = 1000(\alpha - 1) \quad (5)$$

$$216 \quad \left(\frac{\delta_R}{1000} + 1 \right) = \left(\frac{\delta_{R_o}}{1000} + 1 \right) \exp(k[(1 - \alpha)t]) \quad (6)$$

217 where α is the fractionation factor, and k is the rate coefficient for denitrification. The
218 $\delta^{15}\text{N}$ results of the samples collected during the microcosm experiments were to obtain
219 the enrichment factors (ϵ) and fractionation factors (α) that were used to calculate
220 denitrification rate coefficients. Equation 6 was used to quantify denitrification in the
221 laboratory microcosm experiments.

222 Isotopic evidence for denitrification may also be observed in the field if sufficient
223 transformation has occurred to result in a measurable fractionation of ^{15}N . Over time,
224 $\text{NO}_3\text{-N}$ from the source area has been transported down-gradient in the aquifer. If
225 denitrification has occurred in the plume, $\text{NO}_3\text{-N}$ at the leading edge of the plume should
226 be more enriched in ^{15}N than $\text{NO}_3\text{-N}$ closer to the source area. The rate of denitrification
227 in the plume can therefore be calculated by measuring ^{15}N enrichment in samples taken
228 from the plume at increasing distances from the source area. Subsamples of groundwater
229 collected at several monitoring wells along the A-A' transect were analyzed for nitrogen
230 stable isotopes ^{15}N and ^{14}N using the methods discussed above for the microcosm
231 samples but with larger sample volumes (200 ml), and the $\delta^{15}\text{N}$ results were used to
232 obtain the field-scale denitrification rate coefficient (k) (Equation 6) assuming the initial
233 value for $\delta^{15}\text{N}$ (-7) was the most enriched value measured from the groundwater samples.

234

235 *3.4 Numerical Modeling Analysis*

236 Numerical modeling was used to quantify solute transport and attenuation
237 processes including denitrification for the $\text{NO}_3\text{-N}$ plume at the Monument Valley site. A
238 one-dimensional groundwater flow model was developed and calibrated to provide the
239 pore-water velocity for the solute-transport model. The numerical model MODFLOW

240 (Harbaugh and McDonald, 1996) was used for the groundwater flow simulations. The
241 model discretization consisted of 64 cells that were each 30.5 m long, which extended
242 from the source area to beyond Well 650 along the A-A' transect. Constant-head
243 boundary conditions were imposed on the first (1472 m above sea level) and last cell
244 (1455 m above sea level). The results of the groundwater flow modeling were used
245 within the identical model domain for simulating transport of NO₃-N along the A-A'
246 transect.

247 The commonly used numerical solute transport model MT3DMS (Zheng and
248 Wang, 1999) was employed to solve the advection-dispersion equation:

$$249 \quad \frac{\partial(\theta C)}{\partial t} = \frac{\partial}{\partial x_i} \left(\theta D_{ij} \frac{\partial C}{\partial x_j} \right) - \frac{\partial}{\partial x_i} (\theta v_i C) - k \theta C \quad (8)$$

250 where θ is the porosity, C is the groundwater solute concentration, t is time, x is distance,
251 D is the hydrodynamic dispersion coefficient tensor, v is the pore-water velocity, and k is
252 the first-order rate coefficient for denitrification. The dispersion tensor accounts for
253 diffusion/dispersion in three dimensions through the evaluation of the longitudinal,
254 horizontal transverse, and vertical transverse dispersivities and associated velocities. The
255 NO₃-N concentration distribution observed from the monitoring-well data in 1993 was
256 used for the initial condition. Initial simulations indicated that the model required a
257 source boundary condition at the up-gradient boundary to facilitate calibration to the
258 NO₃-N concentration data. A source decay rate (0.02 yr⁻¹) was calculated from the local-
259 composite attenuation rate coefficient at Well 606, which is adjacent to the source zone.

260 The results of miscible-displacement experiments conducted with porous media
261 collected from the alluvial aquifer near Well 606 were used to evaluate adsorption and
262 dispersion properties (Sam, 2006). NO₃-N exhibited minor retardation ($R = 1.2$) due to

263 adsorption, which was accounted for in the transport modeling assuming a linear
264 isotherm ($K_d = 0.028 \text{ L Kg}^{-1}$). The column-scale dispersivity (0.05 cm) was up-scaled to
265 the field scale (14.5 cm) using a standard linear scaling approach (Gelhar et al., 1992).
266 Horizontal and vertical transverse dispersivities were assumed to be 10% of the
267 longitudinal dispersivity. The porosity was assumed to be 0.25, and the molecular
268 diffusion coefficient ($8.64 \times 10^{-5} \text{ m}^2 \text{ day}^{-1}$) was calculated from a correlation relating the
269 diffusion coefficient to the molecular weight (Schwarzenbach et al., 1993). Model
270 simulations were calibrated to the measured $\text{NO}_3\text{-N}$ concentration distribution along the
271 A-A' transect for the years 1998, 2003, and 2007 by varying the denitrification first-order
272 rate coefficient.

273

274 **4.0 RESULTS AND DISCUSSION**

275 *4.1 Laboratory Microcosm Experiments and Analyses*

276 The results of the microcosm experiments are presented in Figure 2 as the
277 biotransformation of $\text{NO}_3\text{-N}$ and production of N_2O over time. The results show that
278 N_2O production, which is the decay product of denitrification in the presence of
279 acetylene, coincides with the decay of $\text{NO}_3\text{-N}$. The denitrification of $\text{NO}_3\text{-N}$ without
280 amendment was relatively slow compared to the decay observed with both ethanol and
281 methanol amendments, which showed nearly complete denitrification of $\text{NO}_3\text{-N}$ over the
282 assay periods. The magnitude and rate of denitrification enhancement was greater for
283 ethanol amended compared to the methanol amended and nonamended microcosms. The
284 denitrification rate coefficients calculated from microcosm concentration results were 0.7

285 yr⁻¹ without substrate amendment, 14.5 yr⁻¹ with methanol amendment, and 17.6 yr⁻¹ with
286 ethanol amendment (Table 1).

287 The NO₃-N isotopic fractionation data obtained from the laboratory microcosm
288 experiments are presented in Figure 3. The nonamended microcosms did not undergo
289 denitrification to the extent required to observe fractionation, and denitrification in the
290 ethanol amended microcosms occurred prior to measurement of fractionation. Thus
291 isotopic analyses were conducted only for the methanol-amended samples. The rate
292 coefficients for the methanol-amended microcosms were very similar for both the
293 concentration decay and isotopic fractionation analyses (Table 1). The results of a linear
294 regression analysis are also shown that was used to calculate the fractionation factor ($\alpha =$
295 $1 + \text{slope}$) attributed to denitrification in the methanol-amended microcosm (Figure 3).

296

297 *4.2 Temporal and Spatial Analysis of Field Data*

298 The concentrations of NH₄, dissolved oxygen, and NO₃-N in groundwater
299 samples collected from monitoring wells along the A-A' transect (Figure 1) were plotted
300 versus time since 1985 to evaluate natural attenuation behavior. NH₄ concentrations
301 (Figure 4a) followed a decreasing trend throughout time for each of the monitoring wells
302 along A-A'. The dissolved oxygen concentrations (data not shown) in the aquifer
303 decreased from 1992 to 1994 to between 0.1 and 1 mg L⁻¹, which is in the range required
304 to initiate denitrification (e.g., Robertson and Kuenen, 1984; Hubner, 1986). Decreases
305 in groundwater NO₃-N concentrations were observed near the source area (Figure 4b),
306 whereas increasing NO₃-N concentrations were observed at distances down-gradient
307 from the source area (e.g., Wells 653 and 650). Regression analyses are also shown for

308 selected wells on the NH_4 and $\text{NO}_3\text{-N}$ plots, and indicate that exponential decay
309 (Equation 1) provides a reasonable description of the data. The local-scale composite
310 rate coefficient calculated with the data from Well 606 (0.02 yr^{-1}) represents the rate of
311 $\text{NO}_3\text{-N}$ attenuation adjacent to the source zone (Table 1). The low magnitude suggests
312 that concentration attenuation at that location is limited. Additionally, the local-scale
313 composite rate coefficients for NH_4 and $\text{NO}_3\text{-N}$ at Well 606 are similar, which suggests
314 that nitrification is acting as the current source of $\text{NO}_3\text{-N}$. The increasing concentration
315 trends at the edge of the plume suggest that the plume is moving or expanding.

316 The spatial behavior of the groundwater contamination plume was evaluated by
317 plotting $\text{NO}_3\text{-N}$ concentrations versus distance along the A-A' transect from the source
318 area. Figures 5a and 5b contain the NH_4 and $\text{NO}_3\text{-N}$ spatial data for selected years,
319 respectively. The concentrations of both NH_4 and $\text{NO}_3\text{-N}$ decrease with distance from
320 the source area for each of the years evaluated. The dissolved oxygen content (data not
321 shown) has decreased over time, especially for the region greater than approximately 610
322 m from the source area. The 1992 data suggest an increase in dissolved oxygen
323 concentration or a concentration spike at approximately 300 m down-gradient of the
324 source area. However, since that time oxygen concentrations have shown a decreasing
325 trend with distance from the source area. The $\text{NO}_3\text{-N}$ plume extends further from the
326 source than the NH_4 plume, which would be expected if nitrification and/or adsorption of
327 NH_4 were occurring. Exponential regression analysis for selected years indicates that
328 exponential decay provides a reasonable description of the data. The field-scale
329 composite rate coefficient calculated for $\text{NO}_3\text{-N}$ from the regression equation was 0.7 yr^{-1}

330 for the 1993 data and 0.6 yr^{-1} for the 2007 data, which suggests a relative consistency in
331 attenuation rates over time at the site (Table 1).

332 The $\text{NO}_3\text{-N}$ isotopic fractionation data obtained from the groundwater analysis are
333 presented in Figure 6. Field-scale denitrification was quantified through $\delta^{15}\text{N}$ enrichment
334 analysis of groundwater samples collected along the A-A' transect monitoring wells. The
335 $\text{NO}_3\text{-N}$ becomes progressively more enriched in ^{15}N relative to ^{14}N with travel
336 time/distance from the source area (Figure 6a), which suggests that denitrification is
337 preferentially transforming ^{14}N as opposed to ^{15}N . The enrichment of ^{15}N increases with
338 decreasing $\text{NO}_3\text{-N}$ concentration, suggesting that ^{15}N fractionation occurs as a result of
339 denitrification and therefore that enrichment can be used to evaluate the magnitude and
340 rate of denitrification. The results of a linear regression analysis are presented that were
341 used to calculate the fractionation factor attributed to denitrification in the alluvial aquifer
342 along transect A-A' (Figure 6b), which was used for the calculation of the denitrification
343 rate coefficient (0.3 yr^{-1} , Table 1).

344

345 *4.4 Numerical Modeling Analysis*

346 The results of the MODFLOW model calibration are presented in Figure 7a along
347 with the observed groundwater elevations from 2002 and 2007. Calibration of the model
348 was accomplished by comparing simulated and measured groundwater elevation data for
349 2007. The simulated groundwater elevations compare favorably with the observed data
350 along A-A' (Figure 7a) with a root mean square error (RMSE) of 0.4 m (0.01% average
351 error).

352 Two zones of different hydraulic conductivities were used in the simulations,
353 which resulted in the change in groundwater elevation gradient observed in Figure 7a.
354 The values calibrated for the two zones were 4.9 m day^{-1} for the region extending from
355 the source zone to 610 m down-gradient, and 7.6 m day^{-1} for the zone from 610 m to
356 1951 m. The previously mentioned hydraulic testing data suggests that hydraulic
357 conductivity increases in the direction of groundwater flow from Well 655 to Well 765,
358 and model calibrated values are within the previously measured range from 0.5 m day^{-1} at
359 Well 655 to 10.8 m day^{-1} at Well 765.

360 The simulated spatial distribution of $\text{NO}_3\text{-N}$ concentrations obtained from
361 calibration of the solute-transport model to the measured data is presented in Figure 7b.
362 The calibrated simulation compares well with the observed concentration data with a
363 RMSE of 3.9 mg L^{-1} (0.7% average error) for 2007. The optimal calibration was
364 achieved by using two zones with different rates of denitrification. The first zone, with a
365 rate coefficient of 0.07 yr^{-1} , was applied from the source area to approximately 610 m
366 down-gradient, and a rate coefficient of 0.44 yr^{-1} was used for the zone from 610 m to
367 1951 m down-gradient of the source. The zone locations were selected based on
368 observation of a change in NH_4 concentrations and redox conditions along the A-A'
369 transect, and correspond to the hydraulic conductivity zones. The apparent spatial
370 variability in denitrification activity may be a result of spatial variability in the
371 nitrification process (greater near the source zone) and in dissolved oxygen
372 concentrations (which are lower down-gradient).

373

374

375 *4.5 Comparison of Rate Coefficient Data*

376 Potential source-zone processes were evaluated through comparison of the local-
377 scale and field-scale composite rate coefficients. The NO₃-N and NH₄ local-scale
378 composite rate coefficients are similar at Well 606. This suggests that nitrification may
379 be a source of NO₃-N at the site. The results of microcosm experiments conducted to
380 evaluate potential nitrification activity indicated a positive potential for nitrification in the
381 area near the source zone (data not shown). These results support the possibility that
382 nitrification is a continuing source of NO₃-N. The local-scale composite NO₃-N decay
383 coefficient was significantly lower than the field-scale composite value (Table 1). This
384 suggests that the source-zone decay rate, as assumed to be represented by the local-scale
385 rate coefficient, is more rate limiting than the solute transport attenuation rate, as
386 provided by the composite-scale rate coefficient. Thus, source-zone decay appears to be
387 the rate-limiting step for NO₃-N attenuation at this site.

388 An integrated characterization approach using various methods was used in this
389 investigation to determine first-order rate coefficients for natural attenuation and
390 denitrification. An interesting result is that the rate coefficients were comparable for the
391 different methods used (Table 1). The spatially-weighted average of the model-calibrated
392 denitrification rate coefficients (0.3 yr⁻¹) is identical to the denitrification rate coefficient
393 calculated from the field isotopic data. These two field-scale values are slightly lower
394 than, but similar to, the laboratory-scale rate coefficient (0.7 yr⁻¹). This observation is
395 contrary to typical observations wherein denitrification rate coefficients determined at the
396 laboratory scale are significantly higher than field-scale rate coefficients. The field-scale
397 denitrification rate coefficients are slightly smaller than but similar to the field-scale

398 composite rate coefficient (which accounts for all natural attenuation processes). This
399 suggests that microbially induced decay primarily controls nitrate attenuation at the site.
400 The rate coefficients reported herein fall within the wide range (0.02 to 6 yr⁻¹) of values
401 reported in prior studies (e.g., McMahon et al., 2008).

402

403 **5.0 SUMMARY**

404 The results of various methods used for the characterization of NO₃-N attenuation
405 at the Monument Valley UMTRA site have been presented herein. Surface remediation
406 of tailing materials at the site occurred prior to 1994. However, NH₄ and NO₃-N remain
407 in the groundwater system, and NO₃-N concentrations measured at monitoring wells
408 continue to exceed the regulatory limit. The feasibility of using MNA for a remediation
409 strategy requires that attenuation occurs at a rate that will achieve cleanup within a
410 reasonable time frame. The rate of denitrification was characterized through a variety of
411 methods including microcosm concentration decay, microcosm isotopic fractionation,
412 field-scale isotopic fractionation, and solute-transport modeling. The field-scale
413 composite rate coefficient as calculated from groundwater concentration data was similar
414 to the field-scale denitrification rate coefficient, which suggests that denitrification is the
415 predominant process contributing to the overall NO₃-N attenuation. The results suggest
416 that NO₃-N in the Monument Valley alluvial aquifer is undergoing natural attenuation.
417 Current work is examining the potential for enhancing denitrification with addition of a
418 substrate. This research highlights the benefits associated with a multiple-method
419 approach for the characterization of natural attenuation.

420

421 **Acknowledgements**

422 The United States Department of Energy is gratefully acknowledged for its support and
423 funding of this project. We would also like to thank Leona Sam, Justin Berkompas,
424 Pamela Gallo, and Christopher Eastoe for their contributions.

425

426 **6.0 REFERENCES**

- 427 Aelion, C.M., Shaw, J.N., Wahl, M., 1997. Impact of suburbanization on ground water
428 quality and denitrification in coastal aquifer sediments. *Journal of Experimental Marine*
429 *Biology and Ecology* 213, 31-51.
- 430 Beller, H.R., Madrid, V., Hudson, G.B., McNab, W.W., Carlsen, T., 2004.
431 Biogeochemistry and natural attenuation of nitrate in groundwater at an explosives test
432 facility. *Applied Geochemistry* 19, 1483-1494.
- 433 Blackmer, A.M., Bremner, J.M., 1977. Denitrification of Nitrate in Soils under Different
434 Atmospheres. *Soil Biology & Biochemistry* 9, 141-142.
- 435 Blicher-Mathiesen, G., McCarty, G.W., Nielsen, L.P., 1998. Denitrification and
436 degassing in groundwater estimated from dissolved dinitrogen and argon. *Journal of*
437 *Hydrology* 208, 16-24.
- 438 Bohlke, J.K., Denver, J.M., 1995. Combined Use of Groundwater Dating, Chemical, and
439 Isotopic Analyses to Resolve the History and Fate of Nitrate Contamination in 2
440 Agricultural Watersheds, Atlantic Coastal-Plain, Maryland. *Water Resources Research*
441 31, 2319-2339.
- 442 Bohlke, J.K., Wanty, R., Tuttle, M., Delin, G., Landon, M., 2002. Denitrification in the
443 recharge area and discharge area of a transient agricultural nitrate plume in a glacial
444 outwash sand aquifer, Minnesota. *Water Resources Research* 38, Doi
445 10.1029/2001wr000663.
- 446 Bottcher, J., Strebel, O., Voerkelius, S., Schmidt, H.L., 1990. Using Isotope Fractionation
447 of Nitrate Nitrogen and Nitrate Oxygen for Evaluation of Microbial Denitrification in a
448 Sandy Aquifer. *Journal of Hydrology* 114, 413-424.
- 449 Chen, J.Y., Tang, C.Y., Yu, J.J., 2006. Use of O-18, H-2 and N-15 to identify nitrate
450 contamination of groundwater in a wastewater irrigated field near the city of
451 Shijiazhuang, China. *Journal of Hydrology* 326, 367-378.
- 452 Clement, T.P., Peyton, B.M., Skeen, R.S., Jennings, D.A., Petersen, J.N., 1997. Microbial
453 growth and transport in porous media under denitrification conditions: Experiments and
454 simulations. *Journal of Contaminant Hydrology* 24, 269-285.

455 Conan, C., Bouraoui, F., Turpin, N., de Marsily, G., Bidoglio, G., 2003. Modeling flow
456 and nitrate fate at catchment scale in Brittany (France). *Journal of Environmental Quality*
457 32, 2026-2032.

458 D'Angelo, E.M., Reddy, K.R., 1999. Regulators of heterotrophic microbial potentials in
459 wetland soils. *Soil Biology & Biochemistry* 31, 815-830.

460 Desimone, L.A., Howes, B.L., 1996. Denitrification and nitrogen transport in a coastal
461 aquifer receiving wastewater discharge. *Environmental Science & Technology* 30, 1152-
462 1162.

463 DeSimone, L.A., Howes, B.L., 1998. Nitrogen transport and transformations in a shallow
464 aquifer receiving wastewater discharge: A mass balance approach. *Water Resources*
465 *Research* 34, 271-285.

466 DOE, 1999. Final Site Observational Work Plan for the UMTRA Project Site at the
467 Monument Valley, Arizona. U.S. Department of Energy, Office of Legacy Management,
468 Document:U0018101.

469 Engesgaard, P., Kipp, K.L., 1992. A Geochemical Transport Model for Redox-Controlled
470 Movement of Mineral Fronts in Groundwater-Flow Systems - a Case of Nitrate Removal
471 by Oxidation of Pyrite. *Water Resources Research* 28, 2829-2843.

472 Feast, N.A., Hiscock, K.M., Dennis, P.F., Andrews, J.N., 1998. Nitrogen isotope
473 hydrochemistry and denitrification within the Chalk aquifer system of north Norfolk, UK.
474 *Journal of Hydrology* 211, 233-252.

475 Ford, R.G., Wilkin, R.T., Puls, R.W., 2007. Monitored Natural Attenuation of Inorganic
476 Contaminants in Ground Water Volume 1 - Technical Basis for Assessment. In: Agency,
477 U.S.E.P. (Ed.). National Risk Management Research Laboratory Office of Research and
478 Development. U.S. Environmental Protection Agency, Cincinnati, Ohio.

479 Fukada, T., Hiscock, K.M., Dennis, P.F., Grischek, T., 2003. A dual isotope approach to
480 identify denitrification in groundwater at a river-bank infiltration site. *Water Research* 37,
481 3070-3078.

482 Gelhar, L.W., Welty, C., Rehfeldt, K.R., 1992. A critical review of data on field-scale
483 dispersion in aquifers. *Water Resources Research* 28, 1955-1974.

484 Groffman, P.M., Altabet, M.A., Bohlke, J.K., Butterbach-Bahl, K., David, M.B.,
485 Firestone, M.K., Giblin, A.E., Kana, T.M., Nielsen, L.P., Voytek, M.A., 2006. Methods
486 for measuring denitrification: Diverse approaches to a difficult problem. *Ecological*
487 *Applications* 16, 2091-2122.

488 Harbaugh, A.W., McDonald, M.G., 1996. User's documentation for MODFLOW-96, an
489 update to the U.S. Geological Survey modular finite-difference ground-water flow model.
490 USGS Open-File Report 96-485.

- 491 Heatwole, K.K., McCray, J.E., 2007. Modeling potential vadose-zone transport of
 492 nitrogen from onsite wastewater systems at the development scale. *Journal of*
 493 *Contaminant Hydrology* 91, 184-201.
- 494 Howard, K.W.F., 1985. Denitrification in a Major Limestone Aquifer. *Journal of*
 495 *Hydrology* 76, 265-280.
- 496 Hubner, H., 1986. Isotope effects of nitrogen in the soil and biosphere. In: Fritz, P.,
 497 Fontes, J.C. (Eds.). *Handbook of Environmental Isotope Geochemistry, Vol 2b, The*
 498 *Terrestrial Environment*. Elsevier, pp. 361-425.
- 499 ITRC, 2000. Emerging Technologies for Enhanced In Situ Bioremediation (EISBD) of
 500 Nitrate-Contaminated Ground Water.
- 501 Jordan, F., Waugh, W.J., Glenn, E.P., Sam, L., Thompson, T., Thompson, T.L., 2008.
 502 Natural bioremediation of a nitrate-contaminated soil-and-aquifer system in a desert
 503 environment. *Journal of Arid Environments* 72, 748-763.
- 504 Kendall, C., Aravena, R., 1999. Nitrate isotopes in groundwater systems. In: Cook, P.,
 505 Herczeg, A. (Eds.). *Environmental Tracers in Subsurface Hydrology*. Kluwer Academic
 506 Publishers, Norwell, MA pp. 261-297.
- 507 Kendall, C., McDonnell, J.J. (Eds.), 1998. *Isotope Tracers in Catchment Hydrology*.
 508 Elsevier, New York.
- 509 Kinzelbach, W., Schafer, W., Herzer, J., 1991. Numerical Modeling of Natural and
 510 Enhanced Denitrification Processes in Aquifers. *Water Resources Research* 27, 1123-
 511 1135.
- 512 Knowles, R., 1982. Denitrification. *Microbiological Reviews* 46, 43-70.
- 513 Korom, S.F., 1992. Natural Denitrification in the Saturated Zone - a Review. *Water*
 514 *Resources Research* 28, 1657-1668.
- 515 Lee, M.S., Lee, K.K., Hyun, Y.J., Clement, T.P., Hamilton, D., 2006. Nitrogen
 516 transformation and transport modeling in groundwater aquifers. *Ecological Modelling*
 517 192, 143-159.
- 518 Lensing, H.J., Vogt, M., Herrling, B., 1994. Modeling of Biologically Mediated Redox
 519 Processes in the Subsurface. *Journal of Hydrology* 159, 125-143.
- 520 Mariotti, A., Landreau, A., Simon, B., 1988. N-15 Isotope Biogeochemistry and Natural
 521 Denitrification Process in Groundwater - Application to the Chalk Aquifer of Northern
 522 France. *Geochimica Et Cosmochimica Acta* 52, 1869-1878.
- 523 McCray, J.E., Kirkland, S.L., Siegrist, R.L., Thyne, G.D., 2005. Model parameters for
 524 simulating fate and transport of on-site wastewater nutrients. *Ground Water* 43, 628-639.

- 525 McGuire, J.T., Long, D.T., Klug, M.J., Haack, S.K., Hyndman, D.W., 2002. Evaluating
526 behavior of oxygen, nitrate, and sulfate during recharge and quantifying reduction rates in
527 a contaminated aquifer. *Environmental Science & Technology* 36, 2693-2700.
- 528 McKeon, C., Glenn, E.P., Waugh, W.J., Eastoe, C., Jordan, F., Nelson, S.G., 2006.
529 Growth and water and nitrate uptake patterns of grazed and ungrazed desert shrubs
530 growing over a nitrate contamination plume. *Journal of Arid Environments* 64, 1-21.
- 531 McKeon, C.A., Jordan, F.L., Glenn, E.P., Waugh, W.J., Nelson, S.G., 2005. Rapid nitrate
532 loss from a contaminated desert soil. *Journal of Arid Environments* 61, 119-136.
- 533 McMahan, P.B., Bohlke, J.K., Bruce, B.W., 1999. Denitrification in marine shales in
534 northeastern Colorado. *Water Resources Research* 35, 1629-1642.
- 535 McMahan, P.B., Bohlke, J.K., Kauffman, L.J., Kipp, K.L., Landon, M.K., Crandall,
536 C.A., Burow, K.R., Brown, C.J., 2008. Source and transport controls on the movement of
537 nitrate to public supply wells in selected principal aquifers of the United States. *Water*
538 *Resources Research* 44, Doi 10.1029/2007wr006252.
- 539 Mengis, M., Schiff, S.L., Harris, M., English, M.C., Aravena, R., Elgood, R.J., MacLean,
540 A., 1999. Multiple geochemical and isotopic approaches for assessing ground water
541 NO₃- elimination in a riparian zone. *Ground Water* 37, 448-457.
- 542 Morrill, P.L., Lacrampe-Couloume, G., Slater, G.F., Sleep, B.E., Edwards, E.A.,
543 McMaster, M.L., Major, D.W., Lollar, B.S., 2005. Quantifying chlorinated ethene
544 degradation during reductive dechlorination at Kelly AFB using stable carbon isotopes.
545 *Journal of Contaminant Hydrology* 76, 279-293.
- 546 Mulvaney, R.L., Khan, S.A., 1999. Use of diffusion to determine inorganic nitrogen in a
547 complex organic matrix. *Soil Science Society of America Journal* 63, 240-246.
- 548 Oa, S.W., Kim, G., Kim, Y., 2006. Determination of electron donors by comparing
549 reaction rates for in situ bioremediation of nitrate-contaminated groundwater. *Journal of*
550 *Environmental Science and Health Part a-Toxic/Hazardous Substances & Environmental*
551 *Engineering* 41, 2359-2372.
- 552 Pauwels, H., Kloppmann, W., Foucher, J.C., Martelat, A., Fritsche, V., 1998. Field tracer
553 test for denitrification in a pyrite-bearing schist aquifer. *Applied Geochemistry* 13, 767-
554 778.
- 555 Postma, D., Boesen, C., Kristiansen, H., Larsen, F., 1991. Nitrate Reduction in an
556 Unconfined Sandy Aquifer - Water Chemistry, Reduction Processes, and Geochemical
557 Modeling. *Water Resources Research* 27, 2027-2045.
- 558 Repert, D.A., Barber, L.B., Hess, K.M., Keefe, S.H., Kent, D.B., Leblanc, D.R., Smith,
559 R.L., 2006. Long-term natural attenuation of carbon and nitrogen within a groundwater
560 plume after removal of the treated wastewater source. *Environmental Science &*
561 *Technology* 40, 1154-1162.

- 562 Robertson, L.A., Kuenen, J.G., 1984. Aerobic Denitrification - a Controversy Revived.
563 Archives of Microbiology 139, 351-354.
- 564 Sam, L.B., 2006. Simulated Natural attenuation and Enhanced Bioremediation of Nitrate-
565 Contaminated Aquifer Materials in Monument Valley, Arizona. Department of Soil,
566 Water, and Environmental Science. University of Arizona, Tucson, p. 52.
- 567 Schurmann, A., Schroth, M.H., Saurer, M., Bernasconi, S.M., Zeyer, J., 2003. Nitrate-
568 consuming processes in a petroleum-contaminated aquifer quantified using push-pull
569 tests combined with N-15 isotope and acetylene-inhibition methods. Journal of
570 Contaminant Hydrology 66, 59-77.
- 571 Schwan, M., Kramer, D., Gericke, C., 1984. Simulation of the Nitrate Degradation in
572 Groundwater. Acta Hydrochimica Et Hydrobiologica 12, 163-171.
- 573 Schwarzenbach, R.P., Gschwend, P.M., Imboden, D.M., 1993. Environmental organic
574 chemistry. J. Wiley, New York.
- 575 Sidle, W.C., Roose, D.L., Yzerman, V.T., 2000. Isotope evaluation of nitrate attenuation
576 in restored and native riparian zones in the Kankakee watershed, Indiana. Wetlands 20,
577 333-345.
- 578 Singleton, M.J., Esser, B.K., Moran, J.E., Hudson, G.B., McNab, W.W., Harter, T., 2007.
579 Saturated zone denitrification: Potential for natural attenuation of nitrate contamination in
580 shallow groundwater under dairy operations. Environmental Science & Technology 41,
581 759-765.
- 582 Smets, B.F., Pritchard, P.H., 2003. Elucidating the microbial component of natural
583 attenuation. Current Opinion in Biotechnology 14, 283-288.
- 584 Smith, R.L., Bohlke, J.K., Garabedian, S.P., Revesz, K.M., Yoshinari, T., 2004.
585 Assessing denitrification in groundwater using natural gradient tracer tests with N-15: In
586 situ measurement of a sequential multistep reaction. Water Resources Research 40, Doi
587 10.1029/2003wr002919.
- 588 Smith, R.L., Duff, J.H., 1988. Denitrification in a Sand and Gravel Aquifer. Applied and
589 Environmental Microbiology 54, 1071-1078.
- 590 Smith, R.L., Garabedian, S.P., Brooks, M.H., 1996. Comparison of denitrification
591 activity measurements in groundwater using cores and natural-gradient tracer tests.
592 Environmental Science & Technology 30, 3448-3456.
- 593 Smith, R.L., Howes, B.L., Duff, J.H., 1991. Denitrification in Nitrate-Contaminated
594 Groundwater - Occurrence in Steep Vertical Geochemical Gradients. Geochimica Et
595 Cosmochimica Acta 55, 1815-1825.
- 596 Starr, J.L., Parlange, J.Y., 1975. Nonlinear Denitrification Kinetics with Continuous-
597 Flow in Soil Columns. Soil Science Society of America Journal 39, 875-880.

598 Whitelaw, K., Rees, J.F., 1980. Nitrate-Reducing and Ammonium-Oxidizing Bacteria in
599 the Vadose Zone of the Chalk Aquifer of England. *Geomicrobiology Journal* 2, 179-187.

600 Widdowson, M.A., Molz, F.J., Benefield, L.D., 1988. A Numerical Transport Model for
601 Oxygen-Based and Nitrate-Based Respiration Linked to Substrate and Nutrient
602 Availability in Porous-Media. *Water Resources Research* 24, 1553-1565.

603 Wiedemeier, T.H., 1999. Natural attenuation of fuels and chlorinated solvents in the
604 subsurface. John Wiley, New York.

605 Wriedt, G., Spindler, J., Neef, T., Meissner, R., Rode, M., 2007. Groundwater dynamics
606 and channel activity as major controls of in-stream nitrate concentrations in a lowland
607 catchment system? *Journal of Hydrology* 343, 154-168.

608 Zheng, C., Wang, P.P., 1999. MT3DMS: A modular three-dimensional multispecies
609 model for simulation of advection, dispersion and chemical reactions of contaminants in
610 groundwater systems; Documentation and Users Guide, Contract Report SERDP-99-1.
611 U.S. Army Engineer Research and Development Center, Vicksburg, MS.
612
613
614
615
616
617
618
619
620
621
622
623
624
625
626

627 Table 1. Compilation of natural, ethanol-, and methanol-enhanced first-order rate
 628 coefficients obtained from laboratory and field data.

<u>Natural and enhanced denitrification-rate coefficients from laboratory microcosm data.</u>			
<u>First-order rate description</u>	<u>Estimation Method</u>	<u>k (yr-1)</u>	<u>Half Life (yr)</u>
Natural (unamended)	Concentration Decay	0.7	< 1
Enhanced (methanol)	Concentration Decay	14.5	< 1
Enhanced (ethanol)	Concentration Decay	17.6	< 1
<u>Natural and enhanced denitrification-rate coefficients obtained from ¹⁵N isotopic enrichment.</u>			
<u>Substrate Description</u>	<u>α</u>	<u>k (yr-1)</u>	<u>Half Life (yr)</u>
Enhanced (methanol) microcosm	0.9824	14.5	< 1
Natural A-A' field data	0.9985	0.3	2
<u>Natural attenuation first-order rate coefficients obtained from field concentration data.</u>			
<u>First-order rate description</u>	<u>Estimation Method</u>	<u>k (yr-1)</u>	<u>Half Life (yr)</u>
Data from Well 606	Local-Scale Composite	0.02	40
Data from Well 655	Local-Scale Composite	0.04	17
Data from 1993	Field-Scale Composite	0.7	1
Data from 2007	Field-Scale Composite	0.6	1
<u>Natural denitrification-rate coefficients obtained from solute transport model calibration.</u>			
<u>Transect Zone of Application</u>	<u>Estimation Method</u>	<u>k (yr-1)</u>	<u>Half Life (yr)</u>
Near source (0-594 m)	Calibration	0.07	9
Away from source (594-1950 m)	Calibration	0.44	2

629

630

631

632

633

634

635

636

637

638

639 **Figure Captions**

640 Figure 1: Site map indicating source zone location (star), groundwater elevation contours
641 (meters above sea level), monitoring wells locations (triangles), and transect A-A' (line
642 with underlined wells labeled).

643

644 Figure 2. Nitrate depletion and nitrous oxide production in soil slurry laboratory
645 microcosms as a function of time. Results designated as natural refer to denitrification
646 without substrate addition, and results designated as methanol or ethanol enhanced refer
647 to carbon substrate amended denitrification.

648

649 Figure 3. Nitrogen stable isotope fractionation (isotopic ratios relative to initial values
650 versus concentrations relative to initial values) observed during laboratory microcosm
651 experiments with and without amendment. The symbols refer to isotopic composition
652 data, and the lines present the results of regression analysis.

653

654 Figure 4. Groundwater ammonium (a) and nitrate (b) concentrations obtained from
655 sampling of monitoring wells along transect A-A' as a function of time. The symbols
656 indicate data for numbered wells, and the lines are the results of exponential regression
657 for selected wells.

658

659 Figure 5. Groundwater ammonium (a) and nitrate (b) concentrations obtained from
660 sampling monitoring wells at various times as a function of distance along transect A-A'.

661 The symbols indicate data for samples collected at the same time, and the lines are the
662 results of exponential regression for selected years.

663

664 Figure 6. Nitrogen stable isotope fractionation (isotopic ratios relative to initial values)
665 observed upon analysis of groundwater samples (without substrate amendment) collected
666 from monitoring wells as a function of distance along transect A-A' (a) and as a function
667 of relative concentration (b). The symbols refer to isotopic composition data, and the
668 lines present the results of regression analysis.

669

670 Figure 7. Comparison of observed (data points) and simulated (lines) groundwater
671 elevation (a) with distance along transect A-A' upon calibration of the MODFLOW
672 model, and comparison of observed (data points) and simulated (lines) groundwater
673 nitrate concentrations (b) with distance along transect A-A' upon calibration of the
674 MT3DMS transport model.

675

676

677

678

679

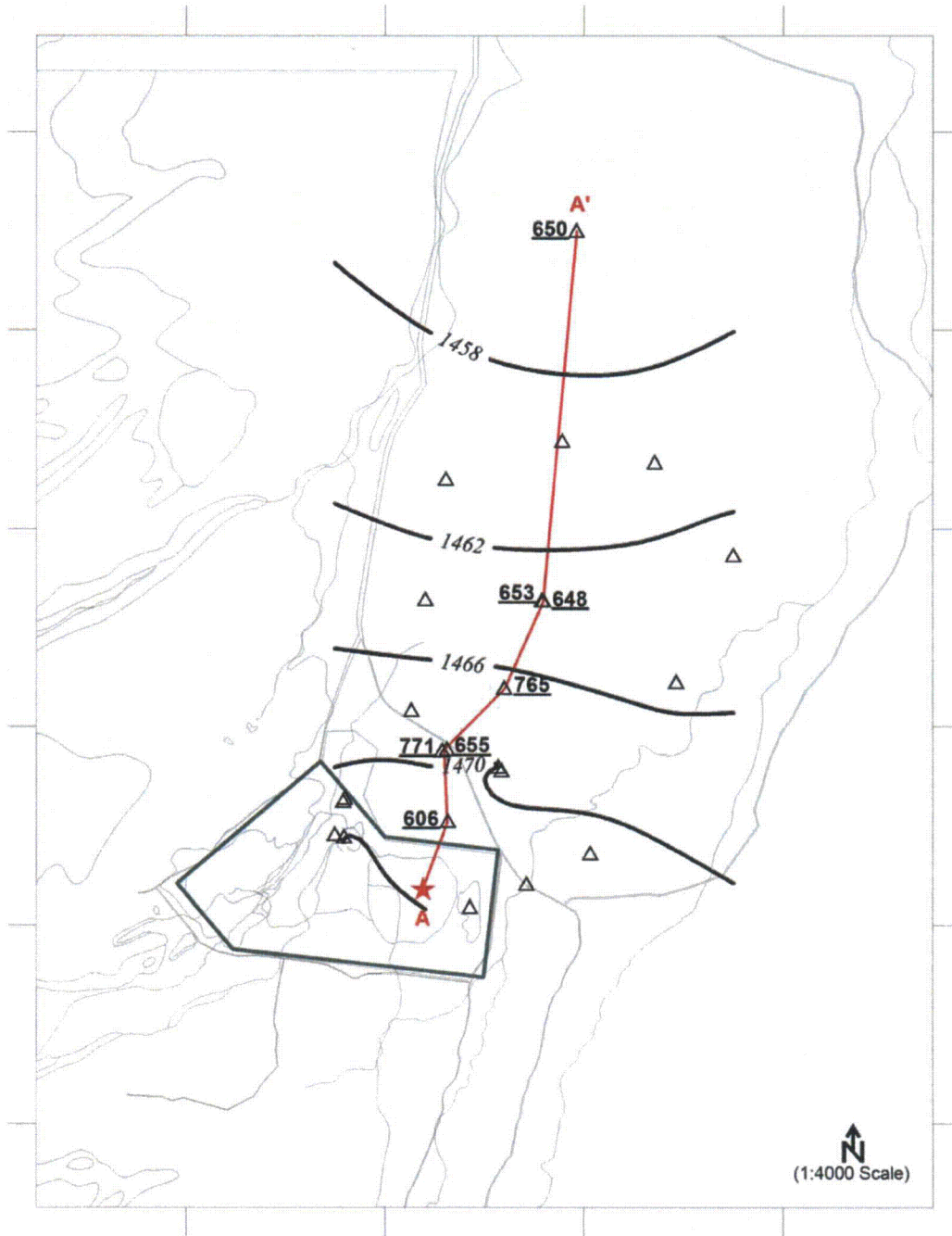
680

681

682

683

684



685

686 Figure 1

687

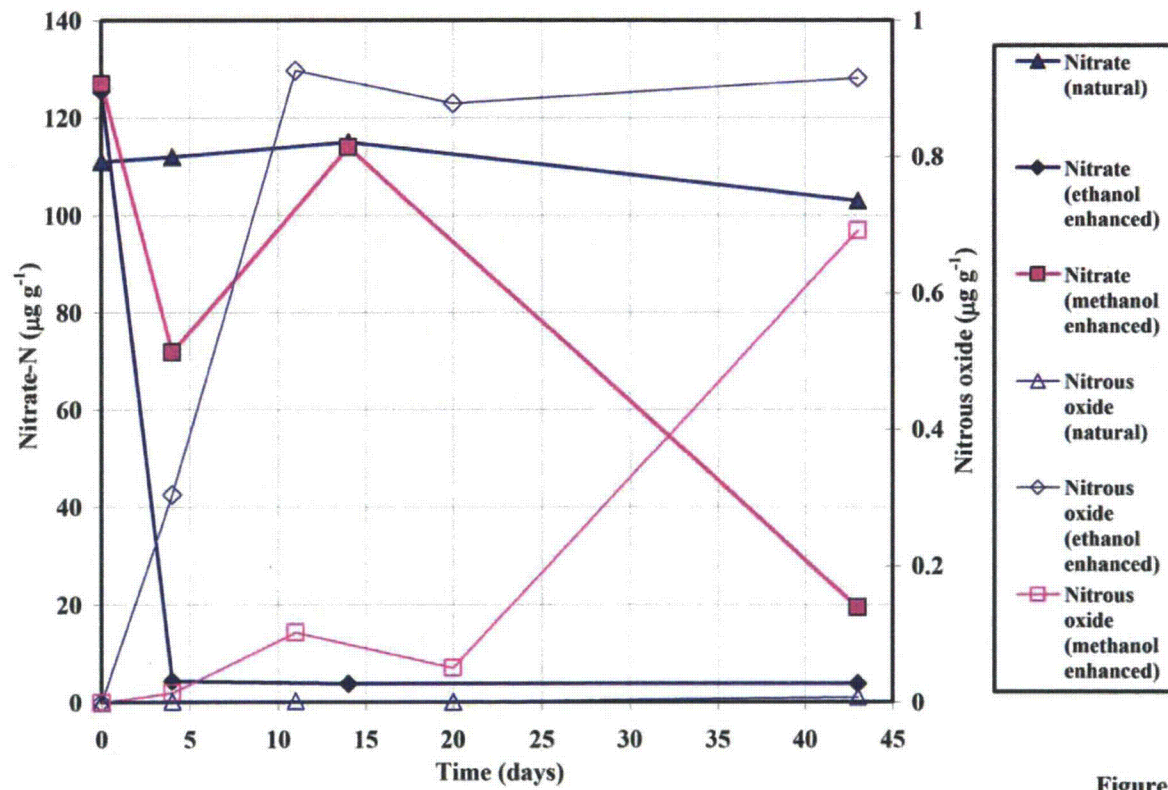


Figure 2

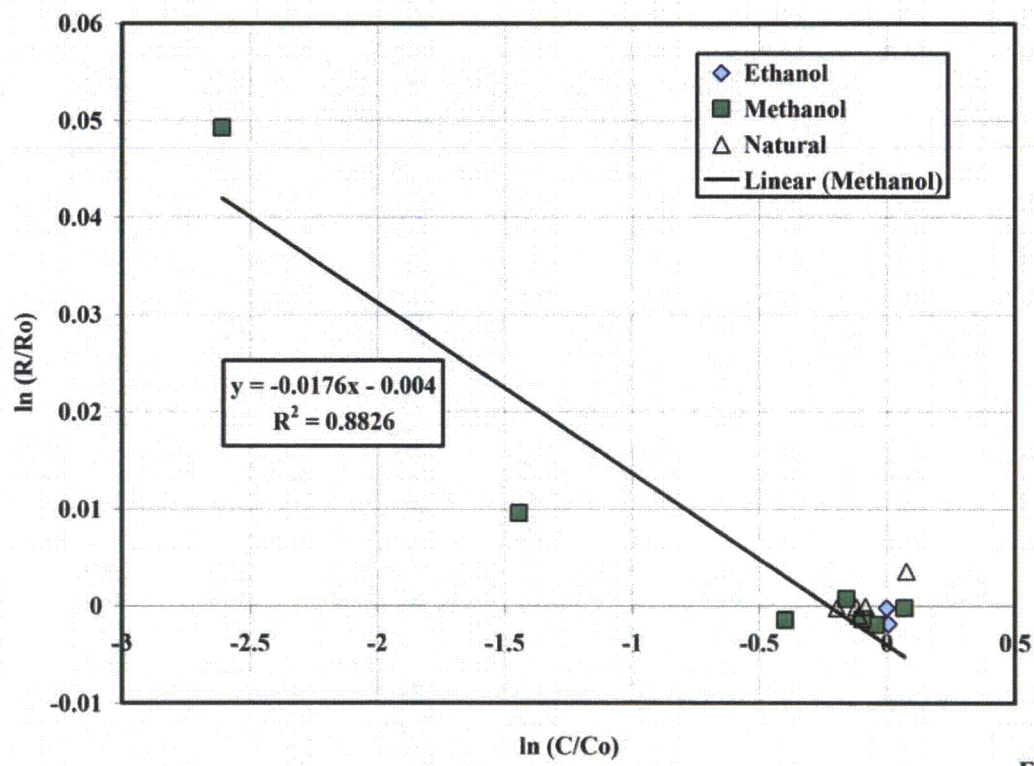


Figure 3

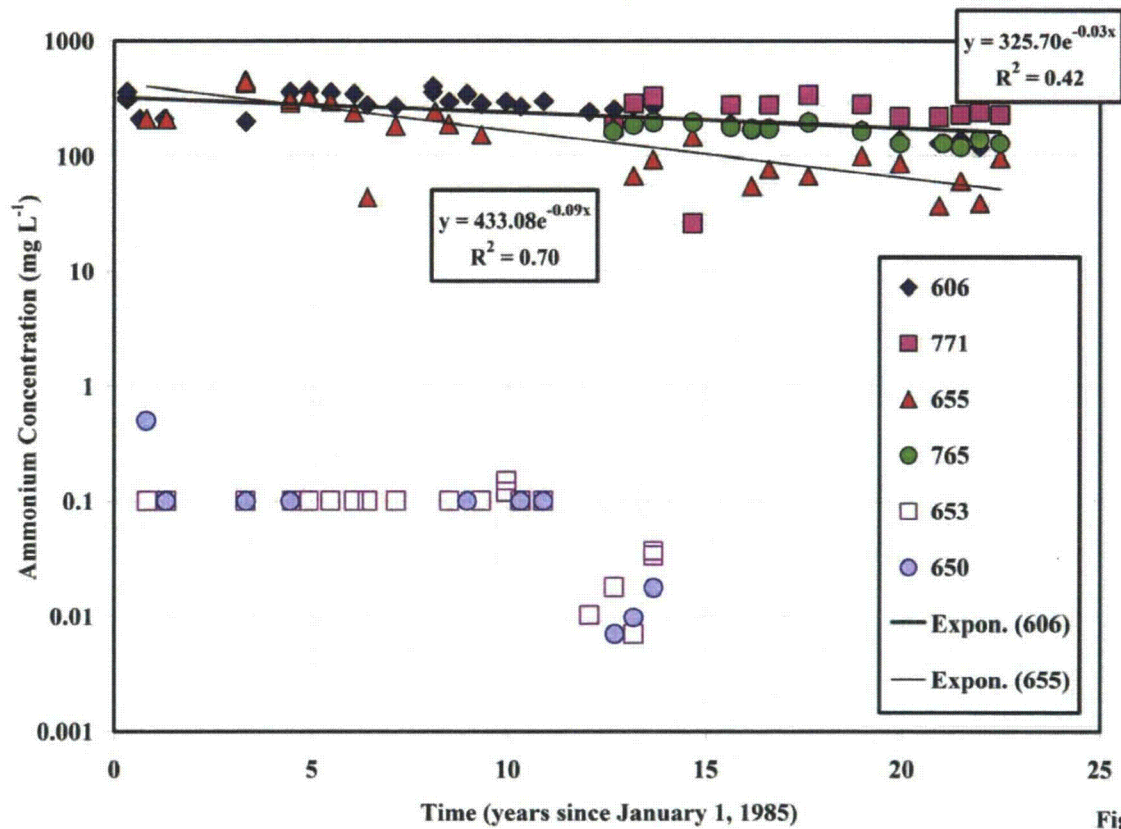


Figure 4a

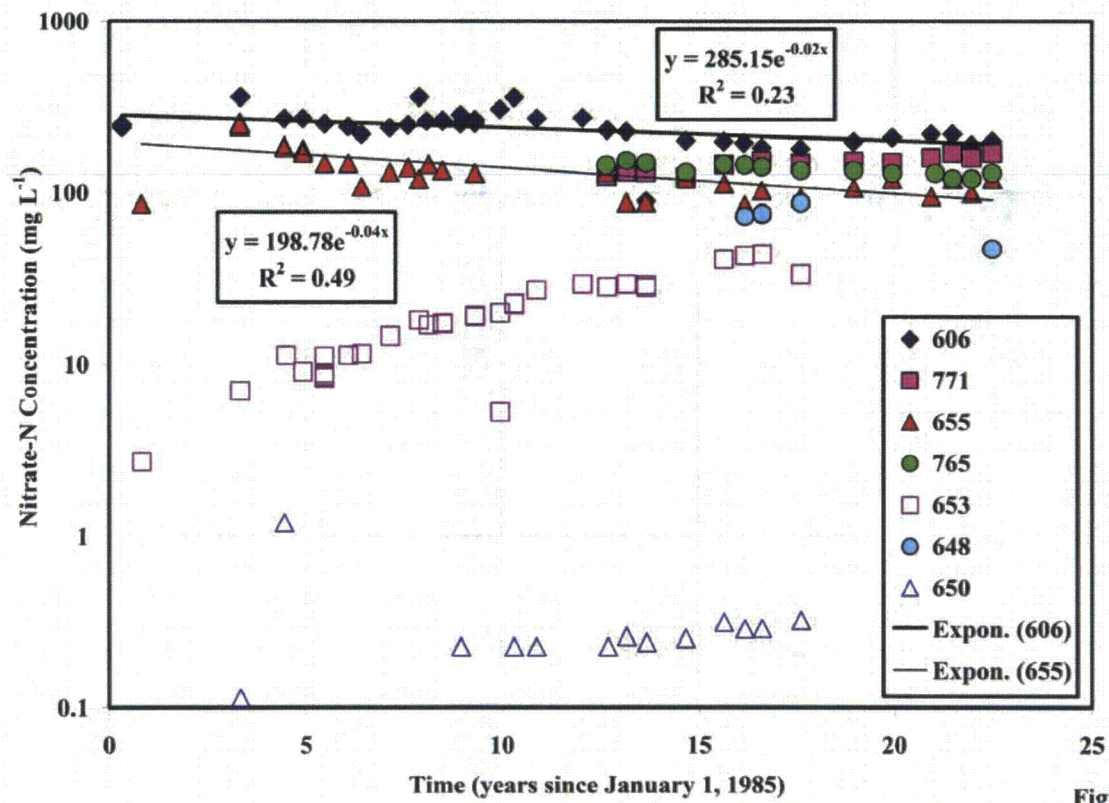


Figure 4b

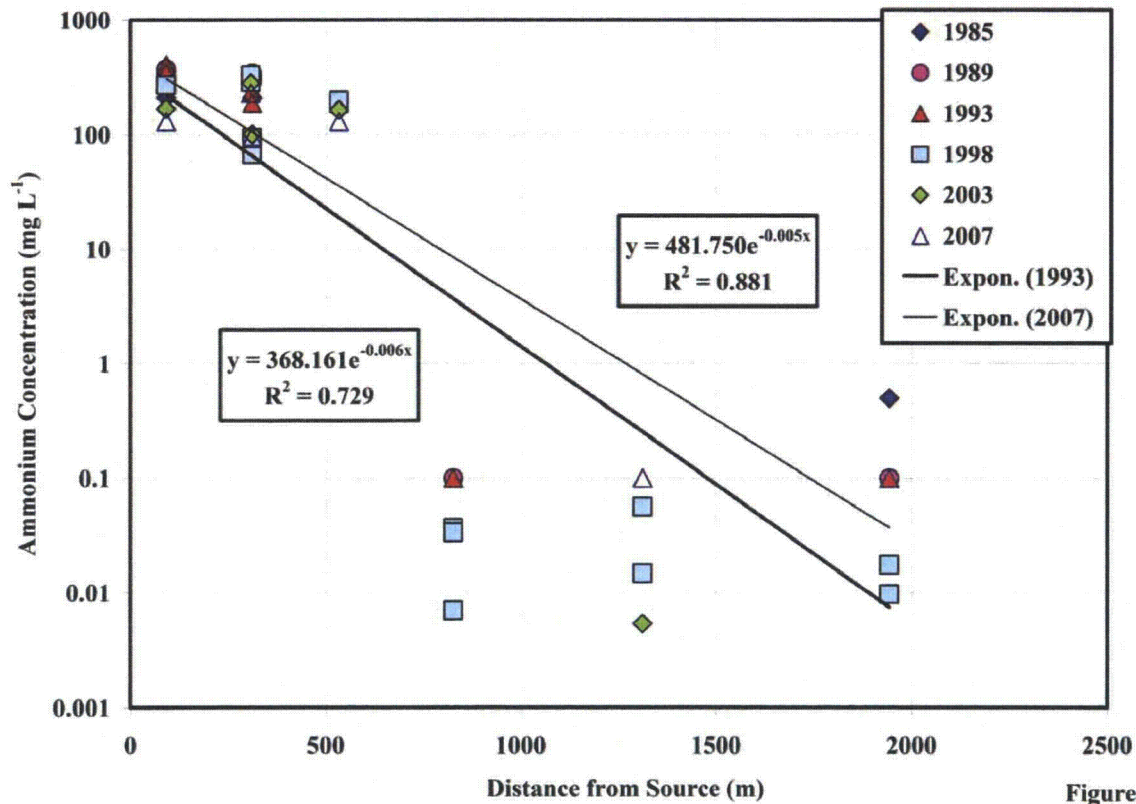


Figure 5a

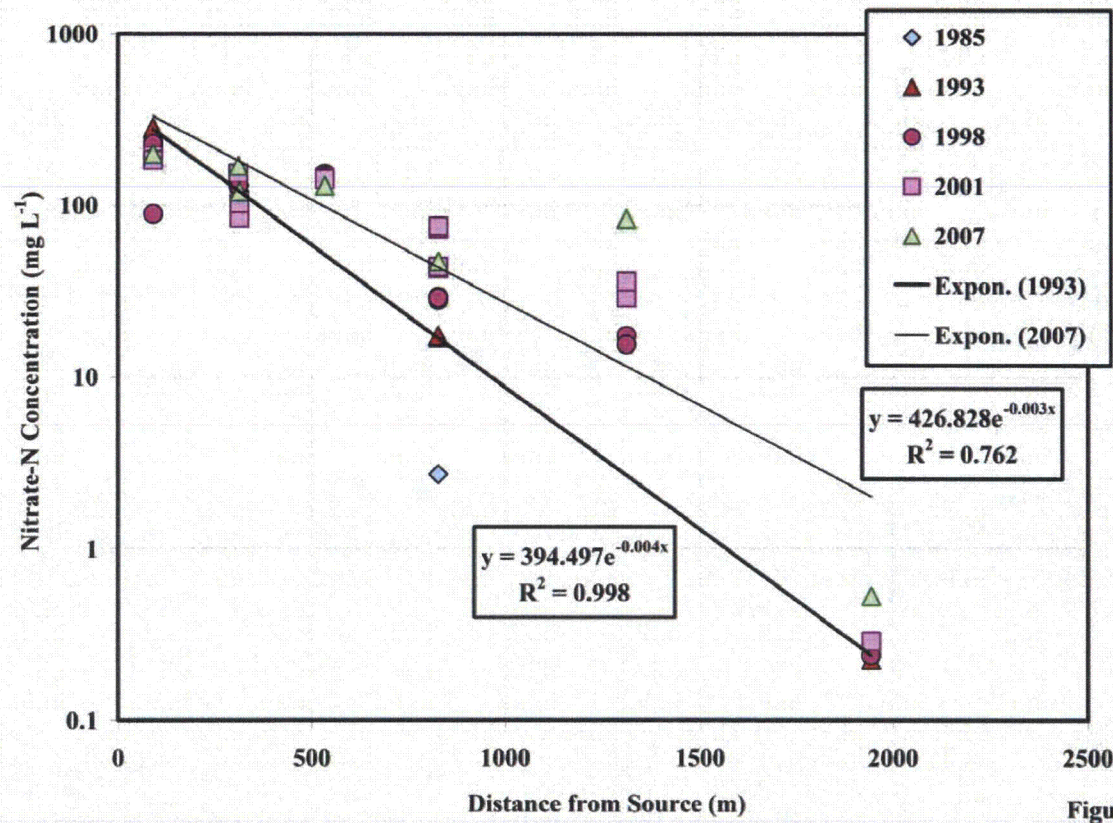


Figure 5b

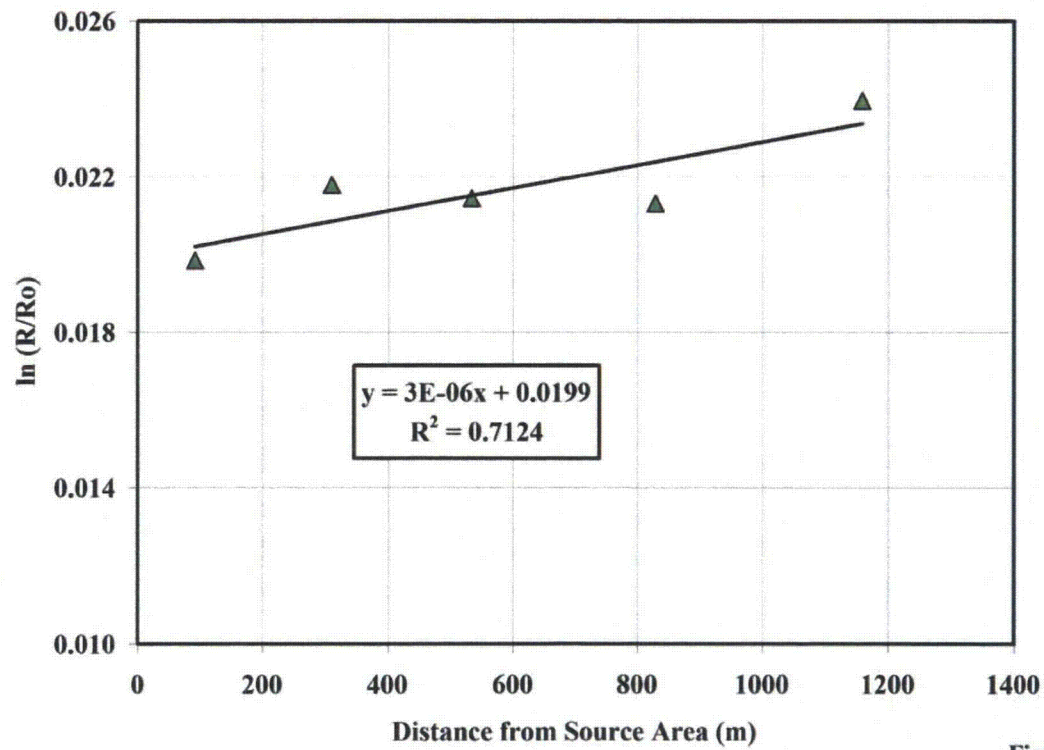


Figure 6a

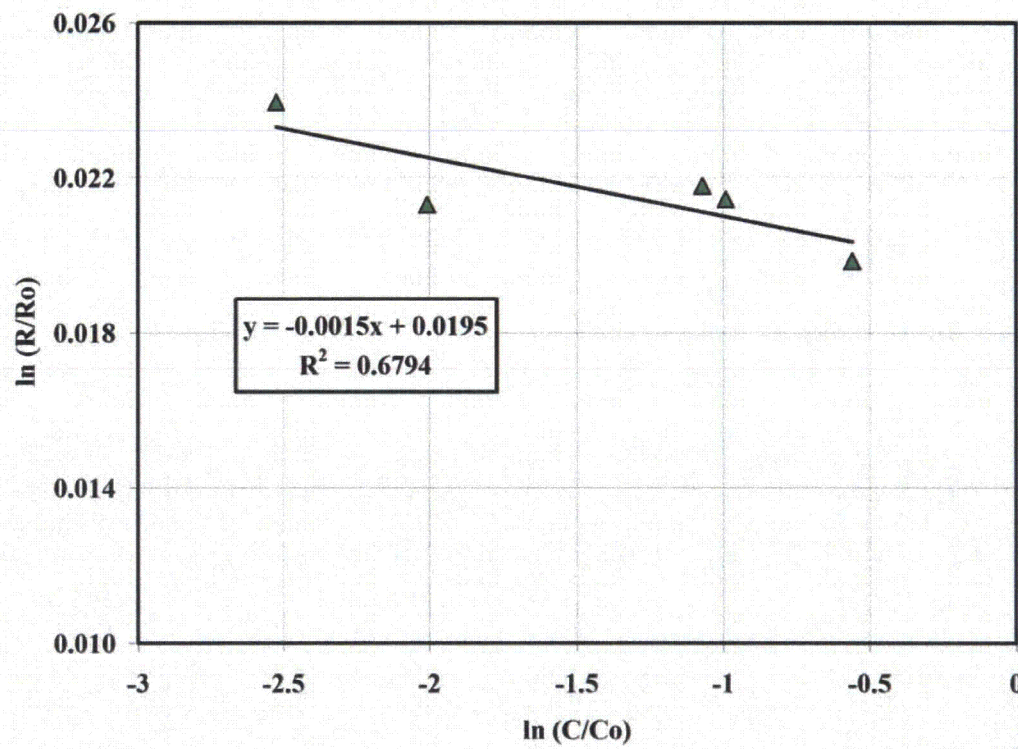


Figure 6b

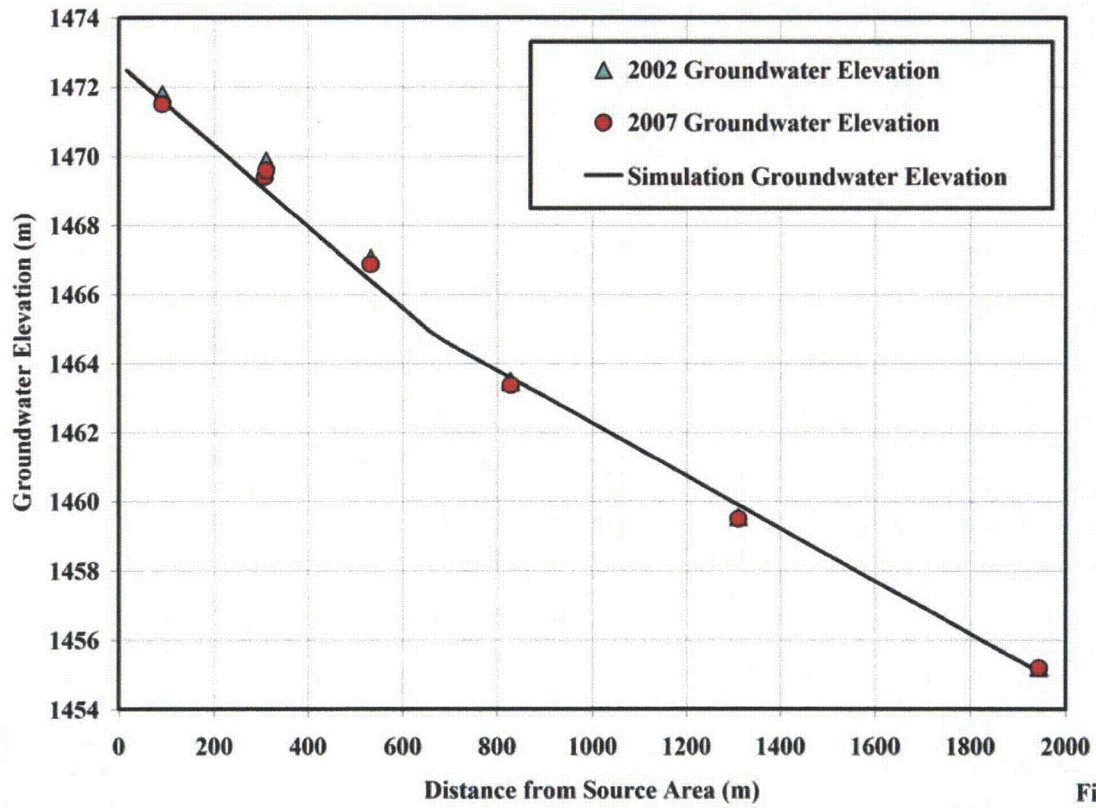


Figure 7a

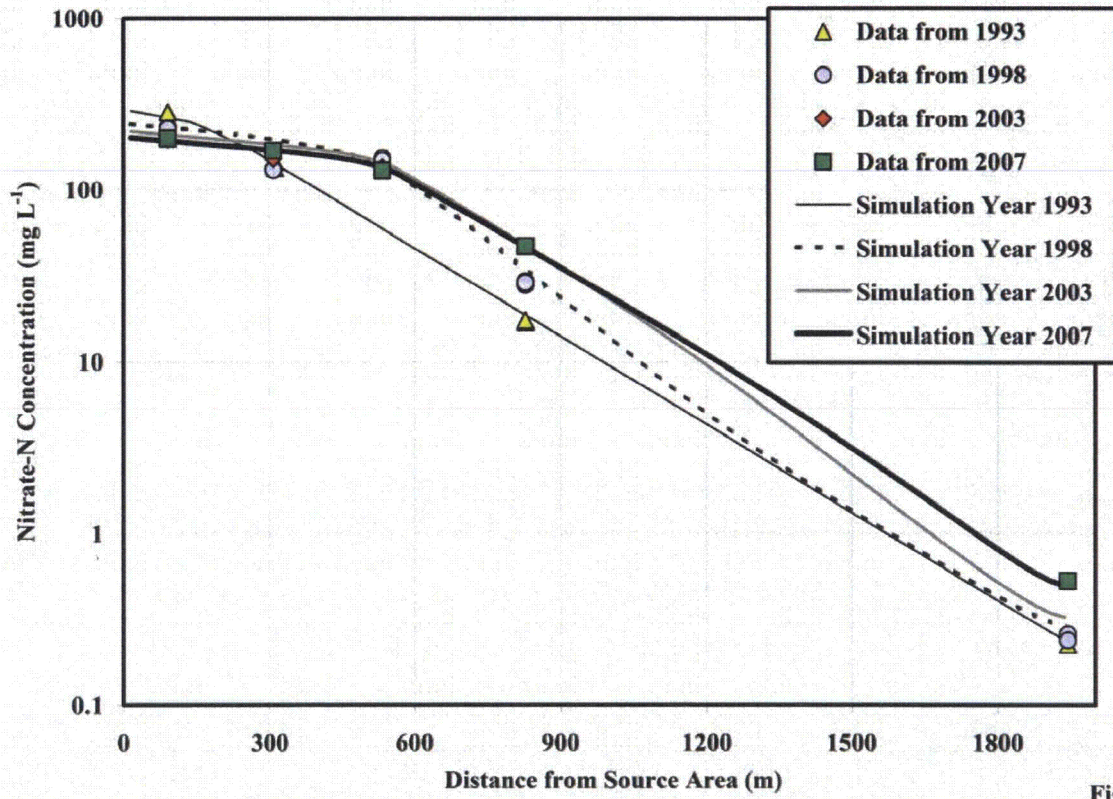


Figure 7b

Appendix E
Ecohydrology Journal Manuscript

This page intentionally left blank

Scaling sap flux measurements of grazed and ungrazed shrub communities with fine and coarse-resolution remote sensing

Edward P. Glenn,^{1*} Kiyomi Morino,² Kamel Didan,³ Fiona Jordan,¹ Kenneth C. Carroll,³ Pamela L. Nagler,⁴ Kevin Hultine,⁵ Linda Sheader⁶ and Jody Waugh⁶

¹ Environmental Research Laboratory of the University of Arizona, Tucson, AZ, USA

² Tree Ring Laboratory, University of Arizona, Tucson, AZ, USA

³ Department of Soil, Water and Environmental Science, University of Arizona, Tucson, AZ, USA

⁴ U.S. Geological Survey, University of Arizona, Tucson, AZ, USA

⁵ Department of Biology, University of Utah, Salt Lake City, UT, USA

⁶ S.M Stoller Corporation, Grand Junction, CO, USA

ABSTRACT

We measured transpiration by black greasewood (*Sarcobatus vermiculatus*) (SAVE) and fourwing saltbush (*Atriplex canescens*) (ATCA) over a nitrate-contaminated aquifer in Monument Valley, Arizona, on the Colorado Plateau. Heat balance sap flow sensors were used to measure transpiration by shrubs in 2006 and 2007 and results were scaled to larger landscape units and longer time scales using leaf area index (LAI), fractional vegetation cover, meteorological data, and the enhanced vegetation index (EVI) from MODIS sensors on the Terra satellite. Transpiration was high depending on leaf area (2.95–6.72 kg m⁻² d⁻¹) and was controlled by vapour pressure deficit (D) in the atmosphere. SAVE tended to have higher transpiration rates than ATCA and had a steeper response to D , but both exhibited midday depression of leaf conductance. Over most of the site, fractional vegetation cover (f_c) and area-wide LAI were low (0.10 and 0.37, respectively) due to heavy grazing by cattle and sheep. However, a portion of the plume that had been protected from grazing for 10 years had $f_c = 0.75$, LAI = 2.88. Transpiration rates on a ground-area basis varied with LAI, with midsummer daily values ranging from 1.44 mm d⁻¹ (LAI = 0.36) to 13.1 mm d⁻¹ (LAI = 2.88 mm) over the site, corresponding to projected annual values of 159–1447 mm year⁻¹. Controlling grazing could, theoretically, slow or halt the movement of the contamination plume by allowing the shrub community to extract more water than is recharged in the aquifer. Copyright © 2008 John Wiley & Sons, Ltd.

KEY WORDS *Atriplex*; *Sarcobatus*; nitrate contamination; transpiration; ground water depletion

Received 3 March 2008; Accepted 19 May 2008

INTRODUCTION

Evapotranspiration by desert phreatophyte shrub communities

Vegetation plays a key role in determining rates of discharge and recharge of aquifers in arid and semi-arid rangelands (Wilcox and Thurow, 2006). Removal of vegetation, as through over-grazing, can result in increased runoff and recharge, whereas an intact vegetation community generally consumes nearly all the annual precipitation (Huxman *et al.*, 2005). The zone of active water uptake by plants can extend deep into desert soils; phreatophytic shrubs and trees can extract water from alluvial aquifers tens of metres from the soil surface, and can be the major biological component of the water cycle in shrub ecosystems (Nichols, 2000; Groeneveld *et al.*, 2007). Determining the rate of ground water discharge by phreatophytes is important in assessing local and regional water budgets, as the area occupied by non-riparian phreatophytes is very large (tens of millions of ha) in the

western USA (Shreve, 1942). Across much of the Colorado Plateau and Great Basin Province of the western USA, phreatophyte communities are the principal or only source of ground water discharge (Nichols, 1994, 2000). Phreatophytes can also influence the rate of migration of contaminants in aquifers through their effects on ground water movement (Jordan *et al.*, 2008). However, only a few studies have attempted to quantify rates of phreatophyte transpiration over wide areas (Nichols, 1993, 1994; Steinwand *et al.*, 2001, 2006; Cooper *et al.*, 2006; Groeneveld *et al.*, 2007; Groeneveld and Baugh, 2007), and different methods have yielded different results (discussed in Nichols, 1994; Cooper *et al.*, 2006).

Methods to estimate phreatophyte transpiration

Early estimates of phreatophyte water consumption depended on indirect approaches, such as growing phreatophytes in concrete tanks to measure water consumption, then extrapolating the results to natural stands of plants. Nichols (1994) used a Bowen ratio micrometeorological method to estimate total evapotranspiration (ET), including plant water consumption and bare soil evaporation, in natural stands of phreatophytes in the Great Basin

* Correspondence to: Edward P. Glenn, Environmental Research Laboratory of the University of Arizona, 2601 East Airport Drive, Tucson, AZ 85706, USA. E-mail: eglenn@ag.arizona.edu

Province, and concluded that the earlier estimates were prone to large errors. Steinwand *et al.* (2001) used porometry to measure stomatal conductance of individual leaves of two phreatophyte shrubs in Owens Valley, California, then developed crop coefficients to scale transpiration over wide areas based on fractional vegetation cover (f_c) and leaf area index (LAI). However, enclosing the leaves in a leaf-chamber may not be representative of natural conductance rates. Furthermore, their use of crop coefficients was criticized as inappropriate for desert plants because it assumes unstressed conditions, which might not apply to desert plants (Mata-Gonzalez *et al.*, 2005).

More recently, Bowen ratio (Cooper *et al.*, 2006) and eddy co-variance (Steinwand *et al.*, 2006; Groeneveld *et al.*, 2007) moisture flux towers have been used to measure ET of phreatophyte communities. Flux towers unobtrusively measure ET over areas of several thousand square metres of uniform vegetation cover, and the measurements can be scaled to larger areas by remote sensing methods. Flux towers measure both bare soil evaporation and plant transpiration, so the plant contribution to ET is not directly measured.

Reported rates of transpiration or ET in non-riparian, arid-zone phreatophyte communities vary widely, from as low as 20 mm year⁻¹ to greater than 600 mm year⁻¹ depending on vegetation type and site characteristics (Cooper *et al.*, 2006; Steinwand *et al.*, 2006; Groeneveld *et al.*, 2007). Transpiration rates are influenced by precipitation (Lin *et al.*, 1996), soil type (Hultine *et al.*, 2006), depth to ground water (Nichols, 1994), fluctuations in ground water level (Naumberg *et al.*, 2005), and land use practices such as grazing (McKeon *et al.*, 2006) and pumping of ground water for human use (Cooper *et al.*, 2006). The percentage of transpired water derived from ground water also varies widely; in the Owens Valley study, ground water accounted for 20–30% of ET from shrubs, but 60–80% of ET from high-cover meadows with ground water 1–3 m beneath the surface (Steinwand *et al.*, 2006). More site-specific information on phreatophyte water consumption is needed for the common phreatophyte associations in the western USA. Remote sensing methods for estimating phreatophyte water use over wide areas are also needed.

Purpose of the present study

This study measured wide-area transpiration in a phreatophyte community growing over a nitrate-contaminated alluvial aquifer at a former uranium mill site in the Great Basin Desert of the USA. The two main shrubs growing over the contamination plume are black greasewood (*Sarcobatus vermiculatus* hereafter referred to as SAVE) and fourwing saltbush (*Atriplex canescens*, hereafter referred to as ATCA). Black greasewood–saltbush plant associations are widely distributed in the western USA, dominating many inter-mountain basins that support alluvial aquifers within 10 m of the surface (Shreve, 1942; Anderson, 2004). The saltbush component can be fourwing saltbush, as in the present study, shadscale

(*Atriplex confertifolia*, hereafter referred to as ATCO), quailbush (*Atriplex lentiformis*), or less widely distributed saltbush species.

Analyses of oxygen, hydrogen and nitrogen isotopes in water samples from soils, the aquifer, and plant stems showed that these shrubs are extracting water and nitrate from the contamination plume, at depths of 6–12 m below the soil surface (McKeon *et al.*, 2005, 2006; Jordan *et al.*, 2008). The site is heavily grazed by sheep and cattle, and previous studies also showed that when shrubs were fenced to prevent grazing, they increased 2- to 3-fold in biomass over just 4 years (McKeon *et al.*, 2006). Therefore, reduction of grazing would allow greater shrub cover, and thus, more transpiration, minimizing the recharge of ground water and thereby reducing the migration of the plume. However, rates of transpiration were not estimated, and it is unknown what actual impact the shrub community has on the local water balance.

In the present study, we used sap flow sensors to estimate transpiration by each shrub type and remote sensing methods to scale the results over larger landscape units and over multiple years (2000–2007) for grazed and ungrazed areas over the plume. We compared transpiration rates to precipitation and to estimates of aquifer recharge. We found that these plants have high rates of transpiration on a leaf area and canopy area basis, and they discharge large volumes of groundwater even when heavily grazed. The results and methods are relevant to other shrub communities in the western USA.

MATERIALS AND METHODS

Site description

The Monument Valley Uranium Mill Tailings Remediation (UMTRA) site is located on the Navajo Nation land in northern Arizona, approximately 24 km southeast of Mexican Hat, Utah, in a high desert (1540 m elevation), dune-and-swale environment on the Colorado Plateau (United States Department of Energy, 1999). Site characteristics and previous research are reported in McKeon *et al.* (2005, 2006); Jordan *et al.* (2008), and in documents from the United States Department of Energy (1999, 2000, 2004, 2006). Annual precipitation is approximately 110 mm, arriving as summer monsoon rains and winter snow and rain. Figure 1 shows the areas of interest at the site covered in the present study. Phreatophyte shrubs growing over the plume consists primarily of ATCA and SAVE shrubs, with some ATCO shrubs, but annual plants and non-phreatophytic perennials augment the flora (United States Department of Energy, 1999; McKeon *et al.*, 2006). The source area, site of the former milling activities, has been fenced since 1997. However, outside the fence the phreatophyte community is heavily grazed, as elsewhere on the Navajo Nation lands (Savage, 1991; McFadden and McAuliffe, 1997).

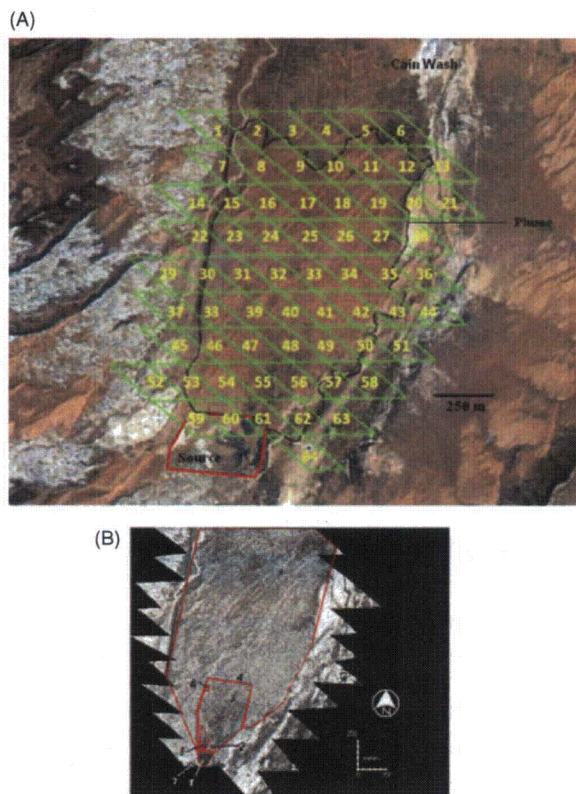


Figure 1. Satellite images used in determining ET and fractional cover, and areas of interest at the Monument Valley UMTRA site. (a) Location of MODIS pixels superimposed on a 2007, panchromatic Quickbird image, showing the extent of the contamination plume in black and the fenced source area in red. (b) Quickbird image classified to show shrub cover as black pixels. Areas of interest in the study were: (Site 1) an area of volunteer plants (mainly *Atriplex canescens*) (ATCA) inside the site fence; (Site 2) a portion of the natural plant stand (mixed *A. canescens* and SAVE) just outside the site fence to compare with (Site 1); (Site 3) the full extent of the naturally dense plant stand over the hot-spot area of the contamination plume north of the fenced area; (Site 4) a large area of sparse cover (mainly ATCA) over the whole plume; (Site 5) the South Exclusion plot (mixed ATCA and SAVE); (Site 6) the North Exclusion plot (mainly ATCA); (Site 7) an irrigated planting (only partly shown).

Research objectives

Our objectives were: (1) to determine rates of leaf-level transpiration (E_L) by representative plants inside and outside animal enclosures (fenced areas) using sap flow sensors; (2) to scale E_L to larger landscape units using plant leaf area determined by leaf harvesting and f_c determined on high-resolution Quickbird satellite images; and (3), to scale plot-level measurements over seasons and years for areas of interest over the contamination plume using imagery from the Moderate Resolution Imaging Spectrometer (MODIS) sensors on the Terra satellite and ground meteorological data. Terminology and units can differ among ET studies; here we follow Ewers and Oren (2000) for sap flux, transpiration and stomatal conductance terminology and units, and Monteith and Unsworth (1990) for other units. In this article we also distinguished between LAI defined as m^2 of leaf area per m^2 of ground area, including both plant canopies and areas of bare soil; and plant leaf area index (LAPS) defined as m^2 of leaf

area per m^2 of plant horizontal surface (Groeneveld and Warren, 1992).

Sap flow measurements

The procedures have been described in detail in Kjelgaard *et al.*, 1997; Grime and Sinclair (1999) and Nagler *et al.* (2003, 2007). We used homemade sensors described in Scott *et al.* (2006), which were validated by measurements of ET by flux towers in that study. In the heat balance method, a branch containing leaves is wrapped by a heating wire and a constant source of low-grade heat is applied to the branch through an electric heating wire (Kjelgaard *et al.*, 1997). Thermocouples embedded in the branch measure temperatures upstream and downstream from the heat source, and a thermopile outside the heating wire in the surrounding layer of insulation measures heat lost radially from the stem. A heat balance equation is then solved to calculate heat transported by convection in the transpiration stream, and the results are expressed in terms of grams of water transported per hour.

The sap flow measurements were made inside and outside two 50×50 m, livestock enclosures at the site (see Figure 1 for locations), which were erected in 2006 for long-term monitoring of grazing effects. ATCA and SAVE are co-dominants at the South Exclusion while ATCA alone dominated the North Exclusion (Table I). Data were collected from 8 September to 18 September 2006, and from 9 July to 15 August 2007. In 2006,

Table I. Fractional cover of plants, litter, and bare soil inside and outside livestock enclosure plots where sap flow measurements were taken at the Monument Valley UMTRA site, November, 2007.

Cover type	South inside	North inside	South outside	North outside
Phreatophyte shrubs				
<i>Atriplex canescens</i>	0.163	0.106	0.016	0.089
<i>Atriplex confertifolia</i>	0.006	—	0.008	—
<i>Sarcobatus vermiculatus</i>	0.104	—	0.041	—
Total phreatophyte shrubs	0.273	0.106	0.065	0.089
Non-phreatophyte shrubs				
<i>Ephedra torreyana</i>	—	0.013	—	—
<i>Ephedra viridis</i>	—	0.002	—	—
<i>Gutierrezia sarothrae</i>	0.003	—	0.009	—
<i>Poliomintha incana</i>	—	0.007	—	0.004
<i>Vanclevea stylosa</i>	—	0.003	—	0.021
<i>Yucca angustifolia</i>	—	—	—	0.006
Total non-phreatophyte shrubs	0.003	0.025	0.009	0.031
Forbs				
<i>Ambrosia acanthicarpa</i>	—	0.009	—	—
<i>Chamaesyce maculate</i>	—	0.005	—	—
<i>Descurainia sophia</i>	0.016	0.034	0.028	0.022
<i>Machaeranthera sp.</i>	—	0.001	—	—
<i>Mentzelia multiflora</i>	0.1	0.2	0.1	0.2
<i>Salsola tragus</i>	0.092	0.036	0.066	0.057
<i>Suaeda torreyana</i>	—	—	0.023	—
Total forbs	0.109	0.087	0.118	0.081
Plant litter	0.156	0.152	0.121	0.128
Bare ground	0.459	0.631	0.687	0.670
Total vegetative cover	0.385	0.217	0.192	0.202

sap flows sensors were attached to—eight to ten individual ATCA and SAVE plants inside and outside each enclosure. In 2007, eight to ten SAVE plants inside and outside the South Enclosure were gauged, and eight to ten ATCA plants inside and outside the North Enclosure were gauged (18 plants per species each year).

Not all sensors produced reliable data throughout the study periods. Some sensors were lost due to rodents chewing the electric cables connecting the sensors to the data logger and voltage regulator. Others were lost to grazing damage by cattle, or to heat damage to the stem from the heating wire. Some sensors produced aberrant diurnal patterns of temperature response, such as higher temperature readings at the thermocouple below the heating wire compared to above the wire during the daytime (the opposite is expected because the heating wire should raise the temperature of water in the transpiration stream). This is attributed to solar heating of the plant stem below the sensor. We screened the sensor data to eliminate sensors that did not survive the entire measurement period or that produced aberrant temperature patterns. We also employed a filtering program that eliminated spikes in the sap flow traces. The final dataset consisted of sap flux per branch (J) in $\text{g H}_2\text{O h}^{-1}$ reported at half-hour intervals. Of the 36 sensors deployed each year, 16 produced complete datasets in 2006 and 20 produced data in 2007.

Determining species composition and fractional cover inside and outside enclosure plots

Ground surveys using a line-intercept method were conducted in November 2007 to compare vegetation inside and outside the enclosure plots. For inside measurements, 20 randomly placed 5-m transects were established in each plot, and cover classes were determined at 10-cm intervals along the transects ($n = 1000$ observations per plot). Cover classes include bare soil, plant litter, or vegetation, determined to species level. The same procedure was used to score outside vegetation, within a $50 \text{ m} \times 50 \text{ m}$ area adjacent to the east side of each enclosure plot.

Scaling sap flux measurements

Sap flux per branch was scaled to a unit leaf area basis as:

$$E_L = J/A_L \quad (1)$$

where A_L is leaf area per branch in square metres. On a daily time step E_L is reported in units of $\text{kg H}_2\text{O m}^{-2} \text{ leaf d}^{-1}$, and on an hourly time step in units of $\text{mmol H}_2\text{O m}^{-2} \text{ s}^{-1}$ for comparison with leaf conductance values (Ewers and Oren, 2000). At the end of the measurement period, all branches with gauges were harvested and returned to the laboratory in paper bags. Plant material was dried in a solar drier, then all leaves on the branch were collected by hand-sorting them from stems and twigs. Dry mass of leaves were converted to square metres of leaf area by determining the specific leaf area (SLA) of sub-samples of leaves. Each year, SLA was

determined during the period of sap flux measurements by collecting a sample of several hundred fresh leaves from ten plants of each species (5 inside and 5 outside the enclosures) (Nagler *et al.*, 2004, 2007). The area of a leaf sample was quantified by placing them on graph paper and counting the area covered by leaves after which the sample was dried to determine m^2 of leaf area per g dry weight of leaves. Leaf area in $\text{m}^2 \text{ g}^{-1}$ was 0.00636 ($\text{SE} = 0.000135$) for fourwing saltbush and 0.00670 ($\text{SE} = 0.000738$) for black greasewood pooled over years and treatments ($P > 0.05$).

E_L was converted to E on a ground-area basis (E_G) as:

$$E_G = E_L \times \text{LAI} \quad (2)$$

with:

$$\text{LAI} = \text{LAPS} \times f_c \quad (3)$$

where f_c is fractional cover of shrubs over the ground and LAPS is the plant LAI (Groeneveld and Warren, 1992). E_G is reported in volumetric units of mm d^{-1} , which are equivalent to units of $\text{kg H}_2\text{O m}^{-2}$ ground area d^{-1} , with 1 mm of H_2O equal to $1 \text{ kg m}^{-2} \text{ H}_2\text{O}$. LAPS was determined by a leaf harvesting method (Nagler *et al.*, 2004) for each plant canopy that received sap flow sensors (total of 36 ATCA and 36 SAVE plants). In 2006, a 0.25 m^2 ($0.5 \text{ m} \times 0.5 \text{ m}$) frame was held horizontal to the ground over a randomly selected portion of the plant canopy, and all leaves within the frame were harvested and dried to determine in grams the leaves m^{-2} of plant canopy area projected on the ground. The procedure was the same in 2007 except that a 0.0625 m^2 ($0.25 \text{ m} \times 0.25 \text{ m}$) frame was used. We then calculated LAPS of a canopy by multiplying g m^{-2} by SLA, determined as described above. Since LAPS and SLA can change over the year, we determined these parameters during the periods of sap flux measurements.

Determining f_c and standing biomass from Quickbird images

Fractional cover was determined on Quickbird images (Digital Globe, Inc., Longmont, CO) acquired on 20 October 2006 and 12 July 2007. The images were sharpened, panchromatic (natural colour) with 0.3 m resolution, and individual shrubs could be resolved on the images. Images were imported into ERDAS Imagine software (Leica Geosystems, Inc., Atlanta, GA) and processed in an unsupervised classification program in which pixels were partitioned into four classes, one of which corresponded to shrubs on the site. However, the shrub class also included shadows cast by the shrubs. We corrected for shadows by measuring the dimensions of individual canopies of ten ATCA and ten SAVE plants on the ground in 2007, then comparing the ground estimates of canopy area to those calculated for the same shrubs from the classified 2007 Quickbird image (Figure 2(A)). A linear equation was fitted to the data for individual shrubs. However, as f_c increases the effect of shadows cast on bare soil decreases, since shadows

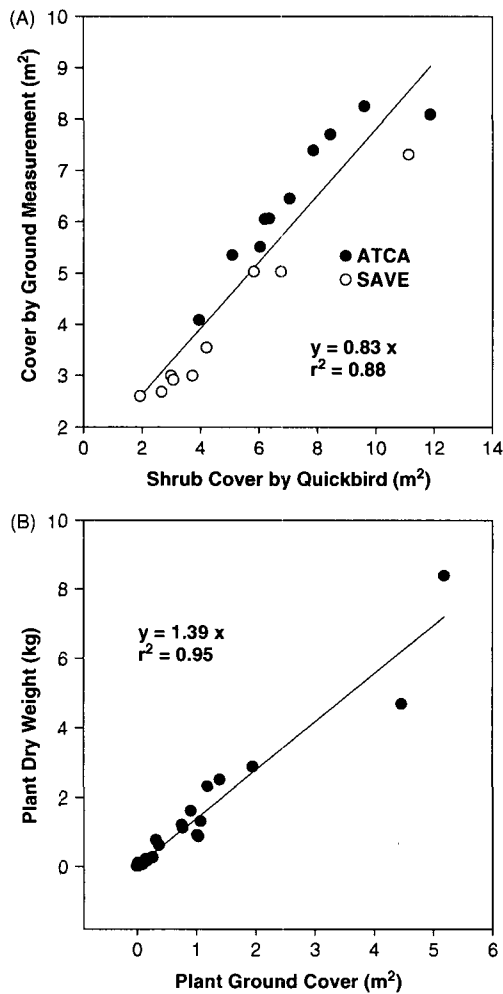


Figure 2. Relationships between shrub cover determined on a classified Quickbird image and ground measurement (A), and between canopy area projected on the ground and dry biomass (B) for shrubs at the Monument Valley UMTRA site.

are an edge effect on clumped vegetation. To correct for shadows, the linear projection of fractional cover (f_{clinear}) in Figure 2(A) was multiplied by a correction factor (C):

$$C = 0.83 + 0.17 \times f_{\text{clinear}} \quad (4)$$

with

$$f_c = f_{\text{clinear}} \times C \quad (5)$$

As f_{clinear} approaches 0, C approaches 0.83, the slope of the linear equation through the origin in Figure 2(A), but as f_{clinear} approaches 1.0, C approaches 1.0, because shadows will be cast within a full canopy. We tested the relationship between f_c estimated by Quickbird and ground estimates of f_c over wider areas within the site where individual canopy dimensions were measured (see section on Results).

Standing dry biomass was estimated from canopy area projected on the ground from a sample of 20 ATCA plants of varying sizes, for which canopy area and dry

biomass were both determined (Figure 2(B)) (McKeon *et al.*, 2005).

MODIS estimates of E_G and LAI

One of the goals of the research was to project how vegetation density and E_G change in response to factors such as rainfall, re-vegetation efforts, and grazing intensity over time. Satellite imagery can be used for this task, as phreatophyte ET is highly correlated with vegetation indices such as NDVI acquired during summer (Groeneveld and Baugh, 2007; Groeneveld *et al.*, 2007). We used a method based on imagery from the MODIS sensor system on the Terra satellite to estimate foliage density and E_G over the site (Nagler *et al.*, 2005). We used the Enhanced Vegetation Index (EVI) product, which estimates foliage density with a pixel resolution of 250 m (Huete *et al.*, 2002, 2008). The data are pre-processed to correct for view angle and atmospheric effects, and only cloud-free images are selected for each 16-day reporting period. EVI is calculated from the blue, red and near-infrared bands as:

$$EVI = 2.5 \times (\delta\text{NIR} - \delta\text{red}) / (1 + \delta\text{NIR} + (6 \times \delta\text{red} - 7.5 \times \delta\text{blue})) \quad (6)$$

where the coefficient '1' accounts for canopy background scattering and the blue and red coefficients, 6 and 7.5, minimize residual aerosol variations. The EVI is one of the two VIs available from the MODIS sensors, and it is widely used in phenological, productivity and ET studies (e.g., Huete *et al.*, 2002, 2008; Waring *et al.*, 2006).

We calculated ET from EVI and maximum daily air temperature (T_a) using a modification of the algorithm developed by Nagler *et al.* (2005). This algorithm was developed by correlating EVI and T_a with ET measured over multiple years at nine moisture flux tower sites in western riparian corridors, and was further tested against sap flow results in a cottonwood planting (Nagler *et al.*, 2007). We first converted EVI to scaled EVI (EVI^*) which stretches the values between 0 (minimum EVI) and 1 (maximum EVI):

$$EVI^* = 1 - (EVI_{\text{max}} - EVI) / (EVI_{\text{max}} - EVI_{\text{min}}) \quad (7)$$

We used 0.542 and 0.091 for EVI_{max} and EVI_{min} , respectively. These values are those from the dataset used to develop the predictive equation for ET in Nagler *et al.* (2005) and represent full vegetation cover and bare soil, respectively:

We then used EVI^* and T_{max} values to calculate ET:

$$E_G \text{ (kg m}^{-2} \text{ d}^{-1}) = 11.5 \times (1 - \exp(-1.63EVI^*)) \times 0.883 / (1 + \exp(-T_{\text{max}} - 27.9) / 2.57)) \quad (8)$$

The expression containing EVI^* is based on the formula for light extinction through a canopy (Monteith and Unsworth, 1990). The temperature term is in the

form of a sigmoidal curve, where there is a minimum temperature due to the physiological status of the plants; a middle, exponential portion of the curve which fits the vapour pressure deficit : temperature response in the Penman-Moneith equation (Allen *et al.*, 1998); and an upper limit, where physiological limitations to E also apply (Hultine *et al.*, 2007). Hence, air temperature is a scalar from 0 to 1.0 that accounts for both atmospheric water demand and the physiological limitations on E , at the low and high ends of the temperature scale (Nagler *et al.*, 2005).

Equation (8) is identical to the one derived in Nagler *et al.* (2005) except that the original algorithm had a constant term representing minimum (bare soil) ET, which was 1.07 mm day^{-1} in the original study of riparian phreatophyte vegetation (Nagler *et al.*, 2005). It was required because none of the tower-based values of ET reached 0 even in winter or when EVI* approached 0, due to bare soil evaporation. However, in this study, the sap flow sensors measured plant transpiration only, and bare soil evaporation is very low due to lack of surface moisture and scant rainfall, so we did not include the constant term in Equation (8).

We estimated LAI from EVI* by calibrating EVI* to f_c values determined on the 2007 Quickbird image. A mask was prepared for the area covered by each MODIS pixel that fell within the site (Figure 1), and the masks were overlain on the Quickbird image. Then f_c was determined for the area covered by each pixel and multiplied by 4.15 (the weighted mean LAPS) over the site determined by leaf harvesting of ATCA and SAVE to give the LAI of each pixel. EVI* values for each pixel were calculated as the mean value of July–August 2007 EVI* values, concurrent with sap flux measurements. A regression equation through the origin gave an expression for LAI:

$$\text{LAI} = 3.21 \times \text{EVI}^* \quad (9)$$

with $r^2 = 0.77$ ($n = 55$, $P < 0.001$).

Other methods and data sources

Daily meteorological data for 2007 were obtained as the mean values from three on-site automated micrometeorological stations (Vista Engineering, Inc., Grand Junction, CO) operated by the US Department of Energy (United States Department of Energy, 2006). The data were reported in hourly increments and included solar radiation (R_s , kW m^{-2}), air temperature (T , $^{\circ}\text{C}$), the partial pressure of water vapour in the air (kPa), wind speed (m s^{-1}) and precipitation (mm). Vapour pressure deficit (D) was determined by subtracting vapour pressure measured at the micrometeorological stations from vapour pressure at saturation as a function of air temperature. Daily values of precipitation and maximum daily air temperature (T_{max}) from 2000–2007 were obtained from the National Oceanic and Atmospheric Administration (NOAA) station at Monument Valley, Arizona, approximately 30 km from the site.

Leaf conductance estimated from sap flux measurements (G_S) was calculated as in Phillips and Oren (1998) from E_L , D and a conductance coefficient (K_G) based on atmospheric pressure:

$$G_S = (K_G \times E_L)/D \quad (10)$$

K_G combines the density of air, the latent heat of vapourization, the specific heat of air at constant pressure, and the psychrometric constant into a single term corrected for temperature, based on a series of regression analyses (Phillips and Oren, 1998):

$$K_G \text{ (kPa)} = 115.8 + 0.4226T \quad (11)$$

K_G ranged from 125–130 kPa in our study. Equation (10) is an approximation of G_S that applies when transpiration is strongly coupled to atmospheric conditions, and it assumes that D in the bulk air above the canopy is the driving force for E_L , and that leaves are at the same temperature as the bulk air over the canopy (Ewers and Oren, 2000). These are appropriate assumptions for small-leaved shrubs with relatively open canopies and a constant supply of water as in the present study (Ewers and Oren, 2000). The term, E_L/D , is the ratio of stand water flux to vapour pressure deficit, and is an indicator of the degree of stomatal opening at a given value of D (Monteith and Unsworth, 1990; Phillips and Oren, 1998; Ewers and Oren, 2000).

Statistical analyses included Analyses of Variance (ANOVA), Analysis of Co-variance (ANCOVA), and linear and non-linear regressions carried out using Systat (Systat Software, Inc., Chicago, IL).

RESULTS

Plant cover inside and outside the enclosure sites

Based on the ground survey, f_c by ATCA, SAVE and ATCO was 0.273 inside the South Enclosure plot and 0.065 in the adjacent control area outside the plot in November, 2007 (Table I). However, inspection of the October, 2006 Quickbird image (the year the enclosure fence was erected) showed that this reflects pre-existing plant cover differences and was not due to fencing the site. Phreatophyte shrub cover was 0.106 and 0.089 inside and outside the North Enclosure, and ATCA was the only phreatophyte species present. At both sites, annual forbs increased total plant cover by approximately 0.10, as this survey was taken at the end of the summer monsoon season when summer annuals were most abundant. By contrast, non-phreatophyte shrubs had f_c of 0.031 or lower. ATCA and SAVE plants ranged in height from 1 to 2 m inside and outside enclosures, whereas ATCO were <0.5 m.

LAPS and E_L by sap flow sensors and correlation with meteorological variables

LAPS and mean daily E_L values were subjected to a three-way ANOVA in which year (2006 or 2007), Plant

Table II. Summary of plant leaf area index (LAPS) and leaf-level transpiration (E_L) at the Monument Valley UMTRA site, 2006–2007, showing means and standard errors in parentheses.

	LAPS 2006	LAPS 2007	E_L 2006 ($\text{kg m}^{-2} \text{d}^{-1}$)	E_L 2007 ($\text{kg m}^{-2} \text{d}^{-1}$)
ATCA	—	—	—	—
In	2.96 (0.45)	3.78 (0.68)	1.66 (0.04)	2.95 (0.34)
Out	3.19 (0.36)	4.47 (0.46)	2.81 (0.09)	4.38 (1.26)
SAVE	—	—	—	—
In	3.71 (0.50)	3.98 (0.45)	3.06 (0.52)	6.72 (1.65)
Out	2.05 (0.20)	4.45 (0.57)	3.07 (0.95)	4.42 (1.25)

ATCA, *Atriplex canescens* (fourwing saltbush); SAVE, *Sarcobatus vermiculatus* (black greasewood).

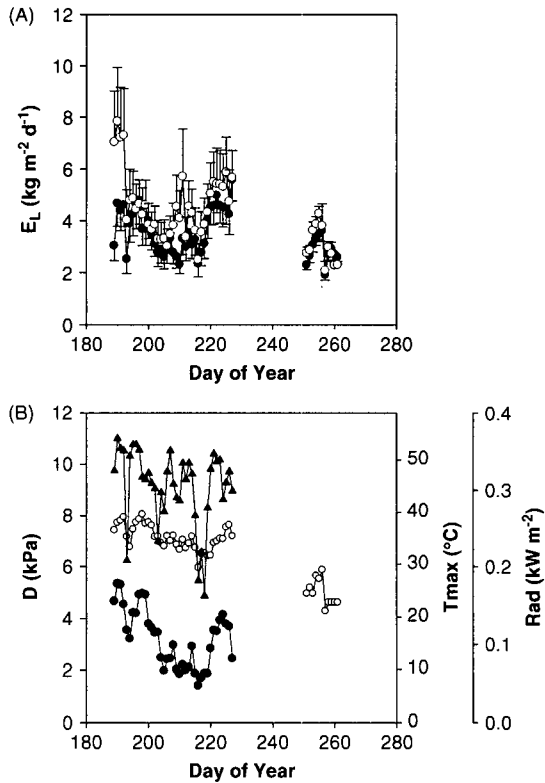


Figure 3. (A) Mean daily values of transpiration (E_L) for ATCA (closed circles) and SAVE in (DOY 251–261) and 2007 (DOY 189–227) at the Monument Valley UMTRA site. Bars show standard errors of means. (B) Mean daily values of vapour pressure deficit (D) (closed circles), maximum daily temperature (T_{max}) (open circles), and daily radiation (Rad) (closed triangles). Only temperature data was available in 2006.

Type (ATCA or SAVE), and Grazing Treatment (in or out of exclosures) were the categorical variables. E_L and LAPS were lower in 2006 than in 2007, but Plant Type and Grazing Treatment were not significant ($P > 0.05$) (Table II). LAPS was high in both years, averaging 2.96 and 3.85 in 2006 and 2007 across species and treatments, respectively. LAPS in 2006 was determined late in the season when plants contained fruits, which lowered LAPS. Although Plant Type was not significant in the ANOVA, E_L of SAVE tended to be higher ATCA

across years and treatments ($P = 0.057$ by Tukey's test across treatments. Figure 3).

On a daily time step, E_L of ATCA and SAVE were strongly correlated with D calculated over daylight hours (0700–1800 h), and less strongly correlated with T_{max} and total daily R_s (Figure 3, Table III). Wind speed averaged 1.66 m s^{-1} ($\text{SE} = 0.10$) over the study and was only weakly correlated with E_L or other meteorological variables. As expected, T_{max} and D were strongly autocorrelated as were SAVE and ATCA E_L . ATCA and SAVE E_L were analysed by ANCOVA against D ; both species responded positively to D ($P < 0.001$), and SAVE had a steeper linear response to D than ATCA ($P = 0.013$). The relationship between E_L and D was best described by an exponential decay function (Figure 4).

On an hourly time step, E_L of SAVE and ATCA both closely tracked the daily radiation curve, whereas T and D peaked later in the day (Figure 5, Tables IV and V). However, G_s peaked at about 10 a.m. for both species and declined gradually for the remainder of the daylight period, then dropped sharply at sunset. G_s was moderately correlated with R_s ($r = 0.62$ and 0.50 for ATCA and SAVE, respectively, $P < 0.01$) but not with other meteorological variables.

Table III. Analysis of Variance (ANOVA) of plant leaf area index (LAI) and leaf-level transpiration (E_L) at the Monument Valley UMTRA site, 2006–2007.

	LAI			E_L		
	F	P	df	F	P	df
Year	6.58	0.013	55	5.88	0.024	22
Plant	1.20	0.279	55	2.85	0.105	22
In/out	1.30	0.259	55	0.01	0.929	22

Mean daily sensor values over each measurement period were subjected to a three-way ANOVA in which year (2006 or 2007), plant (*Atriplex canescens* or *Sarcobatus vermiculatus*), and in or out of the exclosure fences were categorical variables. None of the interaction terms were significant at $P < 0.05$.

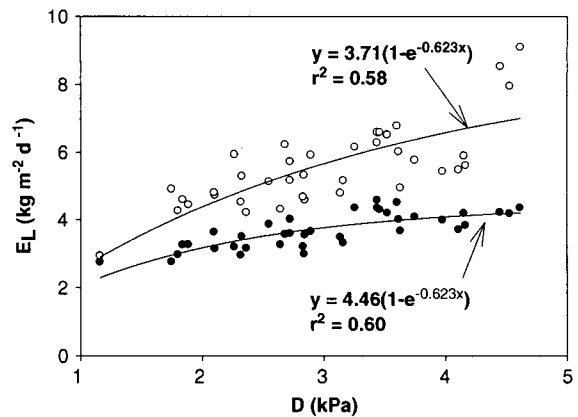


Figure 4. Relationship between vapour pressure deficit (D) and mean daily values of transpiration (E_L) of ATCA (closed circles) and SAVE (open circles) at the Monument Valley UMTRA site. D was determined for daylight hours (5 a.m. to 8 p.m.).

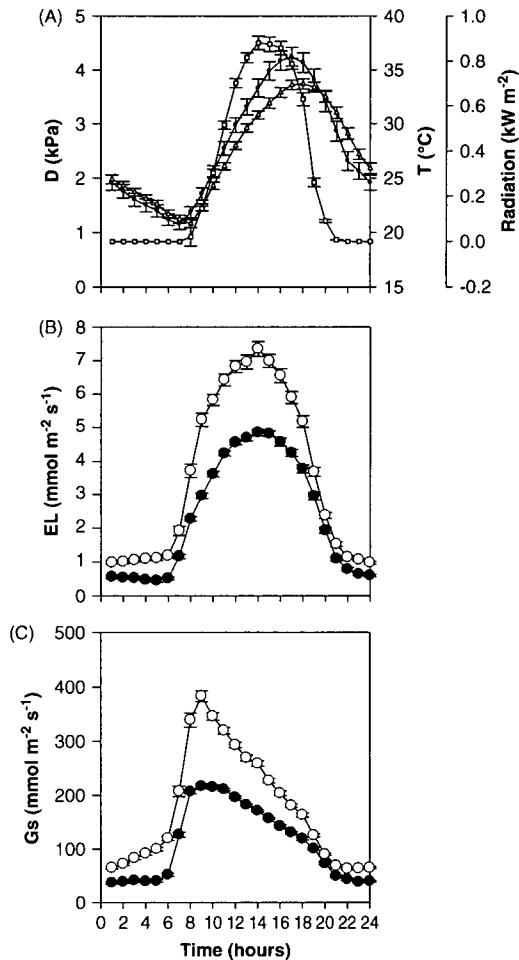


Figure 5. (A) Daily time course of vapour pressure deficit (D) (open circles), air temperature (T) (closed circles) and radiation (open squares) during the period of sap flux data collection at the Monument Valley UMTRA site from 9 July to 15 August 2007. (B) Daily time course of transpiration (E_L) of *Atriplex canescens* (ATCA) (closed circles) and *Sarcobatus vermiculatus* (SAVE) (open circles). (C) Daily time course of leaf conductance (G_s) of ATCA (closed circles) and SAVE (open circles). Error bars are standard errors of hourly measurements.

Table IV. Correlation coefficients between hourly leaf-level transpiration rates of *Atriplex canescens* (ATCA) and *Sarcobatus vermiculatus* (SAVE) plants and meteorological variables at the Monument Valley UMTRA site, 8 July–15 August 2007.

	ATCA	SAVE	D	Temp	Rad	Wind
ATCA	1.00	0.99***	0.749***	0.56**	0.94***	-0.145
SAVE	—	1.00	0.67***	0.45*	0.91***	-0.160
D	—	—	1.00	0.96***	0.84***	-0.103
Temp	—	—	—	1.00	0.68***	-0.183
Rad	—	—	—	—	1.00	-0.106
Wind	—	—	—	—	—	1.00

Asterisks denote significant correlations at $P < 0.05$ (*), $P < 0.01$ (**) or $P < 0.001$ (***).

Because the MODIS remote sensing method for E_G uses T_{max} as the only environmental variable and combines E across species due to the low resolution of the

Table V. Correlation coefficients between hourly leaf-level transpiration rates of *Atriplex canescens* (ATCA) and *Sarcobatus vermiculatus* (SAVE) plants and meteorological variables at the Monument Valley UMTRA site, 8 July–15 August 2007.

	ATCA	SAVE	D	T_{max}	Rad
ATCA	1.00	0.76***	0.78***	0.62***	0.40*
SAVE	—	1.00	0.77***	0.65***	0.47**
D	—	—	1.00	0.92***	0.59*
T_{max}	—	—	—	1.00	0.65**
Rad	—	—	—	—	1.00

Asterisks denote significant correlations at $P < 0.05$ (*), $P < 0.01$ (**) or $P < 0.001$ (***).

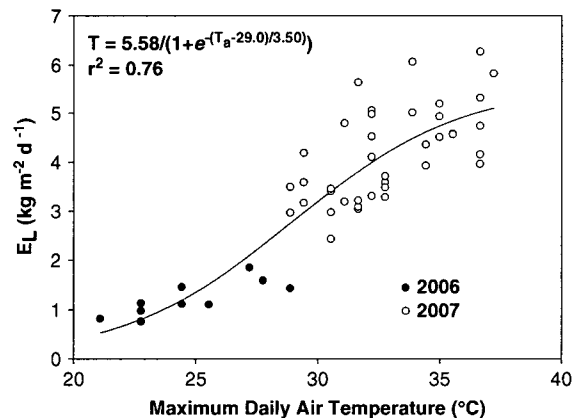


Figure 6. Relationship between pooled mean daily transpiration rates (E_L) of *Atriplex canescens* and *Sarcobatus vermiculatus* and maximum daily air temperature at the Monument Valley UMTRA site during sap flux measurement periods in 2006 and 2007.

images, we tested the strength of this relationship, using a sigmoidal response of E_L to T_{max} for 2006 and 2007 sap flux data (Figure 6). Although the MODIS model of necessity is an oversimplification of the factors controlling E_L , a sigmoidal relationship between T_{max} and combined SAVE and ATCA E_L had a r^2 of 0.76, providing a reasonable approximation of E_L over a seasonal cycle.

Vegetation cover, LAI, standing biomass and E_G over the site

Table VI gives f_c , LAI, standing biomass, and E_G for areas of interest at the site in 2007. Cover was generally low over most of the site (*ca* 0.10) but was very high (0.75) inside a portion of the site that has been fenced since 1997 (Area 1). This area also had very high projected biomass, LAI, and E_G . Estimates of f_c in enclosure plots by Quickbird were reasonably close to those determined by ground survey (Table VI). Figure 7 shows LAI values projected from MODIS EVI* for selected areas from 2000–2007. LAI declined slightly from 2000 to 2003, then increased up to 2007, except for 2006, when LAI values were low. The trends generally fit informal observations we made of grazing pressure at the site, which were high from 2000 to 2003, and declined somewhat in subsequent years. Grazing pressure is not

SCALING SAP FLUX MEASUREMENTS OF GRAZED AND UNGRAZED SHRUB COMMUNITIES

Table VI. Site shrub fractional cover, LAI, biomass, and projected transpiration rates (E_G) over selected areas of the Monument Valley UMTRA site from 8 July to 15 August 2007.

Site	Area (ha)	Fractional cover	LAI	Biomass (kg ha ⁻¹)	Shrubs ratio (ATCA : SAVE : ATCO)			E_G (mm d ⁻¹)
1	1.15	0.749	2.88	10411	1	0.9	0.00	13.1
2	1.57	0.152	0.58	2113	1	8.6	0.80	2.90
3	21.45	0.136	0.52	1890	1	1.2	0.12	2.40
4	182.4	0.094	0.36	1302	1	0.00	0.10	1.42
SE (in)	0.26	0.344 (0.273)	1.32 (1.05)	4782	1	0.64	0.04	5.72
SE (out)	0.26	0.101 (0.065)	0.39 (0.25)	1404	1	2.56	0.5	1.84
NE (in)	0.26	0.095 (0.106)	0.37 (0.41)	1315	1	0.00	0.00	1.44
NE (out)	0.26	0.082 (0.089)	0.32 (0.34)	1140	1	0.00	0.00	1.84
Whole site	318	0.0964	0.37	1340	1	0.20	0.10	1.54

Cover was determined by Quickbird imagery and LAI by cover times leaf area of individual plants. E_G was calculated from sap flux estimates for SAVE and ATCA projected over each area of interest, using values of ATCA for ATCO. The proportion of ATCA, SAVE and ATCO in each area was from ground surveys reported in McKeon *et al.* (2006) or from the present study (areas in Table I). Biomass was determined by an allometric relationship between cover and dry weight of shrubs. For the North and South Exclusion Plots, fractional cover determined by ground surveys is also given in parenthesis. Sites correspond to areas of interest illustrated in Figure 1.

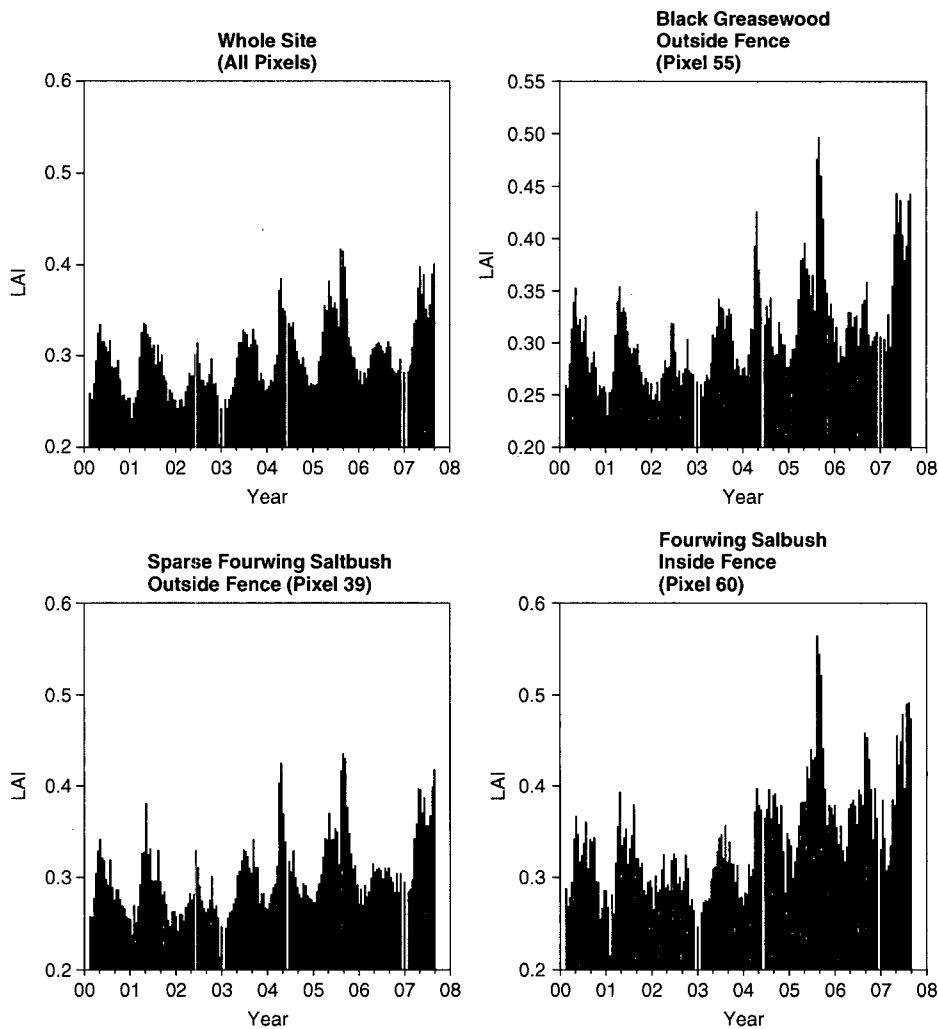


Figure 7. Leaf area index (LAI) values estimated by the Enhanced Vegetation Index (EVI) from MODIS satellite sensors for selected area at the Monument Valley UMTRA site from 2000–2007, showing 16-day composite values of LAI over time. See Figure 1 for pixel locations.

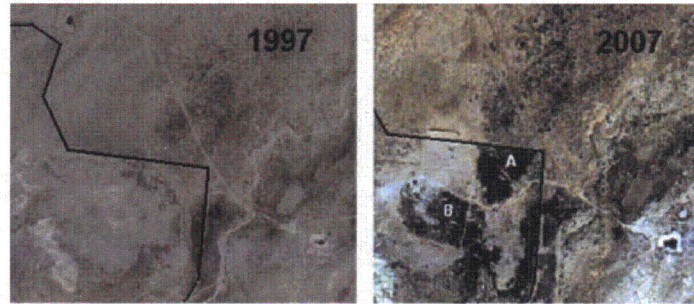


Figure 8. Contrast between shrub density in 1997 and 2007 at the Monument Valley UMTRA site. The line shows the location of the fence enclosing the former mill site. (A) Shows the growth of volunteer plants inside the fence, and (B) shows an irrigated planting over a portion of the source area of contamination at the site.

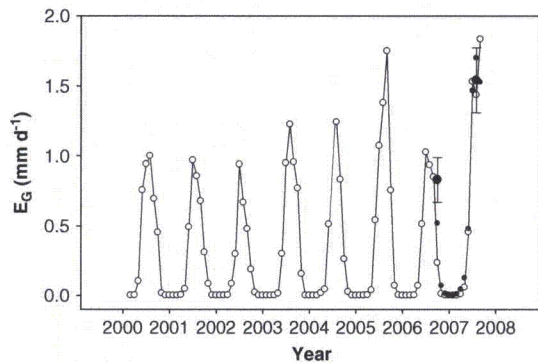


Figure 9. Evapotranspiration at the Monument Valley UMTRA site estimated by the MODIS EVI— T_a method (open circles), by sap flow measurements (large closed circles with standard error bars), and by the relationship between sap flow results and daily maximum temperature projected over the sap flow measurement period in 2006–2007 (small closed circles).

constant, because livestock are moved across the range from year to year to exploit fresh pastures. Although the MODIS pixel encompassing Area 1 only covered part of the area and also included adjacent land outside the fence (Figure 1), MODIS LAI showed a clear increasing trend for this pixel over time due to grazing exclusion. Figure 8 shows Area 1 before and after fencing, going from nearly bare in 1997 to 0.75 cover in 2007.

Estimates of E_G over the whole site by MODIS were in agreement with sap flux estimates in 2006 and 2007 (Figure 9). From 2000 to 2007, E_G by MODIS showed a gradually increasing trend over the site and ranged from 73 to 159 mm year⁻¹ (Table VII). Although E_G was approximately equal to site precipitation over all years, there was no significant relationship ($P > 0.05$) between E_G and precipitation on either on a 16-day or yearly time step, indicating that water from the aquifer was the main source of water for shrubs at this site.

DISCUSSION

Meteorological controls on E_L

Although the diurnal curve of E_L closely tracked R_S , stomatal openings, as indicated by G_S , actually peaked

Table VII. Annual precipitation and pheatophyte transpiration (E_G) at the Monument Valley UMTRA site, 2000–2007. E_G was estimated by the MODIS EVI— T_a method.

Year	Precipitation (mm year ⁻¹)	E_G (mm year ⁻¹)
2000	109	123
2001	117	96
2002	140	73
2003	60	125
2004	74	89
2005	172	163
2006	89	103
2007	117	159
Mean (SE) ^a	110 (12.7)	116 (11.4)

^a Means not significantly different at $P = 0.05$ by paired t -test.

early in the day then decreased. Midday depression of G_S and photosynthesis is common in plants growing in bright, low-humidity environments (Xu and Shen, 2005), and has been noted before for *Atriplex* spp. (das Neves *et al.*, 2008) and SAVE (Donovan *et al.*, 2003). Midday depression of photosynthesis is a complex phenomenon that is controlled by both internal (e.g. metabolic) and external (meteorological) factors (Xu and Shen, 2005). In the present research, peak G_S occurred well before D , T or R_S reached their daily peaks. E_L continued to increase into early afternoon even after G_S peaked due to increasing atmospheric water demand even though, presumably, stomata were partially closed.

On a daily time step, E_L was closely correlated with D , showing a high degree of coupling between ET and atmospheric water demand (the advective term in the Penman-Monteith equation) (Monteith and Unsworth, 1990). Similar to other studies (e.g. Hultine *et al.*, 2007), the response of E_L to D followed an exponential decay function, and SAVE responded more steeply to D and tended to have higher E_L than ATCA. SAVE is a deciduous shrub that develops new leaves in spring and maximizes growth through the summer, whereas ATCA is evergreen and spreads growth and water uptake over a longer annual cycle than SAVE. Similar to the present results, Steinwand *et al.* (2001) reported a one-third higher rate of transpiration as a function of LAI for SAVE compared to *A. lentiformis* in Owens Valley, California, USA.

Table VIII. Comparison of the present results with other studies in which *Sarcobatus vermiculatus* was a dominant or co-dominant species in western US phreatophyte communities.

Study	E_L	G_S	E_G	LAI	LAPS	f_c	Biomass	Location
This study	5.0–7.8	215–395	1.4–5.7	0.33–1.54	3.98–4.47	0.082–0.344	1140–4782	Monument Valley, Arizona
Sperry and Hacke (2002)	—	—	—	—	—	—	—	Skull Valley, Utah
Driese and Reiners (1997)	—	—	—	0.02–0.06	0.27–0.46	0.076–0.349	317–7706	Great Divide Basin, Wyoming
Romo and Haferkamp (1989)	1.7–5.6	89–178	0.86–2.88	—	—	—	—	Southeast Oregon
Groeneveld and Warren (1992)	3.4–10.2	169–335	1.48–7.20	0.57–0.70	0.99–2.70	0.292–0.337	—	Owens Valley, California
Cooper <i>et al.</i> (2006)	—	—	0.9–2.2	—	—	—	—	San Luis Valley, Colorado

Values are the range across phreatophyte shrub species at each site. E_L and G_S are peak diurnal values in $\text{mmol m}^{-2} \text{s}^{-1}$; E_G are mean daily values in mm d^{-1} ; and standing dry biomass is in kg ha^{-1} .

Comparison to other studies

Table VIII compares the present results with other studies in which SAVE was a dominant or co-dominant shrub in western US phreatophyte communities. In general, range of values among studies overlap for E_L , G_S , LAI, f_c and standing biomass. The range of values are wide, as expected, due to the different biological, edaphic, and climatic factors affecting plant growth both within and among sites. Although rates of E_G tend to be moderate ($1.5\text{--}3.0 \text{ mm d}^{-1}$) due to low f_c and LAI, under favourable conditions phreatophyte communities can extract $5\text{--}7 \text{ mm d}^{-1}$ of water from the aquifer, rates that approach potential ET rates for a grass reference crop (Allen *et al.*, 1998). The Monument Valley plants were remarkable for their high LAPS values (*ca* 4.0) compared to other sites, where LAPS ranged from <0.5 to 2.7. This was due to their greater height (1–2 m) compared to other locations, where plant heights were generally 0.3–1 m (e.g. Driese and Reiners, 1997).

Early studies (e.g. Nichols, 1994) emphasized depth to water table as a controlling factor in phreatophyte E_G . However, Cooper *et al.* (2006) and Steinwand *et al.* (2006) found that the relationship between E_G and depth to water was only moderately strong, and it can be mitigated by other factors such as soil type affecting hydraulic conductivity (e.g. Hultine *et al.*, 2006). Depth to water was greater at Monument Valley ($>6 \text{ m}$) than in the other studies in Table VIII (1–3 m), but we still recorded high rates of E_L and high LAPS. The aquifer at Monument Valley is present in sand that supports high hydraulic conductivity (United States Department of Energy, 1999), leading to high rates of water extraction by the shrub community.

Quickbird and MODIS satellite images to project f_c , LAI and E_G over large areas

Desert phreatophyte communities lend themselves to remote sensing analyses for several reasons. Shrubs tend to grow in relatively sparse stands in which f_c can be estimated by high-resolution satellite imagery, as by

Quickbird images in the present study. When LAI is under 4.0, plant communities exhibit a linear response of E_G to LAI (Kelliher *et al.*, 1995; Granier *et al.*, 1999), hence LAI estimated by a vegetation index can be calibrated to estimate seasonal E_G for phreatophyte communities (Groeneveld *et al.*, 2007). In our study, E_G was linear with LAIs ranging from 0.32 to 1.32 over the four stations where sap flow was measured ($r^2 = 0.99$, $P < 0.01$). Furthermore, arid-zone phreatophytes derive most of their water from the aquifer, and the surface soil is normally dry, so transpiration dominates ET (Scott *et al.*, 2006), producing a high correlation between vegetation indices and ET (Nagler *et al.*, 2005; Groeneveld *et al.*, 2007).

In the present study, we used a simple empirical relationship between EVI, T_{max} and ET measured at flux towers for riparian phreatophytes to scale E_G . A more desirable approach would be to use underlying ecophysiological principles to account for E at different levels of organization (Waring, 1993). The Penman-Monteith equation provides a complete model for ET (Allen *et al.*, 1998). An impediment to applying the Penman-Monteith equation is uncertainty about the roughness lengths for sparse shrub communities, which determine turbulent transfer coefficients. Driese and Reiners (1997) found roughness lengths for a sparse shrub community in Wyoming ranging from 0.01 to 0.07 m, lower than used in models, and with no strong relationship to either shrub height or density that could support scaling by remote sensing. However, vegetation in our study tended to be taller than at their site, and the average wind speed and high local turbulence associated with low LAI values and bare soil should create low aerodynamic resistance. The low correlation between E_L and wind speed suggests that atmospheric resistance is not a limiting factor for E_L at our site. Hence, at our site, the components of the Penman-Monteith equation that exercised the greatest control on E_L were bulk atmospheric water demand (D), and apparent partial stomatal closure during midday (G_S).

Steinwand *et al.* (2001) and Groeneveld *et al.* (2007) successfully used the Penman-Monteith equation to

project phreatophyte E_G based on crop coefficients relating phreatophyte E_G to potential ET by a grass reference crop. Although Mata-Gonzalez *et al.* (2005) criticized this approach as inappropriate for desert vegetation, Groeneveld *et al.* (2007) showed that the ratio of actual ET measured at flux towers to potential ET of a reference crop was highly correlated with satellite NDVI values over three different phreatophyte communities and could form the basis of a remote sensing method for phreatophyte ET.

Our simplified method for projecting E_G by MODIS EVI produced reasonable agreement with sap flux results at two sample intervals, but a more rigorous test against long-term flux tower measurements of ET would be desirable. Although D exercised the most important control on E_L at daily time steps, T_{\max} could be used as a proxy for D due to their autocorrelation. T_{\max} can be obtained from thermal bands on satellite images (Glenn *et al.*, 2007), or from the vast array of weather reporting stations in the USA and the rest of the world.

Wide-area E_G estimates and effects of grazing control

E_G was low over the whole site due to low overall plant cover (ca 0.10), similar to the plant cover in North Enclosure. However, some areas, such as the South Enclosure plot over the hot-spot of the plume, had high plant cover (0.34) and high projected E_G compared to the whole site. Protecting vegetation from grazing did not increase rates of E_L , and over the 2 years that the enclosures have been in place, plant cover has not yet significantly increased. However, over longer time periods, grazing control had a marked effect on vegetation cover (McKeon *et al.*, 2006). The area inside the site fence that had been protected from grazing for 10 years developed 0.75 plant cover compared to just 0.15 for plants just over the fence line, and had a projected midsummer E_G of 13 mm d⁻¹. However, this rate was projected from sap flux measurements made in sparser stands, and it is likely that self-shading reduced the actual E_G achieved in this dense stand. Furthermore, we do not know if the increase in cover achieved over this small portion of the site can be projected over the whole site. At the UMTRA site in Tuba City, Arizona, exclusion of livestock for 10 years resulted in an increase in cover from 0.11 to 0.24 (Lash *et al.*, 1999), and similar results were reported along a fence line contrast at the Monument Valley National Monument close to the present site (Brotherson *et al.*, 1983). Hence, over the sparse cover area of the plume, an approximate doubling of shrub cover and ET is a realistic estimate of what can be achieved by control over grazing.

At present, E_G is approximately equal to precipitation over the plume, presumably controlling local recharge, but the volume of the plume has been increasing at a rate of 50000 m³ year⁻¹, providing an estimate of the rate of recharge from other water sources (Jordan *et al.*, 2008). Over 130 ha, this volume is equivalent to a water depth of 38 mm year⁻¹ (24% of the 2007 transpiration rate).

Hence, an increase in E_G by this amount should arrest the movement of the plume, and further E_G increases would be expected to shrink the volume of the plume. The present study shows that these goals are well within the capacity of the phreatophyte community if it were protected from grazing. The water balance at present is tipped slightly in favour of recharge, but could, in theory, be tipped towards discharge even if only part of the plume area was protected from grazing.

Wider relevance of the findings

Like arid and semi-arid rangelands throughout the subtropics (Dregne, 1986), the Navajoan Desert has been extensively altered by over-grazing, starting in the 1830s and continuing to the present (Savage, 1991; McFadden and McAuliffe, 1997). Some studies have concluded that the vegetation changes have resulted in hydrological and geomorphological changes in the landscape over the past 200 years (reviewed in Graf, 1987), but other studies have emphasized the role of climate shifts in producing these changes (e.g. McFadden and McAuliffe, 1997). The present study and previous work at this site show that even small shifts in vegetation cover can potentially impact the site water balance, tipping the balance from extraction to recharge depending on the status of the vegetation.

The nitrate in the alluvial aquifer in this study was of human origin, but southwestern US soils and aquifers can have naturally high levels of nitrates as well (Walvoord *et al.*, 2003). Land use practices such as conversion of grasslands to shrublands, or reduction in overall plant cover, could mobilize these stored nitrates to enter aquifers and drainages where they can conceivably present an environmental hazard to wildlife and humans. Phreatophyte shrub communities can play an important role in controlling the mobility of nitrates in the environment.

REFERENCES

- Allen R, Pereira L, Raes D, Smith M. 1998. *Crop Evapotranspiration—Guidelines for Computing Crop Water Requirements—FAO Irrigation and Drainage Paper 56*. Food and Agriculture Organization of the United Nations: Rome.
- Anderson M. 2004. *Sarcobatus vermiculatus*. *Fire Effects Information System*, [Online]. U.S. Department of Agriculture, Forest Service, Rocky Mountain Research Station, Fire Sciences Laboratory (Producer): Rocky Mountain Research Station, Fort Collins, CO; Available: <http://www.fs.fed.us/database/feis/>.
- Brotherson J, Rushforth S, Johansen J. 1983. Effects of long-term grazing on cryptogam crust cover in Navajo National Monument, Arizona. *Journal of Range Management* **36**: 579–581.
- Cooper D, Sanderson J, Stannard D, Groeneveld D. 2006. Effects of long-term water table drawdown on evapotranspiration and vegetation in an arid region phreatophyte community. *Journal of Hydrology* **325**: 21–34.
- das Neves J, Ferreira L, Vaz M, Gazarini L. 2008. Gas exchange in the salt marsh species *Atriplex portulacoides* L. and *Limoniastrum monopetalum* L. in southern Portugal. *Acta Physiologiae Plantarum* **30**: 91–97.
- Donovan L, Richards J, Linton M. 2003. Magnitude and mechanisms of disequilibrium between predawn plant and soil water potentials. *Ecology* **84**: 463–470.

- Dregne HE. 1986. Desertification of arid lands. In *Physics of Desertification*, El-Baz F, Hassan MHA (eds). Martinus, Nijhoff: Dordrecht.
- Driese K, Reiners W. 1997. Aerodynamic roughness parameters for semi-arid natural shrub communities of Wyoming, USA. *Agricultural and Forest Meteorology* **88**: 1–14.
- Ewers B, Oren R. 2000. Analyses of assumptions and errors in the calculation of stomatal conductance from sap flux measurements. *Tree Physiology* **20**: 579–589.
- Glenn E, Huete A, Nagler P, Hirschboeck K, Brown P. 2007. Integrating remote sensing and ground methods to estimate evapotranspiration. *Critical Reviews in Plant Sciences* **26**: 139–168.
- Graf F. 1987. Geomorphological research in the Colorado Plateau. In *Geomorphic Systems of North America: The Decade of North American Geography*, Vol. 2, Graf W (ed.). Geological Society of America: Centennial Special Issue: Geological Society of America, Boulder, CO: 259–265.
- Granier A, Breda N, Biron P, Villet S. 1999. A lumped water balance model to evaluate duration and intensity of drought constraints in forest stands. *Ecological Modelling* **116**: 269–283.
- Grime V, Sinclair F. 1999. Sources of error in stem heat balance sap flow measurements. *Agricultural and Forest Meteorology* **94**: 103–121.
- Groeneveld D, Baugh W. 2007. Correcting satellite data to detect vegetation signal for eco-hydrologic analyses. *Journal of Hydrology* **344**: 135–145.
- Groeneveld D, Baugh W, Sanderson S, Cooper D. 2007. Annual groundwater evapotranspiration mapped from single satellite scenes. *Journal of Hydrology* **344**: 146–155.
- Groeneveld D, Warren D. 1992. Total transpiration from land areas estimated from hand-held porometer measurements. In *Evapotranspiration Measurements of Native Vegetation, Owens Valley, California, June 1986*, Wilson D, Reginato R, Hollett K (eds). U.S. Geological Survey Water-Resources Investigations Report 91–4159: Sacramento, CA: 49–59.
- Huete A, Didan K, Miura T, Rodriguez E, Gao X, Ferreira L. 2002. Overview of the radiometric and biophysical performance of the MODIS vegetation indices. *Remote Sensing of Environment* **83**: 195–213.
- Huete A, Didan K, van Leeuwen W, Miura T, Glenn E. 2008. MODIS vegetation indices. *Land Remote Sensing and Global Environmental Change: NASA's Earth Observing System and the Science of ASTER and MODIS* (in press).
- Hultine K, Bush S, West A, Ehleringer J. 2007. Effect of gender on sap-flux-scaled transpiration in a dominant riparian tree species: Box elder (*Acer negundo*). *Journal of Geophysical Research* **112**: G03S06, DOI:10.1029/2006JG00232.
- Hultine K, Koepke D, Pockman W, Fravolini A, Sperry J, Williams D. 2006. Influence of soil texture on hydraulic properties and water relations of a dominant warm-desert phreatophyte. *Tree Physiology* **26**: 313–323.
- Huxman T, Wilcox B, Breshears D, Scott R, Snyder K, Small E, Hultine K, Pockman W, Jackson R. 2005. Ecohydrological implications of woody plant encroachment. *Ecology* **86**: 308–319.
- Jordan F, Waugh J, Glenn E, Sam L, Tompson T, Tompson TL. 2008. Natural bioremediation of a nitrate-contaminated soil-and-aquifer system in a desert environment. *Journal of Arid Environments* **72**: 748–763.
- Kelliher F, Leuning M, Raupach R, Schultz E. 1995. Maximum conductances for evaporation from global vegetation types. *Agricultural and Forest Meteorology* **73**: 1–16.
- Kjelgaard J, Stockle C, Black R, Campbell G. 1997. Measuring sap flow with the heat balance approach using constant and variable heat inputs. *Agricultural and Forest Meteorology* **85**: 239–250.
- Lash D, Glenn E, Waugh J, Baumgartner D. 1999. Effects of grazing exclusion and reseeding on a former uranium mill site in the Great Basin desert, Arizona. *Arid Soil Research and Rehabilitation* **13**: 253–264.
- Lin G, Phillips S, Ehleringer J. 1996. Monsoonal precipitation responses of shrubs in a cold desert community on the Colorado Plateau. *Oecologia* **106**: 8–17.
- Mata-Gonzalez R, McClendon T, Martin D. 2005. The inappropriate use of transpiration coefficients (Kc) to estimate evapotranspiration in arid ecosystems: a review. *Arid Land Research and Management* **19**: 285–295.
- McFadden L, McAuliffe J. 1997. Lithologically influenced geomorphic responses to Holocene climatic changes in the Southern Colorado Plateau, Arizona: A soil-geomorphic perspective. *Geomorphology* **19**: 303–332.
- McKeon C, Glenn E, Waugh W, Eastoe C, Jordan F, Nelson S. 2006. Growth and water and nitrate uptake patterns of grazed and ungrazed desert shrubs growing over a nitrate contamination plume. *Journal of Arid Environments* **64**: 1–21.
- McKeon C, Jordan F, Glenn E, Waugh W, Nelson S. 2005. Rapid nitrate loss from a contaminated desert soil. *Journal of Arid Environments* **61**: 119–136.
- Monteith J, Unsworth M. 1990. *Principles of Environmental Physics*, 2nd edn. Edward Arnold: London.
- Nagler P, Glenn E, Thompson T. 2003. Comparison of transpiration rates among saltcedar, cottonwood and willow trees by sap flow and canopy temperature methods. *Agricultural and Forest Meteorology* **116**: 73–89.
- Nagler P, Glenn E, Thompson T, Huete A. 2004. Leaf area index and Normalized Difference Vegetation Index as predictors of canopy characteristics and light interception by riparian species on the Lower Colorado River. *Agricultural and Forest Meteorology* **116**: 103–112.
- Nagler P, Jetton A, Fleming J, Didan K, Glenn E, Erker J, Morino K, Milliken J, Gloss S. 2007. Evapotranspiration in a cottonwood (*Populus fremontii*) restoration plantation estimated by sap flow and remote sensing methods. *Agricultural and Forest Meteorology* **144**: 95–110.
- Nagler P, Scott R, Westenburg C, Cleverly J, Glenn E, Huete A. 2005. Evapotranspiration on western U.S. rivers estimated using the Enhanced Vegetation Index from MODIS and data from eddy covariance and Bowen ratio flux towers. *Remote Sensing of Environment* **97**: 337–351.
- Naumberg E, Mata-gonzalez R, Hunter R, McClendon T, Martin D. 2005. Phreatophytic vegetation and groundwater fluctuations: a review of current research and application of ecosystem response modeling with an emphasis on Great Basin vegetation. *Environmental Management* **35**: 727–740.
- Nichols W. 1993. Estimating discharge of shallow groundwater by transpiration by greasewood in the northern Great Basin. *Water Resources Research* **29**: 2771–2778.
- Nichols W. 1994. Groundwater discharge by phreatophyte shrubs in the Great Basin as related to depth to groundwater. *Water Resources Research* **30**: 3265–3274.
- Nichols W. 2000. Regional ground-water evapotranspiration and ground-water budgets, Great Basin, Nevada, U.S. Geological Survey Professional Paper 1628, 82.
- Phillips N, Oren R. 1998. A comparison of daily representations of canopy conductance based on two conditional time-averaging methods and the dependence of daily conductance on environmental factors. *Annales des Sciences Forestieres* **55**: 217–235.
- Romo J, Haferkamp M. 1989. Water relations of *Artemisia tridentata* ssp. *Wyomingensis* and *Sarcobatus vermiculatus* in the steppe of southeastern Oregon. *American Midland Naturalist* **121**: 155–164.
- Savage M. 1991. Structural dynamics of a southwestern pine forest under chronic human influence. *Annals of the Association of American Geographers* **81**: 271–289.
- Scott R, Huxman T, Cable W, Emmerich W. 2006. Partitioning of evapotranspiration and its relation to carbon dioxide exchange in a Chihuahuan Desert shrubland. *Hydrological Processes* **20**: 3227–3243.
- Shreve F. 1942. The desert vegetation of North America. *Botanical Review* **7**: 195–246.
- Sperry J, Hacke U. 2002. Desert shrub water relations with respect to soil characteristics and plant functional types. *Functional Ecology* **16**: 367–378.
- Steinwand A, Harrington R, Groeneveld D. 2001. Transpiration coefficients for three Great Basin shrubs. *Journal of Arid Environments* **49**: 555–567.
- Steinwand A, Harrington R, Or D. 2006. Water balance for Great Basin phreatophytes derived from eddy covariance, soil water, and water table measurements. *Journal of Hydrology* **329**: 595–605.
- United States Department of Energy. 1999. *Final Site Observational Work Plan for the UMTRA Project Site at Monument Valley, Arizona*, Vol. I, MAC-GWMON 1-1. U.S. United States Department of Energy Department of Energy, Grand Junction Office, Grand Junction.
- United States Department of Energy. 2000. *Evaluation of Active Remediation Alternatives for the Monument Valley, Arizona, UMTRA Project Site*, MAC-GWMON 10-6, US Department of Energy, Grand Junction Office, Grand Junction.
- United States Department of Energy. 2004. *Monument Valley Ground Water Remediation: Pilot Study Work Plan*, DOE-LM/GJ757-2004, Office of Legacy Management, U.S. Department of Energy, Grand Junction.
- United States Department of Energy. 2006. *Soil and Ground Water Phytoremediation Pilot Studies at Monument Valley, Arizona: 2005*

- Status Report*, DOE-LM/1254-2006, Office of Legacy Management, U.S. Department of Energy, Grand Junction.
- Walvoord M, Phillips F, Stonestrom D, Evans R, Hartsough P, Newman B, Striegl R. 2003. A reservoir of nitrate beneath desert soils. *Science* **302**: 1021–1024.
- Waring R. 1993. How ecophysiologicals can help scale from leaves to landscapes. In *Scaling Physiological Processes: Leaf to Globe*, Ehleringer J, Field C (eds). Academic Press, Inc.: San Diego, CA; 159–166.
- Waring R, Milner K, Jolly W, Phillips L, McWethy D. 2006. Assessment of site index and forest growth capacity across Pacific and Inland Norwest USA with a MODIS satellite-derived vegetation index. *Forest Ecology and Management* **228**: 285–291.
- Wilcox B, Thurow T. 2006. Emerging issues in rangeland ecohydrology: vegetation change and the water cycle. *Rangeland Ecology and Management* **59**: 220–224.
- Xu D, Shen Y. 2005. External and internal factors responsible for midday depression of photosynthesis. In *Handbook of Photosynthesis*, 2nd edn, Pessaraki M (ed.). Taylor & Francis: Boca Raton, FL; 297–298.

Appendix F
**Work Plan for Pilot Study of Ethanol-Enhanced
Groundwater Denitrification**

This page intentionally left blank

**PILOT-SCALE EVALUATION WORK PLAN
FOR ETHANOL-ENHANCED DENITRIFICATION AT THE
URANIUM MILL TAILING SITE IN MONUMENT VALLEY,
ARIZONA**

Prepared for:

U.S. DEPARTMENT OF ENERGY
Grand Junction Office
Grand Junction, Colorado

Prepared by:

K.C. Carroll, M.L. Brusseau, and E.P. Glenn
THE SOIL, WATER, AND ENVIRONMENTAL
SCIENCE DEPARTMENT
University of Arizona
Tucson, Arizona

August 3, 2008

TABLE OF CONTENTS

1.0	Introduction.....	3
1.1	Background.....	3
1.2	Potential Applicability for Enhanced Attenuation.....	3
2.0	Project Plan.....	5
2.1	Pilot Test Design.....	5
2.1.1	Pilot Test Site Selection.....	5
2.2	Baseline Groundwater Monitoring.....	5
2.2.1	Groundwater Elevation Monitoring.....	5
2.2.2	Field Monitoring and Groundwater Sample Collection.....	5
2.2.3	Laboratory Analysis.....	6
2.2.4	Microbial Activity Sample Collection and Analysis.....	6
2.3	Ethanol Injection Test.....	6
2.3.1	Ethanol Solution and Nonreactive Tracer Solution.....	6
2.3.2	Injection System.....	7
2.3.3	Injection Test and Post-Injection Monitoring Plan.....	7
2.4	Data Analysis.....	7
3.0	Project Schedule.....	9
4.0	References.....	10

FIGURES

- 1 Site #1 Location
- 2 Site #2 Location
- 3 General Schedule

TABLES

- 1 Proposed Budget

1.0 Introduction

1.1 Background

The Monument Valley site is a former uranium mining site located in northern Arizona (DOE 1999). Uranium was mined at the site from 1943 to 1968, and seepage through mill tailings stockpiles into a shallow alluvial aquifer resulted in a groundwater contamination plume that is the focus of this and other remediation investigations. Surface remediation activities conducted from 1992 through 1994 under the UMTRA Program have removed all of the tailings material from the site (DOE 1999). Ammonium and nitrate concentrations in groundwater have since begun to decrease, which suggests that monitored natural attenuation (MNA) may be a viable remediation strategy for the site. Additionally, the Environmental Research Lab (ERL) conducted a phytoremediation pilot study to remove nitrate from the soil in the former tailings area. The project resulted in reduced nitrate concentrations, and monitoring since then suggests that denitrification is responsible for nitrate transformation at the site (Jordan et al. 2008). However, groundwater at the Monument Valley site continues to exceed the 10 mg/L standard.

1.2 Potential Applicability for Enhanced Attenuation

Enhanced attenuation (EA) can be defined as initiating and/or augmenting natural and sustainable attenuation processes. The goal is to increase the magnitude of attenuation by natural processes beyond that which occurs without intervention. Enhancing in situ biological denitrification through injection of amendments has been deemed a promising method for remediation of nitrate contaminated groundwater (ITRC 2000). A small number of field tests of this method have been reported (e.g., ITRC 2000; Smith et al. 2001; Khan and Spalding 2004). These studies have shown that substantial reductions of nitrate concentrations were achieved upon injection of the chosen amendment. The New Mexico South Valley case study described in the ITRC report (2000) is very similar to the Monument Valley site in terms of volume and area of the plume, nitrate concentrations, and mobility of the plume.

The Monument Valley UMTRA site is an excellent candidate for in situ EA remediation of nitrate in the plume. We have already demonstrated that denitrification can be stimulated in the vadose zone of the source area through irrigation of native shrubs. Nitrate levels in the source area have decreased from 171 mg/L in 2001 to 71 mg/L in 2006. The region of high nitrate contamination in the plume is confined in a relatively small volume of the aquifer. Treatment of this high-concentration portion of the plume could allow natural attenuation of the remainder of the plume, thereby reducing the long-term exposure risk to valley residents, wildlife and livestock.

The degree to which a reagent-injection based method will be successful for a particular site depends greatly on the ability to deliver the reagent to the target zone. Hydrogeologic properties of the subsurface control this aspect, with physical material heterogeneity (i.e., hydraulic conductivity) the primary characteristic of concern. Based on previous site characterization (DOE 1999), the alluvial aquifer consists primarily of fine to medium grained sand deposits that vary in thickness from 0 to 120 ft. Thin, non laterally extensive finer grained layers are found in the thickest sections of the aquifer. The hydraulic conductivity for portions of the aquifer has

been reported to range between 1 and 30 ft/d. A hydraulic gradient of approximately 0.01 has been reported, with average pore water velocities estimated to be approximately 1 ft/day. These properties are relatively ideal for subsurface injection of reagents. The region of elevated nitrate concentrations is contained within an area of the aquifer that has a radius of approximately 800 ft. Therefore, substrate could be injected into this part of the plume within 2 to 3 years, assuming 1 ft/day of pore water velocity.

Considering the information presented above, it appears that enhanced denitrification via reagent injection is a feasible method for the Monument Valley site. Questions that remain to be addressed are the degree of enhancement that can be achieved and the optimal means of implementation. These questions can be addressed with a pilot-scale demonstration test supplemented with mathematical modeling analyses. With this information, the time required to remediate the target zone to a selected cleanup objective can be estimated. Laboratory microcosm evaluations of denitrification have determined that ethanol amendments may increase reaction rate coefficients by approximately a factor of 100, which would decrease remediation times substantially (Jordan et al. 2008). The remediation enhancement with ethanol injection must be tested at the pilot-scale to evaluate the feasibility of this technology.

This project work plan (WP) describes the proposed investigation of field-scale injection of ethanol as a denitrification enhancement substrate at the Monument Valley site. This pilot-scale investigation will focus on a small area of the alluvial aquifer to field test the ethanol application. The results of this pilot study will support the feasibility analysis of full-scale ethanol application at the Monument Valley site for enhanced attenuation of nitrate concentrations and the remediation of groundwater contamination.

2.0 Project Plan

2.1 Pilot Test Design

2.1.1 Pilot Test Site Selection

We propose conducting two simultaneous studies, involving reagent injections at two different locations within the plume. This will allow assessment of potential spatial location dependency of EA feasibility. We have identified two potential locations for the pilot-scale tests. These locations are associated with existing monitoring wells that are sampled as part of the DOE monitoring program as shown in Figures 1 and 2.

- Well 765 Area
- Well 649 Area

Use of these locations would require emplacement of approximately four (two at each site) additional monitoring wells approximately 50 ft downgradient of the injection wells. These four additional monitoring wells will be required to complete the evaluation at a reasonable scale and time frame. It is assumed that the monitoring wells can be installed prior to the scheduling of the preliminary groundwater monitoring. Each of the monitoring wells shown in Figures 1 and 2 will be monitored in addition to the proposed new downgradient monitoring wells. For both cases, the well clusters will span a distance of approximately 50 ft. At each location, the reagent/tracer solution would be injected into a well (765 and 649) at the southern part of the area using a relatively low flow rate. Once injected, the solution would be allowed to migrate under natural gradient conditions. With estimated pore water velocities of approximately 1 ft/day, it is estimated that the solution pulse will traverse the well cluster within two to three months. Ethanol will be tested as the potential carbon source, though the study could be expanded to include methanol amendment, as well.

2.2 Baseline Groundwater Monitoring

2.2.1 Groundwater Elevation Monitoring

Field monitoring of groundwater elevation will be conducted with an electric sounder tape at least once a day prior to injection, during the injection test, and during the post-injection monitoring period. The design of the pilot test is a natural-gradient injection test, which was selected to avoid significant manipulation of the groundwater flow and nitrate transport system except for the application of the substrate ethanol. Water level monitoring will characterize any impact the solution injection will have on the system. Additionally, water level monitoring in the injection wells during the injection may indicate the presence or absence of well-screen biofouling due to enhanced microbial growth.

2.2.2 Field Monitoring and Groundwater Sample Collection

Groundwater samples will be obtained from monitoring wells screened in the alluvial aquifer at and around the ethanol injection wells. Water quality parameters such as pH, dissolved oxygen, redox potential, electrical conductivity, and temperature will be monitored in the field during

sample collection. Samples will be collected and analyzed for nitrate, nitrite, and ammonium, as well as other inorganic chemical analyses including alkalinity and major cations and anions. Prior to sample collection, wells will be purged with a submersible pumping unit for approximately one to three well-bore volumes (based on in-line monitoring of selected water chemistry parameters). Samples will be collected from pump discharge, and subject to traditional methods of filtration, preservation, refrigeration, storage, and transportation custody.

2.2.3 Laboratory Analysis

Samples will be transported to the University of Arizona for laboratory analysis. Ethanol will be determined using gas chromatography (flame ionization detection). Other analyses will include concentrations of nitrate and nitrite by EPA Method 353.2 or ion chromatography (IC) as needed, ammonia by EPA Method 350.1, total nitrogen, total cations by Inductively Coupled Plasma (ICP), total anions by IC, and alkalinity by acid titration.

2.2.4 Microbial Activity Sample Collection and Analysis

Groundwater samples will additionally be analyzed for microbial genetic material to evaluate the microbially mediated denitrification reaction steps occurring in the field. The primary goal of these microbial analyses is to directly monitor denitrification activity through gene expression analysis, which will be accomplished by using Reverse Transcriptase Polymerase Chain Reaction (RT-PCR) targeted for denitrification specific Ribonucleic Acid (RNA) gene products. The efficacy of using RT-PCR to elucidate microbial activity in environmental samples has been previously established for the nitrogen cycle (Burgmann et al. 2003; Hallin and Lindgreen 1999; Cantera et al. 2006).

Template material for the PCR would be obtained from selected monitoring wells in the study area during groundwater sampling before and after the ethanol injection test. Groundwater collected from selected wells will be passed through a sterile filter. Material collected on the filter will be collected using a commercial RNA isolation kit. This RNA will be used as template material in a one tube reverse transcription/Deoxyribonucleic Acid (DNA) amplification reaction (commercially available kit). PCR targets will be conserved regions of denitrification genes, specific to each reaction step in the overall denitrification process. These analyses will allow confirmation of microbial activity in the aquifer for each of the various reaction steps of denitrification. Comparison of pre and post-injection microbial genetic analysis will also provide a qualitative evaluation of changes in microbial activity that will be used to help evaluate EA feasibility.

2.3 Ethanol Injection Test

2.3.1 Ethanol Solution and Nonreactive Tracer Solution

Reagent quality ethanol (99%) will be added to groundwater collected from the site in approximately 50 gallon containers. The concentration of ethanol in the injection solution will be maintained at a constant concentration of 5% by volume during injection at both sites. This

concentration will be adequate to allow detection at monitoring locations, and should minimize potential toxicity issues.

Bromide will be used for a nonreactive tracer due to its low background concentrations at the site. Bromide salt will be mixed with the ethanol injection solution, and injected at a constant concentration during the pilot test. Samples collected from monitoring wells will be analyzed for bromide concentrations using an IC, and field monitoring will be conducted using an ion-specific electrode. Evaluation of bromide transport will be used to determine field-scale transport processes, and comparison of bromide relative to ethanol transport will aid in the evaluation of ethanol utilization for microbial activity.

2.3.2 Injection System

The solutions will be prepared in 50 gallon containers that will be sparged with carbon dioxide gas during the injection period. Additionally, carbon dioxide gas will be injected into the solution container head space to minimize the dissolved oxygen concentration of the injection solution. The injection solution will be added to each container weekly to maintain constant injection. Injection will occur in two locations, Wells 649 and 765. The solution will be discharged at a rate of approximately 6 gallons per day from each container from the bottom through tygon tubing. The injection flow rates will be maintained with peristaltic pumps, and flow rate meters will be attached in-line for monitoring. A power source will be required to operate the pumps. The tygon tubing will be placed into each injection well along the entire well screen to ensure uniform distribution along the length of the screened interval, which should also minimize the biofouling potential. An in-line sampling port will be installed at each injection well-head for monitoring of injection solution concentrations during the test. The duration of the injection portion of the pilot-scale testing will be approximately two months depending on the results of monitoring during the test. It is assumed that any waste derived from the investigation may be collected, contained, and properly disposed of by the site operations personnel.

2.3.3 Injection Test and Post-Injection Monitoring Plan

Groundwater samples will be collected from both injection and monitoring wells on a weekly basis both during and after the conclusion of the ethanol solution injection. Well 649 has two existing downgradient wells within the approximate test zone, and the installation of two more monitoring wells at this site would permit four discrete locations for test monitoring. Well 765 has three existing downgradient wells within the testing area, and the addition of two monitoring wells is required at this location, as well. After initial injection setup, sampling will occur at weekly intervals throughout the duration of the test (approximately 6 months) to monitor the impact of ethanol injection and potential decreases or rebound in nitrate concentrations. In addition, compound specific isotopic analysis will be conducted periodically to help monitor biotransformation processes (e.g., Kendall and Aravena 1999).

2.4 Data Analysis

The data collected during the ethanol-enhanced denitrification pilot-test will be used to evaluate the feasibility of nitrate EA as a remedial alternative for the Monument Valley site. Groundwater elevation monitoring will occur in conjunction with weekly sampling to monitor any changes in

direction and magnitude of the natural gradient. Nitrate, nitrite, ammonia, and cation/anion concentration data will be compared pre, during, and post injection to determine denitrification rates, rebound potential, and the efficacy of enhanced denitrification. Ethanol and bromide transport will be studied to evaluate the mass loss of ethanol and the transport parameters of the injection site. Evaluation of genetic markers of denitrification activity pre, during, and post test will allow us to evaluate microbially mediated reaction steps and impact of ethanol-enhanced denitrification on microbial activity. The results of the field test will be subjected to mathematical modeling to assist in data analysis, including assessment of long term denitrification rates throughout the plume and optimization of the method by which to inject the reagent. The results of the feasibility study can be used to evaluate the efficacy of reagent injection for enhancing rates of denitrification within the groundwater contaminant plume. This information will assist the selection and design a final remediation strategy for the plume.

3.0 Project Schedule

A proposed budget is provided in Table 1, and this section will be used to describe the budget justification. We are requesting funds for salary support towards: 1) a graduate student part time for 6 months to assist with literature review, prep work, sampling, data analysis, and modeling; 2) a research scientist part time for 6 months to assist with prep work, sampling, sample analysis, and reporting, and to model data; 3) the lead scientist and hydrologist overseeing the project personnel. We are also requesting funds to cover the following travel expenses including per diem 1) a week reconnaissance and sampling trip to verify well locations, conduct baseline monitoring, setup injection system, deliver supplies, obtain initial plume sediment characterization samples and assist with additional monitoring well installation, to initiate the study, inject substrate, and begin monitoring; and 2) weekly three-day trips to obtain groundwater monitoring samples, resupply the injection system, and maintain injection over time. Additional funds are requested to conduct chemical and microbiological analysis on samples collected during the investigation. Lastly, we are requesting funds to purchase supplies such as reagents (bromide and ethanol), sampling vials, reagent analysis kits etc.

A generalized project schedule is presented in Figure 3. The project may be initiated upon approval of the project, this Work Plan, and installation of the four additional monitoring wells is completed. It is anticipated that the pre-injection monitoring will require 1 week, the injection period will last approximately 2 months, and the post-injection monitoring period will conclude approximately 4 months after the end of injection. A final report will be provided at the conclusion of the project, which will document the major findings and recommendations.

4.0 References

- Bürgmann, H., F. Widmer, W.V. Sigler, and J. Zeyer, 2003. mRNA Extraction and Reverse Transcription-PCR Protocol for Detection of nifH Gene Expression by *Azotobacter vinelandii* in Soil. *Appl. Envir. Microbiol.* 69: 1928-1935.
- Cantera, J.J.L., F.L. Jordan, and L.Y. Stein, 2006. Effects of irrigation sources on ammonia-oxidizing bacterial communities in a managed turf-covered aridisol. *Biology and Fertility of Soils*, 43: 247-255.
- DOE (U.S. Department of Energy), 1999. Final Site Observational Work Plan for the UMTRA Project Site at Monument Valley, Arizona. Document Number U0018101.
- Hallin, S., and P. E. Lindgren, 1999. PCR detection of genes encoding nitrite reductase in denitrifying bacteria. *Applied and Environmental Microbiology*. 65:1652–1657.
- Interstate Technology and Regulatory Cooperation (ITRC), 2000. Emerging Technologies for Enhanced In Situ Bioremediation (EISBD) of Nitrate-Contaminated Ground Water.
- Jordan, F., W.J. Waugh, E.P. Glenn, L. Sam, T. Thompson, T.L. Thompson, 2008. Natural bioremediation of a nitrate-contaminated soil-and-aquifer system in a desert environment. *Journal of Arid Environments* 72, 748-763.
- Kendall, C., and Aravena, R., 1999. Nitrate isotopes in groundwater systems, in: P. Cook and A. Herczeg (Eds.), *Environmental Tracers in Subsurface Hydrology*. Kluwer Academic Publishers, Norwell, MA pp. 261-297.
- Khan, I.A. and R.F. Spalding, 2004. Enhanced in situ denitrification for a municipal well. *Water Res.*, 38:111-125.
- Smith, R.L., D.N. Miller, M.H. Brooks, M.A. Widdowson, and M.W. Killingstad, 2001. In Situ Stimulation of Groundwater Denitrification with Formate To Remediate Nitrate Contamination. *Environ. Sci. Technol.*, 35, 196-203.

Appendix G
Data Archive Outline

This page intentionally left blank

Data Archive: Outline of Available Files by Topic and Subtopic

- I. Subpile Atrixplex Plantings
 - A. Irrigation Volumes
 - Flow Meter Data
 - use 04.xls
 - USE00.xls
 - USE01.xls
 - B. Moisture Profiles
 - 1999 HP2.xls
 - test plot install hp readings and field.xls
 - 2000 sum00.xls (plus individual hydroprobe files by month)
 - 2001 hp-summary01.xls
 - 2002 moisture content sept 2002 sampling.xls
 - (gravimetric vs. neutron probe calibration)
 - 2004 2004 hp readings.xls
 - mvmoisture00-04.xls
 - 2005 2005 hp readings.xls
 - 2006 2006 hp readings.xls
 - 2007 2007 hp readings.xls
 - 2008 2008 hp readings.xls
 - C. Soil Nitrate, Ammonium and Total N Concentrations
 - 1999 initial nh4 and no3 from 1999.xls
 - 2000 00NH4NO3.xls
 - 2001 01NH4NO3corrected.xls
 - 2002 mv002cno3 and or nh4 ports.xls
 - 2004 2000_2004 stat file_no3&nh4.xls
 - 2005 2000_2005 stat file.xls
 - 2006 MV20053.syd
 - 2007 MV Mar07 Source Area Sampling.xls
 - 2008 MV MAR MAY 08 Source Area Sampling.xls
 - D. Plant Measurements: Area, Volume, Biomass, CNS, Nitrate
 - 2000 00CANOPY.xls, 20plnts00.xls
 - 2001 01CANOPY.xls, 20plnts01.xls
 - 2002 Oct 2002 sampling Shawna.xls
 - 2003 Oct 2003 sampling mort.xls
 - 2004 Oct 2004 sampling mort.xls, sum00-04 zone vol and groundcover.xls,
CANOPY SEPT 2004.xls, harvested biomass sept 2004.xls
 - 2005 CANOPY SEPT 2005.xls, plantn2005.xls
 - harvested biomass sept 2005.xls
 - 2006 plantdata2006.xls, 2006plantBiomassCNS Analysis.xls
 - 2007 plantn&s2007IAS.xls, Plant_Data_2007(1).xls
 - 2008 Plant Census 2008.xls
- II. Salt-balance Study
 - Nitrate, Ammonium, EC
 - reconstituted salts nh4no3.xls

III. Subpile Denitrification Studies

A. Nitrogen Isotope Fractionation

1. Delta N15 over time (2000, 2001, 2002)
Nitrate, % N, total N
Nand15Nofsubpilesoils.xls
2. Delta N15 Established Plants vs. Bare Soil (2005)
Delta N15-NO3
Delta N15-NH4
Ammonium, Nitrate
mulvaneyARIZONA SOIL DELTA-1.xls

B. In-situ Nitrous Oxide Production

- A. Established Plants vs Bare Soil
Nitrous Oxide Measurements
2004 (June, July, August, November)
2004soilcoverdata.xls
MV_N2ostats.xls
MV04_n2o_stats.xls

C. Soil Microcosms

1. On and Off Established Planting
2004 (June, July, August)
Nitrous Oxide Measurements
Soil Moisture
Nitrate
Nitrousstats.xls
MV_N2ostats
MV04_n2o_stats.xls
2. Soil Denitrification Enzyme Activity Slurries (DEA)
On and Off Established Planting
2004 (June, July, August)
Nitrous Oxide Measurements
Soil Moisture
Nitrate
MV_N2ostats.xls
MV04_n2o_stats.xls
3. Effect of Acetylene
 - a. 2005 (individual samples)
Nitrous Oxide Measurements
Soil Moisture
acetylenestudy.xls
 - b. 2006 (composite samples)
Nitrous Oxide Measurements
Soil Moisture
Nitrate
Total Organic Carbon
Ammonium
acetylenestudy2.xls

4. Effect of Moisture
 - a. 2005 (individual samples)
 - Nitrous Oxide Measurements
 - Soil Moisture
 - n2omoisturestudy.xls
 - TOCNHNO3_moisturestudy_SWAPL.xls
 - b. 2006 (composite samples)
 - Nitrous Oxide Measurements
 - Soil Moisture
 - Nitrate
 - Total Organic Carbon
 - Ammonium
 - moisturestudy2.xls

IV. Field Application of Ethanol Solutions- New vs Old Subpile Plantings

- Nitrous Oxide Measurements
- Soil Moisture
- Nitrate, Ammonium
- Total Organic Carbon
- A. 2006 (May, June, July, September)
 - MV ETOH Study 1 (05-18-06).xls
 - MV ETOH Study 2 (06-08-06).xls
 - IASTOCandN(0606).xls
 - MV ETOH fieldstudy 3 (07-13-06)_duplicate.xls
 - MV NO3 and NH4 Data (0706).xls
 - MV ETOH Study 4 (09-17-06).xls
- B. 2007 (May, July, October)
 - 05_2007etohfieldstudy1.xls
 - 07_2007etohfieldstudy2.xls
 - 10_2007etohfieldstudy3.xls

V. Landfarm Study

- A. Greenhouse nitrate uptake study
 - 3 Nitrate Levels
 - Amy's folder (Sorgum, Atriplex, etc.)
 - Plant fresh/dry weight
 - Plant N and C
 - Plant Nitrate
 - GRNDATA.xls
 - GRNDATA2.xls
- B. Field Plot Study
 - Nitrate uptake (4 Nitrate Levels)
 - Soil moisture profiles (0, 250, 500, 750)
 - 2007 hp readings.xls
 - 2006 hp readings.xls
 - Soil nitrate concentrations
 - Plant Measurements
 - Monument Valley Land Farm Planting_06.xls
 - landfarmplants.xls
 - landfarmn&s.xls

Nitrous Oxide Production
Nitrous Oxide Measurements
Soil Moisture
Nitrate, Ammonium
MVLFF Study 08-06.xls

- VI. Stunted Growth Studies
 - A. Casey's initial Stained vs. Unstained Study
 - Plant measurements
 - 2001canopy.xls
 - STAINMAP.xls
 - B. Greenhouse stained soil study
 - 3 Nitrate Levels
 - Amy's folder (Sorgum, Atriplex, etc.)
 - Plant fresh/dry weight
 - Plant N and C
 - Plant Nitrate
 - GRNDATA.xls
 - GRNDATA2.xls
 - C. 2005 Stained vs. Unstained
 - Plant Measurements (Area & Volume)
 - Plant Chemical Analysis
 - Bulk density
 - Soil Chemical Analysis
 - DOEstuntgrowth.xls
 - D. Field fertilizer/mulch study
 - Plant measurements
 - stuntedgrowthfeildstudy06.xls
 - stuntedgrowth122006.xls
 - E. Analysis of Black Mottled Soil
 - blkmottledTOCanalysis.xls
 - MnandTOCanalysis.xls
 - F. Dine Green House Studies
 - 1. 2005 Effect of Soil and Fertilizer
 - Plant survival
 - Relative Growth Rates
 - PLANTWT.xls
 - Greenhouse Plant Data.xls
 - 2. 2006 Effect of Fertilizer
 - Atriplex Biomass, Area, Height, Volume
 - Plant Survival
 - Tables,RGR,appendx.xls
 - Missing Biomass data
 - Greenhouseplantanalysisias.pdf

- VII. Natural Attenuation Plume Studies
 - A. Plant Exclosure Study
 - 1998, 1999, 2000
 - Plant Measurements (groundcover and canopy)
 - 9899002.xls
 - Plant Ash, N, S Content
 - B. Plume Vegetation Densities (2001)
 - 6_28VEG DENSITY.xls
 - 6-28LINE INTERCEPT.xls
 - C. Plant Water Uptake-Isotope Studies
 - 1. 2000
 - Enclosure Plant Water Extract O18 and D
 - Aqueous Well and Rain Samples O18 and D
 - Soil Sample Water Extracts O18 and D
 - ISOTOPE DATA2000.xls
 - O18H2O00.xls
 - isotope samples D and 18O.xls
 - 2. 2005
 - Plant Water Extract O18 and D
 - Aqueous Well and Rain Samples O18 and D
 - Soil Sample Water Extracts O18 and D with depth
 - Gravimetric Soil Moisture with depth
 - Soil Nitrate and Ammonium with depth
 - do18_data.xls
 - wellsoilwater&N.xls
 - D. Plume Nitrogen Enrichment Studies
 - Delta15N measurements
 - Nitrate, Ammonium, Total N
 - 2003, 2005, 2007
 - plumeN_newdatakc.xls

- VIII. Enhanced Natural Attenuation Studies
 - A. Plume Sediment Slurry Denitrification Studies
 - Nitrous oxide production from plume sediment samples
 - Artificial groundwater + nitrate incubated at 6°C
 - MVPlume Study (08-16-06).xls
 - Influence of Carbon Source (none, ethanol, acetate, formate, dextrose)
 - Nitrous Oxide Measurements
 - Soil Moisture
 - Nitrate loss
 - Most Probable Number (MPN) of Denitrifiers
 - 677 BS (Oct05).xls
 - MVPlume Study (25C, 10-03-06).xls
 - B. Comparison of Methanol and Ethanol
 - Nitrous Oxide Measurements
 - N15 Enrichment
 - Nitrate loss
 - ch3ohetohn15analyzed.xls
 - MVPlume ETOHCH3oH Study (25C).xls
 - Compiledetohmeohdata.xls

- C. Plume Sediment Packed Column Studies
 - Influence of Carbon Source (none, ethanol, acetate, formate)
 - Nitrate Concentration Breakthrough Curves
 - 606ColumnNO3data_Aug_05_ETOH.xls
 - ColumnNO3data_July_05_ACETATE.xls
- IX. Evapotranspiration /Plume Water Balance Studies
 - Plant Canopy Cover
 - Area, Volume Biomass
 - Sapflow measurements
 - Grazed vs. Ungrazed
 - 2006 2007
 - A. Sap Flux
 - MV2006 Sapflow03.xls
 - MV07_ed1.xls
 - B. LAI
 - Leaf Area ET Harvest Data 2006.xls
 - ET Harvest Data 2007.xls
 - LAI June 2008.xls
 - C. MODIS and Quickbird Imagery and Analyses
 - September 2006 Quickbird image (GeoTiff)
 - July 2007 Quickbird image (GeoTiff)
 - 2000 – 2009 MODIS EVI (.xls and GeoTiffs)